# Kinom-Analysen des Leberegels *Fasciola hepatica* zur Identifizierung neuer Wirkstoffziele und Wirkstoffkandidaten

JUSTUS-LIEBIG-UNIVERSITÄT GIESSEN

Inaugural-Dissertation

Zur Erlangung des Doktorgrades der Naturwissenschaften

(Dr. rer. nat.)

Im Fachbereich Biologie und Chemie der

Justus-Liebig-Universität Gießen

vorgelegt von

Sagar Ajmera

(M. Sc. Agrobiotechnologie)

aus

Indore, Indien

Gießen 2026

# Exploring the *Fasciola hepatica* kinome for the discovery of novel drug targets and drug candidates

Inaugural Dissertation

To obtain a doctorate in natural sciences

(Dr. rer. nat.)

in the faculty of Biology and Chemistry

of the Justus Liebig University Giessen

submitted by

Sagar Ajmera

(M. Sc. Agrobiotechnology)

from

Indore, India

Giessen 2026

The present work was carried out at the Institute of Parasitology (Faculty 10), Justus Liebig University Giessen, between May 2022 and December 2025 under the supervision of Prof. Dr. Nikola-Michael Prpic-Schäper and PD Dr. Simone Häberlein.

First supervisor: **Prof. Dr. Nikola-Michael Prpic-Schäper**

Institute of Zoology and Developmental Biology, (FB 08)

Justus Liebig University Giessen,

Heinrich-Buff-Ring 38, 35392, Giessen, Germany.

Second supervisor: **PD Dr. Simone Häberlein**

Institute of Parasitology, BFS, (FB 10)

Justus Liebig University Giessen,

Schubertstraße 81, 35392, Giessen, Germany.

**Research is what I'm doing when I don't know what I'm doing.**
**- Wernher von Braun**

# Declarations/Selbstständigkeitserklärung

Ich (Sagar Ajmera) erkläre, dass die vorgelegte Dissertation selbständig und ohne unerlaubte fremde Hilfe und nur mit den in der Dissertation angegebenen Hilfsmitteln angefertigt worden ist. Alle Stellen, die veröffentlichen Schriften wörtlich oder sinngemäß entnommen sind, sowie alle Angaben, die auf mündlichen Auskünften beruhne, habe ich als solche kenntlich gemacht. Ich bin mit einer eventuellen Überprüfung meiner Dissertation durch eine Antiplagiatssoftware einverstanden. Bei den von mir durchgeführten und in der Dissertation erwähnten Untersuchungen habe ich die Grundsätze guter wissenschaftlicher Praxis, wie sie in der „Satzung der Justus-Liebig-Universität Gießen zur Sicherung guter wissenschaftlicher Praxis" niedergelegt sind, eingehalten.

Angaben zu auf künstlicher Intelligenz (KI) basierender Hilfen wie ChatGPT oder SchulKI von OpenAI oder Gemini von Google zur Erstellung meiner Dissertation (Zutreffendes angekreuzt):

☐ Ich habe bei der Erstellung dieses Textes kein KI-Tool verwendet.

☒ Ich habe ein KI-Tool in den folgenden Bereichen eingesetzt:

☐ Ideen finden, meine Kreativität anregen

☐ Verstehen von Konzepten, Recherche von Fakten und Definitionen

☒ Optimierung eines von mir verfassten Textes (Grammatik und Formulierung)

☐ Erstellen ganzer Textpassagen nach meinen Vorgaben

Folgende KI-Tools habe ich verwendet, damit aufgeführte Teile meines Textes von dem Tool wie folgt profitiert haben:

Zur Vorbereitung dieser Arbeit nutzte ich **QuillBot**, um die Lesbarkeit, Grammatik und Sprache ausgewählter Absätze zu optimieren. Anschließend überprüfte und bearbeitete ich die Formulierungen nach meinem Ermessen und übernehme die volle Verantwortung für den Inhalt dieser Arbeit.

**Datum** **Unterschrift**

# Acknowledgements/Danksagung

At the end of this project, I would like to thank all who helped me during my PhD odyssey; without them, this would not have been possible.

Firstly, I would like to express my sincere gratitude to my supervisor, PD Dr. Simone Häberlein, without whom this project would not have existed, and her unwavering mentorship, guidance, and scientific discussion would not have steered this project to its final curve of its voyage. Thank you for your support during my nerve-wracking situation with the „Ausländerbehörde-Gießen", for which I will be grateful beyond measure. I could not have imagined having a better „Doktormutter", advisor, and encourager during my PhD and „Doktorarbeit" writing phase.

I would like to further express my sincere gratitude to Prof. Dr. Christoph Grevelding, who helped me not only shape my scientific insights but also my approach to critical thinking in science. I am also grateful for his help in the bureaucratic work of the university.

I would like to further extend my gratitude to Prof. Dr. Nikola-Michael Prpic-Schäper for agreeing to act as my first supervisor in faculty 08.

I heartily acknowledge the funding organisation for this project: the LOEWE Centre for Novel Drug Targets against Poverty-Related and Neglected Tropical Infectious Diseases (DRUID), which is part of the excellence initiative of the Hessen State Ministry of Higher Education, Research, and the Arts (HMWK). I would also like to thank all DRUID members for the retreats, symposiums, conferences, and scientific discussions.

Many thanks to all the friendly colleagues involved in this project, as well as my fellow lab mates, new and former, in the AG Grevelding, AG Häberlein, and AG Falcone, as well as the BFS building: Oli, Tobi, Max, Sophie, Saranya, Shafqat, and Bernardo, without whom working at the lab or at my desk would be irksome. Cheers Oli for all your help during the coding phase of my project and for letting me use the Linux environment on your working station.

To my friends, who stayed in or near Giessen: Arun, Shirisha, Imran, Srikanth, Tako, Sumit, Tejaswani, Shreenath, Vivek, Sushmita, Carl, Menal, Tobi, Aslı, and Hermann, with whom I shared my problems and received their suggestions and support during my time in Giessen and during my PhD odyssey.

I would also like to thank my family, parents, and my little sister for their love and support during my PhD journey. My cousin, Dr. Ankur Ajmera, whose counselling helped me to pursue a PhD after my master's degree. And Mehul, my other cousin, who helped me grasp the coding concepts in R and Python.

# List of abbreviations

| Abbreviation | Full name |
|---|---|
| PKs | Protein kinases |
| TCBZ | Triclabendazole |
| HITs | High throughput screening |
| NTDs | Neglected tropical diseases |
| WHO | World health organisation |
| NEJs | Newly excysted juveniles |
| BZs | Benzimidazoles |
| PZQ | Praziquantel |
| SAR | Structure activity relationship |
| GPCRs | G-protein-coupled receptors |
| AGC | Protein kinase c-AMP-dependent (A) / Protein kinase c-GMP-dependent (G) / Protein kinase c-CMP-dependent (C) |
| CAMK | Calcium- and calmodulin-regulated kinases |
| CK1 | Caesin kinases 1 |
| CMGC | Cyclin-dependent kinases, MAP kinases, glycogen synthase kinases, and casein kinases 2 |
| RGC | Receptor guanylate cyclases |
| STE | Homologue of yeast sterile 7, 11, and 20 kinases |
| TK | Tyrosine kinases |
| TKL | Tyrosine kinases-like |
| ePKs | Eukaryotic protein kinases |

| Abbreviation | Full name |
|---|---|
| aPKs | Atypical protein kinases |
| PKL | Protein kinase-like |
| MAPKs | Mitogen-activated protein kinases |
| RTKs | Receptor tyrosine kinases |
| PIM | Proviral integration site for moloney murine leukemia virus |
| SMILES | Simplified molecular input line entry system |
| MCCC | Managed chemical compound collection |
| H-bond | Hydrogen bonding |
| DFG | Aspartate-Phenylalanine-Glycine loop |
| Ala (A) | Alanine |
| Arg (R) | Arginine |
| Asn (N) | Asparagine |
| Asp (D) | Aspartic acid |
| Cys (C) | Cysteine |
| Glu (E) | Glutamic acid |
| Gln (Q) | Glutamine |
| Ile (I) | Isoleucine |
| Leu (L) | Leucine |
| Lys (K) | Lysine |
| Met (M) | Methionine |
| Phe (F) | Phenylalanine |

| Abbreviation | Full name |
|---|---|
| Pro (P) | Proline |
| Ser (S) | Serine |
| Thr (T) | Threonine |
| Thr (Y) | Tyrosine |
| Val (V) | Valine |

# List of contents

# Table of contents

## List of figures

## List of supplementary figures

# List of tables

## List of supplementary tables

# 1. Introduction

Infection with parasitic worms (helminths) causes serious disease burden in both animals and humans alike. The World Health Organisation (WHO) has designated several helminths infections as “Neglected Tropical Diseases” (NTDs), because they are often sidelined due to the high cost of a control strategy against them and because they affect poorer populations in the Global South, which often gives them less priority in politics, research and public discussion. At present, millions of people are affected by helminth infection due to either direct infection or infection in animal husbandry, which reduces their socioeconomic capacities (1). Soil-transmitted helminthiases are highly prevalent in developing parts of the world such as Asia, sub-Saharan Africa, and South America (Fig. 1.1) (2,3).

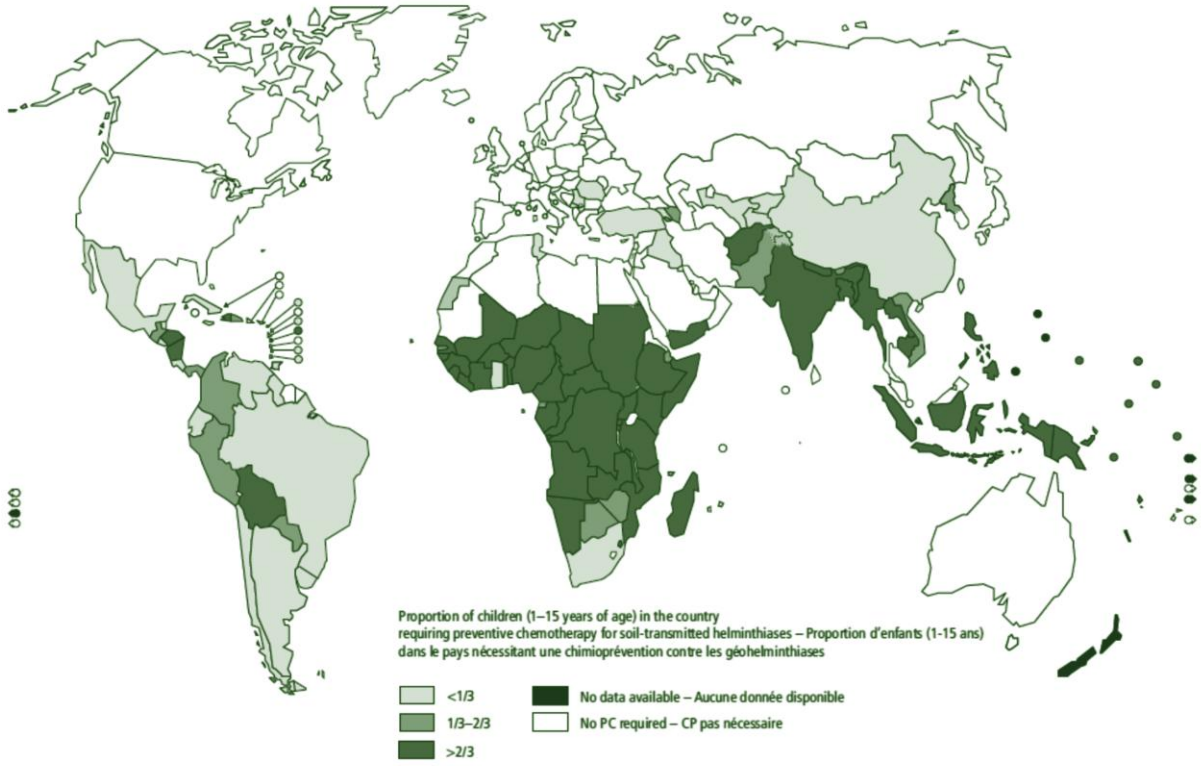


**Figure 1.1: Global prevalence of soil-transmitted helminthiases**. This figure is adapted from (3) with WHO reference number: WER No 25, 2011, 86, 257–266 and is modified with www.biorender.com.

Helminths are polyphyletic and are classified into roundworms (Nematoda), flatworms (Platyhelminthes) and acantocephalins (Acanthocephala) (4). The focus of this thesis will be on *Fasciola hepatica*, or the common liver fluke, a species within Platyhelminthes.

## 1.1 The common liver fluke: *Fasciola hepatica*

*Fasciola hepatica,* known as the common liver fluke, is the causative agent of a vector-borne parasitic disease, fasciolosis, a well-known veterinary problem across the world, and resides

in the liver of the host (1). *Fasciola hepatica* is hermaphroditic in nature (5), i.e., it poses both male and female reproduction systems in a single fluke. The most frequent type of reproduction in flukes is cross-fertilisation, but they can also self-fertilise (6).

### 1.1.1 Phylogeny and epidemiology

Parasitic flatworms belong to the phylum Platyhelminthes, forming a large monophyletic group known as Neodermata (4), which contains three classes: Trematoda, Cestoda, and Monogenea (7). Trematodes are the largest group within Platyhelminthes and are further subclassified into Aspidogastrea (which do not reproduce asexually) and Digenea. Digenea have a complex life cycle involving sexual and asexual reproduction, which relies on multiple hosts (8). There are several digenean trematodes causing debilitating diseases like paragonimiasis, schistosomiasis, etc. The causative agents of schistosomiasis are blood flukes (*Schistosoma mansoni*, *Schistosoma haematobium*, etc.). These organisms are close relatives of the oriental lung fluke, *Paragonimus westermani*, and several other medically important liver fluke species. These liver flukes include two carcinogenic species *Clonorchis sinensis* (the oriental liver fluke) and *Ophisthorchis viverrine* (the southeast Asian liver fluke), as well as the *Fasciola* species: *Fasciola gigantica* (the tropical liver fluke), *F. hepatica* (the common fluke), *Fascioloides magna* (the giant liver fluke), alongside others. The phylogenetic classification of *F. hepatica* is depicted in Fig. 1.2.

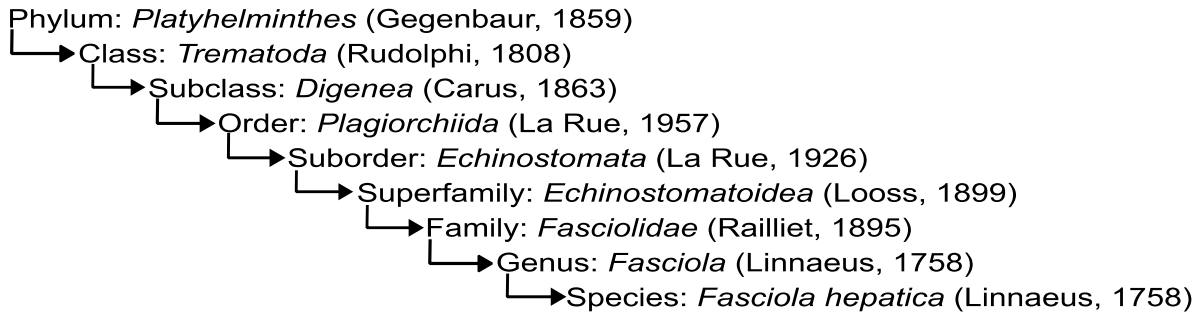


**Figure 1.2: The phylogenetic classification of *F. hepatica***. The information on the phylogenetical classification is collected from (9).

The global distribution of fascioliasis is illustrated in Fig 1.3, which is prevalent on every continent except Antarctica (10). *Fasciola hepatica* infections are found in temperate zones, while *F. gigantica* infections are found in more tropical regions, such as Asia and Africa, but both species can also hybridise simultaneously due to globalisation and the impressive capability to adapt to new vertebrate hosts (6).

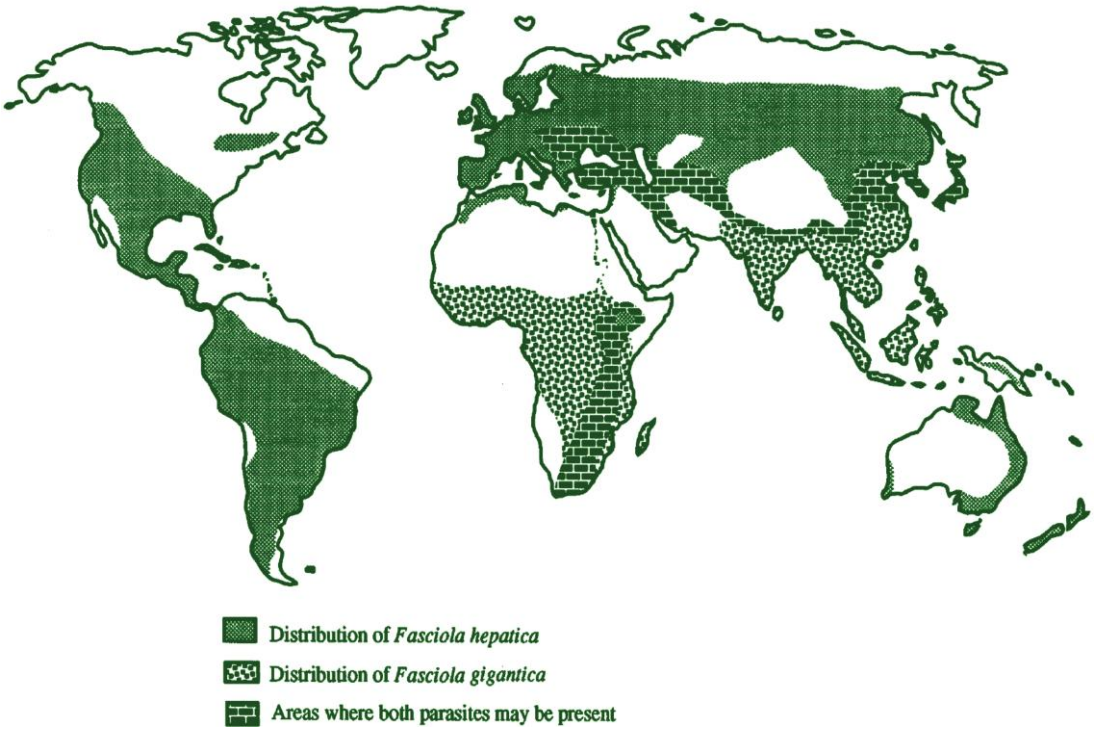


**Figure 1.3: The global distribution of fasciolosis**. This figure is adapted from (11) and is modified with www.biorender.com.

### 1.1.2 Life cycle and the biology of *F. hepatica*

The life cycle of *F. hepatica* (12) (Fig. 1.4) depends on certain environmental conditions and is diheteroxenic, meaning it requires two distinct host species for its development: a gastropod intermediate host from the Lymnaeidae family, such as *Galba truncatula*, and a mammalian definitive host. Liver flukes can infect more than just ruminants like sheep and cattle, and they can also spread to a wide variety of mammals, including humans (8). Fasciolosis infections have also been reported in non-ruminant herbivore species, including horses, deer, donkeys, kangaroos, and camelids, and extend to laboratory animals like mice, rats, hamsters, and rabbits (8).

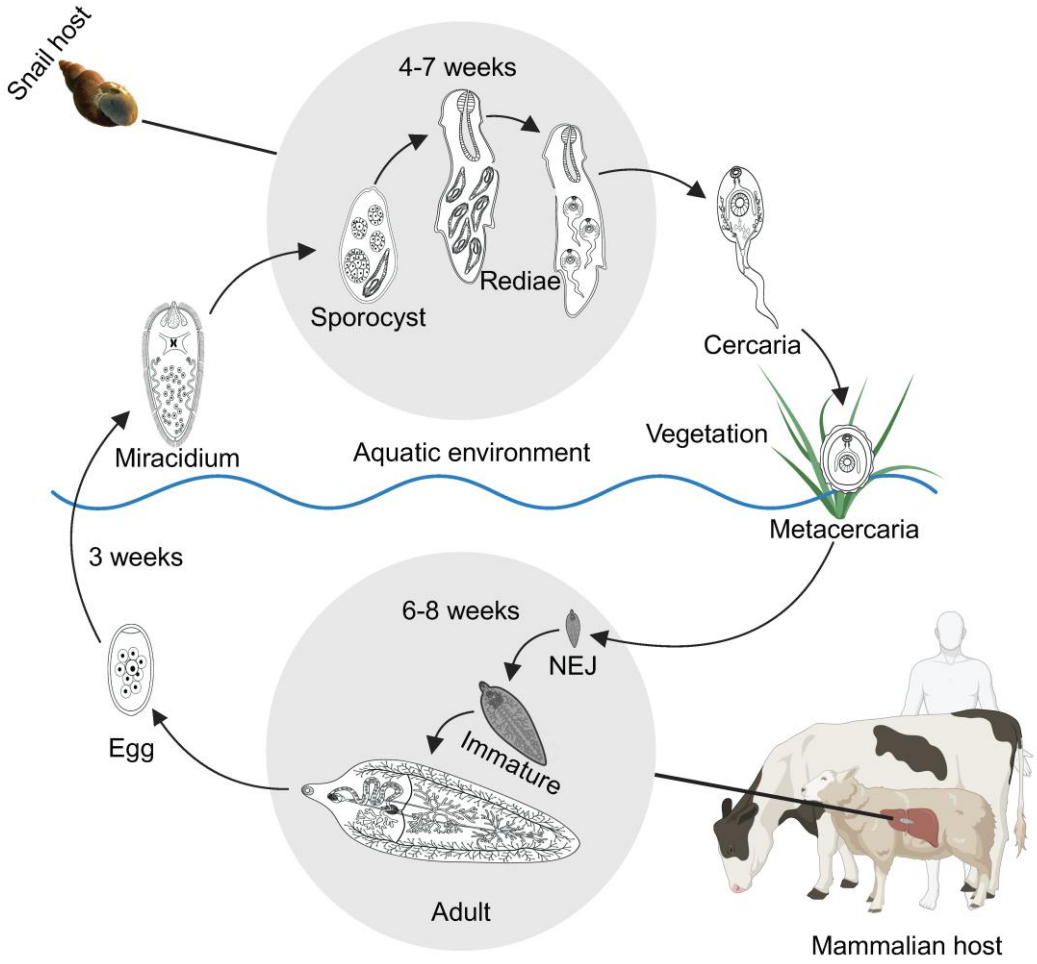


**Figure 1.4: The life cycle of *Fasciola hepatica***. The upper part of the figure (above the blue line) depicts the water-bound part of the life cycle. The illustration of the figure is based on of the book Fasciolosis (13). Credits: [Kayakova Maryia]/Adobe Stock #file no.: 489056005 (cycle, modified) licensed on 05.08.2025. This figure is created with www.biorender.com.

Eggs excreted by mammals infected with liver flukes are in their faeces. The eggs released from the faecal matter and under certain physio-chemical factors go through embryonation (10). Then, the miracidium begins to develop inside the embryonated egg once the optimal environmental conditions are met. After a three-week incubation period, the miracidium-containing egg hatches in an aquatic environment and rapidly searches for a snail host (14). When the miracidium attaches itself to the snail host, it penetrates the skin and develops into a sporocyst (14). The sporocyst reproduces asexually, generating multiple rediae, from which several cercariae emerge after approximately four to seven weeks (15). Cercariae shed from the snail in search of a suitable surface, potentially an aquatic plant, to attach to and encyst into metacercariae (14). In their encysted forms, metacercariae can survive up to several years or even decades if the optimal conditions are met (15). Upon ingestion of the microscopically small metacercariae by a mammal along with an aquatic plant (e.g., watercress) or, less

frequently, with water, the mammal becomes infected. Once in the small intestine of the mammal, juvenile flukes (NEJ: newly excysted juveniles) are released from the metacercariae (13,16). Eventually, these NEJs penetrate the intestinal wall and travel through the peritoneal cavity toward the liver (16). During the following liver-migratory phase, the fluke is not yet sexually mature and hence is known as an immature fluke (13). The immature fluke can burrow into the liver capsule and consume the liver parenchyma until it is sexually mature, which takes on average six to eight weeks (14). After reaching sexual maturity, the adult fluke transmigrates and resides in the large biliary passages (14). A single adult fluke can lay approximately 50,000 eggs per day (17,18), which are then excreted via the faeces of the infected mammal. Depending on the species of host, an adult fluke can survive decades (7,8,13,14).

Adult flukes are multicellular parasites that can reach 3 cm in body length and 1.5 cm in body width (8). All general anatomical features of an adult fluke are displayed in Fig. 1.5. Flukes are dorso-ventrally flattened with a leaf-like shape, which is broad anteriorly and narrow posteriorly. The fluke's outer layer is called tegument, which is covered with numerous spines (7) and glycocalyx (19), which shields the fluke from the host's digestive fluids (20). The oral sucker is the starting point of the digestive tract of the fluke, which is via a muscular pharynx and oesophagus connected to the two branched caeca. Indigestible contents are egested through the oral sucker, as there is no anus (21). A second sucker, the ventral sucker, facilitates attachment to host tissue. Additionally, the flukes have a central nervous system that consists of nerve cords that extend to the posterior portion of the fluke and cerebral ganglia located close to the pharynx (22). Clusters of nerve cells and fibres beneath the tegument, in the oral and ventral suckers, and in relation to the various reproductive organs and ducts, make up the peripheral nervous system (13,20). Flukes, due to their hermaphroditic nature, have a unique reproductive system. They contain two sets of branched testes connected by means of vas deferens to the cirrus sac near the genital pore (it is situated adjacent to the ventral sucker). Furthermore, the genital pore is connected to a uterus with a smaller single-branched ovary in the anterior part of the fluke (23). The primary function of the genital pore is to release eggs, and during copulation, there is an exchange of sperm. Liver fluke eggs comprise an oocyte and numerous vitelline cells derived from the vitellarium (24). The vitellarium consists of numerous vitelline follicles that occupy the posterior and lateral edges of the fluke. A duct that gathers vitelline cells extends along both sides of the fluke and converges with the duct from the opposite side to create the vitelline reservoir. The vitelline duct extends anteriorly to join the oviduct and concludes in the ootype, where egg formation occurs.

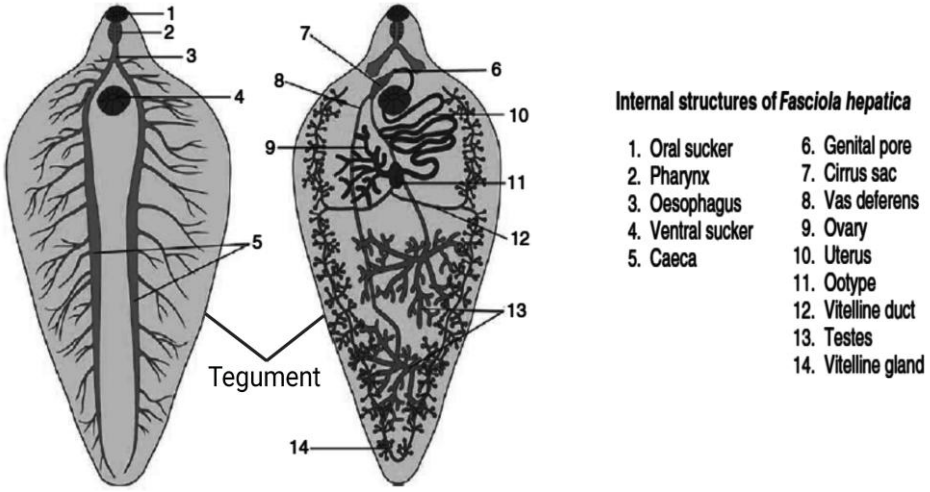


**Figure 1.5: General anatomical features of an adult *F. hepatica*** covering major body structures. This figure is adapted from the book Fasciolosis (13) and was modified with www.biorender.com and Inkscape (25).

### 1.1.3 Neglected tropical disease: Fasciolosis, its economical and health impact

Fasciolosis is a highly pathogenic zoonotic disease, which may be transmitted from vertebrate animals to humans (via a snail host) and vice versa. Fasciolosis is a widespread NTD in tropical areas, affecting up to 90% of livestock (26). WHO also estimated that approximately 17 million people globally are infected with fasciolosis (27), with about 91 million people at risk of infection (28).

The annual socioeconomic impact of fasciolosis infection exceeds $3 billion USD per annum worldwide through the means of death and productivity loss in infected animals (5,10,29,30). This includes a weight loss of the animal (31), decrease in milk yield (32,33), reduction of protein and fat proportions in the milk content (34–36), and fertility of cattle (35,37).

The severity of fasciolosis infection on health is highly detrimental, ranging from asymptomatic cases to life-threatening cases. The next section (1.1.4) describes the manifestation of fasciolosis in humans as well as animals.

### 1.1.4 Symptoms and diagnostics

Symptoms of fasciolosis in humans can be observed as early as one month after metacercaria ingestion. The infection can be divided into two main clinical phases: acute and chronic (6,13,14). When the migrating immature flukes begin the mechanical destruction of the liver tissue, the acute phase - also referred to as the invasive phase - occurs, resulting in toxic and allergic reactions that persist for two to four months. This phase is often characterised by fever, weight loss, abdominal pain, respiratory symptoms like coughing, shortness of breath, haemoptysis, and chest pains, as well as gastrointestinal discomfort-like flatulence, loss of appetite, nausea, and diarrhoea. When the flukes enter the bile ducts and mature into adult

flukes, the chronic phase starts. The enlargement of the flukes causes inflammation, hyperplasia, thickening and dilatation of the duct and gallbladder walls and the fibrosis of the liver. Biliary colic, jaundice, epigastric pain, intolerance to fatty foods, nausea, pruritus, and tenderness in the abdomen are the symptoms of this phase. The chronic phase lasts for up to decades, overlapping with the lifespan of the liver fluke (6,10,30). Livestock exhibits both acute and chronic symptoms that are comparable to those of human infection. However, during the acute phase, sudden death of the animal is possible if the livestock is heavily infested with flukes (38).

There are multiple direct and indirect methods to detect fasciolosis. The most frequently used direct method is to detect eggs of the parasite in the faeces using the conventional sedimentation method (coproscopical) (39). The main drawback of this method is that it is only helpful when the infection is in its chronic phase, as only adult flukes produce eggs (40). The commercial versions of the sedimentation method for detecting many helminths and some protozoan infections are Flukefinder® (41) (Flukefinder® Diagnostic System, Soda Springs, Idaho, USA), FLOTAC® (42) and mini-FLOTAC® (43).

Alternatively, several serological and immunological indirect methods have been adopted for earlier detection of fasciolosis infection, which includes enzyme-linked immunosorbent assays (ELISAs) of stool or serum samples and antibody detection in bulk tank milk samples (44). These methods heavily rely on the detection of antibodies against cathepsin L-like endopeptidase by indirect ELISAs (45). This proteinase is secreted by all *Fasciola spp.* epithelial cells, facilitating the penetration of the host tissue (46,47). These techniques are much more sensitive than direct methods, but they have a disadvantage. Because of their lengthy half-lives, antibodies that the host secretes to combat the fluke can still be found, for example, in milk even after effective treatment (40). Some of the commercially available ELISA kits for detecting fasciolosis are Ildana® (Ildana Biotech, Ireland), IDEXX® (IDEXX, France), and Bio-X® (Bio-X Diagnostics, Belgium).

## 1.2 Control and treatment of fasciolosis

Since the early 1960s, the emergence of a notable class of nitrogen heterocycles in veterinary medicine, known as benzimidazoles, has transformed the development of a new generation of anthelmintics (48). The usage of anthelmintic drugs is currently the principal management intervention against fasciolosis (11).

### 1.2.1 Current control management systems against fasciolosis

Traditional preventative measures against fasciolosis are the same for humans as well as livestock (14). These include avoiding fresh water and raw vegetation consumption from

endemic areas that harbour *Fasciola* metacercariae, as well as breaking the *Fasciola* life cycle at the intermediate host through physical, chemical, or biological means (14). Furthermore, it is crucial to adequately inform the population residing in fasciolosis-endemic areas about the illness, its pathogenicity, and how it spreads (8). Alternatively, farmers can opt for a more controlled animal husbandry approach to reduce the parasite burden in their locality (40). This strategy includes rotational grazing patterns, pasture control, quarantining infected animals and avoiding habitats where intermediate hosts are prevalent (11). But these preventative measurements can only reduce the transmission of the infection, not treat it.

Treatment of fascioliasis involves chemical control with anthelmintics (11). Several different anthelmintics have shown flukicidal activity against fasciolosis (49). Some of the flukicides as well as their effectiveness against different parasitic life stages of *F. hepatica* are illustrated in Fig. 1.6.

<table>
<tr><td></td><td colspan="13">Stage of fluke (weeks post infection)</td></tr>
<tr><td></td><td colspan="4">Immature fluke stage</td><td colspan="9">Adult fluke stage</td></tr>
<tr><td>Flukicide used in host</td><td>1</td><td>2</td><td>3</td><td>4</td><td>5</td><td>6</td><td>7</td><td>8</td><td>9</td><td>10</td><td>11</td><td>12</td><td>12+</td></tr>
<tr><td>Albendazole</td><td rowspan="8"></td><td rowspan="8"></td><td rowspan="8"></td><td rowspan="8"></td><td rowspan="8"></td><td rowspan="8"></td><td rowspan="3"></td><td rowspan="3"></td><td rowspan="3"></td><td colspan="2" rowspan="3">50 - 70%</td><td colspan="2" rowspan="3">80 - 99%</td></tr>
<tr><td>Oxyclozanide</td></tr>
<tr><td>Clorsulon+Ivermectin (inj)</td></tr>
<tr><td>Clorsulon (oral)</td><td colspan="6">90 - 99%</td></tr>
<tr><td>Nitroxynil</td><td colspan="3">50 - 90%</td><td colspan="3">91 - 99 %</td></tr>
<tr><td>Closantel</td><td colspan="2">23 - 73%</td><td>91%</td><td colspan="3">91 - 95%</td><td colspan="3">97 - 100%</td></tr>
<tr><td>Rafoxanide</td><td></td><td colspan="2">45 - 85%</td><td colspan="3">85 - 99%</td><td colspan="3">99 - 100%</td></tr>
<tr><td>Triclabendazole</td><td>90-99%</td><td colspan="12"></td></tr>
</table>

**Figure 1.6: Efficacy spectrum of recommended flukicide used in host** (sheep and cattle) against different life stages of fluke. 'Inj' refers to the administration route of the drug via injection in the host. The figure is adapted from the book Fasciolosis (13).

Flukicides that have been approved against fasciolosis in livestock are used abundantly by farmers, negatively impacting the effectiveness of these flukicides. This active over-usage pattern of monoanthelmintics in the same endemic area has contributed to a real threat of anthelmintic resistance (50). Furthermore, this situation may exacerbate treatment failures and potentially impact the economic stability of the farming sector.

A plethora of compounds have reportedly been used to treat human fasciolosis, but none are as successful as the imidazole derivative TCBZ (14). WHO has also recommended TCBZ to treat human fasciolosis, although EGATEN® (developed by Novartis Pharmaceuticals) is currently in phase IV clinical trials (51), and it is still not approved in several countries for treatment against human fasciolosis.

### 1.2.2 Triclabendazole: mode of action and its resistance in *F. hepatica*

Since 1983, the incorporation of triclabendazole (TCBZ) into standard veterinary practices has been considered the gold standard for controlling fasciolosis infection in both ruminants and humans alike (52). This is because TCBZ is the only known flukicide that is effective against the early pathogenic immature stage of the fluke, beginning from the second week following infection with >90% efficacy in livestock (Fig. 1.6). TCBZ is administered in two separate regimens against human fasciolosis in 10-12 mg/kg dosage (14). The cure rate observed after the first dose of TCBZ is 79.2%, and the second dose is 100% without showing any side effects, even in the case of postnatal and preschool-age children (53). Despite its efficacy, TCBZ is not approved for human use in many countries.

The exact mode of action of TCBZ against *F. hepatica* is still ambiguous. What seems to stand out is that the treatment of TCBZ in *F. hepatica* causes tegument disruption (54–56) and influences apoptosis in the ovaries, testes, and vitelline tissues (23). Additionally, TCBZ inhibits mitotic (germ cell) and meiotic (germ and somatic) cellular division in the liver flukes (57,58). Evidently, these effects are similarly associated with other classical benzimidazoles (BZs), as they bind to β-tubulin, inhibiting the dimerisation of the microtubule network and the polymerisation of heterodimers in helminths (59). But *Fasciola spp*. are insensitive to classical BZs and colchicine (60) because three of the six β-tubulins in *Fasciola spp*. contain a single nucleotide polymorphic (SNP) mutation of F200Y, which means tyrosine (Y or Tyr) is at the 200$^{th}$ residue position instead of phenylalanine (F or Phe) (61). The F200Y mutation in the β-tubulin isotype 1 allele is conjointly associated with resistance to BZs in nematodes, such as *H. contortus*, *A. lumbricoides*, *T. trichiura*, etc. (62). This mutation also hinders the binding ability of the BZ moieties in the binding site, as Tyr forms hydrogen bonds with asparagine$^{165}$ (N or Asn) to close the binding pocket access for the ligands and glutamic acid$^{198}$ (E or Glu), which prevents the binding of BZ ligands at the binding pocket of β-tubulin (63). Furthermore, the study from Olivares-Ferretti and colleagues (64) modelled all six known forms of β-tubulin in *F. hepatica* and indicated that the TCBZ-binding is higher at the nucleotide binding site compared to colchicine and ABZ binding sites. These models are computational, and further experimental validation is still required to solve the exact mode of action of TCBZ.

The significant application, overreliance, and improper dosing of TCBZ have contributed to the development of resistance globally (50). The first documented case of TCBZ resistance was reported in Australia (65); subsequently, various cases of TCBZ resistance have been reported in Europe, New Zealand, and South America (63). Recently, in northern Germany, a TCBZ resistance case documented the death of 300 sheep in the flock due to treatment failure (66). Nonetheless, the resistance has extended beyond TCBZ, as it has spread to other drugs

controlling fasciolosis, such as albendazole (67), clorsulon (68), and closantel (69). And the most distressing aspect is that fasciolosis has developed a multi-drug resistance (70).

The mechanism for TCBZ resistance in *F. hepatica* remains ambiguous. However, three possible hypotheses are suggested: (a) mutation at the TCBZ tubulin binding, (b) enhanced drug efflux, and (c) improved drug metabolism (63). It has been suspected that the mutation of any one of the six β-tubulin binding residues may reduce the drug-tubulin interaction and is linked to TCBZ resistance. However, no concordant evidence of a correlation between the TCBZ-sensitive and -resistant liver fluke strains in terms of amino acid sequence or β-tubulin expression levels has been elucidated (71,72). In cancer cells, efflux pumps such as ABC transporters are associated with the mechanism of multidrug resistance (73). Evidently, the ATP-binding cassette transporter glycoprotein (P-gp), belonging to the ABC subfamily of B member 1 (ABCB1), acts as drug efflux transporter is seemingly involved in TCBZ resistance in nematodes (74). In *F. hepatica*, a small study by Wilkinson and colleagues (75) reported a SNP of T687G (change of thymine to guanine), which caused a S1144R mutation (change of serine to arginine at the 1144 residue) in the P-gp gene, which is linked to reduced accumulation of TCBZ. However, this SNP was not found in TCBZ-sensitive and -resistant isolate fluke populations (76,77). Clearly, determining the function of this SNP in TCBZ resistance requires additional research. Another mechanism of resistance may be based on an altered drug metabolism. A previous study found that TCBZ-resistant isolates have higher expression levels of TCBZ inert metabolites (TCBZ sulphoxide to TCBZ sulphone) than TCBZ-sensitive flukes (78). This study demonstrated that resistant strains rapidly metabolise TCBZ to its inactive form, which may lead to decreased active drug metabolite availability. Furthermore, glutathione S-transferase (GST), an enzyme involved in drug metabolism, is highly expressed in TCBZ-resistant rather than TCBZ-sensitive flukes, resulting in even lower drug concentration accumulation (63). Furthermore, a recent study conducted by Choi and colleagues delineated the differential transcript expression of microtubule-related genes between TCBZ-resistant and TCBZ-sensitive flukes and they observed that TCBZ-resistant flukes exhibited an overexpression of microtubule-related genes (79). This suggests that an overabundance of tubulin targets likely reduces the available TCBZ, thereby hindering the TCBZ required to disrupt microtubule polymerisation and effectively eliminating the flukes. In the future, shedding light on all these mechanisms may improve our understanding of the TCBZ resistance mechanisms in *F. hepatica*.

### 1.2.3 Drug development against fasciolosis

The high cost of drug discovery and compound screening, along with the time spent bringing drugs that are safe for both livestock and humans to the market while ensuring all regulatory and pharmacovigilance compliance (80), contributes to the inability of pharmaceutical companies to be vigilant against an NTD such as fasciolosis. Nonetheless, new molecular entities or *de novo* compounds with known modes of action remain vital for discovering anthelmintics. There are numerous approaches under consideration for drug discovery and development as anthelmintics, with a primary focus on two approaches: phenotypic screening and molecular target-based screening (81).

Phenotypical screening often constitutes the initial discovery of chemical compounds (82), which are then identified and verified for anti-parasitic effects either *in vivo* or *in vitro* (83). Recently traditional natural medicine and natural extracts have been pursued as an alternative treatment for fasciolosis. For example, compounds derived from *Artemisia mexicana* and several other plant extracts used in traditional Mexican medicine have been tested against NEJs, with favourable results (84). Similarly, when a natural naphthoquinone (plumbagin) extract from the roots of *Plumbago indica* was tested on NEJs and 4-week-old immature *F. gigantica* flukes, it showed more detrimental effects than TCBZ at the same concentration (85). Several natural products are currently being tested for anthelmintic properties, such as mirazid (derived from *Commiphora molmol*), which has been commercially distributed in Egypt as a fasciolicide, demonstrated in a preliminary study substantial tissue damage and disruption of egg production in TCBZ-resistant *F. hepatica* (86,87).

Another major aspect of drug discovery for anti-parasitic compounds is the molecular target-based screening approach, which is the dominant strategy when compared to the phenotypic screening (88). The premise of this strategy is based on the hypothesis that a given target is essential for achieving a specific therapeutic aim (89); for example, identifying a chokepoint for biological processes critical for the growth and survival of the parasite. Often, these biological chokepoints are translated from model organisms like *D. melanogaster* or *C. elegans* because they can be manipulated and are phylogenetically close to the target parasite of interest. The next step involves analysing the computational structure activity relationship (SAR) of target inhibitors or antagonists, which is followed by biochemical functional validation. Alternatively, various mammalian families of druggable proteins, such as G protein-coupled receptors (GPCRs), protein kinases (PKs) and ion channels, which can be regulated by the help of small-molecule inhibitors, can also be pursued as anti-parasitic targets (89,90).

Although praziquantel (PZQ) is an effective drug against several parasitic flatworms, it lacks efficacy against *Fasciola*. Recently, Marchant and colleagues recently discovered the

resistance mechanism of PZQ (91), setting a landmark in fasciolicidal research. They found a mutation of a single residue (threonine) at the binding site of PZQ in *Fasciola* instead of asparagine (in sensitive parasitic flatworms) (92). Additionally, Marchant and colleagues computationally discovered (by SAR) new agonists against the *Fasciola* transient receptor potential ion channel, for which our lab contributed by evaluating the activities of these agonists on *Fasciola* and confirming that they are more potent than TCBZ (93). Likewise, PKs are already under investigation for their anthelmintic activities; more on this topic will be covered in section 1.3.

### 1.2.4 Vaccine development against fasciolosis

Vaccination is a valuable preventive measure against any infection and limits the dependency on drug-controlled preventive measures; hence, it controls drug resistance. Several trials have been conducted in the past targeting the secretome of the fluke (collection of bioactive molecules, such as proteins, lipids, and nucleic acids, that the flukes release into their surroundings) (94,95). The lead target groups for vaccine candidates were fatty acid binding proteins, cathepsin L, glutathione S-transferase (GST), and leucine aminopeptidase (94). In the studies, either a combination of vaccines or a singular vaccine was administered against the antigen. The results from most of the trials deduced a substantial reduction in the fluke burden; for instance, targeting native cathepsin L antigen in one trial demonstrated a 34% reduction of fluke burden in sheep (96) and a range of 42 to 69% in cattle (97), although the result could not be replicated. The challenge in developing a vaccine for fasciolosis is to optimise the antigen that elicits acquired immunity against the infection. This situation continues to pose a challenge for the development of a commercially viable vaccine for long-term efficacy against fasciolosis.

Another novel approach for vaccine development against fasciolosis may involve the use of glycoproteins and glycoconjugates secreted by the flukes and present on the outermost part of the tegument (19,98). The glycoproteins from flukes are involved in the T helper 2/TReg immune response via C-type lectin receptors (99). This strategy enables the fluke to ensure its survivability and decrease liver damage inflicted by the host's immune response (100).

An alternative strategy employed for vaccine development against fasciolosis infection (which is under investigation) incorporated cathepsin L mimotopes, which demonstrated reduction in fluke burden by approx. 50% (101) and egg production in sheep (102) and goats (101–103).

## 1.3 Protein kinases: an approach towards antiparasitic compounds

### 1.3.1 Structural aspects and classification of PKs

Protein kinases (PKs) constitute the second most intensely explored class of druggable superfamily of essential proteins after G-protein-coupled receptors (GPCRs) and are regarded as master metabolic switches governing a majority of cellular pathways (104). PKs function by transferring a terminal or gamma (γ) phosphate group from a high-energy molecule, such as adenosine triphosphate (ATP) or guanosine triphosphate (GTP), to the hydroxyl group of a serine/threonine or tyrosine residue of the target protein (105,106). PKs are involved in an abundance of cellular processes, including transcription, translation, and signal transduction cascades associated with cell proliferation, differentiation, apoptosis, migration and metabolism (106–108).

Generally, PKs constitute roughly 2 to 4% of the entire proteome and are among the largest classes of the protein-coding genes found in most of the eukaryotic proteomes. Manning and colleagues mapped the human kinome and discovered 518 PKs (109), which encode approximately 2% of the protein-coding genes. Among the 518 PKs, 478 are eukaryotic PKs (ePKs), and the remaining 40 are atypical PKs (aPKs). Typically, the domain in ePKs is highly conserved and consists of eleven of the twelve subdomains conserved (Fig. 1.7); in contrast, aPKs share limited sequence similarity and are divergent (110). The canonical PK catalytic domain has two main folds, known as lobes, that are connected via a flexible hinge region, establishing a hydrophobic cleft for the ATP binding site (111). The first smaller lobe is the N-terminal lobe, which comprises an α-helix and five β-sheet strands that are distinguished for ATP-binding, while the subsequent larger lobe is the C-terminal lobe, which comprises six α-helices that enable protein substrate binding and phosphorylation catalysis (112,113). The active site, composed of the activation loop and catalytic loop that forms the ATP and substrate binding sites, resides between the N-terminal and the C-terminal lobes (114).

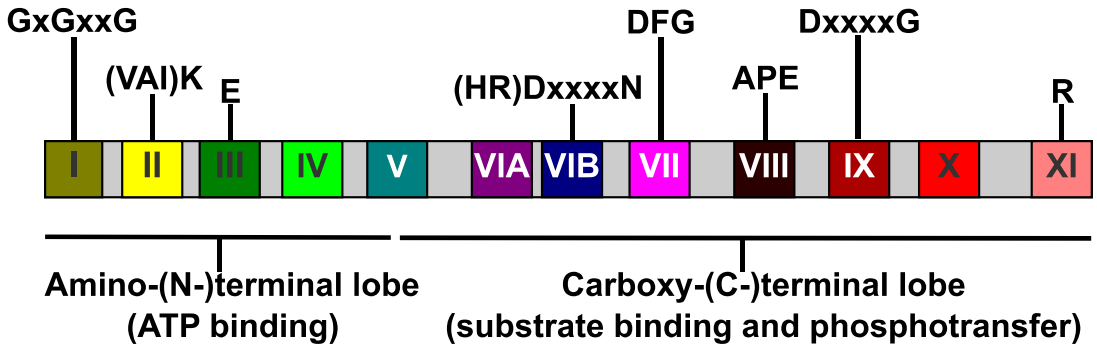


**Figure 1.7: Key structural features of the catalytic domain of eukaryotic protein kinases** (ePKs). The twelve conserved subdomains are depicted in different colour codes (from I to XI), and the grey colour represents the less conserved regions in the protein sequence. This figure is adapted from (110) and created with IBS v2.0 (115) and aesthetically modified in Inkscape (25).

PKs are classified into two main superfamilies based on the residues they phosphorylate: serine/threonine (STK) or tyrosine residues (PTK) (116). Although the majority of PKs phosphorylate only a single type of residue, there are some exceptions known as “dual-specificity kinases”, which can target both serine/threonine and tyrosine residues (117). The “current standard classification scheme” of PKs is based on the initial scheme proposed by Hanks and colleagues (118,119), subsequently refined by Manning and colleagues (109,120) and accessible via KinBase (121). This classification of kinases may alter as new kinases are identified and existing kinases are reclassified into different families and/or subfamilies based on their structure and/or function.

PKs are classified into nine major ePK groups based on their primary sequence and conserved structural features: AGC (protein kinase A, G, and C), CAMK (calcium/calmodulin-dependent kinases), CK1 (casein kinases), CMGC (cyclin-dependent kinases, MAP kinases, glycogen synthase kinases, casein kinases 2), the “Other” group (which shares weak sequence homology to other PK groups), RGC (receptor guanylate cyclases), STE (homologues of yeast sterile 7, 11, and 20), TK (tyrosine kinase), and TKL (tyrosine kinase-like) (109,116,122). Alongside the nine ePKs, some other kinases show a similar prototypical-like fold and catalytic mechanism as ePKs, albeit they lack the canonical sequence motifs features of PK catalytic domains; thus, they are collectively termed “atypical” (aPKs) or simply referred to as “PK-like” (PKL) (123). The aPKs group comprises divergent families, such as Alpha, ABC1 domain-containing (ABC1), phosphatidyl inositol-3-kinase-related kinases (PIKK), and right open reading frame (RIO) (123,124). Consequently, PK groups are split into 240 families and 128 subfamilies (http://kinase.com/kinbase/).

### 1.3.2 PKs as drug targets against cancer and parasitic diseases

Considering the importance of PKs in cancer development, a multitude of small-molecule PK inhibitors serve as therapeutic agents (125), with 94 of these inhibitors currently approved by the USFDA for the treatment of various cancerous types (126,127). Because PK domains are conserved and exhibit analogous roles across phylogenetically distant and divergent organisms, they may also be considered potential targets against parasites (128). Exploring the role of kinases in parasitic worms may help us create innovative interventions, control strategies, and treatment approaches against parasitic worms (129).

Several kinome studies have significantly advanced the drug target research for NTDs caused by various parasites, including cestodes [*T. solium* (130), *D. caninum* (131), etc.], nematodes [*H. contortus* (132), *T. trichiura* (133), etc.], trematodes [*S. japonicum* (134), *S. haematobium* (135), *S. mansoni* (136,137), *F. gigantica* (138), etc.], apicomplexans [*P. falciparum* & *P. vivax* (139,140), *T. annulate* (141), etc.], kinetoplastids [*L. infantum* & *L. braziliensis* (142), Trypanosomatida (143), etc.], etc. The emergence of kinome databases facilitates the search for antiparasitic targets and compounds.

Dissous and Grevelding initially discussed the so-called “piggy-back” approach (144) to repurpose PK inhibitors approved for human diseases as anthelmintics. This so-called “piggy-back” approach was recently adopted and employed by Moreira and colleagues; they showed the effectiveness of repurposed PK inhibitors against *S. mansoni* (145–147). They identified multiple potential schistosomicidal compounds, and following the investigations using an *in vitro* screening assay, they discovered two compounds that induced phenotypical changes in the tegument and gonads as well as impairments in cell proliferation (145–147). This approach was also utilised for malaria and leishmaniasis to uncover numerous lead compounds (142,148,149). This strategy could potentially be extrapolated to for repurposing PK inhibitors in a novel approach to combat fascioliasis.

### 1.3.3 Role of PKs in helminth survival, growth, and signalling

Helminths often inhabit distinct biological niches within their host (150,151) and possess unique defence mechanisms to evade host immune detection and/or attack, often necessitating specialised signalling pathways (152–154). Nevertheless, comprehension of these signalling mechanisms remains scarce; however, understanding these biological chokepoints can be crucial for bolstering the anthelmintic research (155). Considering this, PKs in parasitic helminths are important for several magnitudes of biological and medical reasons, as they are associated with helminth development, including reproduction, growth, cell survival, stress adaptation and apoptosis (156,157).

Mitogen-activated protein kinases (MAPKs) are important for helminth reproduction and stress response and are classified within the CMGC PK group (158). Andrade and colleagues inhibited extracellular signal-regulated kinase (ERK) in *S. mansoni* and established its function in sexual maturation of the blood fluke (159). They additionally reported poorly developed ovaries and a significant reduction of egg burden in mice infected with dsRNA-treated schistosomula (159). The inhibition of c-Jun N-terminal kinase (JNK), another member of the MAPK family, reduced the *in vivo* survival rate of blood flukes by 50% (159). Avelar and colleagues demonstrated that knocking down Smp38 MAPK expression caused tegumental damage and a reduced survival rate of *S. mansoni* (160). The study suggested that Smp38 MAPK serves as a significant defence mechanism against host oxidative stress and facilitates the survival of the blood fluke within the host (160).

Another significant group of PKs is CAMK, which is essential for calcium signalling in helminths. Calcium (Ca2+) is essential for various functions in helminths, including neural activity, fecundity, motility, muscle contraction, and host attachment; therefore, it proves critical for immediate survival within the host (161). In *E. multilocularis*, the CAMK group is implicated in the regulation of larval growth, development, and survival (162). Gao and colleagues reported that inhibiting calcium channels in *Echinococcus* produced significant inhibitory effects on the parasite, its germinal layer cells, and metacestode, hypothesising the involvement of CAMKII in the maintenance and completion of the life cycle (163).

Another subfamily of the tyrosine PK group represents receptor tyrosine kinases (RTKs), which are particularly significant due to their involvement in host-induced stress signalling in helminths. Through studying the insulin signalling mechanism in *S. mansoni*, Vicogne and colleagues identified an unconventional receptor exhibiting significant homological similarity to the mammalian insulin receptor, which they designated as venus kinase receptors (VKRs), belonging to the RTKs (164). Initially characterised in schistosomes, an additional VKR was afterwards identified in insects, exhibiting several identical VKR domain compositions (165), thereby establishing them as invertebrate-specific insulin-like receptors which are absent in mammals (166–168).

### 1.3.4 PKs in *F. hepatica* and knowledge gaps

To date, only few studies investigated PKs as drug target candidates in *F. hepatica*. Previous work of our lab aimed at steering the drug discovery research for *F. hepatica* towards PKs by investigating the effects of the abelson tyrosine kinase 1 (ABL1) inhibitor imatinib (Gleevec®) and the PLK1 inhibitor BI2506 *in vitro* against adult and immature flukes (169). They demonstrated, utilising matrix-assisted laser desorption/ionization (MALDI) and mass spectrometry imaging (MSI), the absorption route of the ABL1 inhibitor imatinib, predominantly

via oral ingestion by the fluke. The accumulation of imatinib induced abnormalities in the tegument and reproductive organs, leading to interruptions in egg production and fluke mortality *in vitro* (169). Moreover, they demonstrated the effects of BI2536, which diminished the viability of 4-week-old immature flukes (169). Subsequently, McCusker and colleagues further characterised PLK1 through gene silencing (RNAi) in juvenile flukes and demonstrated a rapid stunting of fluke growth and proliferation of neoblast cells (170).

Recently, Gramberg and colleagues from our research group identified PKs with preferential expression in certain tissues by applying spatial transcriptomics. PKCβ was expressed in the tegument of adult flukes and treatment with the PKCβ inhibitor ruboxistaurin had lethal effects *in vitro* (171). This finding establishes a link for PKCβ as a druggable target essential for the survival of the liver fluke.

Although there has been recent progress in comprehending certain functions of PKs in *Fasciola*, substantial challenges persist in our knowledge, resulting in a considerable gap that necessitates extensive effort to address. The critical challenges are as follows:

(a) The absence of a kinome for *F. hepatica* hinders comprehensive research on PKs in this parasite. As kinome analysis would facilitate the prioritisation of proteins associated with lethal phenotypes of etiological agents (such as the liver fluke) for target selection upon inhibition (172). (b) The connection between TCBZ resistance and PKs, such as MAPKs, suggests a potential role in TCBZ resistance. The specific phosphorylation targets associated with this resistance remain unidentified. The precise kinases that activate the drug efflux pumps remain unknown. A recent genomics study of *F. hepatica*, conducted by Chio and colleagues, has established a foundation for future research on the correlation between resistance-associated genes in the EGFR-PI3K-mTOR-S6K signalling pathway, microtubule function, and the survival of the fluke following TCBZ exposure (79). (c) The absence of experimentally resolved crystal structures of PKs necessitates that current drug-designing strategies rely heavily on homology modelling of these structures, which poses a risk of host toxicity due to the high conservation of kinase active sites.

### 1.3.5 Function of PIM kinase

The proviral integration site for murine leukaemia virus (PIM) kinases are an example of a PK family not yet well studies in parasitic flatworms including *F. hepatica*. PIM kinases belong to the CAMK PK group and were initially recognised in the 1980s as potent oncogenes in mouse cells, phosphorylating serine and threonine residues (173). The PIM kinase family constitutes three genes: PIM1, PIM2, and PIM3, which exhibit over 60% sequence similarity among themselves (174). All PIM kinases are overexpressed in various malignancies, including prostate cancer, myeloma, leukaemia, non-Hodgkin lymphoma, and breast cancer (175). PIM

kinases have emerged as a focal point in cancer drug research, being extensively used to reduce glycolysis, increase T cell longevity, and regulate tumour processes (176,177).

Human PIM kinases exhibit a distinctive characteristic: they possess shorter amino acid sequences at both the N-terminal and the C-terminal regions, which are external to the kinase domain and lack regulatory domains within their protein structures (178). Nearly all the kinases and phosphatases activate and deactivate one another via phosphorylation and dephosphorylation; however, PIM kinases are hypothesised to be constitutively active (179,180). PIM kinases are regulated through translational, transcriptional, post-transcriptional, and proteasomal degradation (181).

PIM kinases are mainly attributed to the cell cycle (182) and have also been reported to modulate immune microenvironments and regulate immune cells (183). The initial evidence of PIM1 activity in cellular progression was identified in 1999 when PIM1 phosphorylated the cell-division cycle 25A (Cdc25A) phosphatase. The G1/S phase of the cell cycle is regulated by Cdc25A, and elevated expression of Cdc25A facilitates the transition from G1 to S phase (184). The G1/S phase inhibitor p21 was found to be phosphorylated by PIM1, leading to the inhibition of cyclin kinase, thereby confirming a PIM1 role in regulating cell apoptosis (185). PIM1 also affects the M-phase of the cell cycle through the phosphorylation of nuclear mitotic apoptosis protein (NuMA) (186). Similarly, a rapid transition to mitosis from the G2 phase was reported when PIM1 inactivates Cdc twenty-five-associated kinase 1 (C-TAK1) and activates Cdc25C phosphatase, with PIM kinase functioning as a regulation factor (187). PIM1 also negatively regulates Bcl-2-associated agonist of cell death (BAD) protein, indicating that PIM1 affects cell apoptosis (188).

In addition to cell cycle regulation, PIM1 has been reported to be regulated by the Janus kinase/Signal Transducer and Activator of Transcription (JAK/STAT) pathway (189). The initiation of this pathway occurs through interleukins, which subsequently transduce the JAK signal to phosphorylate STATs, thereby enhancing the expression level of PIM1 by binding to the promoter gene (189). Following the reduction of PIM1 expression through the feedback mechanism, JAK activity reduces due to the phosphorylation of the SOCS protein, subsequently blocking STAT activation (190).

All the metabolic pathways related to PIM1 can also be derived from the KEGG orthology of PIM kinase (K04702) for the JAK/STAT pathway in cancer, specifically for the anti-apoptosis process (map04630), as well as for the pathways in cancer (map05200) (191,192). The pathways are depicted in the supplementary section of this thesis in supplementary figures 6.1 and 6.2, respectively.

SGI-1776 is a pan-PIM kinase ATP-competitive inhibitor and was first introduced as an anticancer drug for non-Hodgkin's lymphoma, prostate cancer, and leukaemia (193,194). The $IC_{50}$ value of SGI-1776 against human PIM1, PIM2, and PIM3 was found to be 7, 363, and 69 nM, respectively (195). Chen and colleagues reported that this inhibitor targets not only human PIM kinases but also FLT-3 at 44 nM and haspin at 34 nM (195). CX-6258 is a second-generation pan-PIM kinase ATP-competitive inhibitor, initially identified by Haddach and colleagues (196). The $IC_{50}$ value of CX-6258 against human PIM1, PIM2, and PIM3 was found to be 5, 25, and 16 nM, respectively (196). This inhibitor exhibited modest activity against FLT3 at 134 nM (197) and against haspin at 10 nM (198). The current clinical trial status for both the pan-PIM inhibitors (SGI-1776 and CX-6258) can be found in the supplementary table 6.11 Of this thesis. The 2D structures of SGI-1776 and CX-6258 can be found in the supplementary table 6.8 of this thesis.

Recently, PIM kinases have been established as crucial drug target in cestodes, whereas their therapeutic potential in parasitic flukes remains completely unstudied. No studies have yet characterised this PK in the common liver fluke (*F. hepatica*), indicating a substantial deficiency in the molecular research of liver flukes.

## 1.4 Aim of this research

Fasciolosis is a globally prevalent zoonotic NTD, infecting both humans and important veterinary animals alike. Benzimidazoles are utilised in the treatment of fasciolosis, with TCBZ regarded as the gold standard due to its efficacy in targeting flukes during their early migratory phase. While TCBZ is exceptionally effective against the premature flukes, mass drug administration (MSA) has led to the prevalent emergence of TCBZ resistance (50). Therefore, it necessitates uncovering new control approaches and drugs, especially due to the unavailability of efficient vaccines.

According to the hypothesis initially proposed by Dissous and Grevelding (144), repurposing PK inhibitors from human cancer can be used for the treatment of helminthic infection. This new strategy might potentially be a new avenue for discovering druggable interventions in combating fasciolosis, but to target PKs, first we need to identify how many PKs do exist in *F. hepatica* and which of them can be pursued as druggable targets. Therefore, the subsequent objectives were laid out for this work:

1. Elucidating the kinome of *F. hepatica* through a refined genomic-bioinformatic pipeline.
2. Conduct kinome-wide comparisons among closely related parasitic flatworm species and the human host.
3. Identify and report *in vitro* inhibitory data for selected commercially available small-molecule PK inhibitors evaluated against the immature and adult life stages of liver flukes.
4. Homology modelling of FhPIM kinase for virtual screening of a compound library to identify additional inhibitors having fasciolicidal specificity.

# 2. Materials and Methods

## 2.1 Materials

### 2.1.1 Animal model and *F. hepatica* strain

A list of animals as well as the strain of *F. hepatica* used in this work can be found in Table 1.

**Table 1: List of animals and strains**.

| Species, Strain | Source | Identifier |
|---|---|---|
| *Rattus norvegicus*, Wistar | Janvier Labs | RjHan:WI |
| *Fasciola hepatica*, Italian strain | Ridgeway Research | https://ridgewayresearch.co.uk/parasite-diagnostics-laboratory/available-parasites/ |

### 2.1.2 Reagents, chemicals, and media supplements

A list of reagents and chemicals used in this work can be found in Table 2.

**Table 2: List of reagents and chemicals**.

| Reagent/Chemical | Supplier | # Cat. no. | Application |
|---|---|---|---|
| ABAM [10,000 units/ml penicillin, 10 mg/ml streptomycin, 25 mg/ml amphotericin B] | c.c.pro GmbH | 2-18-M | *In vitro* culture |
| Chicken serum | Thermo Fisher Scientific | 16110082 | *In vitro* culture and oral infection |
| Diethyl pyrocarbonate (DEPC) | Carl Roth® | P030.1 | Buffer preparation |
| Dimethyl sulfoxide (DMSO) | Sigma-Aldrich® | D4540 | Solvent for small molecule inhibitors |
| Disodium hydrogen phosphate ($Na_2HPO_4$) | Carl Roth® | P030.1 | Buffer preparation |
| Double distilled $H_2O$ | Carl Roth® | 3478.1 | Buffer preparation |
| Ethanol | Carl Roth® | 9065.4 | Solvent |
| Potassium chloride (KCl) | Carl Roth® | P017.2 | Buffer preparation |
| Potassium dihydrogen phosphate ($KH_2PO_4$) | Carl Roth® | 3904.1 | Buffer preparation |

| | | | |
|---|---|---|---|
| RPMI 1640 medium [1x] | GIBCO™, Thermo Fisher Scientific | 11835-030 | Flukes *in vitro* culture |
| Sodium chloride (NaCl) | Carl Roth® | 6885.1 | Buffer preparation |
| TRIS | Carl Roth® | 4855.2 | Buffer preparation |

### 2.1.3 Buffers and solutions

A list of buffers and solutions used in this work, which were stored at room temperature unless otherwise stated, can be found in Table 3.

**Table 3: List of buffers and solutions**.

| Buffer | Ingredients | Application |
|---|---|---|
| DEPC $H_2O$ | 0.1% (v/v) DEPC in $ddH_2O$ | Multipurpose buffer |
| PBS (10x) | 1.37 mM NaCl<br>27 mM KCl<br>65 mM $Na_2HPO_4$<br>15 mM $KH_2PO_4$<br>In $dH_2O$<br>pH = 7.0 - 7.2 | Multipurpose buffer |
| Saline solution | 0.9% (w/v) NaCl with 1% (v/v) ABAM in $ddH_2O$ | Immature fluke harvest |
| Sugar water | 1 g saccharose in 20 ml $dH_2O$ | Oral infection |
| Fluke *in vitro* culture medium | RPMI 1640<br>5% chicken serum (**not** heat-inactivated)<br>1% ABAM | Flukes *in vitro* culture |

### 2.1.4 Commercially available small-molecule inhibitors

Commercially available small-molecule inhibitors used in this work were first dissolved in DMSO (as recommended by the manufacturer to create a stock of 50 mM) and were stored at -80°C for long-term storage (one year). Prior to the initiation of an inhibitor treatment experiment, the inhibitors were stored at -20°C, and upon the conclusion of the experiment, they were returned to -80°C for storage. The list of these inhibitors can be found in Table 4.

**Table 4: List of small-molecule inhibitors available commercially**.

| Inhibitor | Supplier | # Cat. no. | Molecular weight (Da) |
|---|---|---|---|
| vandetanib (ZD6474) | Selleck Chemicals | S1046 | 475.35 |
| ruboxistaurin (LY333531) HCl | Selleck Chemicals | S7663 | 505.01 |
| tyrosine kinase-IN-1 (XL999) | MedChemExpress® | HY-100315 | 445.53 |
| foretinib (XL880) | Selleck Chemicals | S1111 | 632.65 |
| SGI-1776 | Cayman Chemical Company | Cay16423-1 | 405.42 |
| CX-6258 HCl | Cayman Chemical Company | Cay16245-1 | 498.40 |
| triclabendazole (TCBZ) | Sigma-Aldrich® | 32802 | 359.66 |

### 2.1.5 Software and online databases

List of software and online databases used in this thesis can be found in Table 5.

**Table 5: List of software and online databases.**

| Software/Online databases | Methodology application | References | Website |
|---|---|---|---|
| AlphaFold v2 | Molecular docking | (199–201) | https://www.alphafold.ebi.ac.uk/ |
| Anaconda | Kinome generation and molecular docking | (202) | https://www.anaconda.org/ |
| AutoDock Vina v1.1.2 | Molecular docking | (203,204) | https://vina.scripps.edu/ |
| BEDTools v 2.31.1 | Kinome generation | (205) | https://bedtools.readthedocs.io/en/latest/ |
| BLAST + v2.2.24 and v2.15.0 | Kinome generation and phylogenetic tree construction | (206,207) | https://ftp.ncbi.nlm.nih.gov/blast/executables/blast+/ |

| | | | |
|---|---|---|---|
| BlastKOALA | Kinome generation | (208) | https://www.kegg.jp/blastkoala/ |
| ColabFold v1.5.5 | Molecular docking | (209) | https://colab.research.google.com/github/sokrypton/ColabFold/blob/main/AlphaFold2.ipynb |
| EMBL-Clustal Omega | Kinome generation and molecular docking | (210) | https://www.ebi.ac.uk/jdispatcher/msa/clustalo |
| EMBOSS needle v6.6.0.0 | Kinome generation | (210,211) | https://emboss.sourceforge.net/apps/cvs/emboss/apps/needle.html https://ssbio.readthedocs.io/en/latest/instructions/emboss.html# |
| Exonerate v2.4.0 | Kinome generation | (212) | https://www.anaconda.org/bioconda/exonerate |
| Figtree v1.4.4 | Kinome generation and phylogenetic tree construction | (213) | https://tree.bio.ed.ac.uk/software/figtree/ |
| GFFRead v0.12.7 | Kinome generation | (214) | https://anaconda.org/bioconda/gffread |
| HMMER v2.3.2 and v3.3.2 | Kinome generation | (215,216) | https://www.ebi.ac.uk/Tools/hmmer/home |
| Inkscape v1.4 | Figure compilation | (25) | https://www.inkscape.org |
| InterProScan v5.63-95.0 | Kinome generation | (217) | https://www.ebi.ac.uk/interpro/ |
| Kinnanote v1.0 | Kinome generation | (218) | https://sourceforge.net/projects/kinannote/ |

| | | | |
|---|---|---|---|
| MAFFT v7.520 | Kinome generation | (219) | https://mafft.cbrc.jp/alignment/software/ |
| MEGA v11 | Phylogenetic tree construction | (220) | https://www.megasoftware.net/ |
| MrBayes v3.2.7a | Phylogenetic tree construction | (221) | https://nbisweden.github.io/MrBayes/ |
| MUSCLE v5 | Phylogenetic tree construction | (222,223) | https://www.drive5.com/muscle/ |
| NCBI | protein sequence database | (9) | https://www.ncbi.nlm.nih.gov/ |
| Open Babel v3.1.1 | Molecular docking | (224) | https://openbabel.org/index.html |
| OrthoFinder v3 | Kinome generation | (225) | https://github.com/davidemms/OrthoFinder |
| OrthoMCL v2.0.9 | Kinome generation | (226,227) | https://orthomcl.org/orthomcl/app |
| PANTHER v16 | Kinome generation | (228) | https://pantherdb.org/ |
| pBLAT v2.5.1 | Kinome generation | (229) | https://anaconda.org/bioconda/pblat |
| Pfam v63.0 | Kinome generation | (230) | https://www.ebi.ac.uk/interpro/download/pfam/ |
| PyMOL v3.1 | Molecular docking | (231) | https://www.pymol.org/ |
| Python v2.7 and v3 | Kinome generation and molecular docking | (232) | https://www.python.org/ |
| R v4.3.4 | Kinome generation | (233) | https://www.r-project.org/ |
| RCSB PDB | Molecular docking | (234) | https://www.rcsb.org/ |
| Smart v9.0 | Kinome generation | (235) | https://smart.embl.de/ |

| | | | |
|---|---|---|---|
| SmartChemist webserver | Molecular docking | (236) | https://chemist.smarts.plus/ |
| SUPERFAMILY v2 | Kinome generation | (237) | https://www.supfam.org/ |
| SWISS-MODEL | Molecular docking | (238) | https://swissmodel.expasy.org/ |
| Tidyverse (R package) | Kinome generation | (239) | https://tidyverse.org/ |
| TLDR webserver | Molecular docking | (240) | https://tldr.docking.org/ |
| Uniprot | Kinome generation, molecular docking, and protein sequence database | (241,242) | https://www.uniprot.org/ |
| USCF ChimeraX v1.8 | Molecular docking | (243,244) | https://www.rbvi.ucsf.edu/chimerax/ |
| WormBase Parasite vWBP18-19 | Kinome generation and protein sequence database | (245) | https://www.parasite.wormbase.org/index.html |

### 2.1.6 Laboratory equipment

List of laboratory equipment used in this works can be found in Table 6.

**Table 6: List of laboratory equipment**.

| Equipment | Manufacturer | Application |
|---|---|---|
| DFC3000G | Leica | B&W camera for DMIL |
| DMC2900 | Leica | Colour camera for DMIL, TL3000 Ergo and DMi8 |
| HERACELL VIOS 160i CO2 incubator | Thermo Fisher Scientific | Flukes *in vitro* culture |
| M 125 C | Leica | Stereo microscope for fluke scoring & imaging |
| TL3000 Ergo | Leica | Light transmitted base of microscope (light plate) for fluke scoring & imaging |

## 2.2 Methods

### 2.2.1 Ethical statement

Animal experiments with rats (*Rattus norvegicus*) as model hosts were performed, obeying the EU-directive 2010/63/EU on the protection of animals used for scientific purposes and the German Animal Welfare Act “Tierschutzgesetz”. To cultivate and harvest liver flukes from rats, the Regional Council (Regierungspräsidium) Giessen approved the infection experiments (V54-19c20 15 h 02 GI 18/10 Nr. V 6/2023).

### 2.2.2 Maintenance, harvest, and *in vitro* culture of *F. hepatica*

#### 2.2.2.1 Infection of rats with *F. hepatica*

One week before the initiation of the oral infection procedure, the rats were trained with freshly prepared sugar water with a 200 µl pipette tip to get them adapted to the infection procedure. Metacercariae of an Italian *F. hepatica* strain were obtained from Ridgeway Research (UK), and the day before the oral infection, they were collected in desired numbers in a microcentrifuge tube (eppi). The procedure to collect them is as follows: Metacercariae were obtained on plastic sheets from Ridgeway Research (UK) and were kept in sterile refrigerated conditions. Firstly, one sheet containing metacercariae was unrolled in a petri dish containing autoclaved $dH_2O$ using plastic tweezers. Metacercariae were scraped (under microscopic conditions) from the plastic sheet using a scalpel or 100 µl pipette tip. A pipette tip lined with chicken serum (CS) was used to collect the desired number of metacercariae (20 or 25) and to prevent them from sticking to the tip (the reason for lining the pipette tip with CS). After the collection of the metacercariae, firstly, the sheet was rolled back and placed back in the sterile refrigerated conditions; later, all the used equipment was subjected to bleach treatment for sterilising them before autoclaving them.

The oral infection was conducted on Wistar rats (RjHan: WI, Janvier, France) at an age of four to five weeks with 20 (adult flukes) or 25 (immature flukes) metacercariae. The procedure for oral infection is similar to sugar feeding with few extra steps. Firstly, the supernatant of the collected metacercariae was decanted, and then a fresh pipette tip was lined with CS (reason stated above). Subsequently, freshly prepared sugar water was carefully added to the eppi containing metacercariae, which was later fed dropwise directly into the mouth of the rat. After feeding the suspension to the rat, the eppi was flushed with sugar water and was fed once again to the rat. A new pipette tip was used for each rat to prevent accidental overinfection. After four weeks (for harvesting immature flukes) or twelve weeks (for harvesting adult flukes) post infection (p.i.), rats were subjected to cervical dislocation after $CO_2$ euthanasia. The collection conditions of flukes are stated in the next section (2.2.2.2.).

#### 2.2.2.2 Harvest of immature and adult flukes

Immature flukes were collected after 4 weeks p.i. via the chopped livers of the rats, whereas adult flukes were collected after 12 weeks p.i. from the bile ducts of the rats. The collected flukes were cultured in RPMI-1640 medium containing 1% ABAM solution and 5% CS for one hour to regurgitate their gut contents, followed by overnight culture in RPMI-1640 medium containing 1% ABAM and 5% CS. **Please note** that the CS used for the preparation of the fluke *in vitro* culture medium was **not** heat-inactivated. Flukes were either used to test small-molecule inhibitors or stored in protect buffer at -80°C until RNA extraction.

#### 2.2.2.3 *In* vitro culture of immature flukes

Immature flukes were cultured in a 48-well plate (one-two flukes per well) with 650 µl of RPMI-1640 medium containing 1% ABAM and 5% CS at 37°C in 5% $CO_2$. Before the start of an experiment, medium was always prepared freshly under sterile conditions and then stored at 4°C. If the medium was not used within three to five days, then fresh ABAM was added to the medium. **Please note** that the CS used for the preparation of the fluke *in vitro* culture medium was **not** heat-inactivated.

Conditions for small-molecule inhibitor evaluation: First, the medium was added to the plate under a laminar flow hood, which was incubated at 37°C for one hour to warm the medium. Before the start of the fluke relocation, all the equipment, light plate and workbench were sterilised with 70% ethanol to avoid the risk of contamination. Then, flukes were relocated from their overnight culture plate to the warmed plate containing the medium; this procedure was done with the help of spring steel tweezers. Fresh medium was replenished to a new plate every 24 h, and after the plate was warmed to 37°C, then the flukes were transferred to the new plate containing the medium. A motility score was assigned to each worm prior to transferring the flukes to a new plate with fresh medium. Scores were recorded for up to 72 h after every 24 h, after which the worms were subjected to photography and/or videography to record their motility at the end of the experiment and later were stored in RNA protect buffer at -80°C. Flukes were scored with a microscope (Leica M125 C) at 2x magnification and photography and/or videography was conducted with the same microscope at 4x magnification.

#### *2.2.2.4 In* vitro culture of adult flukes

Adult flukes were cultured in 12-well plate (one to two flukes per well) with 3 ml of RPMI-1640 medium containing 1% ABAM and 5% CS, at 37°C in 5% $CO_2$. **Please note** that the CS used for the preparation of the fluke *in vitro* culture medium was **not** heat-inactivated. The conditions for handling the flukes were the same as for immature flukes specified in the above section (2.2.2.3).

#### 2.2.2.5 Scoring grades for the flukes

The scoring of the flukes was adapted from Morawietz and colleagues (169). Scoring grades were as follows: 0 (no movement even after mechanical stimulation with tweezers or dead flukes), 1 (minimal or irregular movement), 2 (slightly reduced motility than normal), and 3 (normal motility).

#### 2.2.2.6 *In vitro* small-molecule inhibitor treatment on immature and adult flukes

The small-molecule inhibitors specified in table 4 were evaluated for their anthelminthic activities on immature and adult flukes. Dimethyl sulfoxide (DMSO) was used to prepare stock solutions of 50 mM. At different concentrations (25 µM, 50 µM, and 100 µM), the small-molecule inhibitors were used to treat flukes. As a negative control, DMSO was used in the same volume as the highest concentration of a small-molecule PK inhibitor, specifically 0.2% for immature flukes and 0.3% for adult flukes. The final dilution of the DMSO in the fluke *in vitro* culture medium was achieved by initially vortexing the DMSO or the small-molecule inhibitor in an eppi with the culture medium, which was subsequently transferred to the 12- or 48-well plate. The *in vitro* handling conditions for immature and adult flukes, along with their scoring grades, are specified in sections 2.2.2.3, 2.2.2.4, and 2.2.2.5 respectively.

### 2.2.3 Assembly of the *F. hepatica* kinome

#### 2.2.3.1 Identification, prediction, and curation of the kinome

A bioinformatic pipeline developed for the generation of *Schistosoma haematobium* kinome (135) was adapted and refined (Fig. 2.1) to identify, predict, and curate PKs in the proteome of *F. hepatica* (PRJNA179522, v2021-12-WormBase) published at WormBase Parasite vWBP18 (245). Initially, I employed Kinannote (218) using the metazoan (-m) option on the genome using the usage command line specified in the usage section of the program, which generated a draft kinome containing PKs classified into groups, families, and sub-families.

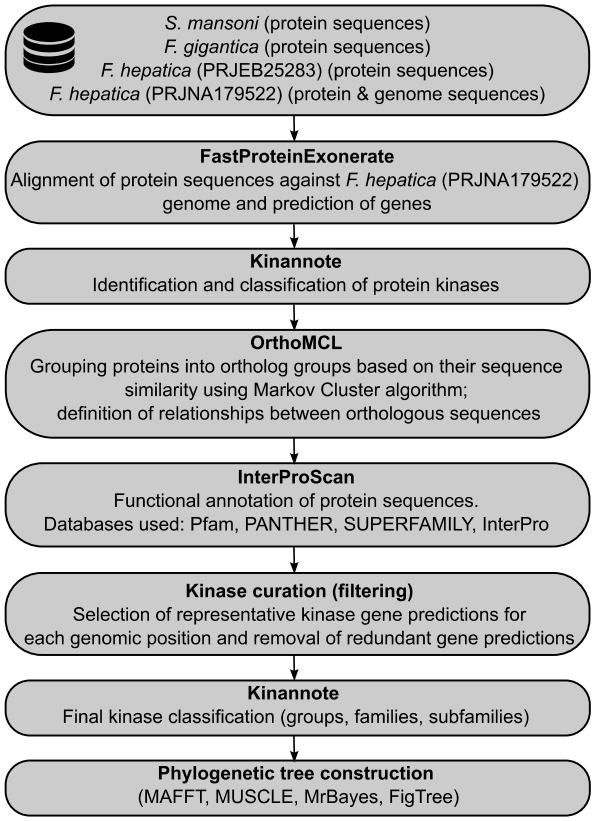


**Figure 2.1: Modified bioinformatic pipeline for the kinome generation of *F. hepatica***. This figure presents a detailed overview of the genomic-bioinformatic pipeline employed for the generation of the kinome of *F. hepatica*. This figure is adapted and modified from Ajmera et al., 2026 (246).

Subsequently, to further curate the kinome, I employed the FastProteinExonerate wrapper script (https://github.com/stroehleina/FastProteinExonerate) alongside the inferred proteomes of closely related species to *F. hepatica*, such as *Schistosoma mansoni* (PRJEA36577), *Fasciola gigantica* (PRJNA230515), and an additional proteome of *F. hepatica* (PRJEB25283), which all were published at WormBase vWBPS18. This step augmented the existing gene models in our query genome of *F. hepatica* (PRJNA179522). FastProteinExonerate necessitates the installation of pBLAT (229), BEDTools (205), Exonerate (212), and GFFRead (214) as prerequisites. This supplementary procedure ensures the alignment of protein sequences to the genome scaffolds of *F. hepatica* (PRJNA179522) and predicts genes in the matching regions as well as addresses the gaps in the fragmented genes.

Subsequently, I employed OrthoMCL (226,227) to define the orthologous relationship among the protein sequences of the four previously inferred proteomes of species closely related to *F. hepatica* and to provide orthologous grouping. OrthoMCL ensured efficient and accurate functional annotation of orthologs by facilitating scalable multi-species analysis, utilising the BLAST (206) and the Markov clustering algorithm (247). MySQL installation is a prerequisite for OrthoMCL to perform local clustering of the protein sequences.

Additionally, I provided functional annotations using InterProScan v5.63-95.0 (217), which gave insights about PK domains using Pfam v63.0 (230), PANTHER v16 (228), and SUPERFAMILY v2 (237) databases.

With the aggregated data from OrthoMCL and InterProScan, I subsequently filtered the dataset using the Tidyverse (239) package in R v4.3.4 (233). The data filtering was carried out to remove the redundancies and overlapping genes in the dataset. The conditions for the data filtering can be found in sections 2.2.3.1.1 and 2.2.3.1.2. This was carried out by subsetting the data by filtering the database domain ID/ accession numbers for Pfam “PF00069 - Protein kinase domain” and “PF07714 - Protein tyrosine and serine/threonine kinase”, for SUPERFAMILY “SSF56112 - Protein kinase-like (PK-like)”, and for InterProScan “IPR011009 - Protein kinase-like domain superfamily”, “IPR000719 - Protein kinase domain”, and “IPR001245 - Serine-threonine/tyrosine-protein kinase, catalytic domain”.

Then, I further reduced the redundancies and overlapping genes using the “FOR” nested loop with “IF” conditions (the code used for filtering loops are specified in the supplementary code section of this thesis 6.3.1 and 6.3.2). The nested loop iterates to reduce the redundancies by selecting the distinct unique sequence identifier for a single gene locus using the Tidyverse package in R v4.3.4. The new predicted genes were given a new numeric identifier with the prefix “FhPK_00” in the final dataset and can be found in the supplementary table 6.12 of this thesis and the complete kinome information is accessible in the online version of supplementary data file 1 in Ajmera et al. 2026 (246).

#### 2.2.3.1.1 Nested loop iteration conditions for reducing the redundancies

“FOR” nested loop iteration was built on four “IF” conditions, which are as follows:

1. Sequence should be on the same contig.
2. Sequence should be on the same strand.
3. The start position of the sequence should be smaller or equal to the current start.
4. The end position of the sequence should be larger or equal to the current end.

Code for the nested loop iteration with “IF” conditions for reducing the redundancies in R v4.3.4 (233) is stated in supplementary code section 6.3.1 of this thesis.

#### 2.2.3.1.2 Nested loop iteration conditions for reducing the overlapping genes

“FOR” nested loop iteration was built on three “IF” conditions, which are as follows:

1. Sequence should have the longest gene length on the genomic location.
2. Sequence should have the longest protein sequence length on the genomic location.
3. Sequence should have the highest overlapping ratio.

Code for the nested loop iteration with “IF” conditions for reducing the overlapping genes in R v4.3.4 (233) is stated in supplementary code section 6.3.2 of this thesis.

#### 2.2.3.2 Functional annotation via KEGG pathway

Upon the complete procurement of PKs in *F. hepatica*, they were further subjected to functional annotation using the KEGG metabolic pathway via the BlastKOALA (208) webserver with its default setting and selecting the eukaryotes gene dataset.

#### 2.2.3.3 Kinome comparison

I further collated the kinome of *F. hepatica* with accessible kinomes of *S. mansoni* (136,137), *S. haematobium* (135) and *H. sapiens* (109,121). Initially, the PK domains of the sequences were needed to be identified, for which I developed a Hidden Markov Model (HMM) using the webserver HMMER v3.3.2 (215,216) utilising Pfam-A database (230) with “PF00069 - protein kinase domain” and “PF07714 - protein tyrosine and serine/threonine kinase”. The HMM was employed to accurately identify and classify PKs among the selected species by detecting conserved sequence motifs within PK domains. Profile HMM encompass position-specific residue probabilities and insertion/deletion patterns, enabling the identification of both canonical and divergent PK sequences. This method guaranteed reliable and consistent kinome annotation for interspecies comparative analysis. Moreover, protein sequences containing fragmented domains, specifically those comprising of two or more domains each shorter than 140 amino acids, were consolidated. Furthermore, sequences were grouped utilising OrthoFinder (225). OrthoFinder clusters PK sequences into orthologues groups based on sequence similarity and phylogenetic relationships, facilitating the identification of conserved and lineage-specific PK families across the selected species. It employs gene tree inference to differentiate orthologs from paralogs, yielding a more evolutionarily precise classification of PKs. This enables comprehensive comparative analysis of kinome expansion, contraction, and functional diversification. Subsequently, I conducted comprehensive all-vs-all groupwise global alignment of the PK sequences utilising EMBOSS needle v6.6.0.0 (210,211). Later, only the best alignment representation (based on the percent identity between the query and target sequences) was selected using a self-written script in R v4.3.4 (233). Atypical PK exhibit minimal sequence similarity to the HMM protein kinase profiles (123); therefore, I performed the comparison utilising solely the full-length sequences via local BLAST (206). All relevant information regarding the kinome comparison is available in the online version of supplementary data file 1 in Ajmera et al. 2026 (246).

## 2.2.4 Phylogenetic tree construction

### 2.2.4.1 Phylogenetic tree construction for PK groups

I constructed individual phylogenetic trees for classified PK groups of *F. hepatica* and the orthologous kinases from the already available kinome of *S. mansoni* (136,137) excluding the unclassified genes. For the construction of the trees, I first aligned the protein sequences of an individual PK group with MAFFT v7.520 (219) utilising the most accurate alignment option (L-INS-i; parameters *-local -maxirate* 1000), which provided a multi-sequence alignment (MSA). Then, I further refined the MSA output from MAFFT, utilising the refine option (*-refine*) in MUSCLE v5 (222,223) to boost the homologous characters in the MSA. Later, these refined alignments were converted to a NEXUS format file using MEGA v11 (220). Then these NEXUS format files were subjected to Bayesian Inference (BI) analysis using MrBayes v3.2.7a (221) to estimate evolutionary relationships and assess statistical support for the inferred phylogenetic tree clades. The BI analysis utilised a fixed LG (Le and Gascuel) model, incorporating empirical amino acid sequence frequencies and rate heterogeneity modelled through an invariant sites plus gamma distribution with four discrete groups. Markov chain Monte Carlo (MCMC) sampling was conducted for 1,000,000 generations using eight chains, with samples taken every 100 generations. 25% of the samples were discarded as burn-in to ensure that only samples from the stationary phase of the Markov chain were utilised. At the start of the MCMC run (the core BI analysis command), the chain initiates from a random initial tree and parameter values, which are generally distinct from the high-probability areas of the posterior distribution. In this initial phase, the probability and parameter values shift as the chain progresses towards convergence. Additionally, the posterior probabilities for each clade were calculated as the ratio of post-burn-in sampled trees that contained that clade. This is how Bayes' theorem suggests the probability of that clade is based on the data and model. The algorithm of MrBayes, with the help of majority-rule consensus, selects only the best tree representation from the remaining trees, typically by utilising the **sumt** command. The constructed phylogenetic trees were aesthetically visualised and illustrated in the program Figtree v1.4.4 (213). The high-definition representations of all the phylogenetic trees, along with their branched nodal support values, are available in the supplementary figure section of this thesis (supplementary figures 6.6 to 6.15) and in the online version of supplementary data file 2 in Ajmera et al. 2026 (246).

### 2.2.4.2 Phylogenetic tree construction for homologues PIM kinases

Initially, I identified homologues of PIM kinase between *F. hepatica* (D915_000232) and various selected species using BLAST (206,207), which I obtained from WormBase Parasite (245), NCBI (9) and Uniprot (241,242). Subsequently, I constructed a phylogenetic tree for all the procured homologues of PIM kinase sequences from the selected species and employed

*F. hepatica* BRSK (D915_001295) as an outgroup sequence. The procedure for construction and visualisation of the tree was identical to 2.2.4.1.

### 2.2.5 Molecular docking calculations

For one selected PK, the *Fasciola* PIM kinase FhPIM (D915_000232), I followed the aim to identify new small-molecule inhibitors by a virtual screening approach. The complete molecular docking calculations were conducted on a Simple Virtual Machine (SimpleVM) cloud environment (High Performance Cluster) supplemented by the de.NBI (German Network for Bioinformatics Infrastructure). The molecular docking calculations were performed in the Anaconda environment (202) with Python v2.7 and v3 (232). The complete workflow of the molecular docking calculations can be found in Fig. 2.2.

The main steps involved in molecular docking calculations studies are as follows:

1. The generation and preparation of the protein structure (FhPIM kinase)
2. The preparation of the ligands (the MCCC compound library)
3. Selection of the docking parameters, i.e., the location and the size of the binding box and the intensity of the docking run
4. The filtration, energy minimisation, and preparation of the top-ranked docked ligands were performed for different software-readable formats
5. Finally, the visualisation and evaluation of the docked ligands in PyMOL v3.1

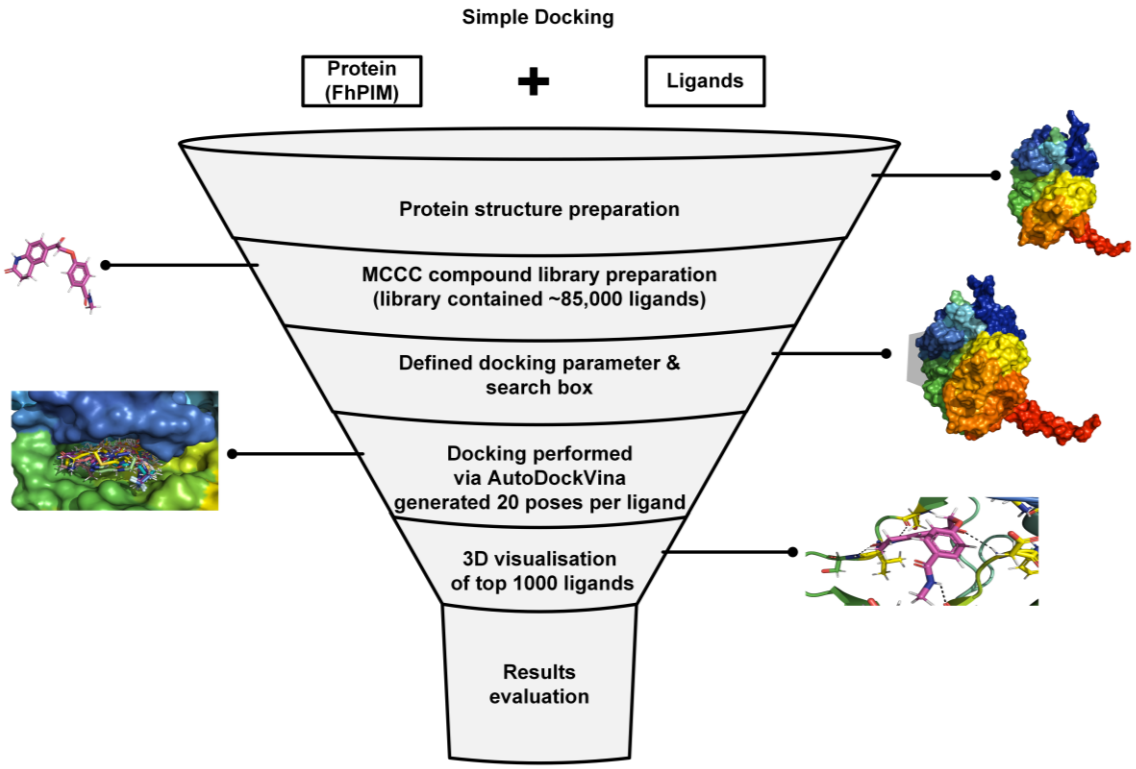


**Figure 2.2: The workflow of the molecular docking and virtual screening of MCCC library**. A simple type of molecular docking was performed, utilising the binding pocket of a protein (FhPIM kinase) to dock ligands from the MCCC compound library for target-based drug discovery. This figure provides a concise overview on the different processes involved in the comprehensive molecular docking calculation procedure.

### 2.2.5.1 Protein structure preparation for docking calculations

The protein structure is essential for executing computer-simulated docking algorithms, which necessitate a chemically precise model to predict how a ligand will dock in the binding pocket of the protein. The predicted 3D protein structure often lacks hydrogen bonds and may include crystallisation salts or unwanted water molecules at the binding site. If these issues are not addressed during the protein preparation phase, then the docking engine will misinterpret the electrostatics or steric boundaries, leading to inaccurate results. The critical phase in the preparation of a protein structure encompasses the elimination of water molecules, the incorporation of hydrogen (to establish hydrogen bond networks), the adjustment of the protonation state of the residues (typically at 7.4 pH), the restoration of absent atoms (by filling in missing side chains or small loops through homology modelling), and energy minimisation (to rectify unnatural internal clashes or strained bonds formed during the protein prediction step).

Due to the absence of an experimentally determined 3D structure for FhPIM (D915_000232) kinase, I utilised the protein sequence of FhPIM kinase in ColabFold (209) to predict its 3D structure, employing a num_relaxed value of 1. This procedure entailed the energy

minimisation of the highest-ranked generated model, utilising the AMBER force field for relaxation to rectify stereochemical violation and structural clashing in the predicted protein structure (248). Subsequently, the predicted structure was further refined by SWISS-MODEL (238), employing human PIM1 kinase as the template model (RCSB PDB ID: 4JX7) (Fig. 2.3.A), which exhibited a 49.4% sequence identity upon a multiple sequence alignment between the Hs and Fh PIM kinase domains (246). This refinement adjusted the conformation of Phe59 in the predicted structure of FhPIM to precisely align with the conformation of Phe54 observed in human PIM1. Additionally, I employed a different 3D structure for the second molecular docking calculation run, which was predicted from the AlphaFold database (199–201) (Uniprot: A0A4E0YG3; AlphaFold database: AF-A0A4E0RYG3-F1-v6). The second predicted structure was further refined using the TLDR webserver (240), which also changed the conformation of Phe59. This refinement yielded a slightly improved binding conformation for staurosporine, the small-molecule inhibitor employed to analyse the binding pocket of FhPIM, as staurosporine has been extensively investigated within the binding pocket of human PIM1 (RCSB PDB ID: 1YHS) (249–251).

**Please note** that there were two rounds of molecular docking performed. The first round was performed using the AlphaFold generated model with num_relaxed value 1 which was further modified using homology modelling (SWISS-MODEL). The second round was performed by using the FhPIM model available in AlphaFold database (AF-A0A4E0RYG3-F1-v6) which was further modified using homology modelling (SWISS-MODEL) followed by TLDR webserver. Both the protein sequence of FhPIM and HsPIM1 kinase can be found in the supplementary information section 6.4 of this thesis.

Upon aligning both refined structures of FhPIM, only two primary deviations were noted in the side chains, like the conformations of residues Phe54 and Arg64 in the second model. These conformation changes were modified by the TLDR webserver and resulted in creating more space for ligand binding in the second predicted structure of the FhPIM kinase. However, the overall modified structures of both FhPIM remained symmetrical and exhibited identical conformational shifts at FhPIM Phe59; the second predicted structure, further refined through SWISS-MODEL and TLDR webserver, produced more favourable staurosporine binding conformations. Moreover, the slight structural discrepancies between the two modelled structures are limited to residues located outside the binding pocket and do not influence the binding analysis.

Subsequently, utilising USCF ChimeraX v1.8 (243,244), I selected, trimmed, and retained only the predicted 3D structures of the kinase domains of both the FhPIM (Fig. 2.3.B). Furthermore, I visually inspected the protonation states of histidine residues in the predicted structures of

FhPIM using ChimeraX v1.8. Finally, I assigned the protonation states of the histidine residues to HIE, HID, or HIP accordingly. These protonated states (HIE, HID, and HIP) refers to the presence of a proton (hydrogen) on the delta (δ) nitrogen, epsilon (ε) nitrogen, or both nitrogens in the imidazole sidechain of histidines. The receptor (3D structures of FhPIM kinase domain) was prepared for docking utilising the AutoDock Vina v1.1.2 (203,204) script (prepare_receptor.py). This script eventually prepares the 3D protein structure of FhPIM kinase for molecular docking by eliminating water molecules, non-standard ions, and existing co-crystallised ligands and subsequently converting it to pdbqt format, the sole input format recognised by the docking engine (AutoDock Vina) for its operation.

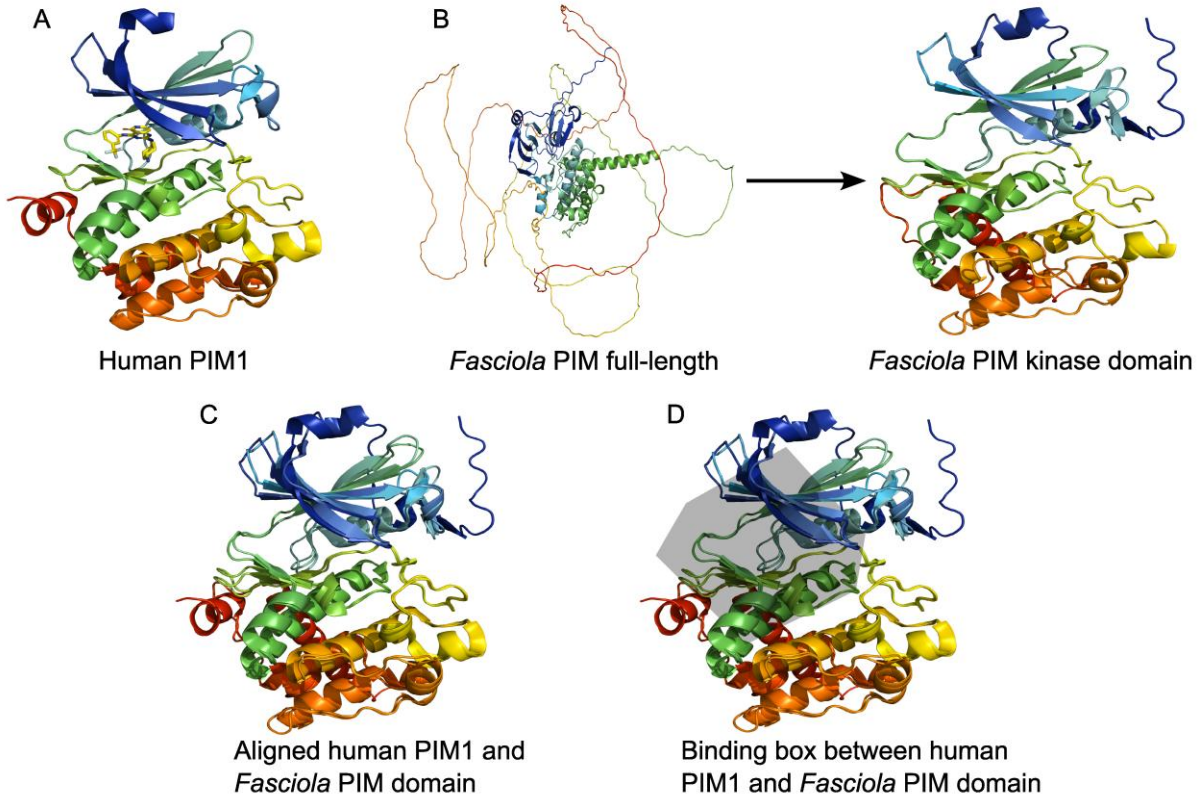


**Figure 2.3: 3D models of human PIM1 and *Fasciola* PIM kinase**. All 3D models are from N-terminus coloured in blue to the C-terminus coloured in red (labelled according to the rainbow spectrum setting in PyMOL v3.1 (231)). **(A)** The full-length 3D model of a small-molecule inhibitor (in yellow) in the binding pocket of the human PIM1 kinase obtained from the protein database (234) (RCSB ID: 4JX7). **(B)** AlphaFold generated full-length model of *Fasciola* PIM kinase (D915_000232) which is further trimmed in ChimeraX v1.8 (243,244) to retain only the kinase domain with adjusted protonation states of histidine residues. **(C)** Aligned 3D models of human PIM kinase and *Fasciola* PIM kinase domain in PyMOL v3.1 (231). **(D)** Location of the binding box between human PIM1 and *Fasciola* PIM kinase.

### 2.2.5.2 Ligand preparation for docking calculations

The Managed Chemical Compound Collection (MCCC) library from Nottingham is a specially curated diverse library for lead-likeness containing approximately 85,000 compounds, which follows Lipinski's "rule of five" (252,253). The MCCC library which was initially in 2D sdf (structure data file) format. This format was processed and converted to individual mol2 format

using Open Babel v3.1.1 (224) for the first iteration of molecular docking. This conversion resulted in individual 3D structure files that contained hydrogens and the parameters equivalent to 7.4 pH and MMFF94 force field minimisation (254). Later, for the second iteration of molecular docking calculation, the library was processed using Molecular Operating Environment (MOE) 2022 (255) platform to prevent the generation of broken molecules and incorrect protonation states of the ligands. At last, the ligand files were prepared for molecular docking calculation using the AutoDock Vina script (prepare_ligand.py). The script verifies the presence of polar hydrogens (specifically those attached to oxygen and nitrogen) in the ligand. If absent, it adds them and then converts the mol2 format file to pdbqt format, the sole input format recognised by the docking engine (AutoDock Vina) for its operation. Please note that in the first round of virtual screening, ligands prepared with the Python script and Open Babel were utilised. In the second round of virtual screening, ligands prepared from the MOE platform were utilised. The rationale for employing two distinct ligand preparation approaches was that Open Babel generated some ligands with broken molecules and unusual protonated states across different molecules, resulting in a significant number of stranded donors that could not be salvaged through water molecules. The MOE automates the 3D protonation processes to ensure that ligands possess the appropriate bond lengths, angles, and electronic characteristics necessary for precise evaluation by the docking engine.

#### 2.2.5.3 Docking parameters

To define the size and the centre coordinates of the binding box, I aligned the HsPIM1 (RCSB PDB ID: 4JX7) with a small-molecule inhibitor (2-[(trans-4-aminocyclohexyl)amino]-4-{[3-(trifluoromethyl)phenyl]amino}pyrido[4,3-d]pyrimidin-5(6H)-one commonly referred as 1N6) in the binding site against the FhPIM kinase domain in PyMOL using the align function (Fig. 2.3. C). The alignment of HsPIM1 and kinase domain of FhPIM delineated the binding box location (Fig. 2.3. D), which had a size of x = 21, y = 20, and z = 21 and the location coordinates of the binding box were x position = 20.52, y position = -38.76, and z position = -1.82. The exhaustiveness parameter was set to 32, which resulted in the generation of pdbqt files (approximately 85,000 files in total), yielding 20 conformer poses for every docked ligand.

#### 2.2.5.4 Energy minimisation of the docked ligand files

Five custom-made bash scripts (written under the guidance of Dr. Jamal Shamsara) were built in Python v3 and were utilised for energy minimisation of the ligand. The scripts and their functions can be found in Table 7.

**Table 7: List of custom scripts and their functions** which were used for the preparation of docked ligands for visual inspection.

| Scripts | Function |
|---|---|
| 1 | Converted the AutoDock Vina output results from pdbqt to sdf format |
| 2 | Extracted binding affinity energy (kcal/mol) for all the docked ligand conformers, i.e., filtered out only the best conformer pose from the 20 conformer poses for every docked ligand |
| 3 | Filtered out only the top 500 ranked compounds. This filtration step involves selecting them based on the lowest binding affinity energy and a lower root-mean-square deviation (RMSD) value |
| 4 | Converted the top 500 ranked compounds from sdf to mol2 format |
| 5 | Energy was minimised for the top 500 ranked ligands using ChimeraX v1.8, and then the individual mol2 files were concatenated into one file and prepared into a suitable file format for visual inspection in PyMOL |

Molecular docking calculations were conducted separately with both predicted structures of FhPIM, yielding in total the top 1000 compounds (500 compounds each from both first and second molecular docking iterations) for visual evaluation. The criteria for evaluating the docked ligands is explained in the next section 2.2.5.5.

#### 2.2.5.5 Visualisation and evaluation criteria for docked ligand poses

The visualisation of docked ligand poses was performed in PyMOL v3.1 (231). The evaluation criteria were taken from published guidelines (256,257). In detail the ligand poses were graded from A to D/X, which are described in Table 8. A more detailed explanation on the selection criteria of the docked ligands is also available on the wiki website of AG-Kolblab from the Institute of Pharmaceutical Chemistry at the University of Marburg (https://kolblab-wiki.pharmazie.uni-marburg.de/index.php/Compound_evaluation).

**Table 8: Evaluation criteria for docked ligands**.

| Scoring grade | Criteria |
|---|---|
| A | Absolutely no intramolecular clashes, no internal strain, and no stranded hydrogen bond donors (like nonpolar amide groups) or hydrogen bond acceptors (etheric oxygen) and must look plausible (aromatic-aromatic stacking) |
| B | No intramolecular clashes, one or fewer stranded hydrogen bond donors/acceptors with some rational expectations (can be fine-tuned with +/-) |
| C* | More than one stranded hydrogen bond donor/acceptor and charge-charge mismatches |
| D/X* | Bad clashes with multiple stranded hydrogen bond donors/acceptors, abnormal protonation states, broken molecules, twisted amides etc. |
| Fine-tuning (+/-) | Unsatisfied hydrogen bond donors/acceptors in the hydrophobic pocket of the binding site of the target receptor often have high desolvation value. Therefore, for donors, one unsatisfied hydrogen bond or below, and for acceptors, three or below, are accepted. However, priority is given to the donor, as rejecting a donor can incur greater penalty than an acceptor. |
| (*) grades of C or D/X | These molecules are eliminated due to greater strain energy or lack of key interactions in the binding site of the receptor or unrealistic interactions (having a longer interaction distance range (in Å) than average than suggested (256,257)) |

### 2.2.6 Statistics

Statistical analyses were conducted using the programming language R v4.3.0 (233). A non-parametric analysis of variance was conducted using a Wilcoxon rank-sum test. P-values less than 0.05 were considered statistically significant. All relevant statistical data for the SGI-1776 and CX-6258 PIM kinase inhibitors are stated in supplementary tables 6.1 and 6.2. All the remaining statistical data for the small-molecule PK inhibitors used in this thesis at section 3.1.4 are stated in supplementary tables 6.3 to 6.7.

# 3. Results

The results part of this thesis has been divided into two main parts. The first part (3.1) covers the generation of kinome and *in vitro* activity of the selected small-molecule PK inhibitors on immature and adult flukes. The data presented in this part has been published in Ajmera et al., 2026 (246). The second part (3.2) covers the druggability aspect of targeting *Fasciola* PIM kinase, which is planned to be published in the future.

## 3.1 Generation of the *Fasciola hepatica* kinome

This section of the results presents the kinome generation, with all the required data accessible in the supplementary files of Ajmera et al., 2026 (246), in the supplementary section of this thesis, or as otherwise stated.

### 3.1.1 Kinome prediction and curation

A preliminary run of Kinnanote (218) made use of the proteome of *F. hepatica*, resulting in the creation of a draft kinome. This draft kinome comprised 212 PKs, of which 200 were ePKs that are categorised into various groups, families, and subfamilies (Table 9). Furthermore, Kinnanote identified four aPKs, and the remaining eight PKs were classified as unclassifiable (STK).

**Table 9: Summary of draft and curated kinome of *F. hepatica*.**

| PK group | Draft kinome | Curated kinome | Distribution of PK group in the curated kinome |
|---|---|---|---|
| AGC | 26 | 34 | 14.11% |
| Atypical | 4 | 4 | - |
| CAMK | 35 | 38 | 15.77% |
| CK1 | 5 | 8 | 3.32% |
| CMGC | 41 | 43 | 17.84% |
| Other | 30 | 35 | 14.52% |
| RGC | 4 | 4 | 1.66% |
| STE | 18 | 20 | 8.30% |
| TK | 29 | 33 | 13.69% |
| TKL | 12 | 14 | 5.81% |
| STK (unclassifiable) | 8 | 12 | 4.98% |
| Total | 212 | 245 | 100% |

I subsequently employed a bioinformatics pipeline (135) originally established for the kinome generation of *S. haematobium*, which I later adapted (mentioned in the method section 2.2.3 and Fig. 2.1) to predict, identify, and curate the PK sequences within the proteome of *F. hepatica*. I also minimised redundancies and overlapping genes by employing the "FOR" nested loop with "IF" conditions. After manually curating the dataset, I successfully integrated 29 additional PKs, resulting in a total of 241 ePKs and four aPKs. The curated kinome comprises 245 PKs, accounting for 2.15% of the 11,217 protein-coding genes in the *F. hepatica* genome.

The ePKs were further categorised into nine major groups of PKs (AGC, CAMK, CK1, CMGC, Other, RGC, STE, TK, and TKL), which were subsequently divided into families and sub-families (supplementary data 1 of the online version of Ajmera et al., 2026). Kinnanote was unable to classify 31 PKs into their corresponding PK families but recognised them in their PK groups. 19 of the 31 PKs were subsequently classified to their respective PK families through pairwise alignment of *F. hepatica* and *S. mansoni* protein sequences. Subsequently, I constructed phylogenetic trees for each individual PK group of the *F. hepatica* kinome (which has 233 classified PKs) and the polished kinome of *S. mansoni* (which has 263 PKs) as a reference. The constructed phylogenetic trees further bolstered the classification of these remaining unassigned PKs into their respective PK families and subfamilies within the ACG group (two PKs), CAMK (five PKs), and TK group (twelve PKs); this information can be found in supplementary data 1/table S2 of Ajmera et al., 2026 (246), and I will elaborate more on these genes in the 3.1.1.2 section of this thesis.

I further compared the distribution of the PKs in the curated kinome of *F. hepatica* with other published kinomes of various species (Fig. 3.1). The majority of the ePKs within the helminths were clearly distributed in a similar pattern across multiple helminth species. On average, the CMGC within helminths possesses the highest number of PKs. In nematodes, the highest number of PKs are found within the CK1 PK group. *G. lamblia*, an excavate protozoan, is an outlier in the Other group, possessing 226 PKs, which is more than double the number of PKs found in all the compared species (Fig. 3.1). Both mammals (*H. sapiens* and *M. musculus*) possess the highest average number of PKs across all groups, excluding the Other, CK1, and RGC groups. Notably, the compared protozoan species, *G. lamblia* and *L. major*, both lack RGC, TK, and TKL PKs.

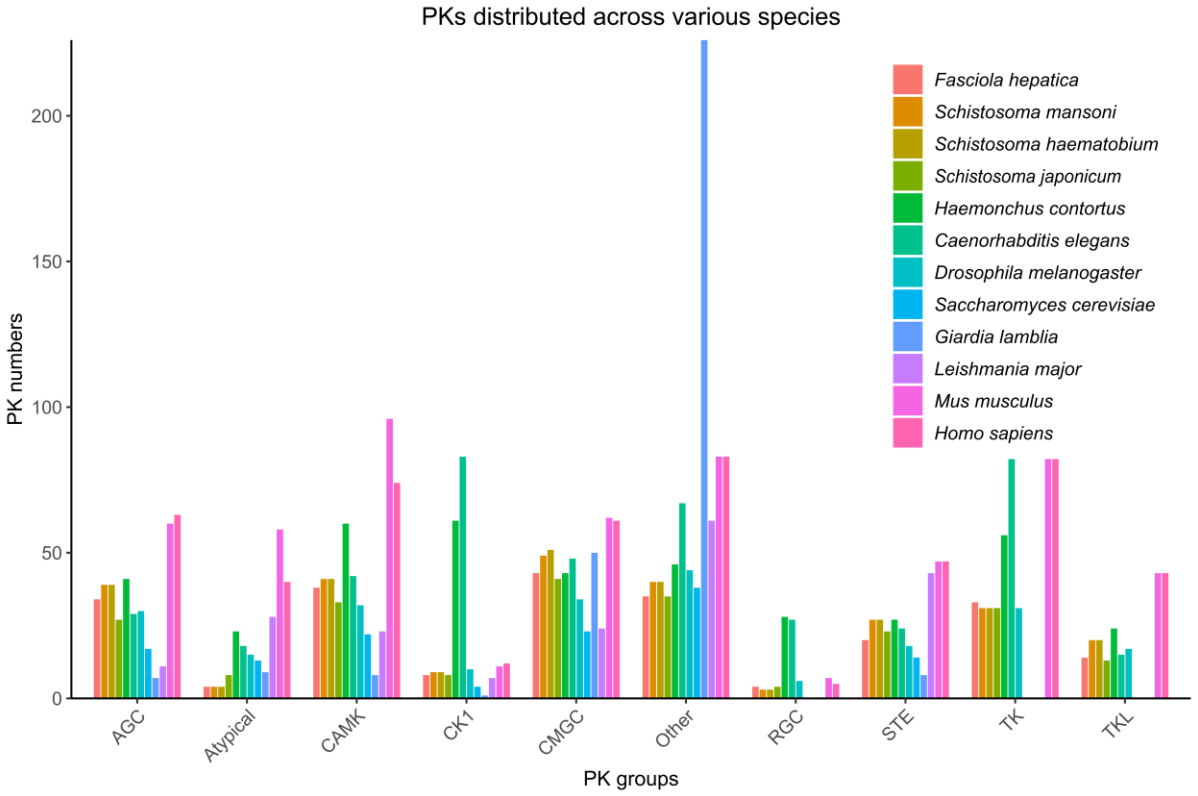


**Figure 3.1: PKs distribution in *F. hepatica* across ten distinct PK groups** and a comparison with the selected kinomes of various species. The information for the kinomes of *S. mansoni* (136,137), *S. haematobium* (135), *S. japonicum* (134), and *H. contortus* (132) is obtained from readily published kinomes, and the remaining kinomes (*C. elegans*, *D. melanogaster*, *S. cerevisiae*, *G. lamblia*, *L. major*, *M. musculus*, and *H. sapiens*) are obtained from KinBase (121).

After the creation of individual PK group phylogenetic trees, I assembled all the trees into a singular comprehensive figure (Fig. 3.2) and eliminated all gene identifiers, branch nodal support, and posterior probabilities to produce a cleaner version. The original high-resolution phylogenetic trees, which include their gene identifiers, branch nodal support, and posterior probabilities, are available in supplementary data 2 of Ajmera et al., 2026 (246), and in supplementary figures 6.6 to 6.15 of this thesis.

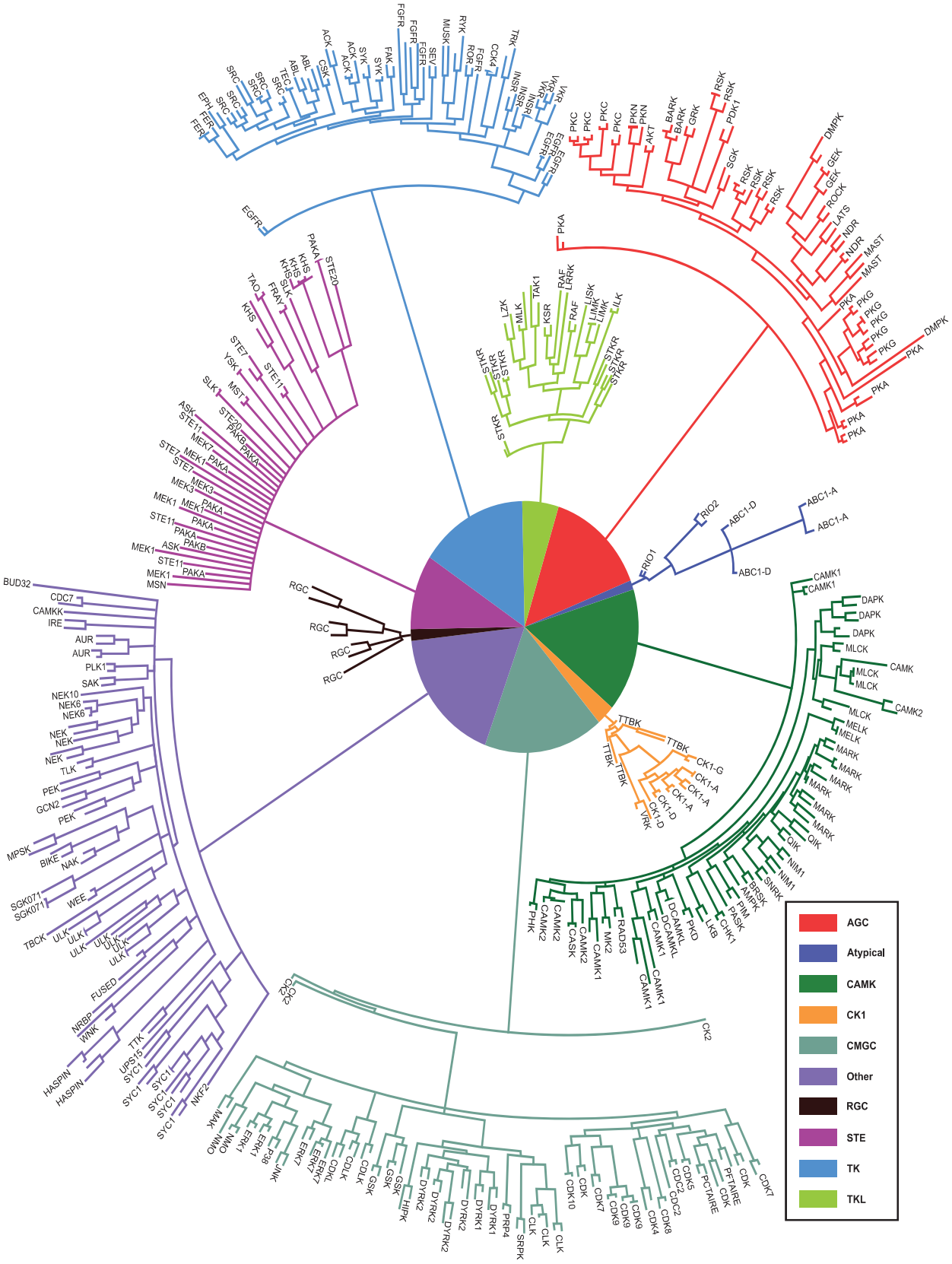


**Figure 3.2: The kinome of *F. hepatica*** includes phylogenetic tree analyses of PKs between *F. hepatica* and *S. mansoni* across all ten major PK groups, which are indicated by different colours. Comprehensive phylogenetic trees exhibiting posterior probabilities, nodal support values, and gene identifiers can be found in supplementary figures 6.6 to 6.15 of this thesis. This figure is reproduced from Ajmera et al., 2026 (246).

#### 3.1.1.1 Eukaryotic PKs in the kinome of *F. hepatica*

The largest ePK group is CMGC (n = 43), which constitutes 17.84% of the ePKs distribution within the kinome. The CMGC group is depicted in a muted green-cyan colour (Inkscape colour code: 6ea092ff) as a branch of Fig. 3.2. The CMGC PK group comprises four members: cyclin-dependent kinases (CDKs), mitogen-activated protein kinases (MAPKs), glycogen synthase kinases (GSKs), and CDC-like and dual-specificity tyrosine-phosphorylation-regulated kinases (CLK/DYRKs). CMGC kinases are crucial in cellular signalling pathways, including proliferation, differentiation, and apoptosis (258). Mammalian MAPKs comprise of three key PKs: extracellular signal-related kinases (ERKs), which are generally activated by growth-related signals; c-Jun N-terminal kinases (JNK); and p38, both of which are triggered by stress stimuli (258). The curated kinome includes the following CMGC PK family members: 16 cyclin-dependent kinases (CDKs), eight dual specificity tyrosine-phosphorylation-regulated kinases (DYRK2), seven MAPKs (which include four ERKs, one JNK, one p38, and one NMO kinase), three cyclin-dependent kinase-like kinases (CDKL), three GSK-3, two dual specificity protein kinases (CLK), two casein kinase II subunits (CK II), one serine-arginine protein kinase (SRPK), and one male germ-associated kinase (MAK).

The second largest ePK group is made up of calcium- and calmodulin-regulated kinases (CAMK) (n = 38), which constitutes 15.77% of the ePKs distribution within the kinome. The CAMK group is depicted in a dark teal/green colour (Inkscape colour code: 288240ff) as a branch of Fig. 3.2. CAMKs play a crucial role in helminth biology, such as muscle contraction to nerve impulse transmission (161,259). The group comprises nine CAMKs (CAMK1 and CAMK2), 16 calcium- and calmodulin-regulated kinase-like (CAMKL) members, three myosin light chain kinases (MLCK), three death-associated protein kinases (DAPK), and one representative from each of the families doublecortin-like and CAM kinase-like (DCAMKL), calcium/calmodulin-dependent serine protein kinase (CASK), proviral integration site for murine leukaemia virus-1 (PIM), MAP kinase-associated protein kinase (MAPKAPK), checkpoint kinase 2 (RAD53), protein kinase D (PKD), and phosphorylase kinase (PHK). The five CAMKs, which Kinannote could not classify, were later classified via the pairwise alignment and the phylogenetic tree analysis. The unclassified CAMKs included D915_000952, D915_003510, and FhPK_0029, which are identified as CAMK1; D915_003510 as CAMK2; and D915_004391 as myosin light chain kinases (MLCK).

A marginally smaller group (n = 35), which constitutes 14.52% of the ePKs within the kinome, is classified as “Other” due to distinct sequence characteristics that differentiate it from the eight major ePK groups. The Other group is depicted in a purple colour (Inkscape colour code 7f6cafff) as a branch of Fig. 3.2. These PKs include five Unc-51-like kinases (ULK), five SCY1-like protein 1 (SCY1) members, four pancreatic eukaryotic translation initiation factor 2 alpha

kinase 3 (PEK) members, four NIMA-related kinases (NEK), three numb-associated kinases (NAK), two aurora kinases (AUR), two polo-like kinases (PLK), and one family member each representing a sugen kinase 071 (SGK071), calcium/calmodulin-regulated kinase kinase (CAMKK), dual specificity protein kinase TTK (TTK), tousled-like kinase (TLK), histone H3-associated protein kinase (HASPIN), inositol-requiring kinase (IRE), WEE1-G2 checkpoint kinase (WEE), nuclear receptor-binding protein (NRBP), cell division control 7 (CDC7) kinase, and a with-no lysine kinase (WNK).

The AGC is the next ePK group composed of Ser/Thr PKs and derives its name from three representative families: protein kinase A, G, and C (260). The ACG group is depicted in a bright red colour (Inkscape colour code: ee393aff) as a branch of Fig. 3.2. This group (n = 34), which constitutes 14.10% of the ePKs within the kinome, comprises 13 families: five ribosomal protein S6 kinases (RSK), five protein kinases G (PKG), five protein kinases A (PKA), five myotonic dystrophy protein kinases (DMPK), four protein kinases C (PKC), three G-protein coupled receptor kinases (GRK), two nuclear DBF2-related kinases (NDR), and one family member each representing microtubule-associated serine/threonine kinase (MAST), protein kinase B (AKT), serum and glucocorticoid responsive kinase (SGK), protein kinase N (PKN), and phosphoinositide-dependent protein kinase 1 (PDK1). The two AGCs, which Kinannote could not classify, were later classified via the pairwise alignment and the phylogenetic tree analysis. The unclassified AGCs included D915_002893 and FhPK_0023, which were identified as PKA and DAMK, respectively.

The fifth ePK group is the TK, comprising 13.70% of the ePKs distribution within the kinome. The TK group is depicted in a sky-blue colour (Inkscape colour code: 5290cdff) as a branch of Fig. 3.2. This group (n = 33) is functionally divided into receptor TKs (RTKs) and non-receptor TKs or cytoplasmic TKs (CTKs). The RTKs consist of 18 PKs, which include four fibroblast growth factor receptors (FGFR), three epidermal growth factor receptors (EGFR), two venus kinase receptors (VKR), two insulin receptors (INSR), and one family member each representing ephrin receptor (EPH), receptor tyrosine kinase-like orphan receptor (ROR), receptor-like tyrosine kinase (RYK), muscle and skeletal associated receptor tyrosine kinase (MUSK), colon carcinoma kinase 4 (CCK4), sevenless tyrosine kinase (SEV), and tropomyosin receptor tyrosine kinase (TKR). The other 15 TKs were classified into cytoplasmic TKs (CTKs), which included five SRC proto-oncogene non-receptor tyrosine kinases (SRC), two activated Cdc42-associated tyrosine kinases (ACK), two spleen-associated tyrosine kinases (SYK), two abelson murine leukaemia homologs (ABL), and one family member each representing feline encephalitis virus-related kinase (FER), focal adhesion kinase (FAK), tec protein tyrosine kinase (TEC), and C-terminal SRC kinase (CSK). The 12 TKs, which Kinannote could not classify, were classified via the pairwise alignment and the phylogenetic

tree analysis. The unclassified TKs included FhPK_0008 as VKR, FhPK_0023 as SEV, D915_001277 as SRC, D915_003307 as CCK4, D915_003399 as SRC, D915_003619 as FGFR, D915_004177 as SRC, D915_005671 as SYK, D915_005801 as SRC, D915_006326 as TRK, D915_006582 as SRC, and D915_008445 as MUSK.

The sixth ePK group is the STE, comprising 8.30% of the ePKs distribution within the kinome. The STE group is depicted in a magenta colour (Inkscape colour code: a84599ff) as a branch of Fig. 3.2. This group (n = 20) consists of several PKs involved in the MAPK cascade, such as 13 MAP kinase kinase kinase kinases (MAP4K) homologous to yeast Ste 20 (STE20), four MAP kinase kinases (MAP2K) homologous to yeast Ste 7 (STE7), and three MAP kinase kinase kinases (MAP3K) homologous to yeast Ste 11 (STE11).

The seventh ePK group is the TK, comprising 5.80% of the ePKs within the kinome. The TKL group is depicted in a lime green colour (Inkscape colour code: 97c840ff) as a branch of Fig. 3.2. This group (n = 14) consists of seven serine/threonine kinase receptors (STKR), four mixed lineage kinases (MLK), one LIM domain kinase (LIMK), one kinase suppressor of Ras1 (KSR), and one rapidly accelerated fibrosarcoma proto-oncogene serine/threonine kinase (RAF).

The eighth ePK group is the CK1, comprising 3.32% of the ePKs within the kinome. The CK1 group is depicted in an orange colour (Inkscape colour code: f8983cff) as a branch of Fig. 3.2. This group (n = 8) consists of five CK kinases (CK1-A, D, and G), two tau tubulin kinases (TTBK), and one vaccinia-related kinase (VRK).

The smallest ePK group is the RGC, comprising 1.65% of the ePKs within the kinome. The RGC group is depicted in a dark brown colour (Inkscape colour code: 2e1212ff) as a branch of Fig. 3.2. This group (n = 4) consists of four RGC members.

**Please note** for additional classification into the subfamilies of PK groups, please refer to supplementary data 1 of Ajmera et al., 2026 (246). And the “current standard classification scheme” is subject to change, as mentioned in the introduction section (1.3.1) of this thesis.

#### 3.1.1.2 Atypical, unclassified, and twilight PKs in the kinome of *F. hepatica*

In cohort to the ePKs, four atypical PKs (aPKs) were identified, comprising two right open reading frame kinases (RIOK-1 & 2) and two ABC1-domain-containing kinases (ABC1-A & D) (123,124). The aPKs group is depicted in the shade of blue colour (Inkscape colour code: 515da9ff) as a branch of Fig. 3.2.

Moreover, Kinannote identified 12 additional genes as serine/threonine PKs (STK) but was unable to classify them into specific PK groups. These PKs included FhPK_0032, FhPK_0028, FhPK_0019, D915_009626, D915_008949, D915_007212, D915_006916, D915_006252,

D915_004196, D915_004132, D915_003160, and D915_002076. Although these 12 PKs scored below the threshold cut-off HMM value for the classification into PK groups or families, they were included in the final kinome to ensure a comprehensive analysis. To further corroborate the results from Kinannote, I performed the domain architecture analysis for these STK genes via the SMART webserver (235) and noticed that all 12 aforementioned genes have a PK catalytic domain with unclassified specificity (supplementary figure 6.3).

Lastly, the six remaining genes, D915_007708, D915_005953, D915_003717, D915_003040, D915_001945, and FhPK_0010, were classified as twilight hits (218), i.e., PK subdomain-containing proteins, which can be potential distant homologs of ePKs. These twilight hits are excluded from the final kinome but can function as seed sequences for illustrating novel PK-like families. Their domain architecture analysis via the SMART webserver (235) can be found in the supplementary figure 6.4.

### 3.1.2 Functional annotation associated to KEGG metabolic pathways

To enhance the functionality of the curated kinome of *F. hepatica*, I used the BlastKOALA webserver (208) with the default setting on the 245 PKs. A total of 110 PKs, constituting 49.4% of all the PKs, were functionally annotated according to human orthology using the KEGG metabolic pathways. In the first level of functional annotation, the PKs were assigned to eight categories of metabolic pathway (Table 10). The relevant genes can be found in supplementary data 3 of Ajmera et al., 2026 (246).

**Table 10: Functional level one of KEGG-associated metabolic pathways of *F. hepatica*** annotated via BlastKOALA (208). Associated genes can be found in the supplementary data file 3 of Ajmera et al., 2026 (246).

| KEGG pathway categories | Number of associated pathways |
|---|---|
| Environment information processing | 61 |
| Metabolism | 22 |
| Genetic information processing | 9 |
| Cellular processes | 8 |
| Organismal systems | 7 |
| Human diseases | 1 |
| Nucleotide metabolism | 1 |
| Carbohydrate metabolism | 1 |

Subsequently, I extracted the second level of functional annotation for these 110 annotated PKs (Fig. 3.3). According to the KEGG-associated terms, the majority of PK functions were

linked to the cancer pathways (24.54%) (Table 11), the endocrine system-associated pathways (20%), the immune system-associated pathways (15.45%), the cell growth and death-associated pathways (9.10%), the nervous system-associated pathways (8.20%), the transport and catabolism-associated pathways (7.29%), the development-associated pathways (6.36%), the cell communication-associated pathways (4.54%), the genetic information processing-associated pathways (2.72%), and the cell motility and folding, sorting, and degradation-associated pathways (0.90%), respectively.

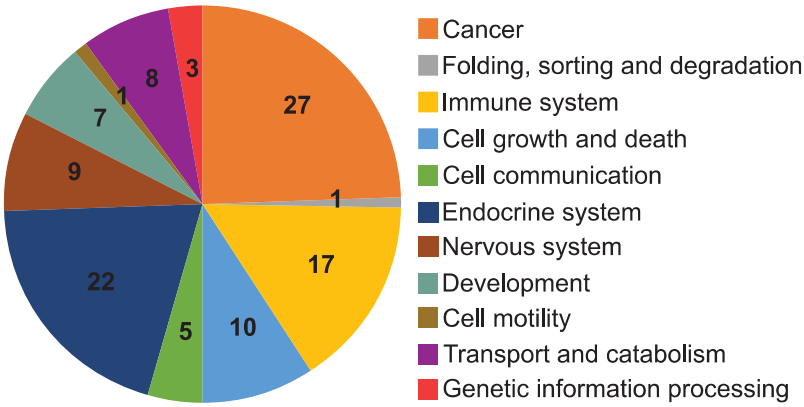


**Figure 3.3: Functional level two of KEGG-associated metabolic pathways of *F. hepatica*** annotated via BlastKOALA (208). This figure is adapted, and the associated genes can be found in supplementary data 3 of Ajmera et al., 2026 (246).

**Table 11: KEGG orthology terms for cancer metabolic pathway** of *F. hepatica* annotated PKs. The other remaining KEGG associated pathways and KEGG orthology (KO) terms can be found in supplementary data 3 of Ajmera er al., 2026 (246).

| KEGG orthology (KO) term | KEGG pathways (2nd level) | *F. hepatica* gene identifiers |
|---|---|---|
| KO2087 | Vc | D915_002458 |
| KO2206 | Pic, Vc, Gc, Pc, Sclc | FhPK_0027 |
| KO2211 | Tmic | D915_000509, D915_001553, D915_002174 |
| KO2216 | Vc | D915_002663 |
| KO2677 | Pic, Mic, Pgic, Ccra, Cmic, Hcc, G, Nsclc | D915_002081, D915_006901 |
| KO3083 | Pic, CC, Hcc, Gc, Bcc, Pc, Ec, Bc | D915_003190, D915_006277 |
| KO3097 | PPcpic | D915_000427, D915_004801 |
| KO4345 | Pic, Pgic, Ccra, Vc | D915_000165, D915_004618, D915_006227, FhPK_0017 |

| | | |
|---|---|---|
| KO4361 | Pic, Mic, Pgic, Ccra, Ccros, Ccmic, Cmic, PPcpic, Coc, Panc, Hcc, Gc, G, M, Blc, Pc, Endc, Bc, Nsclc | FhPK_0030 |
| KO4365 | Pic, Pgic, Ccros, Coc, Panc, Hcc, Gc, G, Tc, Aml, Cml, M, Rcc, Blc, Pc, Endc, Bc, Nsclc | D915_006185 |
| KO4368 | Pic, Mic, Pgic, Ccra, Ccros, Ccmic, Cmic, PPcpic, Coc, Panc, Hcc, Gc, G, Tc, Aml, Cml, M, Rcc, Blc, Pc, Endc, Bc, Nsclc | D915_001287, D915_002477 |
| KO4371 | Pic, Mic, Pgic, Ccra, Ccros, Vc, Ccmic, Cmic, PPcpic, Coc, Panc, Hcc, Gc, G, Tc, Aml, Cml, M, Rcc, Blc, Pc, Endc, Bc, Nsclc | D915_001614, D915_006871 |
| KO4373 | Ccra | D915_000217, D915_004859 |
| KO4432 | PPcpic | D915_005833 |
| KO4440 | Pic, Ccros, Cmic, Coc, Panc | D915_006573 |
| KO4441 | Pgic, Ccros, PPcpic | D915_005042 |
| KO4443 | Vc | D915_007665 |
| KO4456 | Pic, Pgic, Ccra, Ccros, Ccmic, Cmic, PPcpic, Coc, Panc, Hcc, Gc, G, Aml, Cml, M, Rcc, Pc, Endc, Bc, Sclc, Nsclc | FhPK_0014 |
| KO4514 | Pic, Mic, Pgic | D915_002343 |
| KO4515 | Pic, Pgic, G | D915_001189, D915_002206 |
| KO4688 | Pic, Pgic, Ccra, Cmic, PPcpic, Coc, Panc, Hcc, Gc, Aml, Bc | D915_009964, FhPK_0026 |
| KO5733 | Rcc | D915_006992, FhPK_0036 |

| | | |
|---|---|---|
| KO5869 | G | D915_007891 |
| KO6272 | Ec | FhPK_0009 |
| KO8794 | G | D915_002235, D915_007740 |
| KO8957 | Hcc, Gc, Bc | D915_001641, D915_007708, D915_010101, FhPK_0025 |
| KO18050 | Mic | D915_000022 |

Vc = Viral carcinogenesis, Pic = Pathways in cancer, Gc = Gastric cancer, Pc = Prostate cancer, Sclc = Small cell lung cancer, Tmic = Transcriptional misregulation in cancer, Mic = MicroRNAs in cancer, Pgic = Proteoglycans in cancer, Ccra= Chemical carcinogenesis - receptor activation, Cmic = Choline metabolism in cancer, Hcc = Hepatocellular carcinoma, G = Glioma, Nsclc = Non-small cell lung cancer, Cc = Colorectal cancer, Bcc = Basal cell carcinoma, Ec = Endometrial cancer, Bc = Breast cancer, PPcpic = PD-L1 expression and PD-1 checkpoint pathway in cancer, Ccros = Chemical carcinogenesis - reactive oxygen species, Ccmic = Central carbon metabolism in cancer, Coc = Colorectal cancer, Panc = Pancreatic cancer, M = Melanoma, Blc = Bladder cancer, Endc = Endometrial cancer, Tc = Thyroid cancer, Aml = Acute myeloid leukemia, Cml = Chronic myeloid leukemia, Rcc = Renal cell carcinoma.

### 3.1.3 Kinome comparison and a basis for drug repurposing?

After the curation of the *Fasciola* kinome, I compared it with the kinome of its closely related parasitic flatworm species (*S. mansoni* (136,137) and *S. haematobium* (135)) and *H. sapiens* (109,121) to provide understanding of evolutionary relationships and functional similarities with trematodes and the human host and to identify potential trematode-specific PKs. The kinomes comprised 233, 263, 265, and 518 PKs for *F. hepatica*, *S. mansoni*, *S. haematobium*, and *H. sapiens*, respectively.

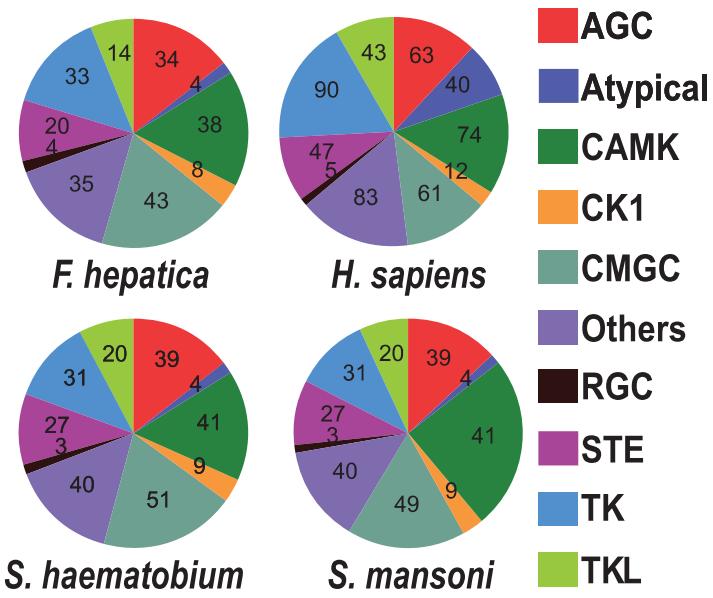


**Figure 3.4: Comparison of trematode and human kinomes**. The number of kinases per group is indicated. This figure is adapted and modified from Ajmera et al., 2026 (246).

A PK group-level analysis showed the quantity of the PKs identified for the nine ePK groups and the aPK group in the kinomes of *F. hepatica*, *S. mansoni*, *S. haematobium*, and *H. sapiens* (Fig. 3.4). The PK group sizes were predominantly similar across all three trematode species, with CMGC and CAMK representing the largest groups. Nevertheless, the PK group sizes within the human kinome distinctly varied from those of the trematodes. In humans, the Other and TK groups constitute larger proportions (16% and 18%, respectively) in the kinome, whereas the CMGC group represents a smaller proportion (12%) compared to the trematode kinomes; the CMGC group represents the largest fraction (18% for Fh, 19% for Sh, and 19% for Sm). Additionally, the total number of PKs in humans exceeds that in trematodes across all PK groups, highlighting the enhanced diversity of the human kinome.

A comprehensive global-pairwise comparison of the PK domains across the four kinomes identified 67 PKs in *Fasciola* for which either no human homologs were identified or the sequence identity of the human PK domains were notably low (> 30%). The majority of these PKs possessed a homolog in one or both of the schistosome species. An instance in the TK group, where the human homolog was absent, is the VKR genes (FhPK_0008, D915_003706, Smp_019790, Smp_153500, ShRTK, and ShVKR2). Upon comparing these PKs with the means of reciprocal BLAST, the closest homologs within the human kinome were the insulin receptors, bolstering the assertion by Vicogne and colleagues that VKRs are invertebrate-specific insulin-like receptor genes that are absent in mammals (164,166–168).

After the analysis of ePK comparison within the trematode and the human kinomes, only four PKs were identified in *Fasciola* that lack homologs in schistosome species as well as the

human host: D915_005277 (STE), FhPK_0027 (CMGC), D915_001682 (CAMK), and FhPK_0018 (Other).

The path of identifying trematode-specific PKs and those with a minimal sequence identity and similarity to the human homologs is advantageous, as it allows for therapeutic targeting without the risk of off-target effects in the humans. I identified the closest human homolog for *F. hepatica* PKs through global-pairwise analysis and acquired percentages of sequence identity and sequence similarity for the PK domains. I have compiled the top five PKs (Table 12), which exhibit notably low conservation of PK domains between *F. hepatica* and humans (< 30% sequence identity). **Please note** that a total of 23 PKs were identified with the highest sequence divergence compared to human orthologs; however, only the top five PKs are presented in Table 12. The Other PK group exhibited the lowest identity and similarity values, specifically in the SCY1-like pseudokinase 3 (SCYL3), with an identity and similarity of 8.5% and 13.1%, respectively. In total, I identified 23 PKs exhibiting a low level of conservation with human PKs (data can be found in table 2 of Ajmera et al., 2026 (246)).

**Table 12: Summary of PK domain sequence identity of less than 30%** among the top five *F. hepatica* PKs in comparison to the most closely related Hs PK hits. **Please note** a total of 23 PKs were identified with the highest sequence divergence compared to human orthologs; however, only the top five PKs are presented in this table.

| PK group | Fh identifier | Hs identifier | % Sequence identity | % Sequence similarity |
|---|---|---|---|---|
| Other | D915_009688 | SCYL3 | 8.5 | 13.1 |
| Other | D915_007882 | PRPK | 13.5 | 18.7 |
| AGC | D915_002893 | LATS1 | 14.7 | 21 |
| AGC | D915_008016 | LATS1 | 16.2 | 19.3 |
| AGC | FhPK_0023 | PKG2 | 17.8 | 25.9 |

In contrast, notable sequence similarity between human and trematode PKs may facilitate a drug repurposing strategy, allowing existing inhibitors of human PKs to demonstrate substantial efficacy against the trematode PKs. I have compiled the top five PKs (Table 13), which exhibit notably high conservation of PK domains between *F. hepatica* and humans (> 75% sequence identity). **Please note** that a total of 16 PKs were identified with the highest sequence convergence compared to human orthologs; however, only the top five PKs are presented in Table 13. The highest identity and similarity values (84.1% and 94%, respectively) were identified for a microtubule affinity regulating kinase 1 homolog (MARK1, D915_002194), a constituent of the CAMK group. In total, I identified 16 PKs exhibiting a high degree of conservation with the human PKs (data can be found in table 3 of Ajmera et al., 2026 (246)).

**Table 13: Summary of PK domain sequence identity of more than 75%** among the top five *F. hepatica* PKs in comparison to the most closely related Hs PK hits. **Please note** a total of 16 PKs were identified with the highest sequence convergence compared to human orthologs; however, only the top five PKs are presented in this table.

| PK group | Fh identifier | Hs identifier | % Sequence identity | % Sequence similarity |
|---|---|---|---|---|
| CAMK | D915_002194 | MARK1 | 84.1 | 94.0 |
| CMGC | D915_004801 | CK2a1 | 83.9 | 92.7 |
| AGC | D915_000165 | PKACa | 81.6 | 91.8 |
| STE | D915_001478 | PAK3 | 80.6 | 90.9 |
| CK1 | FhPK_0002 | CK1g3 | 80.3 | 89.0 |

### 3.1.4 *In vitro* testing of PK inhibitors on immature and adult flukes

To identify whether a drug repurposing strategy could effectively deliver a PK inhibitor with fasciolicidal activity, I employed small-molecule PK inhibitors that are either FDA-approved for human use or have advanced to clinical trials II or further for the treatment of human diseases, for which homologues to the human host can be found in the curated *Fasciola* kinome dataset from the previous sections 3.1.2 and 3.1.3. All the clinical data relevant of the small-molecule PK inhibitors used in this thesis can be found in supplementary table 6.11.

I selected four small-molecule PK inhibitors to target both the immature and the adult life stages of the liver fluke: vandetanib (ZD6474) (261), ruboxistaurin (262), foretinib (XL880) (263), and tyrosine kinase-IN-1 (XL999) (264). Vandetanib inhibits human endothelial growth factor receptor (VEGFR 2/3), RET, EGFR, and FGFR and is an FDA-approved small-molecule inhibitor for the treatment of medullary thyroid cancer (261,265–269). Foretinib is an investigational small-molecule PK inhibitor in clinical phase II trials involved in cancer development, targeting PDGFR-β, MET, VEGFR2, RON, FLT3, and ERK (263,270,271). Tyrosine kinase-IN-1 is an inhibitor that targets multi-RTKs (FGFR 1/3, KIT, FLT3, VEGFR2, and PDGFR α/β) (264). Ruboxistaurin is a selective inhibitor of the PKCβ isoform (262). In the curated kinome of *F. hepatica*, I annotated D915_006901 as PKCβ. All the putative targets in *F. hepatica* were linked to cancer pathways according to the KEGG functional analysis (data can be found in supplementary data 3 of the online version of Ajmera et al., 2026 (246)).

The parameters for *in vitro* treatment and motility assessment of the liver flukes are mentioned in sections 2.2.2.3, 2.2.2.4, 2.2.2.5, and 2.2.2.6 of this thesis. The motility score assessment for the fluke ranges from 3 to 0, where 3 = normal motility, 2 = slightly reduced motility than normal, 1 = minimal or irregular movement, and 0 = no movement even upon mechanical stimulation with tweezers or dead flukes. I also utilised TCBZ to treat the fluke under identical

conditions, which served as the positive control, whereas the negative control comprised medium containing the drug solvent DMSO. For each different condition (25 µM, 50 µM, and 100 µM), I employed 4 flukes (n = 4, both immature and adult flukes). Subsequently, I evaluated their survival and motility every 24 h over a total of a 72 h culture period, with each experiment condition replicated three times. All the statistical data related to the selected small-molecule PK inhibitors is available in supplementary tables 6.3 to 6.7.

For all inhibitors and concentrations, immature flukes (Fig. 3.5 B and D) exhibited more sensitivity than adult flukes, as their motility was significantly reduced (score 0.5 and 1) compared to the control group (score 3). After 24 h, vandetanib at 25 µM concentration exhibited the highest potency against the immature flukes, followed by ruboxistaurin. Both inhibitors lowered the motility of the flukes by 50% when compared to the control group. Following a prolonged duration of 72 h, vandetanib, ruboxistaurin, and foretinib significantly lowered the motility to a minimal level, whereas tyrosine kinase-IN-1 exhibited reduced efficacy. At a concentration of 50 µM, ruboxistaurin exhibited the highest efficacy in reducing the motility of the flukes and eventually killing them within 24 h, whereas the others followed after 48-72 h. TCBZ (the reference drug) required higher concentration and/or extended treatment duration to attain the equivalent effect.

On adult flukes, all inhibitors, including TCBZ, resulted in a minor decrease in the motility (scores 1.5 and 2.5) at 25 µM, (Fig. 3.5 A and C). At a concentration of 50 µM, ruboxistaurin significantly reduced the motility of the flukes after 24 h and proved lethal to the flukes after 72 h. At the same concentration, TCBZ was sublethal (score 1) and exhibited more potency in reducing the motility of the flukes than vandetanib (score 1.5). Foretinib and tyrosine kinase-IN-1 exhibited less efficacy, resulting in a late reduction in motility after 72 h for foretinib and an overall small effect (score 2) for tyrosine kinase-IN-1. At a concentration of 100 µM, ruboxistaurin proved lethal within the first 24 h, succeeded by vandetanib, tyrosine kinase-IN-1, and TCBZ after 48 h. Conversely, the flukes tolerated foretinib treatment even after 72 h.

At the low concentration, all the selected small-molecule PK inhibitors exhibited more efficacy than TCBZ (the reference drug) against the immature flukes. Conversely, in adult flukes, only ruboxistaurin exhibited a significant reduction in the motility against TCBZ.

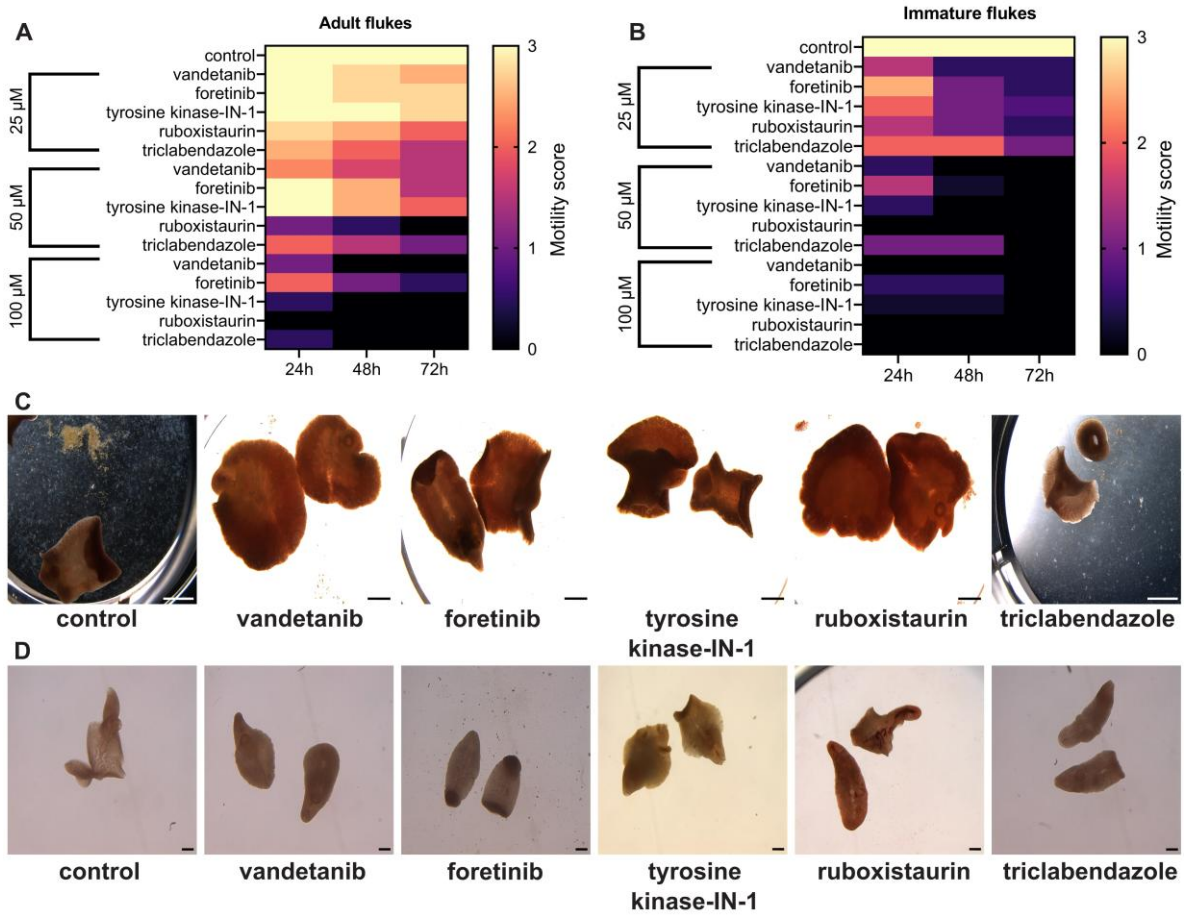


**Figure 3.5: Heatmaps depict the motility scores of flukes** following the treatment of PK inhibitors compared to TCBZ at different concentrations of 25 µM, 50 µM, and 100 µM. **(A)** Illustrates the motility scores of adult flukes. **(B)** Illustrates the motility scores of immature flukes. The flukes were cultured for 72 h, and the motility scores were recorded every 24 h for the different time points of 24 h, 48 h, and 72 h. After the scoring, the media was replenished with fresh media with 1% ABAM and 5% chicken serum. DMSO, which served as a drug-dissolving vehicle, was used as a negative control and was added during the culturing of the control flukes. The scale bar represents the motility scores from 0 to 3 (3 = normal movement, 2 = slightly reduced movement, 1 = severely reduced movement, and 0 = no movement/dead). For each condition of PK inhibitor treatment as well as TCBZ against adult and immature flukes, the number of biological replicates was four (n = 4). **(C)** Representative images of the adult flukes treated with selected PK inhibitors at a concentration of 50 µM after 72 h time point (scale bar = 1000 µM). **(D)** Representative images of the immature flukes treated with selected PK inhibitors at a concentration of 50 µM after 72 h time point (scale bar = 500 µM). This figure is adapted, and the statistical data related to this figure is available in supplementary data 2 of the online version of Ajmera et al., 2026 (246) as well as the supplementary tables 6.3 to 6.7 of this thesis. **Please note** that the representative images of the adult flukes **(C)** and immature flukes **(D)** are related just to the 72 h time point and 50 µM PK inhibitor concentration.

## 3.2 Assessment of the druggability of PIM kinase in the common liver fluke

In this section of the thesis, I will examine the druggability aspect of PIM kinase in the common liver fluke.

Koike and colleagues screened several commercially available small-molecule PK inhibitors and observed the adverse effects of the pan-PIM kinase inhibitors (SGI-1776 and CX-6258) on *E. multilocularis* (272). Additionally, Koike and colleagues conducted molecular docking with several compounds to establish a potential affinity for targeting EmPIM kinase. In my work, I aimed to foster the exploration of the FhPIM kinase, identified as D915_000232 in the curated kinome of the common liver fluke (246), for the identification of novel compounds. In the subsequent sections, I will elucidate the druggability of PIM kinase in the common liver fluke. Additionally, to identify the orthologues of *Fasciola* PIM kinase, I performed reciprocal BLASTp searches of FhPIM kinase (D915_000232) against model organisms and related species in WormBase (245), NCBI (9), and Uniprot (241,242).

### 3.2.1 Transcriptomics data of PIM kinase in liver flukes

Characterising the transcriptomic profile of a potential drug target is crucial for validating its therapeutic efficacy in the complex, multi-stage life cycle of the common liver fluke. This parasite undergoes significant physiological transformations between its intermediate snail host and definitive mammalian host. Furthermore, delineating these expression patterns at the cell-type level and within essential tissues facilitates the prediction of physiological outcomes from inhibition and assesses the availability of the target for potential chemotherapeutic agents. This transcriptomic evidence provides a biological justification for exploring a gene as a prospective target for fascioliasis treatment. Therefore, I obtained gene expression data, single-cell RNA-seq data, and spatial transcriptomic data to investigate the expression of PIM kinase in liver flukes, which are detailed in the subsequent sections of this thesis.

#### 3.2.1.1 PIM kinase expression data in different life stages of liver flukes

To explore the expression data across the different life stages of the liver fluke, I used the published life stage gene expression data that was furnished from the raw reads produced in (5,273). The data was analysed and remapped by Dr. Oliver Puckelwaldt in our research working group at the institute.

The gene expression data (Fig. 3.6) revealed elevated levels of transcripts per million (TPM) of PIM kinase in adult flukes compared to other life stages of the liver flukes. The expression of PIM kinase is nominally expressed in the egg and metacercaria but significantly increases

post-excystation of newly excysted juveniles (NEJs) after 3 hours, subsequently declines after 24 hours, remains constant during the immature stage, and then markedly increases after reaching sexual maturity.

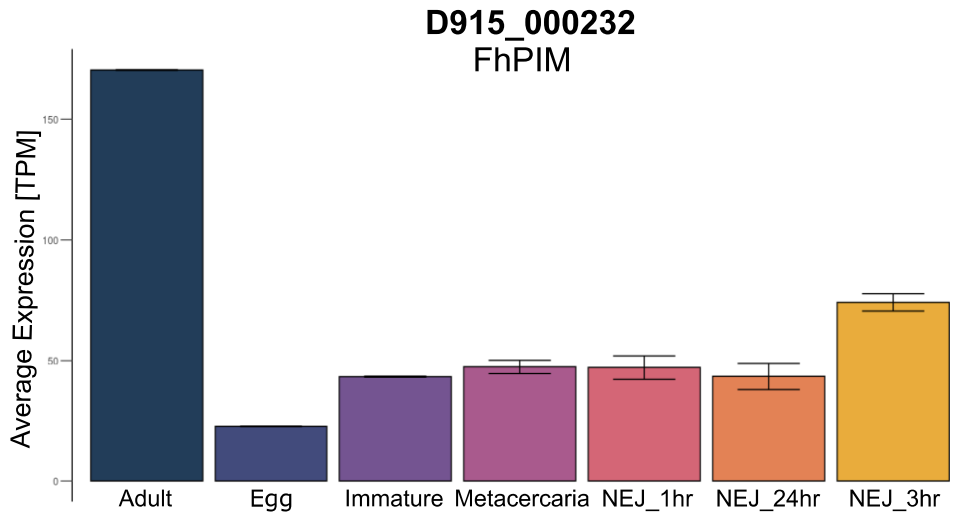


**Figure 3.6: The expression plot of *Fasciola* PIM kinase**. RNA-seq of different *Fasciola* life stages of PIM kinase (D915_000232) encoded in the *F. hepatica* genome. Raw reads were produced by (5,273), which were remapped (by Dr. Oliver Puckelwaldt) to the genome used in this work. TPM = transcripts per million, and NEJ = newly excysted juvenile.

### 3.2.1.2 Single-cell RNA-seq gene expression data of PIM kinase in liver flukes

The single-cell RNA-seq gene expression data for the liver fluke was generated and analysed by Dr. Oliver Puckelwaldt in our research working group at the institute. He delineated a total of 15 clusters identified subsequent to his analysis (Fig. 3.7 A). The clusters were mapped to cells associated with the following tissues: testes (3 clusters), gut (1 cluster), ovary (2 clusters), stem cells (1 cluster), muscle and muscle-associated (2 clusters), vitellarium (2 clusters), Mehlis gland (1 cluster), and three clusters for which no annotation was found (274).

The expression pattern of PIM kinase is distributed among various cell types, as illustrated in figure 3.7 B, predominantly expressed in female germ cells (oocytes) and to a lesser extent in the early vitellocyte cell cluster. The observed expression in the unidentified cluster 3 may be attributable to the oocytes and most likely be a background expression signal. Of note, some muscle cells appear also positive.

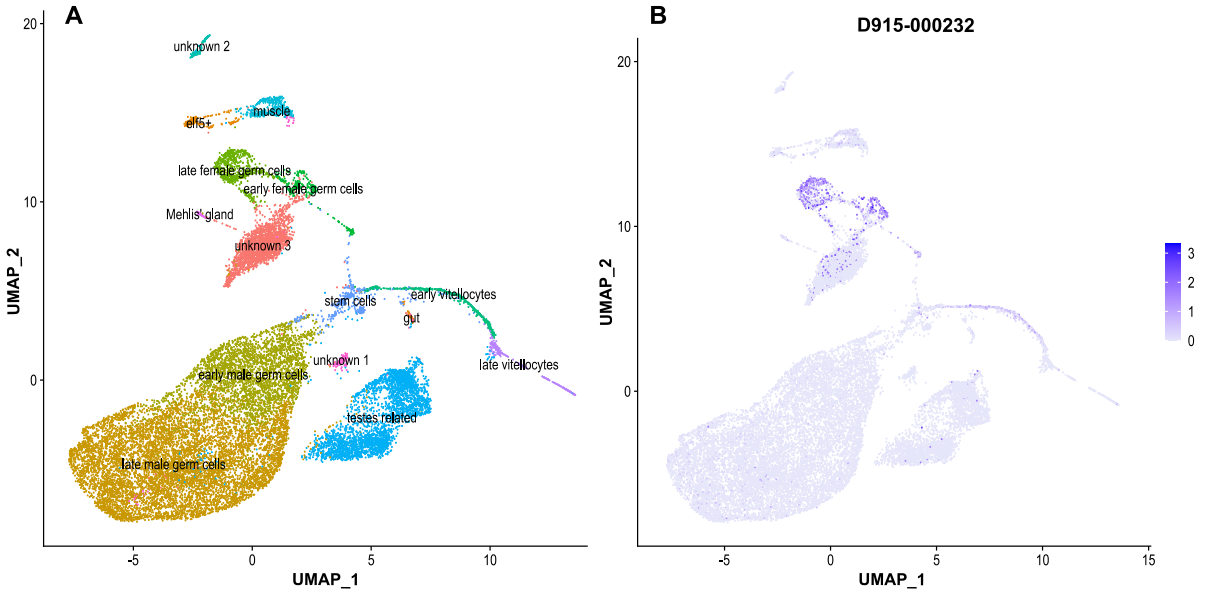


**Figure 3.7: Single-cell RNA-seq gene expression pattern of PIM kinase in *F. hepatica*. (A)** Uniform Manifold Approximation and Projection (UMAP) of scRNA-seq analysis of 19,581 cells of the liver fluke. Clusters are coloured, and labels are added. **(B)** UMAP feature plot for FhPIM kinase (D915_000232). The images for this figure were generated by Dr. Oliver Puckelwaldt.

### 3.2.1.3 Tissue expression of PIM kinase in liver flukes

The spatial transcriptomic data for the liver fluke was produced in our research working group at the institute and can be accessed via the following link (https://www.uni-giessen.de/haeberlein-lab/en/info). Furthermore, Gramberg and colleagues (171) published the spatial transcriptomic data of *F. hepatica*.

The spatial transcriptome of *F. hepatica* corroborated the findings observed in the single-cell RNA-seq data, indicating that PIM kinase is primarily expressed in oocyte cell clusters. Alongside the insights from the single-cell RNA-seq data, the spatial mapping (Fig. 3.8 B) demonstrated that the transcripts were specifically enriched in the parenchyma, as well as within the areas of ovaries, gut, and tegument (Fig. 3.8 C).

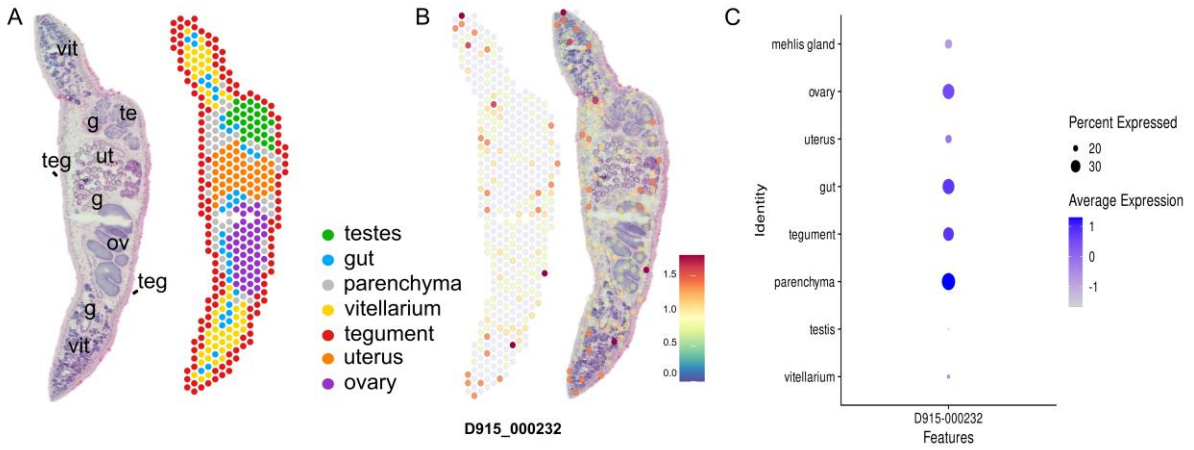


**Figure 3.8: Tissue expression of PIM kinase in *F. hepatica*. (A)** H&E-stained tissue section (left) and spatial projection of spots covering the tissue modified from Gramberg et al. 2025 (171), g: gastrointestinal tract, ov: ovary, par: parenchyma, teg: tegument, te: testis, ut: uterus, vit: vitellarium. **(B)** Spatial projection and overlay sections illustrating the prediction of expression clusters of PIM kinase in the spatial transcriptome of the liver fluke. Gene expression is indicated by colour (blue = low, red = high). **(C)** DotPlot illustrating the expression profile of PIM kinase (D915_000232) in selected tissue markers of different clusters. The colour of the dot represents the average expression level (Z-score scaled counts; grey = low, blue = high) across all spots within a cluster. The size of the dot represents the percentage of spots within a cluster that have captured this transcript. The images for this figure were generated by Dr. Oliver Puckelwaldt.

### 3.2.2 Phylogenetic analysis of PIM kinases

Upon identifying the orthologs of FhPIM kinase, I determined the orthologous relationships of FhPIM kinase (D915_000232) with other PIM kinases across various selected species. I conducted a phylogenetic analysis using the Bayesian Inference (BI) method from MrBayes (221) on the amino acid sequences of different vertebrate and invertebrate PIM kinases. Consequently, I constructed a phylogenetic tree using MrBayes v3.2.7a for all the PIM kinases (Fig. 3.9) across various selected species. The PIM kinases for vertebrates, PIM1, PIM2 and PIM3 (shown in the pure blue box in Fig. 3.9), are classified within the same clade; notably, each distinct PIM kinase occupies separate branches. The *Holothuria leucospilota* (sea cucumber) PIM kinase, although classified within the invertebrate clade (shown in the patriarch purple box in Fig. 3.9), is anticipated to share similarities with vertebrates, as *H. leucospilota* is part of the phylum Echinodermata, which is phylogenetically closer to Chordata (vertebrates) than the more distantly related protostome invertebrate species such as *Rhipicephalus sanguineus*, *Aplysia californica*, and *Biomphalaria glabrata* that were used in the phylogenetic tree construction. All remaining PIM kinases of the flatworm species (shown in the grass green box in Fig. 3.9) are grouped within the same clade of the flatworms in the phylogenetic tree (shown in the cyan box in Fig. 3.9), forming different branches for trematodes (shown in the cyan box in Fig. 3.9), cestodes (shown in the reddish orange box in Fig. 3.9), and planarians (shown in the dark blue-violet box in Fig. 3.9) with a strong nodal support (100%). Furthermore, the *F. hepatica* PIM kinase was grouped in the same tree node

as the *F. gigantica* PIM kinase (FGIG_09449) in the trematode branch of the flatworm species clade of the phylogenetic tree with a strong nodal support (100%). The BR serine/threonine-protein kinase (BRSK) of *F. hepatica* was used as an outgroup to establish the root of the phylogenetic tree (Fig. 3.9).

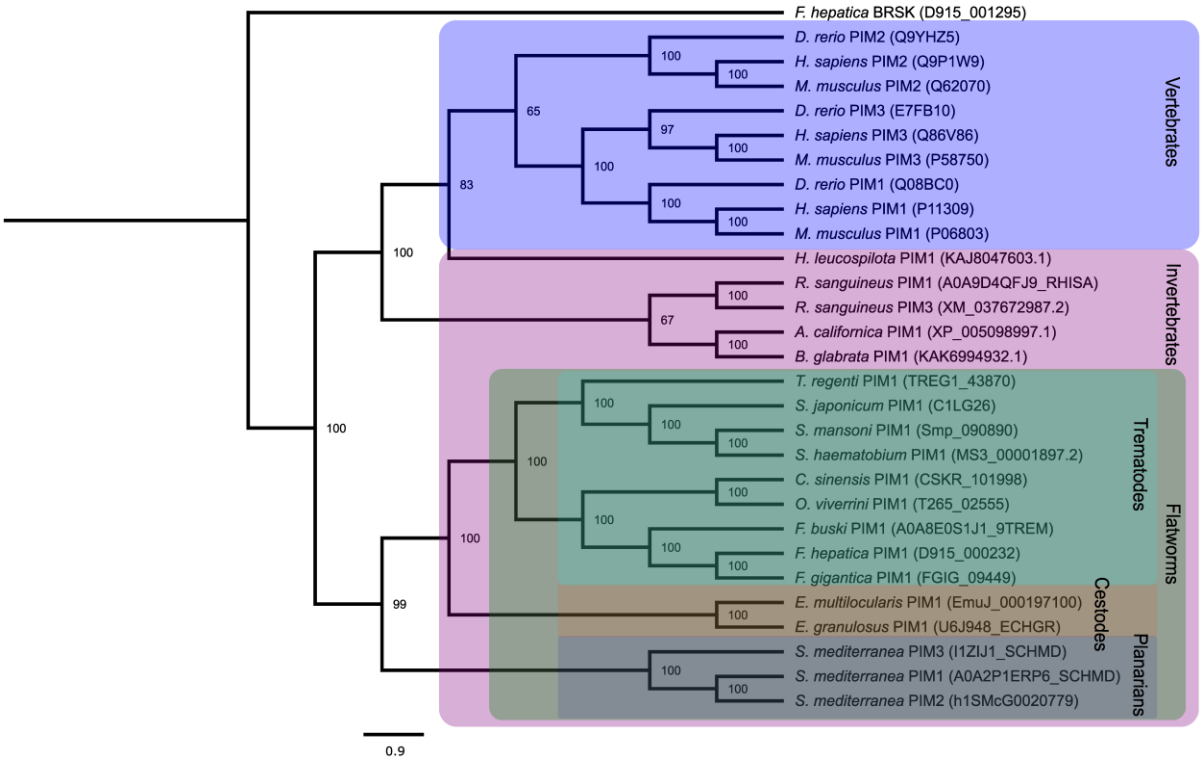


**Figure 3.9: Bayesian Inference (BI) tree of *F. hepatica* PIM kinase**, comprising homologous PIM kinases from various selected species. The selected species included three vertebrates: *D. rerio*, *H. sapiens*, and *M. musculus* (shown in the pure blue box, Inkscape colour code 0000ffff), as well as 16 invertebrates, such as *H. leucospilota*, *R. sanguineus*, *A. californica*, and *B. glabrata* (shown in the patriarch purple box, Inkscape colour code 800080ff). The remaining twelve species are flatworms, grouped into trematodes, cestodes, and planarians (shown in the grass green box, Inkscape colour code 008000ff). Trematodes include *T. regenti*, *S. japonicum*, *S. mansoni*, *S. haematobium*, *C. sinensis*, *O. viverrini*, *F. buski*, *F. hepatica*, and *F. gigantica* (shown in the cyan box, Inkscape colour code 00ffff66); cestodes include *E. multilocularis* and *E. granulosus* (shown in the reddish orange box, Inkscape colour code ff3d0066); and planarians include *S. mediterranea* (shown in the dark blue-violet box, Inkscape colour code 13009b66). *F. hepatica* BRSK (D915_001295) served as the outgroup to root the tree. Percentage posterior probabilities/bootstrap values are displayed at the nodal supports of the branches in the tree. The gene identifiers for each species are indicated in the tree.

### 3.2.3 Effect of pan-PIM kinase inhibitors on immature and adult flukes

After gathering the promising data promising, I thought of using the pan-PIM inhibitors (SGI-1776 and CX-6258) to evaluate their effects on immature and adult liver flukes. The control comprised a medium containing the drug solvent DMSO. For each different condition (25 µM, 50 µM, and 100 µM), I employed 4 flukes (n = 4, both immature and adult flukes). Subsequently, I evaluated their survival and motility every 24 h over a total of a 72 h culture period. All the statistical data related to the selected small-molecule PK inhibitors is available in supplementary tables 6.1 and 6.2 of this thesis.

Immature flukes (Fig. 3.10 B and D) exhibited greater sensitivity to both inhibitors compared to adult flukes. At a concentration of 25 µM of both the inhibitors, the immature flukes exhibited only a slight reduction in their motility after 24 h; however, after 72 h, SGI-1776 impaired the motility of the immature flukes, in contrast to CX-6258, which only slightly reduced their motility. At a concentration of 50 µM, both the inhibitors exhibited severe motility reduction within 24 h and proved lethal to the immature flukes after 72 h. At a concentration of 100 µM, both the inhibitors exhibited lethal potency to the immature flukes within 24 h.

Adult flukes (Fig. 3.10 A and C) exhibited no significant reduction in their motility after 72 h at a concentration of 25 µM. At a concentration of 50 µM, CX-6258 exhibited slight reduction in the motility of the adult flukes, whereas SGI-1776 exhibited a significant impairment in their motility. At a concentration of 100 µM, SGI-1776 was lethal to the adult flukes within 48 h; conversely, CX-6258 exhibited significant motility impairment but was not lethal to the adult flukes.

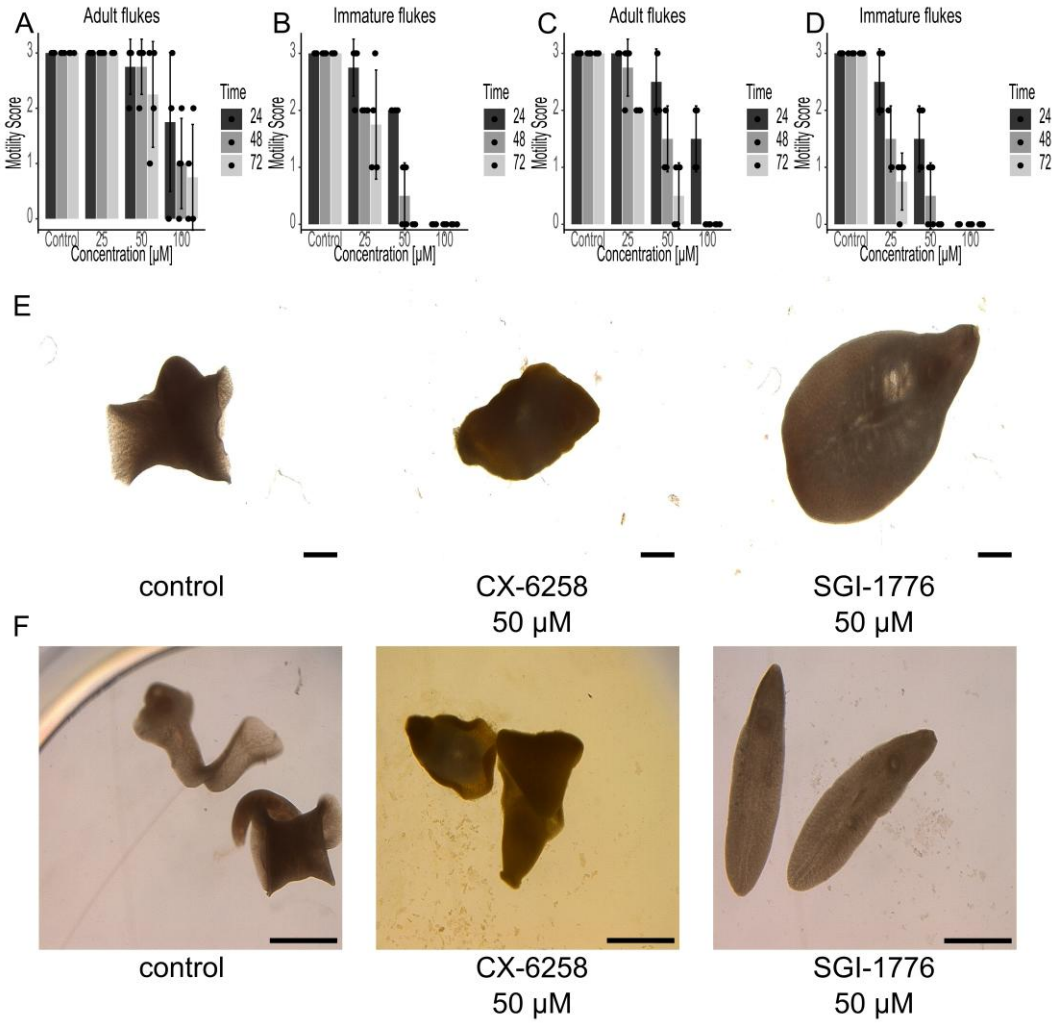


**Figure 3.10: Motility score of flukes treated with CX-6258 and SGI-1776** at different concentrations of 25 µM, 50 µM, and 100 µM. **(A)** Illustrates the motility scores of adult flukes treated with CX-6258. **(B)** Illustrates the motility scores of immature flukes treated with CX-6258. **(C)** Illustrates the motility scores of adult flukes treated with SGI-1776. **(D)** Illustrates the motility scores of immature flukes treated with SGI-1776. The flukes were cultured for 72 h, and the motility scores were recorded every 24 h for the different time points of 24 h, 48 h, and 72 h. After the scoring, the media was replenished with fresh media with 1% ABAM and 5% chicken serum. DMSO, which served as a drug-dissolving vehicle, was used as a negative control and was added during the culturing of the control flukes. The motility scores are recorded from 0 to 3 (3 = normal movement, 2 = slightly reduced movement, 1 = severely reduced movement, and 0 = no movement/dead). **(E)** Representative images of the adult flukes treated with CX-6258 and SGI-1776 at a concentration of 50 µM after 72 h time point (scale bar = 500 µM). **(F)** Representative images of the immature flukes treated with CX-6258 and SGI-1776 at a concentration of 50 µM after 72 h time point (scale bar = 1000 µM). For each condition of CX-6258 and SGI-1776 of immature and adult flukes, the number of biological replicates was four (n = 4). The statistical values for all the conditions are stated in the supplementary tables 6.1 and 6.2. **Please note** that the representative images of the adult flukes **(E)** and immature flukes **(F)** are related just to the 72 h time point and 50 µM concentration.

### 3.2.4 Multi-sequence alignment and KLIFS domain architecture of Hs and Fh PIM kinases

Upon comparing the kinome of all four species mentioned in section 3.1.3, I found a 49.4% sequence identity and a 65.1% sequence similarity between the PIM kinase domains of Hs and Fh. To further ascertain the start and end of the PK domain in both *Fasciola* (D915_000232) and human (P11309) PIM1 kinase, I conducted a SMART protein domain analysis using the webserver (235), with the results illustrated in the supplementary figure 6.5. Then, I used the EMBL-Clustal Omega alignment webserver (210) to compare the Hs and Fh PIM kinase domains, which helped me gather important details about the drug binding sites and the key structure of the PIM kinase. Furthermore, upon aligning the PK domains, I acquired the conserved structural elements of the catalytic PK domain from the KLIFS webserver (275), utilising RCSB PDB IDs 4JX7 and 5O13 for Hs PIM1 kinase (234).

Important pharmacophores/residues for PIM kinase inhibition, illustrated with red arrows in Fig. 3.11, were obtained from the HsPIM1 kinase interaction described by Heyder and colleagues (250). The important residues described for Hs PIM1 kinase are Lys67, Glu121, Arg122, Pro123, Asp128, Asp131, Glu171, and Asp186. The catalytic Lys67, located in the β-sheet III of the N-terminal loop, forms the back pocket of the HsPIM1 kinase alongside Glu89; both residues are conserved in the FhPIM kinase as Lys77 and Glu98 (276,277). The Glu89 establishes a salt bridge with Lys67 to enhance the catalytic activity of the HsPIM1 kinase (278). The subsequent three residues, Glu121, Arg122, and Pro123, are located within the flexible hinge loop region between the N-terminal and C-terminal of human PIM1 kinase. In FhPIM, only arginine is conserved as Arg130, while Glu121 (Hs) is substituted by Asp129 and Pro123 (Hs) is substituted with Val131. Additionally, another residue in FhPIM kinase, Ser132, also contributes to the hinge region. The other important residues are conserved between Hs and Fh PIM kinases: these are Asp128 in the linker loop between the hinge and the αD-helix, Asp131 in the αD-helix, Glu171 in the catalytic loop, and Asp186 in the DFG loop from Hs PIM1 kinase, which correspond to Asp137, Asp140, Glu180, and Asp195, respectively in FhPIM kinase.

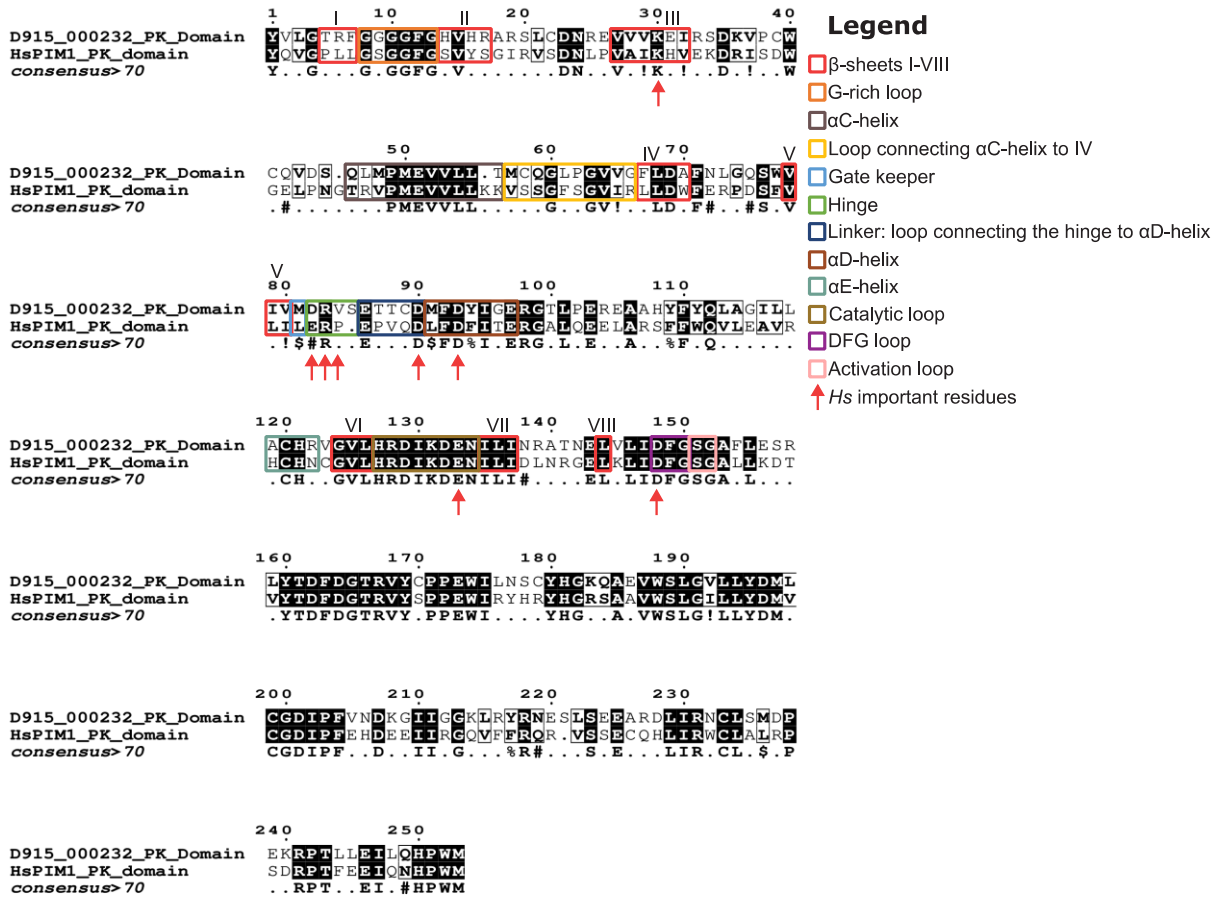


**Figure 3.11: Multiple sequence alignment of Hs and Fh PIM kinase domains**. The alignment was created using the EMBL-Clustal Omega alignment webserver (210) and visualised using the ESPript v3.2 webserver (279), and later the figure was compiled in Inkscape (25). Additional information described in the legend was retrieved from the 4JX7 and 5O13 (RCSB PBD IDs) stored on the KLIFS webserver (275). The important Hs residues depicted in the legends were taken from Heyder and colleagues (250). Conserved residues (*) are depicted with uppercase letters at the consensus>70 line below the aligned residues as well as with a black background; conserved substituted residues (:) are depicted with a white background box as well as (.) at the consensus>70 line below the aligned residues; semi-conserved substituted residues (.) are depicted with (.) instead of the residue as well as below the residues in the consensus>70 line; the character '!' stands for I (Ile) or V (Val); the character '#' stands for N (Asn), D (Asp), Q (Gln), or E (Glu); the character '$' stands for L (Leu) or M (Met); and the character '%' stands for F (Phe) or Y (Tyr).

Additionally, I observed a significant substitution of the gatekeeper residue from Leu120 in HsPIM1 to Met128 in FhPIM kinase. Furthermore, I observed that in the linker loop connecting the hinge to the αD-helix, all residues from Pro125, Val126, and Gln127 (HsPIM1) to Thr134, Thr135, and Cys136 are notably semi-conserved substitutions in the *Fasciola* PIM kinase.

### 3.2.5 Molecular docking of MCCC library in the FhPIM kinase domain

Molecular docking is a computational simulation that predicts the optimum position (pose) and binding affinity of a small-molecule interacting within the active site of a target protein (280). This method was designed to efficiently and economically assess large chemical libraries, facilitating the prioritisation of the most effective inhibitors for NTDs before commencing expensive laboratory trials (172,281). By modelling these interactions, I can provide a structural foundation for the systematic design of pharmaceuticals targeting FhPIM.

To prepare the FhPIM kinase domain (from 39 to 350 amino acids long) for molecular docking, the protonation states of histidines were first virtually examined and were later changed to the following protonation states: 38 to HID, 41 to HIP, 61 to HIE, 63 to HIE, 155 to HIE, 168 to HIE, 174 to HID, 228 to HIP and 297 to HIE. I conducted two rounds of molecular docking, utilising two FhPIM kinase structures: the initial round employed the AlphaFold generated model, which was subsequently modified through homology modelling (SWISS-MODEL). The second round utilised the FhPIM model from AlphaFold database (AF-A0A4E0RYG3-F1-v6), which was subsequently modified using homology modelling (SWISS-MODEL) and followed by the TLDR webserver.

The managed chemical compound collection (MCCC) library from Nottingham functions as a curated repository of lead-likeness small-molecules intended to enable extensive target-based screening, consisting of approximately 85,000 compounds. Furthermore, the MCCC library follows Lipinski's "rule of five" (252,253). I conducted two rounds of molecular docking with the MCCC library employing two distinct ligand preparation methodologies: initially using Open Babel v3.1.1 (224) and subsequently utilising the Molecular Operating Environment (MOE) 2022 (255) platform. The rationale for employing two distinct ligand preparation approaches was that Open Babel generated some ligands with broken molecules and unusual protonated states across different molecules, resulting in a significant number of stranded donors that could not be salvaged through water molecules. The MOE automates the 3D protonation processes to ensure that ligands possess the appropriate bond lengths, angles, and electronic characteristics necessary for precise evaluation by the docking engine.

After performing two runs of molecular docking of the MCCC library using AutoDockVina (203,204), the top 500 ranked compounds from each run (a total of 1000 top-ranked compounds) were visualised and evaluated in PyMOL v3.1 (231).

The detailed evaluation criteria for selecting the interaction between the FhPIM kinase domain and the ligands are specified in section 2.2.5.5. The primary evaluation criteria are the absence of intramolecular clashes, no stranded hydrogen bond donor, and a reduced number of stranded hydrogen bond acceptor.

The SmartChemist webserver (236) was used to obtain information on the MCCC library ligand moieties using their Simplified Molecular Input Line Entry System (SMILES) specified in the supplementary tables 6.9 and 6.10.

In the following, the top five grade of the ligands and their docking poses from each of the docking runs are presented (in total ten ligands), while the remaining 24 ligands are displayed in supplementary figures 6.16 to 6.39. **Please note** that the top five ligands were initially selected to be illustrated in the following sections and the selection was based on their evaluation grades and, subsequently, on their ranks as determined by the script.

#### 3.2.5.1 First virtual screening round of the MCCC library in FhPIM kinase

Upon evaluating the 500 top-ranked compounds from the first virtual screening round, only 16 were found to have polar interactions satisfying the criteria within the FhPIM binding pocket. While none of these ligands reached the best score A, there were one classified as B+, five as B, and ten as B-. Details of these ligands, their rankings, and grades can be found in Table 14. This section describes only the top five ligands according to their grades, while the remaining ligands are further displayed in the supplementary figures (from 6.16 to 6.26). **Please note** that the top five ligands were initially selected based on their evaluation grades and subsequently on their ranks as determined by the script. All the rejected 484 compounds can be found in the supplementary table 6.13 of this thesis.

2D structures, SMILES, molecular weight, and molecular formula of the docked ligands are kept in the supplementary table 6.9.

**Table 14: List of the top 16 ligands identified from the first round of virtual screening**.

| Ligand name | AutoDock Vina generated energy (kcal/mol) | Ranking according to the script | Grade according to the evaluation criteria | Interacting residue in the FhPIM binding pocket with the ligand |
|---|---|---|---|---|
| NCC-00008538 | -10.9 | 9 | B- | **Lys77** and **Asp195** |
| NCC-00077290 | -10.9 | 10 | B- | **Lys77** and **Asp195** |
| NCC-00072436* | -10.7 | 15 | B | **Lys77**, Ser132, and **Asp195** |
| NCC-00032341 | -10.5 | 30 | B- | **Arg130**, Val131, and **Asp195** |
| NCC-00044825 | -10.3 | 71 | B- | **Arg130** and **Asp195** |
| NCC-00074481 | -10.2 | 94 | B- | **Arg130**, Glu133 and Thr135 |
| NCC-00009414 | -10.2 | 98 | B- | **Arg130**, Thr135, and **Asp137** |
| NCC-00044623 | -10.2 | 100 | B- | **Asp137** and **Glu180** |
| NCC-00061091* | -10.1 | 171 | B+ | **Lys77**, Ser132, and **Asp195** |
| NCC-00032141* | -10 | 188 | B | **Lys77**, Val131, Ser132, and **Asp137** |
| NCC-00057583 | -10 | 195 | B- | **Arg130**, **Lys178**, and **Asp195** |
| NCC-00032797* | -10 | 245 | B | **Lys178**, **Glu180**, and **Asp195** |
| NCC-00090515* | -9.9 | 288 | B | **Lys77**, Thr135, and **Asp137** |
| NCC-00015704 | -9.9 | 299 | B- | Gly56, **Arg130**, Glu133, Thr135, **Asp137**, and **Glu180** |
| NCC-00058509 | -9.8 | 420 | B- | **Lys77**, **Arg130**, Val131, **Asp137**, and **Asp195** |
| NCC-00032487 | -9.8 | 497 | B | **Lys77**, **Asp137**, and **Asp195** |

**Please note** that the bolded residues are conserved between Fh and Hs PIM kinases, and these residues are predicted to be significant for ligand binding in the HsPIM1. The molecular docking results of ligands denoted with (*) are illustrated in Fig. 3.12 to 3.16, while the remaining ligands are illustrated in supplementary figures 6.16 to 6.26.

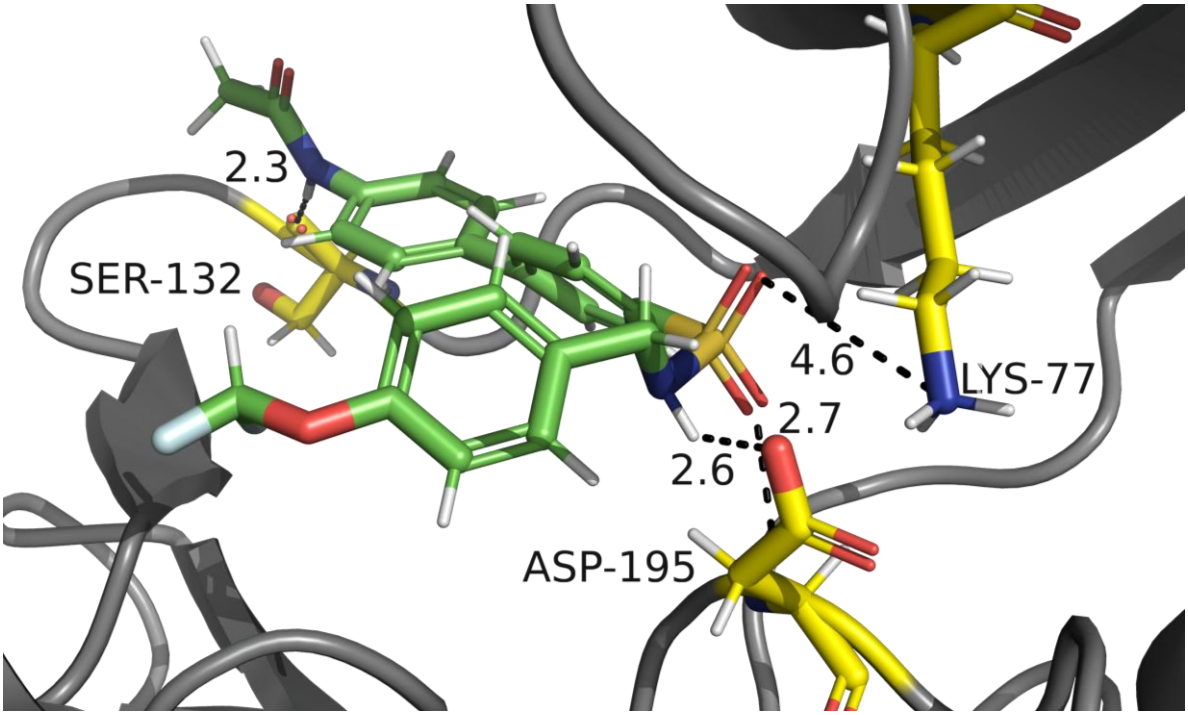


**Figure 3.12: Polar interactions of NCC-00072436** in the binding pocket of FhPIM kinase. NCC-00072436 (ligand) is displayed as sticks with green-coloured carbon atoms. The structure of FhPIM is illustrated as a cartoon in grey colour. The polar interactions are depicted as black dashed lines and their distances in angstroms (Å). Residues depicted in yellow colour are the polar interacting residues (Lys77, Ser132, and Asp195) in the binding pocket of FhPIM kinase. All nitrogen, oxygen, fluorine and sulphur atoms are in blue, red, palecyan, and yelloworange colours, respectively.

Based on the visual evaluation, I assigned the ligand NCC-00072436 a grade of B-, as it meets several criteria outlined in section 2.2.5.5 of this thesis. The ligand interacts with three important pharmacophores in the binding pocket of FhPIM kinase through multiple polar interactions. The most stable conformer out of 20 generated by AutoDock Vina exhibited a binding affinity of -10.7 kcal/mol. The DFG motif (Asp195), hinge region (Ser132), and VVVK motif (catalytic Lys77) are some of the essential pharmacophores depicted in the binding pocket of the FhPIM kinase (Fig. 3.12), as described in the previous section 3.2.4.

The ligand donates a hydrogen bond (H-bond) to the carboxylic acid side chain of Asp195 (2.7 Å). Furthermore, the ligand accepts an H-bond from the protein through the backbone nitrogen of Asp195 (2.6 Å) via the bridging sulphonamide moiety. The ligand also donates to the anionic carboxylate group of Ser132 (2.3 Å), another H-bond. The last contact with the protein occurs via a salt bridge between the ammonium group of Lys77 and the bridging sulphonamide moiety of the ligand (4.6 Å). Moreover, no other polar interactions were observed with the linker loop, the αD-helix, or the ribose pocket of the FhPIM kinase.

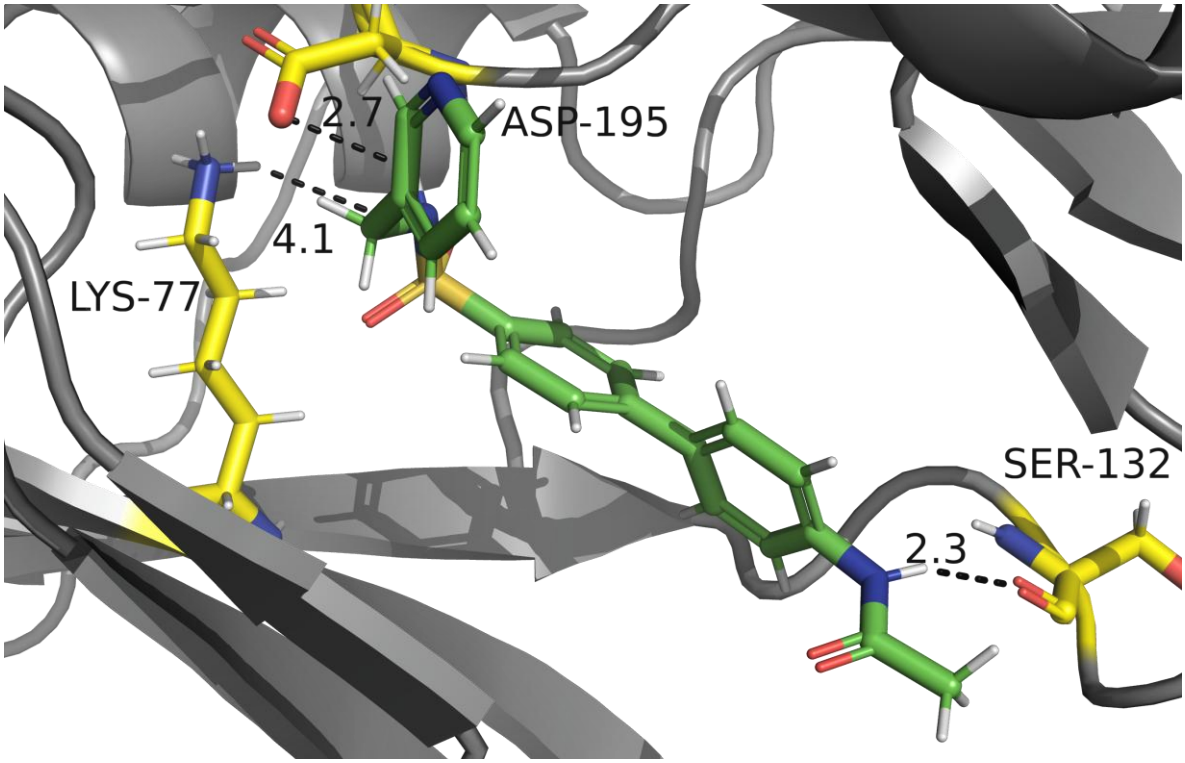


**Figure 3.13: Polar interactions of NCC-00061091** in the binding pocket of FhPIM kinase. NCC-00061091 (ligand) is displayed as sticks with green-coloured carbon atoms. The structure of FhPIM is illustrated as a cartoon in grey colour. The polar interactions are depicted as black dashed lines and their distances in angstroms (Å). Residues depicted in yellow colour are the polar interacting residues (Lys77, Ser132, and Asp195) in the binding pocket of FhPIM kinase. All nitrogen, oxygen, and sulphur atoms are in blue, red, and yelloworange colours, respectively.

After visual inspection, I assigned a grade of B+ to ligand NCC-00061091, as depicted in Fig. 3.13. At first glance, this ligand appears to be a structural homolog of the previous ligand (NCC-00072436), as it also incorporates a bridging sulphonamide moiety and establishes three polar interactions with the identical essential pharmacophores as the prior ligand (Asp195, Ser132, and Lys77). The most stable conformer exhibits a weaker binding affinity of -10.1 kcal/mol in comparison to the previous ligand. The most significant difference I observed is the varying H-bond distances, as this ligand establishes an acceptor H-bond with the ammonium group of Lys77 (4.1 Å) and forms a single donor H-bond with Asp195 (the carboxylic acid side chain) in the DFG motif (2.7 Å), instead of both acceptor and donor H-bonds. The last polar interaction is with Ser132, exhibiting an identical H-bond distance (2.3 Å) to that of the previous ligand.

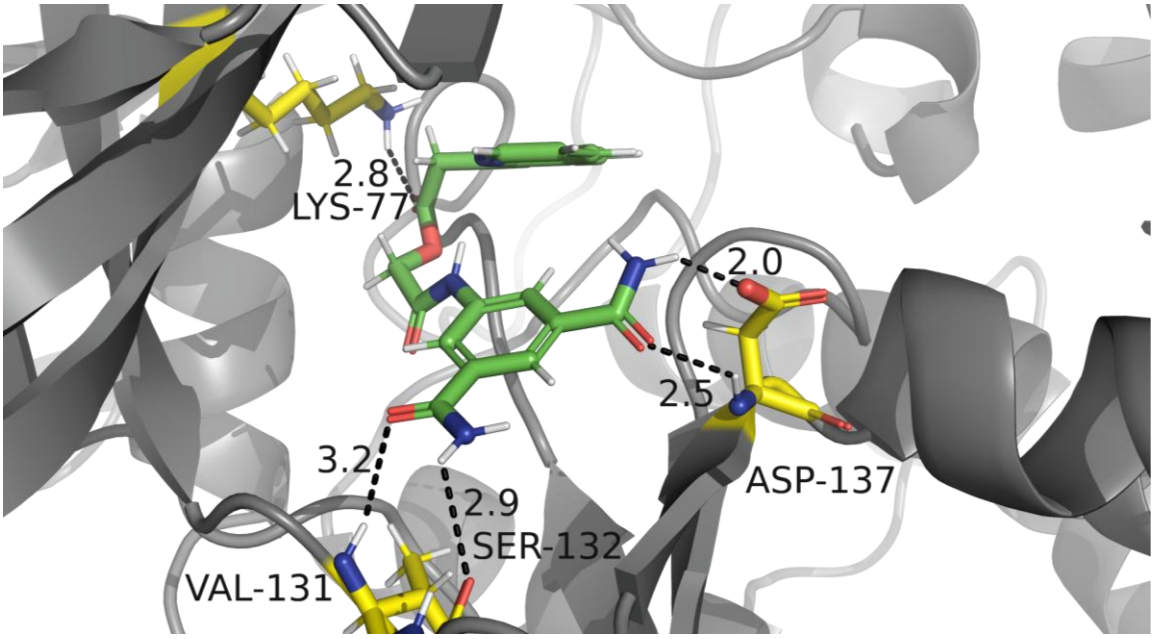


**Figure 3.14: Polar interactions of NCC-00032141** in the binding pocket of FhPIM kinase. NCC-00032141 (ligand) is displayed as sticks with green-coloured carbon atoms. The structure of FhPIM is illustrated as a cartoon in grey colour. The polar interactions are depicted as black dashed lines and their distances in angstroms (Å). Residues depicted in yellow colour are the polar interacting residues (Lys77, Val131, Ser132, and Asp137) in the binding pocket of FhPIM kinase. All nitrogen and oxygen atoms are in blue and red colours, respectively.

The ligand NCC-00032141 efficiently occupies the ATP-binding pocket of the FhPIM kinase (Fig. 3.14), demonstrating a binding affinity of -10 kcal/mol and demonstrating polar interactions with four essential pharmacophores: the linker loop connecting the hinge to the αD-helix (Asp137), the hinge region (Ser132 and Val131), and the VVVK motif (catalytic Lys77). I assigned this ligand a grade of B due to its ability to both donate and accept H-bonds from the protein through Asp137, facilitated by the C3 carboxamide group in the benzene-1,3,5-tricarboxamide moiety of the ligand (with H-bond distances of 2.0 Å and 2.5 Å, respectively). This ligand similarly donates and accepts H-bonds from the protein through the hinge region (Ser132 and Val131) via the C5 carboxamide group of the benzene-1,3,5-tricarboxamide moiety (with H-bond distances of 3.2 Å and 2.9 Å, respectively). The final contact with the protein occurs through a salt bridge formed between the ammonium group of Lys77 and the carbonyl portion of the linker ester to the terminal quinoline moiety of the ligand (2.8 Å). Furthermore, no significant H-bond was detected between Asp195 in the DFG motif and the ligand.

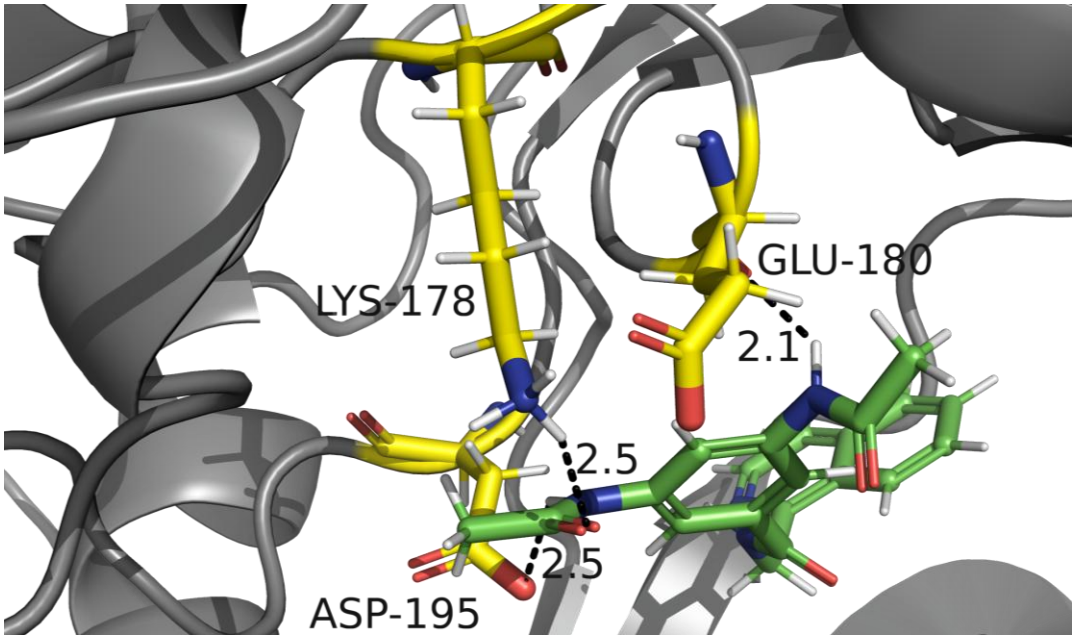


**Figure 3.15: Polar interactions of NCC-00032797** in the binding pocket of FhPIM kinase. NCC-00032797 (ligand) is displayed as sticks with green-coloured carbon atoms. The structure of FhPIM is illustrated as a cartoon in grey colour. The polar interactions are depicted as black dashed lines and their distances in angstroms (Å). Residues depicted in yellow colour are the polar interacting residues (Lys178, Glu180, and Asp195) in the binding pocket of FhPIM kinase. All nitrogen and oxygen atoms are in blue and red colours, respectively.

I assigned the ligand NCC-00032797 a grade of B, as it demonstrated three polar interactions (Fig. 3.15) within the binding pocket of FhPIM kinase, exhibiting a binding affinity of -10 kcal/mol. Among these three interactions, two occur within the catalytic loop region of the FhPIM binding pocket (Lys178 and Glu180), which are conserved in HsPIM1 kinase as Lys169 and Glu171. Bogusz and colleagues have shown that Lys169 in HsPIM1 is a part of the activation domain, along with Lys67, Glu89, Asn172, and Asp186, which are essential for the ATP-binding in HsPIM1 (197). Moreover, the aforementioned study also indicated that the Glu171 can interact with the Lys169, facilitating structural interactions within the binding pocket and influencing binding of inhibitors to the active site (197). Additionally, Asp128 and Glu171 form the ribose pocket within the binding pocket of HsPIM1 (282). Glu171 (conserved as Glu180 in FhPIM) constitutes a component of an acidic patch that is often in conjunction with Asp128 (conserved as Asp137 in FhPIM) within the ATP-binding pocket, establishing H-bonds with potent pan-PIM inhibitors (250,283,284).

The ligand features an H-bond donor to the backbone carbonyl atom of Glu180 (2.1 Å). Furthermore, the ligand constitutes another H-bond donation to the carboxylic acid side chain of Asp195 in the DFG motif (2.5 Å). The last polar interaction occurs between the ammonium group of Lys178 and the carbonyl part of the C3 carboxamide group of the terminal at the benzene-1,3,5-tricarboxamide moiety of the ligand, forming a salt bridge (2.5 Å).

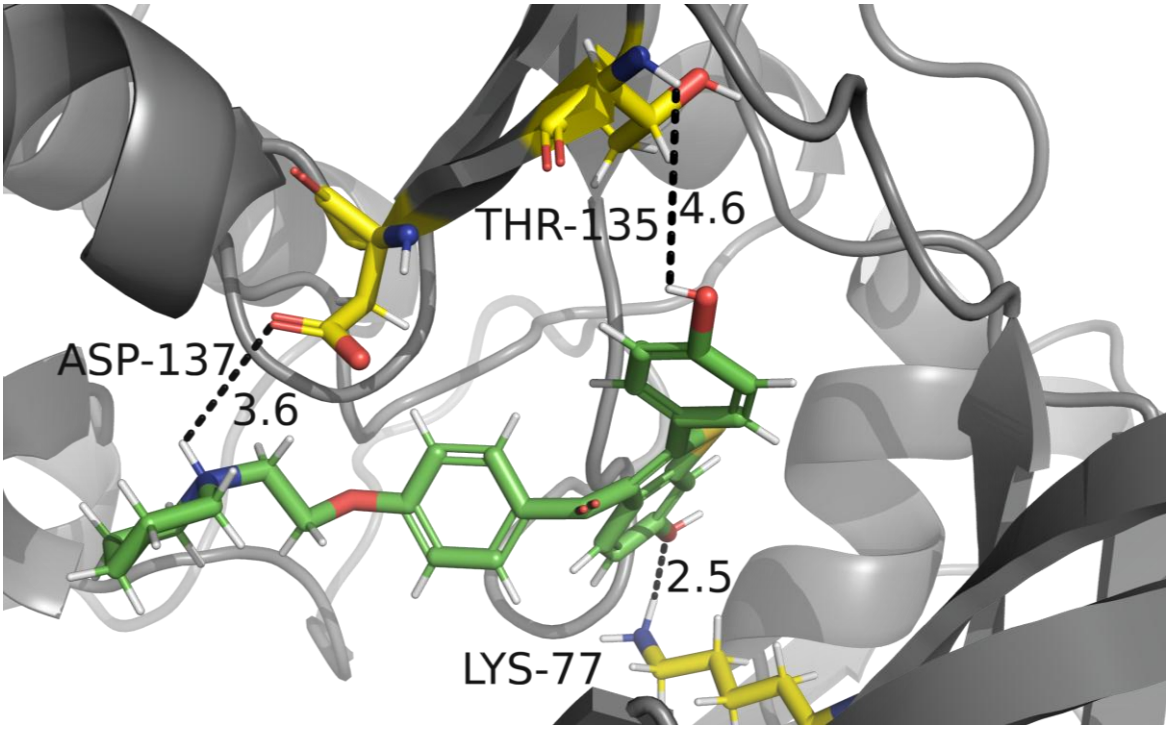


**Figure 3.16: Polar interactions of NCC-00090515** in the binding pocket of FhPIM kinase. NCC-00090515 (ligand) is displayed as sticks with green-coloured carbon atoms. The structure of FhPIM is illustrated as a cartoon in grey colour. The polar interactions are depicted as black dashed lines and their distances in angstroms (Å). Residues depicted in yellow colour are the polar interacting residues (Lys77, Thr135, and Asp137) in the binding pocket of FhPIM kinase. All nitrogen, oxygen, and sulphur atoms are in blue, red, and yelloworange colours, respectively.

The ligand NCC-00090515 exhibited a binding affinity of -9.9 kcal/mol, establishing three polar interactions (Fig. 3.16) with different pharmacophores located in the linker loop connecting the hinge to the αD-helix (Thr135 and Asp137) and VVVK motif (catalytic Lys77). I assessed this docked ligand as B. In HsPIM1, Val126 (substituted by Thr135 in FhPIM) creates a distinct hydrophobic pocket, with the side chains of Val126 contributing substantial hydrophobic interactions with the inhibitor, and the presence of Val126 imparts selectivity to the inhibitor, as it is substituted in other PIM kinases (197).

In the first polar interaction, the ligand donates an H-bond through the tertiary amine of the piperidine moiety to the side chain carboxylate group of the Asp137 in the αD-helix loop (3.6 Å). Despite the distance exceeding the average range of H-bonds, the ligand accepts an H-bond from the protein through the α-amino group of Thr135 (4.6 Å). The last polar interaction occurs between the ammonium group of catalytic Lys77 and the 4-hydroxyl group of the 2-(4-hydroxyphenyl)benzo(b)thiophen-6-ol moiety of the ligand, wherein the protein donates an H-bond to the ligand and forms a salt bridge (2.5 Å).

### 3.2.5.2 Second virtual screening round of the MCCC library in FhPIM kinase

Upon evaluating the second virtual screening round of the 500 top-ranked compounds, only 18 were found to have polar interactions satisfying the criteria within the FhPIM binding pocket. While none of these ligands reached the best score A, there were one classified as A-, four as B+, six as B, and seven as B-. Details of these ligands, their rankings, and grades can be found in Table 15. This section describes only the top five ligands according to their grades, while the remaining ligands are further displayed in the supplementary figures (from 6.27 to 6.39). **Please note** that the top five ligands were initially selected based on their evaluation grades and subsequently on their ranks as determined by the script. All the rejected 482 compounds can be found in the supplementary table 6.14 of this thesis.

2D structures, SMILES, molecular weight, and molecular formula of the docked ligands are kept in the supplementary table 6.10.

**Table 15: List of the top 18 ligands identified from the second round of virtual screening**.

| Ligand name | AutoDock Vina generated energy (kcal/mol) | Ranking according to the script | Grade according to the evaluation criteria | Interacting residue in the FhPIM binding pocket with the ligand |
|---|---|---|---|---|
| NCC-00011396* | -10.5 | 52 | B+ | **Lys77**, Val131, and **Asp195** |
| NCC-00082673* | -10.4 | 86 | B+ | **Glu180** and **Asp195** |
| NCC-00089972 | -10.3 | 111 | B- | **Lys77**, **Arg130**, and **Asp195** |
| NCC-00069794 | -10.3 | 115 | B- | **Glu180** and **Asp195** |
| NCC-00090340 | -10.3 | 134 | B | Val131 |
| NCC-00071469* | -10.2 | 188 | A- | Asp129, Val131, **Glu180**, and **Asp195** |
| NCC-00007132 | -10.2 | 214 | B- | **Lys77**, Asp129, Val131, and **Asp195** |
| NCC-00059610 | -10.2 | 220 | B | Val131 and Thr135 |
| NCC-00064956 | -10.2 | 221 | B | **Lys77**, Val131, and **Asp195** |
| NCC-00087073* | -10.1 | 240 | B+ | Asp129, **Arg130**, and Val131 |
| NCC-00081502 | -10.1 | 250 | B- | **Lys77**, Arg130, and **Asp195** |
| NCC-00009498* | -10.1 | 281 | B+ | **Lys77**, Asp129, Val131, and **Asp195** |
| NCC-00059926 | -10.1 | 308 | B- | Asp129, Val131, and **Asp195** |

| | | | | |
|---|---|---|---|---|
| NCC-00046881 | -10.1 | 318 | B | Val131 and Ser132 |
| NCC-00030002 | -10.1 | 340 | B- | Lys77, Val131, and **Asp195** |
| NCC-00019088 | -10 | 394 | B- | Val131 and **Asp137** |
| NCC-00082340 | -10 | 472 | B | **Arg130** and Ser132 |
| NCC-00016401 | -10 | 485 | B | Asp129 and Val131 |

**Please note** that the bolded residues are conserved between Fh and Hs PIM kinases, and these residues are predicted to be significant for ligand binding in the HsPIM1. The ligands denoted with (*) are illustrated in Fig. 3.17 to 3.21, while the remaining ligands are illustrated in supplementary figures 6.27 to 6.39.

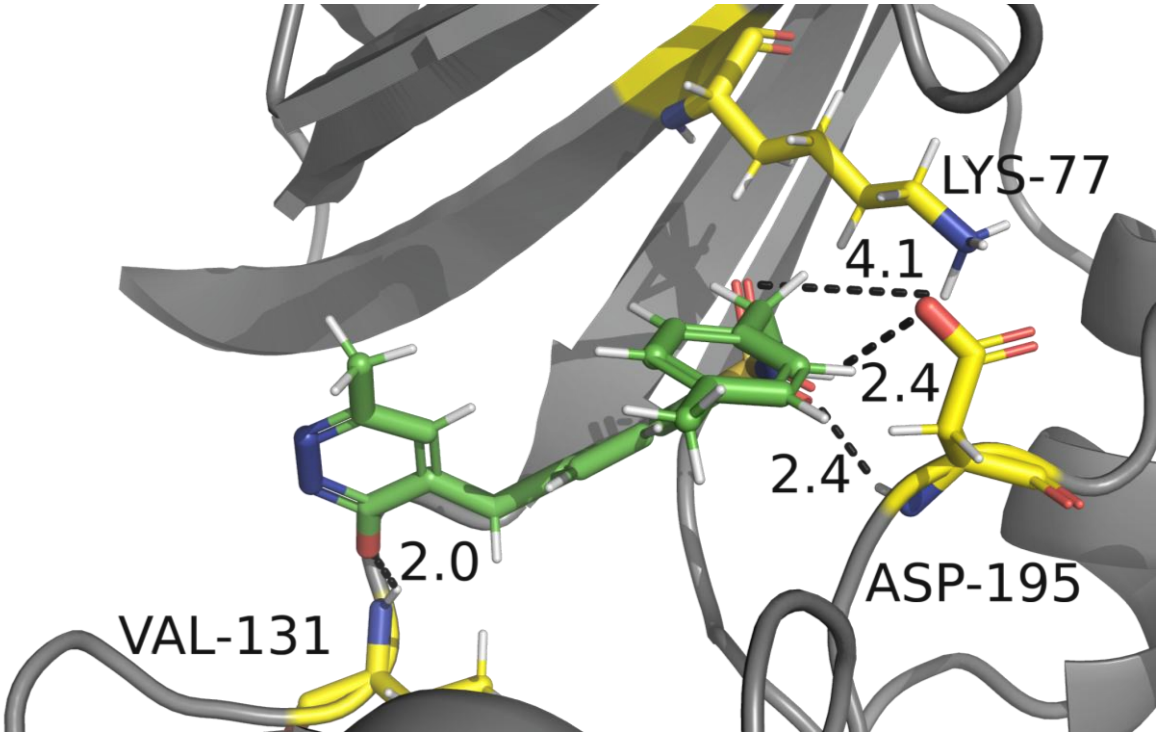


**Figure 3.17: Polar interactions of NCC-00011396** in the binding pocket of FhPIM kinase. NCC-00011396 (ligand) is displayed as sticks in green-coloured carbon atoms. The structure of FhPIM is illustrated as a cartoon with grey colour. The polar interactions are depicted as black dashed lines and their distances in angstroms (Å). Residues depicted in yellow colour are the polar interacting residues (Lys77, Val131, and Asp195) in the binding pocket of FhPIM kinase. All nitrogen, oxygen, and sulphur atoms are in blue, red, and yelloworange colours, respectively.

The ligand (NCC-00011396) effectively occupies the ATP-binding pocket of the FhPIM kinase (Fig. 3.17), exhibiting a binding affinity of -10.5 kcal/mol and forming polar interactions with three critical pharmacophores: the DFG motif (Asp195), the hinge region (Val131), and the VVVK motif (catalytic Lys77). I assigned this ligand a grade of B+ due to the capacity of the bridging sulphonamide moiety to establish three salt bridges with the protein: the first with the ammonium group of Lys77 (4.1 Å), the second and third with the negatively charged carboxylate group and the backbone nitrogen of Asp195 (2.4 Å each). The last interaction occurs between the α-amino group of Val131 on the protein's hinge region and the hydroxyl

group of the terminal 3-hydroxypyridazine moiety of the ligand, establishing an acceptor H-bond to the ligand (2.0 Å).

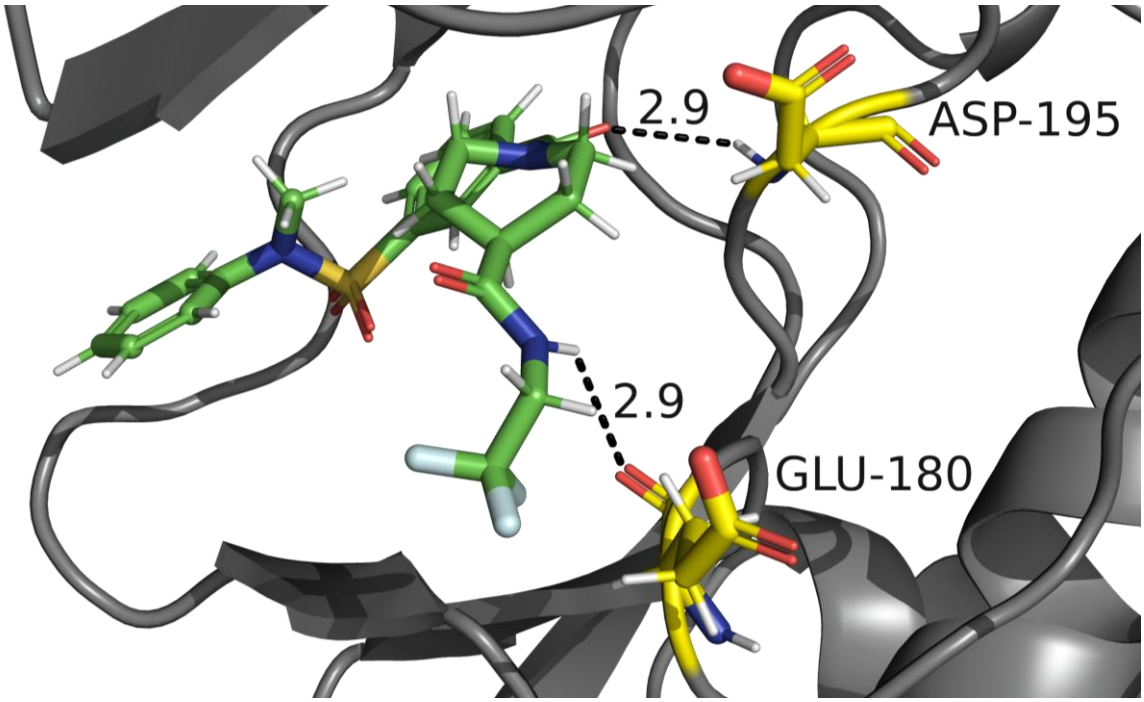


**Figure 3.18: Polar interactions of NCC-00082673** in the binding pocket of FhPIM kinase. NCC-00082673 (ligand) is displayed as sticks with green-coloured carbon atoms. The structure of FhPIM is illustrated as a cartoon in grey colour. The polar interactions are depicted as black dashed lines and their distances in angstroms (Å). Residues depicted in yellow colour are the polar interacting residues (Glu180 and Asp195) in the binding pocket of FhPIM kinase. All nitrogen, oxygen, fluorine and sulphur atoms are in blue, red, palecyan, and yelloworange colours, respectively.

The result regarding the ligand NCC-00082673 highlights the polar interactions of Asp195 and Glu180, within the binding pocket of FhPIM kinase (Fig. 3.18). I assigned this ligand a grade of B+ because it establishes two polar interactions with the DFG motif (Asp195) and the ribose pocket (Glu180), exhibiting a binding affinity of -10.4 kcal/mol. The ligand accepts an H-bond from the backbone nitrogen of the Asp195 in the protein (2.9 Å). Additionally, the ligand donates an H-bond to the backbone carbonyl oxygen of Glu180 (2.9 Å).

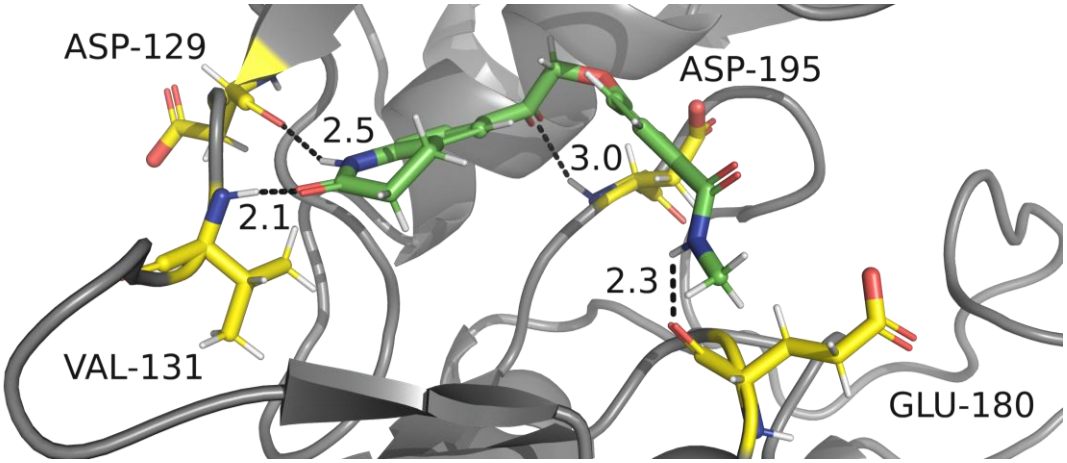


**Figure 3.19: Polar interactions of NCC-00071469** in the binding pocket of FhPIM kinase. NCC-00071469 (ligand) is displayed as sticks with green-coloured carbon atoms. The structure of FhPIM is illustrated as a cartoon in grey colour. The polar interactions are depicted as black dashed lines and their distances in angstroms (Å). Residues depicted in yellow colour are the polar interacting residues (Asp129, Val131, Glu180, and Asp195) in the binding pocket of FhPIM kinase. All nitrogen and oxygen atoms are in blue and red colours, respectively.

AutoDock Vina estimated a binding affinity of -10.2 kcal/mol for ligand NCC-00071469, indicating multiple polar interactions (Fig. 3.19). Polar interactions were predicted with the hinge region (Asp129 and Val 131), the ribose pocket (Glu180), and the DFG motif (Asp195). I assigned this ligand a grade of A- due to its adequate placement in the catalytic cleft of the binding pocket of FhPIM. Bissantz and colleagues described the average typical distance of non-covalent interactions in their study (256), and this ligand represents the average distance for all the polar interactions.

The carboxamide part of the ligand's 3,4-dihydro-2(1H)-quinolinone moiety forms both acceptor and donor H-bonds within the hinge region (Asp129 and Val131) of the protein, exhibiting distances of 2.5 Å and 2.1 Å, respectively. Moreover, within the ribose pocket, the ligand donates an H-bond to the protein through the backbone carbonyl oxygen of Glu180 (2.3 Å). Additionally, the DFG motif enables the ligand to accept an H-bond via the backbone nitrogen of the Asp195 (3.0 Å).

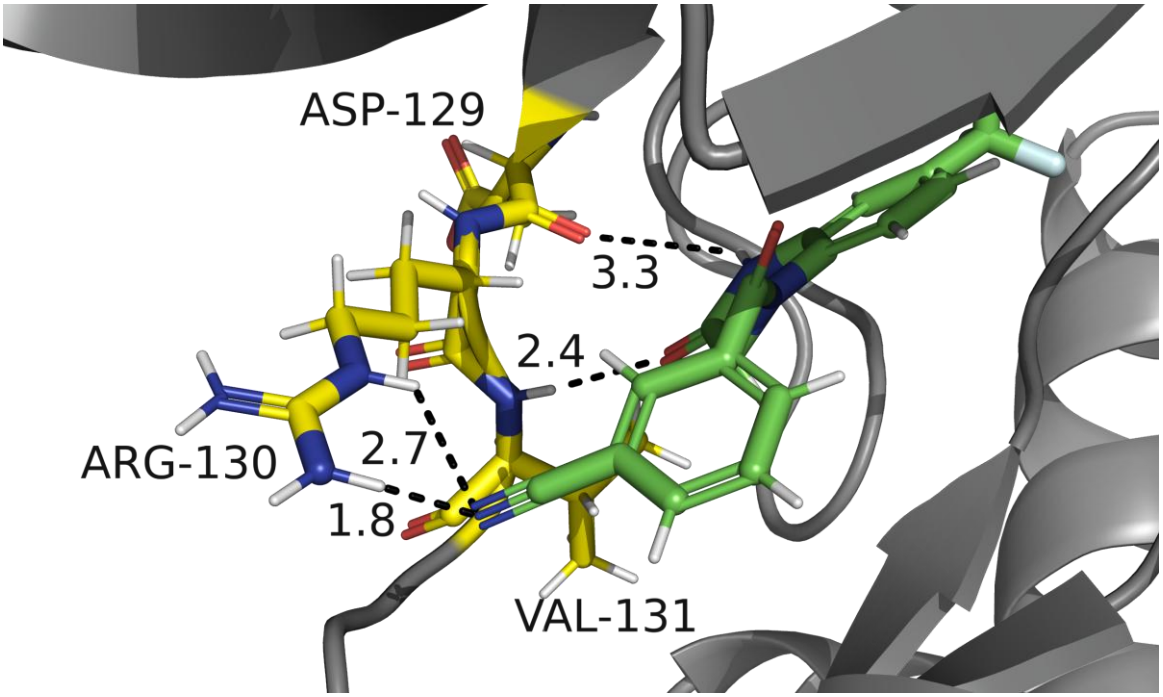


**Figure 3.20: Polar interactions of NCC-00087073** in the binding pocket of FhPIM kinase. NCC-00087073 (ligand) is displayed as sticks with green-coloured carbon atoms. The structure of FhPIM is illustrated as a cartoon in grey colour. The polar interactions are depicted as black dashed lines and their distances in angstroms (Å). Residues depicted in yellow colour are the polar interacting residues (Asp129, Arg130, and Val131) in the binding pocket of FhPIM kinase. All nitrogen, oxygen, and fluorine atoms are in blue, red, and palecyan colours, respectively.

The ligand NCC-00087073 establishes polar interactions (Fig. 3.20) within the hinge region (Val131, Arg130, and Asp129) of the FhPIM binding pocket, exhibiting a binding affinity of -10.1 kcal/mol; therefore, I assigned this ligand a grade of B+. The hinge region consists of Glu121, Arg122, and Pro123 in HsPIM1; however, only Arg130 is conserved, while the other two residues are substituted with Asp129 and Val131 in the FhPIM. The ligand donates an H-bond to the protein via the 3,4-dihydro-1H-quinoxalin-2-one moiety to the negatively charged carboxylate side chain of Asp 129 (3.3 Å). Additionally, the protein donates two H-bonds from the positively charged guanidino group of Arg130 to the negatively charged terminal cyanide group of the ligand (1.8 and 2.7 Å, respectively). The last polar interaction was predicted between the α-amino group of the Val131 of the protein and the hydroxyl part of the carbonyl group of the 3,4-dihydro-1H-quinoxalin-2-one moiety, forming an acceptor H-bond to the ligand (2.4 Å).

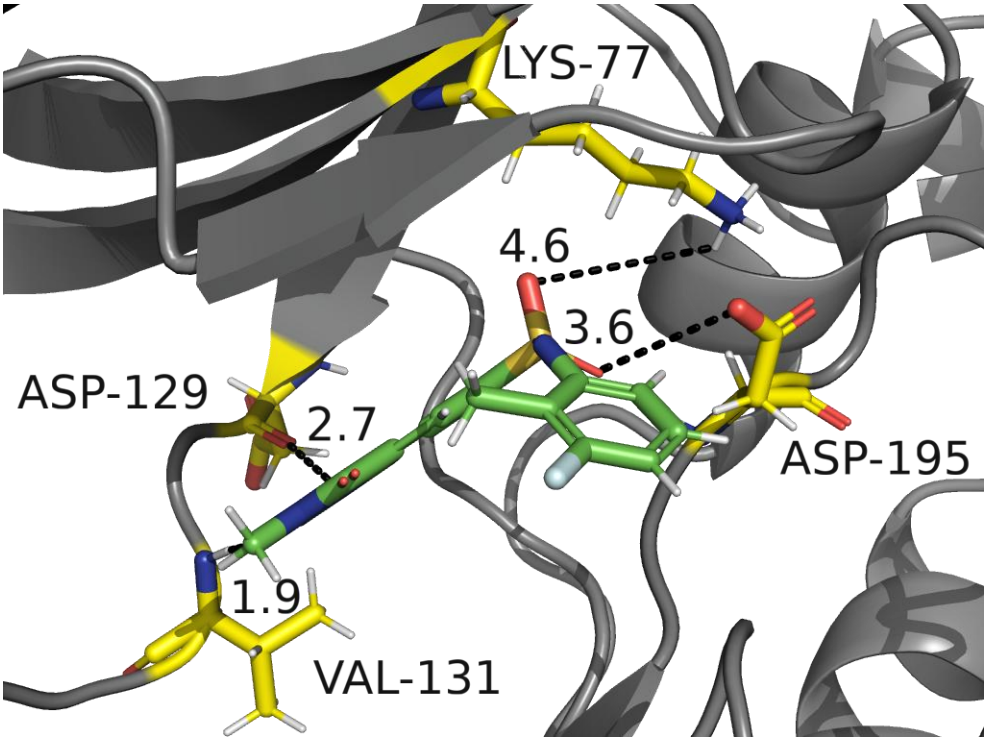


**Figure 3.21: Polar interactions of NCC-00009498** in the binding pocket of FhPIM kinase. NCC-00009498 (ligand) is displayed as sticks with green-coloured carbon atoms. The structure of FhPIM is illustrated as a cartoon in grey colour. The polar interactions are depicted as black dashed lines and their distances in angstroms (Å). Residues depicted in yellow colour are the polar interacting residues (Lys77, Asp129, Val131, and Asp195) in the binding pocket of FhPIM kinase. All nitrogen, oxygen, fluorine, and sulphur atoms are in blue, red, palecyan, and yelloworange colours, respectively.

The ligand NCC-00009498 effectively occupies the ATP-binding pocket of the FhPIM kinase (Fig. 3.21), exhibiting a binding affinity of -10.1 kcal/mol and forming polar interactions with four essential pharmacophores: the DFG motif (Asp195), the hinge region (Val131 and Asp129), and the VVVK motif (catalytic Lys77). I assigned this ligand a grade of B+ owing to its capability to form two salt bridges via the bridging sulphonamide moiety: the first with the carboxylic acid side chain of Asp195 and the second with the ammonium group of Lys77 in the protein, exhibiting H-bonds of 3.6 Å and 4.6 Å, respectively. Additionally, in the hinge region of the protein, this ligand accepts an H-bond from the α-amino group of Val131 (1.9 Å) and donates an H-bond to the negatively charged carboxylate side chain of Asp129 (2.7 Å).

The docking results verify that the identified scaffolds exhibit the structural complementarity necessary to effectively occupy the active binding site of the FhPIM kinase. The primary polar interactions identified between the binding pocket of FhPIM kinase and the ligands included Lys77, Asp129, Arg130, Val131, Ser132, Asp137, Glu180, and Asp195. These findings provide a compelling structural basis for advancing these candidates into subsequent *in vitro* and, thereafter, *in vivo* bioassays to validate their effectiveness as novel treatments for the neglected tropical disease fasciolosis.

# 4. Discussion

The significant consequences of helminth infections on the health of humans and animals call for critical intervention strategies. Despite the implementation of various measures, consisting of enhanced sanitation and environmental parasite removal, the primary strategy for controlling helminthic infections is still the administration of a limited selection of anthelmintics, given the lack of commercial vaccines for most helminths (285,286). The management of cestodes and trematodes often depends on some classes of anthelmintics, with two primary classes of anthelmintics drugs being isoquinolines, such as praziquantel (PZQ) (287), and benzimidazoles (BZs), such as TCBZ (288). BZs are a versatile group of heterocyclic aromatic compounds containing a fused benzene nucleus and an imidazole ring (289). BZs revolutionised the management of trematodes by specifically targeting the cytoskeleton of the parasite and binding to the β-tubulin to inhibit microtubule formation (59,290). Among the trematodes is the common liver fluke, a causative agent of fasciolosis, which is a neglected pathogen.

## 4.1 The rationale for the protein kinase research in the liver fluke

Liver flukes cause annual costs in the billions of USD, resulting in devastating economic losses in the livestock sector and affecting the human population. TCBZ is an excellent pharmaceutical option for managing fasciolosis; however, long-standing challenges associated with mass drug administration (MDA) initiatives to mitigate the spread of fasciolosis have necessitated persistent efforts to discover novel compounds and characterise new drug targets. This approach has become especially vital due to the emergence and spread of TCBZ resistance across various continents. Recently, a substantial flock of approximately 300 sheep in Germany succumbed to the liver flukes due to TCBZ resistance (66). One way to tackle the resistance aspect is to identify new intervention strategies through drug discovery that target different biological key choke points in the liver flukes. PKs are especially interesting from the pharmaceutical point of view for drug development, being the second most pursued group of targeted enzymes after GPCRs (106). They are also crucial in combating parasitic helminths due to their significant roles in essential biological processes, such as cell cycle, migration, signal transduction, and apoptosis (145,147). Several small-molecule inhibitors derived from oncological research provide novel prospects for drug repurposing, potentially expediting the drug development process significantly (144). This thesis aimed to delineate a kinome for the common liver fluke (*F. hepatica*), to assess the hypothesis of repurposing PK inhibitors against the liver flukes, and to evaluate the utilisation of the MCCC library for drug discovery to identify novel compounds targeting the liver flukes.

### 4.1.1 The kinome landscape of the liver fluke

This thesis offers a comprehensive annotation and analysis of the PKs in *F. hepatica*, initially identifying 212 PKs, which were subsequently extended to 245 PKs through manual curation. The kinome constitutes approximately 2.15% of the 11,217 protein-coding genes in the genome of the liver fluke, a proportion consistent with that of other studied kinomes across various species (130). The liver fluke kinome exhibits a symmetrical distribution of PK groups comparable to other studied trematodes, such as *S. mansoni*, *S. haematobium*, etc. The annotated kinome encompasses all nine major ePK groups and a single aPK group. I would emphasise the AGC, CAMK, CMGC, and TK groups, as various members from these groups are recognised as significant for the development of blood flukes and have been further discussed as anti-parasitic targets (137,145,291).

The CMGC group, with 43 members, has emerged as the largest PK group, comprising 17.84% of PKs within the kinome of liver flukes. This group is significant for its diverse roles in cell cycle control, transcriptional regulation, splicing, and other processes (292,293), and it encompasses several MAPKs, including all the major members of the MAPK signalling cascade. The MAPK signalling pathways are essential for regulating various cellular processes, including proliferation, differentiation, and apoptosis (293,294). In *S. mansoni*, RNAi-mediated functional analysis of the MAPK family members (SmJNK and SmERK1) elucidated their role in the development of adult blood flukes (137,159). As the fundamental signalling cascades, such as the MAPK signalling pathways, are evolutionarily conserved, I identified that the PK domain of FhJNK (D915_006573) exhibits a PK domain identity of 69.7% and a PK domain similarity of 81.5% to SmJNK (Smp_172240), indicating a high degree of functional conservation among these divergent trematode species. Additionally, FhERK1 homologs (D915_001614 and D915_006871) demonstrate a PK domain identity of 83.1% and 90.7%, along with PK domain similarity of 83% and 92.4%, respectively to SmERK1 homologs (Smp_047900 and Smp_142050). This high degree of conservation encourages the assessment of JNK and ERK1 in the future as potential pan-trematode drug targets effective against both *S. mansoni* and *F. hepatica*. Recently, Moreira and colleagues have focused on MAPK in *S. mansoni*, emphasising the significance of SmJNK, SmERK, Smp38, and SmFES to identify compounds having similar drug-like properties to PZQ, thereby enhancing the *in vitro* screening of compounds obtained from docking-based virtual screening (145,146). This methodology may prove advantageous, and the significant sequence similarity could facilitate the identification of novel broad-spectrum fasciolicidal agents targeting both parasite groups.

The CAMK is another significant group of PKs, comprising 38 members and accounting for 15.77% of PK in the liver fluke kinome. It plays a crucial part in calcium signalling in various

helminths, influencing neural activity, fecundity, motility, muscle contraction, host attachment and a range of homeostatic roles (161,259,295). Consequently, it is vital for immediate survival within the host and has been suggested as a potential anthelmintic target (161,259). In *S. mansoni*, CAMKs exhibited increased expression and activity after administration of the paralysis-inducing drug PZQ, while RNAi diminished motility and viability, which indicated that CAMKII is implicated in the motor function and motility of the worms (296,297). *F. hepatica* and *S. mansoni* are digenetic trematodes that exhibit significant evolutionary and molecular conservation. Given that CAMKII inhibition in *S. mansoni* has demonstrated a reduction in motor function, it is reasonable to hypothesise that a similar effect might be achieved by targeting CAMKs in *F. hepatica*.

The AGC-PK group, characterised by a 14.11% of PKs, is significant for its pivotal downstream function in T-cell receptor (TCR) and B-cell antigen receptor (BCR) signalling (298), as well as its involvement in the negative regulation of MAPK signalling (299). Additionally, AGC serves as a mechanistic regulator of critical functions in cell signalling, metabolism, growth, migration, stress responses, muscle contraction, and focal adhesion in vertebrates (300–302). In *S. mansoni*, PKCs are linked to the neural mass, excretory vesicle, ridge cyton, tegument, and germinal cells in schistosomula and miracidium, indicating potential roles in larval transformation (303–305). In adult blood flukes, they are involved in neuromuscular functions related to movement, attachment, pairing, and egg release (306,307). In liver flukes, the roles of PKCs in body contraction and muscle function have been delineated (308). Furthermore, I identified four PKC isoforms (D915_000022, D915_002081, D915_006901, and D915_008611) in liver flukes, based on their homology to *S. mansoni*, *S. haematobium*, and *H. sapiens*. The spatial transcriptomics data, generated by Gramberg and colleagues at our institute, indicate that one of the four PKC isoforms (D915_006901) was expressed across the tegument, whereas the others were linked to the Mehlis' gland, ovary and testis (171). The single-cell RNA-seq dataset, generated by Puckelwaldt and colleagues at our institute, identified the same PKC isoform within the neuromuscular elf5+ cluster (274,309). Moreover, the same PKC isoform exhibits a PK domain identity of 83.1% and similarity of 91.8% to a homologue in *S. mansoni* (Smp_128480). This suggests a future investigation of PKC in liver flukes as a viable target due to its role as a critical survival mechanism in the host, mediated through the tegument and the neuromuscular elf5+ cluster.

The TK group, with 33 members, constitutes a significant fraction of the kinome of the liver fluke, representing 13.69% of PKs and comprising 18 receptor tyrosine kinases (RTKs) and 15 cytoplasmic tyrosine kinases (CTKs). RTKs constitute a class of membrane-bound receptors that react to external stimuli, including growth factors, and serve as signal transducers, facilitating intercellular communication (310,311). RTKs phosphorylate tyrosine

residues on essential intracellular substrate proteins, thereby affecting cell fate, including proliferation, migration and differentiation (312). RTKs, among others, influence the members of the aforementioned MAPK signalling cascade members (313,314). A unique RTK family for invertebrates comprises venus kinase receptors (VKRs), which have a TK domain analogous to that of insulin receptors (166). In *S. mansoni*, VKRs play a pivotal role in reproduction, oocyte maturation, and larval development (164,167,168). Gene silencing demonstrated the involvement of SmVKR1 and SmVKR2 in gametogenesis (137,167). Furthermore, SmVKR1 (Smp_019790) was found to interact with a multi-kinase complex consisting of the Src-kinase SmTK3 and the Src/Abl hybrid-kinase SmTK6, which controls cell growth, mitosis, and cytoskeleton functions (315). The phylogenetic analysis of *S. mansoni* and *F. hepatica* revealed that FhPK_0008 and D915_003706 are homologous to SmVKR1 and SmVKR2, respectively, demonstrating 78.2 and 78.4% identity and 86.6 and 88% similarity in their PK domains compared to the schistosomal kinase domains. Although kinase research in *F. hepatica* is still nascent relative to schistosomes, it will be intriguing to compare functional aspects of PK signalling between these two evolutionary related, yet distinct, parasites. A notable distinction lies in their reproduction strategies; liver flukes are hermaphrodites, while blood flukes are dioecious parasites. Moreover, this promotes a thorough investigation of RTKs in liver flukes concerning their potential as drug targets, given that RTKs activate the stress signalling MAPK cascade (316).

Although 245 PKs in the liver fluke kinome have been identified and annotated *in silico*, a valuable milestone, subsequent steps necessitate thorough functional validation and characterisation. Consequently, future investigations should use tools such as RNA interference (RNAi) and enzyme activity assays to validate the essentiality of these PKs, thereby identifying a lucrative drug target for developing an effective intervention strategy for controlling fasciolosis.

### 4.1.2 Constraints in the annotation of the liver fluke genome

A significant bottleneck in the comprehensive kinome curation of a non-model organism is the quality of the genome annotation. The Benchmarking Universal Single-Copy Orthologs (BUSCO) score, which delineates genome annotation quality (317), for *F. hepatica* (PRJNA179522), was only 71%, consisting of 1.2% duplicated genes and a significant gene fragmentation frequency of 9.5%, with approximately 18% of genes remaining unannotated. The significant fragmentation and the existence of unannotated genes restrict the comprehensive curation of a species' kinome. Kinannote is a proficient programme that identifies and classifies PKs within the selected species, achieving a sensitivity rate of 70% and a precision rate of 80% (218). Kinnanote operates by establishing stochastic models,

including Hidden Markov Models (HMMs) and Position-Specific Scoring Matrices (PSSM), to identify and classify PKs (218). This method alone is inadequate for an accurate curation of the kinome of *F. hepatica*. The absence of annotation necessitates the integration of Kinannote with complementary resources, including orthology- (226) or phylogenetic-based (318) methodologies, InterProScan (217), and the bash wrapper script FastProteinExonerate (129,319). This script uses protein sequences from closely related species of the target species to fill sequence gaps and predict genes with novel information, thereby greatly enhancing the curation of the kinome for this parasite. Kinnanote surpasses other PK-identifying programs, such as Kinomer (320), which exhibits reduced sensitivity for detecting PKs in helminths. Another significant limitation of Kinomer is its capability to classify PKs only at the group level, with a severely restricted ability to classify them into families, and subsequent classification into subfamilies is unfeasible (129).

If the constraints in the annotation of PKs can be subsided by substantially enhancing putative gene models and advancing the long-read sequencing technologies, this would resolve genomic regions that could not be assembled, thereby significantly diminishing the necessity for sequence curation (129). Enhancements in functional annotation may also be realised through a systems biology approach, which integrates transcriptomic, proteomic, and metabolomic data into the annotation process, thereby minimising fragmented and duplicate genes and further annotating the unannotated genes. Nevertheless, the newly generated, diverse, and extensive datasets must be integrated into the existing data. Therefore, experimental investigations should be followed by technical enhancements and expansions. Ultimately, creating an enhanced dataset that enables a more comprehensive annotation of the genome, thereby reducing the number of undiscovered PKs.

### 4.1.3 Comparison of the selected trematode and human kinomes

A primary hurdle in anthelmintic development is attaining selective toxicity, eradicating the parasite without harming the host. The comparative bioinformatics analysis yields actionable insights into this challenge and suggests potential prioritisation of therapeutic targets that are adequately divergent, maybe even parasite-specific, while balancing the efficacy and toxicity of anthelmintic compounds to the host (149).

The kinome of the liver fluke is significantly smaller than the human kinome, yet it exhibits the same number of PKs within their respective groups, comparable to the other trematode kinomes of *S. mansoni* and *S. haematobium*. The comparative analysis of these kinomes indicated homologous PKs present in the trematode kinomes but are absent in the human kinome. As the kinome landscape sub-chapter previously described, the biological functions of invertebrate-specific VKRs are crucial for lifecycle development by regulating oocyte

maturation and larval development. Their absence in humans renders them viable drug targets for fascioliasis. Furthermore, multiple PKs exhibiting a low level of sequence similarity between the liver fluke and humans were identified. Particularly, the genes exhibiting minimal sequence similarity to the human PKs are within the Other PK group (D915_009688, D915_007882, FhPK_0018, D915_007720, D915_004111, D915_004720, D915_008234, D915_005804, and D915_006868). Both types may be advantageous for drug designs focused on minimising side effects. Such drugs are less prone to induce off-target effects in humans because humans either do not have the target or the orthologous protein has a too divergent structure, which impedes the binding of the drug molecule. Additionally, in the comparison of the three trematode kinomes, only four genes were recognised as *Fasciola*-specific (D915_005277, D915_001682, FhPK_0027, and FhPK_0018). The STE11 family member D915_005277 might be exclusive to the order Plagiorchiida, whereas the CAMK family member D915_001682 might be exclusive to the Fasciolidae family. The CMGC group member FhPK_0027 exhibited no distinct schistosome homologs but seemed to be associated with cyclin-dependent kinases (Smp_080730 and D915_002458), as determined by whole protein sequences and phylogenetic analyses. At last, FhPK_0018 (Other PK group) lacked a schistosome homolog, potentially indicating an incomplete kinase sequence, which has likely hindered the homology search. Subsequent work should concentrate on the functional characterisation of these *Fasciola*- and parasite-specific PKs, in order to identify genes critical for liver fluke survival. The recombinant expression of these PKs could facilitate high-throughput screenings of compound libraries to discover potential inhibitors.

The repurposing of existing PK inhibitors, used in the treatment of human diseases, represents an alternative intervention strategy previously studied in anthelmintic research (83,134,144,145,291,321,322). To refine the list of potential inhibitors, researchers can employ the repurposing of FDA-approved drugs to reliably identify the orthologous “chokepoints”, which are essential enzymes within the biochemical network of the pathogen that, when blocked or inhibited, impede its survival. By focusing on these chokepoints that are orthologous to known human drug targets, we can use *in silico* molecular docking to determine whether these FDA-approved drugs will effectively bind to and inhibit the essential parasite proteins, leading to the discovery of new intervention methods. Furthermore, a KEGG-based functional annotation of the liver fluke PKs indicated that of 110 KEGG-annotated PKs, 24.54% were linked to human orthologs involved in cancer pathways. Numerous PK inhibitors with anti-cancer activity are recognised for their ability to inhibit the differentiation of cancer stem cells (116,323). In trematodes, neoblasts represent the unique group of proliferating somatic stem cells, acting as the key components for tissue regeneration and the substantial reproductive capacity distinctive of these parasites (324–326). Thus, interfering with the

maintenance or differentiation of these totipotent cells offers a strategic method to undermine the survival of the parasite and impede egg production, which is predominantly responsible for clinical pathology (324–326). Therefore, it would be advantageous to assess pertinent PK inhibitors *in vitro* for their ability to impede the growth, development, and/or viability of liver flukes. The repurposing of FDA-approved small-molecule PK inhibitors could substantially decrease the time required to develop a new control strategy for fascioliasis. Simultaneously targeting a protein in both the pathogen and the host poses the risk of adverse side effects in the host, but choosing inhibitors that have successfully undergone clinical trials and have demonstrated their safety can mitigate this risk. Clinical trials offer a significant safety margin, as acute or short-term dosing is required for anthelmintic treatment, whereas oncological treatments usually necessitate prolonged and continuous administration of doses over months or years (145). This substantial decrease in the treatment duration restricts systemic exposure and effectively eradicates the risk of cumulative toxicity (145). Furthermore, subtle structural variations in the ATP-binding pockets of parasite PKs can be utilised to achieve significant selectivity, thereby ensuring a viable therapeutic window even when targeting highly conserved orthologs (145).

Subsequent to the completion of the kinome analysis for this thesis, an alternative study adopted a different methodology to generate the kinome of the liver fluke. The research conducted by McCusker and colleagues identified a total of 271 putative PKs (170), whereas the kinome analysis presented in this thesis identified 245 PKs. McCusker and colleagues utilised two genomes of *F. hepatica*: one was published by the University of Liverpool, comprising approximately 14,628 genes (5), and the second genome was published by Washington University, which contains 11,217 genes (273). The difference in the number of PKs may be related to the methodology, as using basic homology searches (such as BLAST or basic HMMER) with more flexible statistical thresholds (higher E-values) will encompass a higher number of sequences. This approach inherently encompasses distantly related PKs, aPKs, and possibly some false positives or pseudokinases that lack catalytic activity yet maintain structural similarity. In contrast, I employed stricter cutoffs, excluding partial or fragmented gene models and manually validating domain integrity for the curation of the kinome in this thesis, resulting in a high-confidence dataset. By employing this conservative methodology, the final number was inherently reduced as borderline sequences were systematically eliminated.

## 4.2 Therapeutic and druggability potential of PKs in liver flukes

Recent advancements in bioinformatic kinome mining have enabled the comprehensive mapping of the PKs of multiple helminths. PKs regulate essential helminth-specific processes, including tegumental maintenance, neoblast proliferation, and reproductive organ development, through the phosphorylation of serine, threonine, and tyrosine residues (156,327). The objective of the kinome curation is to identify druggable targets, as PKs and their inhibitors, which are considered as “magic bullets”, a concept established by Paul Ehrlich (328) that functions as central nodes of eukaryotic signal transduction (104). Traditional drug discovery typically employs a “one target, one model” strategy; however, in parasitology, such an approach often results in resistance development. A polypharmacological therapeutic approach that typically involves the design of molecules capable of binding to multiple targets, thereby enhancing efficacy and diminishing the potential of drug resistance in comparison to conventional highly selective therapies (329). Consequently, multi-target kinase inhibition (MKI) originated from the premise of polypharmacology and serves as an effective method whereby a single inhibitor can concurrently inhibit multiple PKs. The synergistic impact of MKI enhances its efficacy and prevents the emergence of resistant strains (330).

A more profound understanding of PKs and their architectures may enable innovative strategies for targeting them with small-molecule PK inhibitors, aimed at overcoming resistance and achieving greater target selectivity. This task was once deemed arduous, if not impossible, because of the high intracellular ATP concentration that a small-molecule PK inhibitor must navigate, along with the complexities associate with the precise targeting of a structurally conserved ATP recognition site (105).

### 4.2.1 Application of drug and target repurposing for fasciolicidal drugs

The absence of investments from private companies in the development of *de novo* compounds for NTDs often results in their neglect, as the high cost associated with the development and screening of compounds deters pharmaceutical companies; therefore, academic laboratories frequently conduct the drug discovery process. In an attempt to minimise cost and time, numerous academic groups employ various “repurposing” strategies, including “drug repurposing” and “target repurposing” (321). The “drug repurposing” strategy frequently employs approved compounds to discover alternatives that were not initially sanctioned, thereby minimising research duration and pharmaceutical development expenses (321,331). The “target repurposing” commences with finding homologs of certain targets, with the goal of initialising drug design for these targets based on approved compounds or clinical options that are equivalent to it.

As numerous PKs of species that are causative vectors for NTDs share the catalytic domain of human kinases, such types of inhibition can be further exploited. A comparative structure activity-relationship (SAR) analysis of PK inhibitors indicated that kinases exhibiting over 60% of sequence similarity generally demonstrate high SAR similarity with their inhibitors (332). Given the significant conservation of PKs between the host and the animal, targeting the specific PK of interest and determining the necessary dosage for the expulsion of the liver fluke may represent a viable strategy for treating fasciolosis; therefore, extensive *in vitro* and *in vivo* research would still be essential to establish their safety for veterinary application. The FDA has presently approved 94 PK inhibitors, with numerous additional candidates in clinical trials (125–127). This may illustrate the possibility of repurposing PK inhibitors to provide innovative therapeutic strategies for fascioliasis. This potential is further emphasised by previous works at our institute, which demonstrated the *in vitro* efficacy of imatinib (a TK inhibitor approved by the FDA as Gleevec® for gastrointestinal stromal tumours (333)) against all pathogenic life stages of the liver fluke, alongside a significant transcriptional expression of the presumed target ABL1 in those stages (169,334).

In addition to functioning as significant drug targets, the PKs may provide essential information about the mechanisms underlying anthelmintic resistance. Resistance to TCBZ is hypothesised to be multifactorial, potentially involving modified drug uptake, increased efflux mechanisms, and metabolic detoxification (63). If TCBZ induces cellular stress that the parasite mitigates via hyperactive signalling of specific stress-activated protein kinases (SAPKs), primarily JNK, p38, and MAPKKKs such as MLK, TAK1, TAO, ABL, CK1, etc. (335), then targeting these PKs could theoretically resensitise resistant flukes to TCBZ. A "combination therapy" strategy, employing a PK inhibitor to disrupt the resistance mechanisms of the parasite in conjunction with a conventional anthelmintic, may signify a highly viable avenue for forthcoming *in vitro* and *in vivo* research.

### 4.2.2 Evaluation of small-molecule PK inhibitors on liver flukes

To evaluate the hypothesis that repurposing of existing small-molecule PK inhibitors constitutes an effective strategy for discovering new fasciolicidal compounds, I chose four suitable inhibitors. I focused on vandetanib, foretinib, and TK-IN-1, as these are anti-cancer compounds that target multiple RTKs. Cancer is frequently linked to the dysregulation of RTKs, such as EGFRs, FGFRs, or VEGFRs; consequently, numerous RTK-targeting inhibitors have been designed for biomedical application (310,312). Ruboxistaurin, the fourth inhibitor, is a selective inhibitor of PKCβ1 (IC50 = 4.7 nM) and PKCβ2 (IC50 = 5.9 nM) (262), but at elevated levels, it also inhibits PDK1, which plays a role in the insulin-like growth factor signalling pathway (336). The *in vitro* evaluation demonstrated significant efficacy of ruboxistaurin and

vandetanib against both immature and adult liver flukes, comparable to or exceeding that of TCBZ at identical concentrations *in vitro*.

Ruboxistaurin, a selective PKC inhibitor (262,337), has undergone phase III clinical trials for diabetic neuropathy treatment, exhibiting safety and oral bioavailability in patients (338). The drug is predominantly eliminated through bile, with its metabolites maintaining activity against PKCβ, indicating that parasites would encounter the active substance *in vivo* (339). The binding site for ruboxistaurin between human PKCβ and the PKCβ of the liver fluke is highly conserved, rendering it a compelling potential for treating liver fluke infections. A spatial transcriptomics study by Gramberg and colleagues at our institute demonstrated that PKCβ is primarily expressed near the surface of the fluke. Additionally, a concentration of 50 µM ruboxistaurin resulted in the lethality of adult liver flukes within 72 hours of culture (171), a dosage comparable to the *in vitro* potent dosage of TCBZ and within the range of maximum bile concentrations of TCBZ metabolites in sheep (340,341). I have now expanded this discovery and can demonstrate significant efficacy against immature liver flukes. Given a tolerated dose of 800 mg/kg body weight in rats (342), subsequent studies may evaluate the efficacy of ruboxistaurin in diminishing fluke burden *in vivo*.

Given the significant *in vitro* efficacy of ruboxistaurin and its previously reported pharmacokinetic characteristics (338,343,344), it may represent a compelling inhibitor for subsequent investigations, including *in vivo* assay assessment in infected animals. Alternatively, investigators can employ structure-based drug design using *in silico* modelling of the liver fluke's PKCβ, followed by molecular docking of virtual compound libraries, to identify compounds with enhanced binding affinity to the liver fluke PKCβ enzyme.

The multi-RTK inhibitor vandetanib was nearly as effective as ruboxistaurin. The enhanced efficacy of vandetanib compared to the other two multi-RTK inhibitors may have been attributed to several factors, including the critical role of the PK targeted by vandetanib in liver fluke survival or by varying uptake mechanisms within the parasites. Vandetanib is an inhibitor of human VEGFR-2 (KDR) (345) and also inhibits two other growth factors, EGFR and FGFR (265). Vandetanib substantially diminished the survival rate of the liver flukes in the *in vitro* assays. The lack of VEGFR receptors in invertebrates (346) indicates that metazoan VEGFR, PDGFR, and FGFR share a common RTK ancestor in their evolutionary lineage (347). A gene duplication event resulted in the emergence of FGFR and VEGFR/PDGFR-like genes. Consequently, FGFR is the sole representative among invertebrates, including the liver flukes. Vandetanib is an FDA-approved compound for the treatment of thyroid cancer and exhibits exceptional oral bioavailability (268,269,348–350). Moreover, Gustafson and colleagues reported a preclinical tissue distribution profile revealing that vandetanib significantly

bioaccumulates in the liver tissue of the host, attaining concentrations up to 212 µg/g (approximately 450 µM) subsequent to standard oral administration (349). The *in vitro* screening revealed in this thesis that vandetanib induced lethal effects on immature flukes at a concentration of 50 µM. Furthermore, a single dose of 400 mg/kg body weight of vandetanib mitigated the fluke burden by 48% in the *S. mansoni*-infected mice model (322). Additionally, a pharmacokinetic study conducted by Weil and colleagues following phase III clinical trials of vandetanib noted the substantial accumulation of vandetanib concentrations in the liver and bile, which considerably exceed systemic plasma levels (351). This significant biliary accumulation is highly beneficial for the *in vivo* efficacy against liver flukes, as the immature flukes would migrate to the liver and mature into adult flukes, subsequently residing in the bile ducts of the host and being exposed to the persistent, high-dose accumulation of vandetanib. The notable fasciolicidal activity observed in the *in vitro* assay supports the evaluation of vandetanib as another potential inhibitor for *in vivo* investigation targeting liver flukes. Given that vandetanib is a multi-RTK inhibitor, it is pertinent to identify which targeted PKs are essential for the liver fluke and to evaluate the cellular downstream effects of their inhibition in the liver flukes. This insight may illuminate more effective methods to eradicate the parasite.

All four inhibitors assessed against liver flukes were anticipated to exhibit efficacy against a related trematode, *S. haematobium*, according to a prior *in silico* analysis of its kinome (135). The significance of these inhibitors' target for parasite survival was indicated by lethal knock-out phenotypes in model organisms and their association to unique biological chokepoints in critical pathways (135,155). While the antiparasitic efficacy of the proposed inhibitors has not been experimentally evaluated against *S. haematobium*, this would be a compelling avenue for future investigation, as I observed *in vitro* efficacy for a few inhibitors against liver flukes. Prospective inhibitors may subsequently be validated via enzyme activity assays and *in vivo* inhibitor screenings.

## 4.3 Harnessing PIM kinase for its fasciolicidal properties

The scarcity of fasciolicidal compounds necessitate the development of new drugs against fascioliasis. Fortunately, the identification of new drug targets is relatively straight forward due to the readily accessible availability of transcriptomic data of the common liver fluke.

Several PIM kinase inhibitors have recently been examined for their anthelmintic efficacy against various helminths, including *E. multilocularis*, *A. ceylanicum*, and *T. muris* (272,352). Both the studies examined the pan-PIM kinase inhibitors CX-6258 and SGI-1776. Koike and colleagues reported adverse *in vitro* effects of CX-6258 and SGI-1776 on *Echinococcus* primary cells, along with a deterioration in the structural integrity of the parasite metacestode vesicles upon treatment with 10 µM (272). Banas and colleagues reported a

substantial decrease in worm burden by 61% and a further reduction in faecal egg counts by 86% in *T. muris*-infected mice (352). Following the concept of anthelmintic activity outlined in both studies, I examined the efficacy of the pan-PIM kinase inhibitors *in vitro* against immature and adult liver flukes, observing significant reduction in motility within 72 h of culture at a concentration of 50 µM. The evaluation of both inhibitors against liver flukes demonstrated the proof of concept that PIM kinase is crucial for the survival of the parasite. This motivated me to investigate FhPIM kinase as a target for discovering additional compounds that may exhibit potential fasciolicidal properties.

A subsequent literature review indicated that the pan-PIM inhibitors, CX-6258 and SGI-1776, target not only PIM kinases but also FLT3, MYLK4, and HASPIN in humans (195,196,198). The whole protein sequence analysis of D915_006326 in *F. hepatica* identified it as a homolog of HsFLT3, exhibiting 23.23% sequence identity and 40.12% sequence similarity. Moreover, the PK domain analysis of D915_003545 identified it as a homologue of MYLK4 (smooth muscle myosin light chain kinase: HGNC id 7590), exhibiting 55.9% sequence identity and 76.6% sequence similarity. Additionally, with the PK domain analysis, two homologues of HsHASPINs were identified (D915_006868 and D915_008234), exhibiting 29.6% and 26.8% sequence identity, along with 42.2% and 39.3% sequence similarity, respectively. Melms and colleagues demonstrated the off-target effects of CX-6258 and SGI-1776 on HsHASPINs, suggesting that the significant effects of CX-6258 and SGI-1776 may arise not only from their affinity for FhPIM but also for FhHASPINs. However, this hypothesis will be investigated in a separate independent research study in the future, as it is beyond the scope of this thesis.

### 4.3.1 Information mining of *Fasciola* Pim kinase

The reduction in motility of liver flukes prompted a comprehensive investigation of PIM kinase for fasciolicidal properties. Consequently, I acquired the gene expression, single-cell RNAseq, and spatial transcriptomics data generated by my colleagues at the institute (171,274,309). The significant increase in expression levels immediately after excystment, followed by a reversion to pre-excystment levels during the immature stage, aligns with the upregulation of PIM kinase during cell proliferation event in liver flukes, as the rate of cellular replication event peaks in the flukes post-excystment (353) and further escalates upon reaching sexual maturity.

The single-cell RNAseq data revealed the expression of FhPIM kinase in the ovaries, further substantiating the assertion that the expression levels rise after sexual maturity. The spatial transcriptomics data also indicated that expression occurs not only in ovaries but also in the parenchyma, tegument, gut, and sparsely in the uterus, thereby further supporting the hypothesis that PIM expression in liver flukes increases upon attending the adult stage of their

life cycle. Single-cell RNAseq and spatial transcriptomics described the expression of PIM kinase in oocyte, tegument, parenchyma, and uterus during cellular replication events, as PIM kinases are mainly associated with the cell cycle and are typically active during the G and S phases of the cell cycle (182).

The constructed phylogenetic tree of PIM kinases (Fig. 3.9) across various species distinctly groups them into vertebrates and invertebrates with high nodal support value (100%). The invertebrate clade of flatworms in the phylogenetic tree of PIM kinases is further divided into trematodes, cestodes, and planarians. Upon meticulous inspection of the trematode clade, the *F. hepatica* PIM kinase organised itself within the clade of the liver fluke, with the adjacent group comprising the clade of the blood fluke (comprising *S. mansoni*, *S. haematobium*, *S. japonicum*, and *T. regenti*), which aligns with the expectation that liver flukes are evolutionarily closer to blood flukes. Moreover, the cestode clade (including *E. multilocularis* and *E. granulosus*) is positioned adjacent to the trematode, exhibiting a 100% nodal support value, indicating a closer evolutionary relationship to trematodes. Furthermore, Koike and colleagues have examined PIM kinase for its anti-parasitic properties in *E. multilocularis* (272) and suggested EmPIM kinase as a viable target for the treatment of alveolar echinococcosis. This outcome prompted me to explore FhPIM kinase as a potential drug target for the treatment of fasciolosis with fasciolicidal properties.

The multiple sequence alignment along with KLIFS domain architecture of the Hs and Fh PIM kinase domains revealed two distinct differences between the domains. The first is the “gatekeeper” residue in HsPIM1 kinase, Leu120, while FhPIM kinase contains a hydrophobic Met128 as the gatekeeper residue (354,355). Leu and Met are both bulky, nonpolar, and aliphatic amino acids; however, methionine possesses a longer, unbranched side chain, whereas Leu features a branched side chain at the beta-carbon (354,356). The gatekeeper is deeply integrated within the PKs, regulating access to a deeper hydrophobic pocket, where PK inhibitors can exert their effects by binding (355). Mutations to the gatekeeper residue obstruct the entry of the drug, diminishing its efficacy and fostering PK inhibitor resistance (355). Consequently, the gatekeeper of the FhPIM kinase can facilitate the deeper penetration of the ligand into the hydrophobic pocket or its more ready rotation, a characteristic constrained by the inflexible Leu in HsPIM1, while also containing a sulphur atom. The sulphur atom is highly polarised and can engage in S-aromatic interactions or even weak H-bonds (356), which branching Leu cannot provide. This occurrence of a Met serving as a gatekeeper in the liver flukes, in contrast to Leu in HsPIM1, highlights the exploitable conformational plasticity of PKs and the development of selective inhibitors (357–359). Additionally, I observed another distinct difference between the PIM kinase domains in the hinge region, a shift from the rigid HsPIM1 Glu121-Arg122-Pro123 motif to a longer, more flexible Asp129-Arg130-

Val131-Ser132 motif, indicating a significant topological modification in the hinge region (111,116). The positioning and conformation of proline (Pro123) in HsPim1 preclude the interaction of ligands with residues apart from Glu121, which represents the canonical hinge-ATP interaction, providing its backbone carbonyl as an H-bond acceptor (250). This four-residue hinge likely contributes to the high structural flexibility of the binding pocket of FhPIM kinase, making it an ideal target for diverse compound libraries during virtual docking, as the entry gate to the ATP-binding pocket is physically broader and deeper in FhPIM kinase compared to HsPIM1. The increased flexibility and polar characteristics (contributed by Ser in FhPIM kinase) permit a wider array of pharmacophores to potentially develop stable H-bond networks that are sterically or electronically unfavourable in the HsPIM1 ATP-binding pocket, thereby significantly enhancing the therapeutic range while minimising the off-target effects and toxicity of PK inhibitors in the hosts.

### 4.3.2 Insights on the druggability of FhPIM from homologs modelling

In contrast to conventional commercial compound libraries that frequently emphasise "drug-like" complexity, the managed chemical compound collection (MCCC) library from the university of Nottingham is deliberately curated for lead-likeness (360). This distinction is essential; maintaining a low pairwise Tanimoto coefficient score facilitates the exploration of the protein's pocket, thereby enhancing the chances of discovering new scaffolds (360). By employing compounds with lower molecular weights and lipophilicity, the chemical diversity in the library ensures that the resulting "hits" possess sufficient chemical headspace for subsequent medicinal chemistry optimisation while conforming to Lipinski's "rule of five" in later iterations (252,253). The rules are as follows: (1) fewer than 5 H-bond donors, (2) fewer than 10 H-bond acceptors, (3) a molecular weight of less than 500 Daltons, and (4) a calculated octanol-water partition coefficient (Clog P) not exceeding 5 (252,253). In drug discovery, there should be no more than one infraction of the aforementioned rules concerning the lead-likeness of a compound.

In the absence of a crystalline 3D structure of FhPIM, I initially generated a high-fidelity 3D structure employing advanced predictive models like AlphaFold2 (199–201) and SWISS-MODEL (238) using HsPIM1 (RCSB PDB ID: 4JX7) as a reference. The 3D structure of the FhPIM kinase was trimmed to retain the PIM kinase domain, and the molecular docking was conducted within this domain, which exhibited a 49.4% identity between Hs and Fh PIM kinase domains (246). For reliable homology modelling of PKs, the percentage identity should surpass the gold standard of more than 30% of the whole sequence identity (361–364). This threshold serves as a crucial empirical threshold, indicating overall conservation of the 3D fold of the protein (361). Below 30% sequence identity, a protein may exhibit a similar sequence

yet possess an entirely different structure, undermining the reliability of the protein backbone (364–366).

Subsequent to predicting the crystalline structure of FhPIM, I identified the protonation states of histidines. This step is essential prior to docking, as it determines the H-bond network, electrostatic environment, and ligand-binding mode within the ATP-binding site (367). Histidines typically exist in three different states: two that are neutral (HID and HIE) and one that is protonated (HIP) (368,369). The neutral states can function as either an H-bond donor or acceptor, depending upon which nitrogen is protonated, while the protonated state solely functions as an H-bond donor (369,370). Moreover, histidine residues predominantly occupy the hinge region and catalytic loop region in PKs, significantly affecting the binding of ATP-competitive inhibitors and regulating their conformational flexibility (367).

The majority of PIM kinase inhibitors reported in the protein data bank (PDB) target Lys67 and establish further interactions with Asp128 and/or Glu171, either directly or via water mediation (250,283). Another set of interactions in HsPIM1 involves Lys67, Glu121, and Asp128, which are crucial for the discovery of pan-PIM kinase inhibitors in HsPIM1, HsPIM2, and HsPIM3 (282).

As previously outlined, Met, substituted as the gatekeeper in liver fluke PIM kinase, establishes a more plausible hydrophobic boundary, and its side chain flexibility enables it to reposition itself, thereby facilitating accessibility to the hydrophobic pocket (327,354,356,371). Furthermore, the hinge region serves as the axis for the conformational transition between the active and inactive states of PKs, while flexibility promotes canonical ATP-binding and PK activation (111,250,282). Selective toxicity may be achieved by designing a ligand to fill the extra space provided by the flexible FhPIM hinge or the flexible Met gatekeeper. Within the human host, that same compound would encounter steric hindrance due to molecular overcrowding, impeding its effective binding to the HsPIM1.

The back pocket in HsPIM1 comprises the residues Lys67 and Glu89; thus, it is plausible to assume that Lys77 and Glu98 in FhPIM kinase will similarly constitute the back pocket, as these residues are conserved between Hs and Fh PIM kinases. The VAIK motif is significant due to the presence of the catalytic Lys67 in HsPIM1 (VVVK motif, with Lys77 conserved in FhPIM), which engages with the inhibitor in an “ATP-competitive” manner (372) and establishes ligand interactions essential for anchoring and stabilising the α and β phosphate groups of a bound ATP-molecule (373,374). The carboxylate side chain of Glu89 is adjacent to the ammonium group of Lys67, which facilitates the positioning of Lys67 within the binding pocket of HsPIM1 (373). Designing a ligand that targets Lys77 within the VVVK motif of FhPIM

kinase can competitively inhibit ATP, thereby blocking the energy transfer necessary for activating its signalling pathway in the common liver fluke.

Hayder and colleagues indicated that the ribose pocket in HsPIM1 is constituted by Asp128 and Glu171 (250), both of which are conserved in FhPIM kinase as Asp137 and Glu180. Therefore, it is plausible to assume that these residues similarly form the ribose pocket in FhPIM kinase as in HsPIM1. The targeting of residues at the specificity surface (Asp128, Asp131, and Glu171) is considered less prevalent; however, staurosporine has demonstrated the ability to bind in an ATP-mimetic manner to the hinge and Asp128 through its methylamino group (375). A HITS- and structure-guided optimisation study yielded highly effective inhibitors that targeted the hinge region, Lys67 and Asp128 in HsPIM1 using short yet rigid chain linkers between ring groups (282,283). A recent optimisation study of diamino pyrazoles indicated PIM kinase inhibition by targeting residues adjacent to the specificity surface (376). Their findings indicate that the requirements for rigidity on the hinge region of the binding pocket may be less critical on the lysine side, allowing for some flexibility in shape complementarity and, therefore, in the targeting of less conserved or solvent-exposed residues in this region (374,376). Given that all the aforementioned residues are conserved in FhPIM kinase, I hypothesise that if a ligand binds to the same residues in FhPIM kinase, then the effects of the ligand might be similar to the inhibition of HsPIM1 and obstruct the signalling pathways of PIM kinase in liver flukes during the cellular replication event.

The side chain of Asp in the DFG motif interacts with magnesium ions adjacent to the ATP unit (373). The conformation of the DFG motif in HsPIM1 is characterised as being “in loop”, representing the active state of this motif (111,116,377). The Asp in the DFG motif is a conserved catalytic residue that chelates magnesium, positioning the phosphates for phosphotransfer (378–380). The magnesium ion-binding motif is a component of a crucial regulatory structural element, the activation segment, which activates the PKs; other components include a short β9-strand, the activation loop, and the P+1 loop (111,116). The DFG motif is conserved in FhPIM kinase, serving as a critical regulatory switch and promoting catalytic activity as well as ATP binding in the FhPIM kinase.

### 4.3.3 Virtual screening of the MCCC library in FhPIM for the discovery of new fasciolicidal compounds

As previously discussed, the significant pharmacophore residues in HsPIM1 kinase are the sites to which various ligands bind. The majority of the ligands from the MCCC library engage with residues located in the back pocket, hinge region, linker loop, αD-helix, ribose pocket, and aspartate of the DFG motif of FhPIM kinase. I identified 34 compounds from the MCCC library that demonstrated potential interactions within the FhPIM binding pocket following two

rounds of virtual screening. The top ligand (NCC-00071469) from the second round of virtual screening, graded A-, established four interactions with Asp129, Val131, Glu180, and Asp195 within the binding pocket of FhPIM. The significance of the interactions was previously articulated. Moreover, the molecular docking studies demonstrated that the remaining top ligands identified in the MCCC library form a network of interactions with the significant pharmacophore residues in the binding pocket of FhPIM. The involvement of the Lys in the VVVK (VAIK in HsPIM1) motif and the aspartate in the DFG motif suggests that this ligand proficiently displaces the ATP-phosphate binding cluster and the magnesium coordination sphere, and the unique interaction with Asp residues in the αD-helix and linker loop suggests a deep-pocket binding mode. This multi-point anchorage, extending from the hinge to the C-lobe, is likely to impose a substantial entropic penalty on the conformational flexibility of FhPIM, potentially resulting in irreversible inhibition of the survival signalling of *F. hepatica*. The diversity of these residues indicates that the FhPIM kinase can accommodate different hydrophobic moieties, offering a clear avenue for future SAR optimisation to enhance fasciolicidal potency and efficacy while reducing host cross-reactivity.

The encouraging results from the molecular docking of MCCC library compounds within the FhPIM indicate a significant milestone; however, translating these computational findings into drug discovery for liver fluke research necessitates a stringent, multi-faceted experimental framework. The future drug discovery pipeline would involve the following steps:

1. The immediate next step should involve conducting a functional characterisation of FhPIM via RNAi to assess the morphological, reproductive, and motility phenotypes. Furthermore, it is crucial to validate genetic knockdown phenotypes, which can be achieved through CRISPR-induced drug resistance or total knockdown of the target, ensuring that the effect of the compound stems from a specific target interaction rather than off-target toxicity.
2. The subsequent step involves evaluating these compounds from the MCCC library for motility reduction or adverse effects *in vitro* on both immature and adult flukes to identify the potent new compounds suitable for preclinical and clinical studies.
3. Subsequent to genetic validation and *in vitro* screening, biochemical assays, including time-resolved fluorescence energy transfer (TR-FRET) and thermal shift assays (TSA), should be conducted to ascertain the half-maximal inhibitory concentration (IC50), binding kinetics, conformational changes, and stabilisation of the *Fasciola* protein versus the human protein upon ligand binding, thereby ensuring a definitive selectivity index to mitigate the off-target toxicity in the host.
4. ADMET and pharmacokinetics are essential to verify that the hit compounds exhibit drug-like characteristics appropriate for systemic or gastrointestinal administration. Hit-

to-lead progression necessitates the evaluation of metabolic stability in human, murine, and, importantly, ovine or bovine, given the veterinary burden of fascioliasis. Simultaneously, cytotoxicity must be evaluated in mammalian hepatic cell lines (e.g., HepG2) to verify a safe therapeutic range.

5. Optimised lead compounds must be assessed *in vivo* using rodent models to evaluate reductions in hepatic fluke burden, faecal egg count, and the improvement of hepatobiliary pathology through histological analysis.
6. Candidates exhibiting significant *in vivo* efficacy against liver flukes, along with an extensive therapeutic range, should be permitted to progress as investigational new drugs (INDs) in clinical trials, adhering to the strict guidelines established by the International Council of Harmonisation on good clinical practices (ICH-GCP E6 R3). Clinical translation must advance through various phases, including phase I safety trials in healthy volunteers, phase II proof-of-concept trials in endemic populations, and phase III randomised controlled trials evaluating novel FhPIM inhibitors in comparison to existing standards, such as TCBZ.

## 4.4 Conclusion

In conclusion, addressing the existential threat of TCBZ resistance necessitates a fundamental transformation of flukicide discovery. This thesis presents a comprehensive dataset of PKs in the common liver fluke (*F. hepatica*). This dataset may serve as a robust basis for future research on drug targets and pathogen cell biology in this parasite. The comparative analysis of PK domains between trematode and human hosts demonstrated a substantial therapeutic prospect for two concurrent strategies: repurposing of human PK inhibitors and developing trematode-specific drugs. This thesis demonstrated the feasibility of repurposing approved small-molecule PK inhibitors, evidenced by the successful *in vitro* evaluation of the FDA-approved multi-RTK inhibitor vandetanib and the PKCβ inhibitor ruboxistaurin against the common liver fluke. Moreover, following the significant *in vitro* effects of vandetanib on liver flukes, it can be promoted as a strong candidate for its investigation in *in vivo* studies. Leveraging the kinome curation, I envision the thesis-curated dataset serving as a guide for the investigation of other neglected multicellular parasites, thereby enhancing our understanding of their biology and facilitating the identification of novel treatment interventions. Through structure-based molecular docking studies of the broad MCCC library, I identified a subset of novel, multivalent ligands. These top-ranking ligands effectively formed H-bonds within the essential pharmacophore while concurrently targeting the unique hydrophobic topology of the FhPIM activation loop. These unique binding modes suggest potential selectivity over HsPIM1, such as the key substitutions within the FhPIM kinase hinge region, which provide distinct structural motifs that can be exploited to avoid off-target HsPIM1 inhibition. Finally, the kinome curation and identification of these MCCC library ligands within the FhPIM kinase through virtual screening confirm the importance of the kinome and the FhPIM kinase as essential milestones for confronting parasitic infections, providing both immediate repurposing candidates and robust pharmacophores for the development of PK-directed anthelmintics.

# 5. Summary/Zusammenfassung

## 5.1 Summary

Fasciolosis is a worldwide prevalent parasitic infection and considered a neglected tropical disease (NTD). It is caused by the liver flukes *Fasciola hepatica* and *F. gigantica*, which imposes considerable economic burdens and significantly affects both humans and animals. Parasites resistant to Triclabendazole (TCBZ), the predominant treatment for fasciolosis, have emerged on all continents, complicating the global management of fasciolosis, particularly in the absence of an effective vaccine. Protein kinases (PKs) are increasingly recognised as promising drug targets due to their crucial role in the survival and development of parasites, including the common liver fluke (*F. hepatica*). The cognisance of PKs in liver flukes remains scarce, with only a limited number of studies having explored PKs as potential therapeutic targets in this organism.

An advanced and refined genomic-bioinformatic computational pipeline was employed to identify, curate, and classify a comprehensive kinome of the liver fluke, which accounted for 245 PKs and represented 2.14% of the liver fluke's proteome. A comparative analysis with closely related trematode species and the human host revealed substantial orthology. Furthermore, the KEGG functional annotation indicated that 25% of the annotated PKs participate in conserved cancer-associated metabolic signalling pathways. This overlap emphasises the feasibility of a "drug repurposing" strategy, which was experimentally confirmed through the *in vitro* evaluation of approved small-molecule PK inhibitors. PK inhibitors associated with the PKs expressed in cells and tissues that are potentially crucial for parasite survival, including stem cells and muscle cells, were prioritised. The PKCβ inhibitor ruboxistaurin demonstrated lethal effects on both immature and adult liver flukes at a concentration of 50 µM, whereas the multi-RTK inhibitor vandetanib was lethal to immature liver flukes and significantly reduced the motility of adult liver flukes, indicating the efficacy of small-molecule PK inhibitors across different life stages of the liver fluke. Furthermore, these prioritised PK inhibitors demonstrated higher efficacy compared to TCBZ at equivalent concentration.

Subsequently, a structure-based virtual screening of the prioritised FhPIM kinase using molecular docking was conducted. A managed chemical compound collection (MCCC) library, which consists of 85,000 compounds optimised for lead-likeness, was docked into the FhPIM kinase binding pocket. As a result, 34 novel compounds exhibiting high predicted binding affinity for the FhPIM kinase were identified. In the docking models, these ligands produced essential hydrogen-bonding networks within the conserved pharmacophores and effectively

exploited the unique topology of the FhPIM kinase activation loop compared to the human PIM1 kinase, indicating significant potential for species-specific selectivity and reduced host toxicity. In the future, these 34 compounds will be subjected to *in vitro* evaluation to determine their capacity to inhibit the liver fluke vitality.

Overall, this study identified and curated the kinome of the common liver fluke using *in silico* analyses; it demonstrated the potential for PKs as drug targets and identified active fasciolicidal compounds. Moreover, this study also provides evidence for the “drug-repurposing” of small-molecule PK inhibitors, which may represent an alternative intervention strategy in combating liver flukes. Additionally, the discovery of potential FhPIM kinase inhibitors derived from the MCCC library signifies a clear trajectory for the progression of target-based fasciolicidal strategies. Overall, this work establishes a solid basis for exploring future helminthic interventions based on PK inhibitors and for advancing basic research into the functions of PKs in the cell biology of liver flukes.

## 5.2 Zusammenfassung

Faziolose ist eine weltweit verbereitete parasitäre Infektionskrankheit die zu den vernachlässigten Tropenkrankheiten (NTD) gezählt wird. Sie wird durch die Leberegel *Fasciola heptica* und *F. gigantica* verursacht und hat, neben erheblichen wirtschaftlichen Schäden, negative Auswirkungen auf die Gesundheit von sowohl Menschen als auch Tieren. Außerdem wird die Behandlung der Krankheit durch das weltweite Auftreten von Resistenzen gegen das hauptsächlich verwendete Medikament Triclabendazol (TCBZ) und den Mangel einer effektive Impfung, weiter verkompliziert. Proteinkinasen (PKs) werden aufgrund ihrer wichtigen Rolle für das Überleben und Entwicklung von Parasiten, einschließlich des Leberegels *F. hepatica*, als vielversprechende Wirkstoffziele diskutiert. Das Wissen über PKs in Leberegeln ist allerdings auf einige wenige Studien zum Potential von PKs als Wirkstoffziele begrenzt.

In dieser Studie wurde eine optimierte bioinformatische Pipeline zur Identifikation und Klassifikation der PKs des Leberegels genutzt. Das so erstellte Kinom enthielt 245 PKs, was etwa 2,14% des Proteoms des Leberegels ausmacht. Eine vergleichende Analyse mit verwandten Spezies und dem humanen Wirt zeigte eine substanzielle Orthologie. Außerdem zeigte KEGG-Annotation, dass 25% der identifizierten PKs Teil von konservierten Krebs-assoziierten Stoffwechselwegen sind. Dieser Sachverhalt legt die Möglichkeit einer „drug repurposing“-Strategie nahe, welche in dieser Studie durch die *in vitro*-Testung zugelasser PK-Inhibitoren bestätigt werden konnte. Ein besonderer Fokus wurde auf Inhibitoren von PKs mit Expression in Zellen und Geweben gelegt, die für das Überleben des Wurms von essentieller Wichtigkeit sind, zum Beispiel Muskeln oder Stammzellen. Der PKCβ-Inhibitor

Ruboxistaurin zeigte letale Effekte auf sowohl immature als auch adulte Würmer in einer Konzentration von 50 µM, wohingegen der Inhibitor Vandetanib, welcher auf multiple RTKs wirkt, letale Effekte auf immature Würmer zeigte und die Beweglichkeit der adulten Würmer signifikant verminderte. Diese Ergebnisse bestätigten die Wirkung von PK-Inhibitoren auf verschiedene Lebenstadien des Leberegels. Außerdem zeigten ausgewählte Inhibitoren bei gleicher Konzentration eine höhere Wirksamkeit als TCBZ.

Ein strukturbasiertes virtuelles Screening für die priorisierte Kinase FhPIM wurde mithilfe von molekularem Docking durchgeführt. Dabei wurde eine aus 85.000 chemischen Verbindungen bestehende Sammlung (MCCC), die für Wirkstoffentwicklung vorselektioniert ist, in die Bindestelle der FhPIM-Kinase gedockt. Am Ende der Analyse wurde für 34 der getesteten Verbindungen eine hohe Bindeaffinität vorhergesagt. In den Docking-Modellen bildeten diese Liganden Wasserstoffbrücken mit konservierten Pharmakophoren unter der Nutzung der für den Leberegel eigenen Topologie der Aktivierungschleife. Die unterschiedliche Struktur der FhPIM-Kinase zum humanen Ortholog dieser Kinase weißt auf ein erhebliches Potential für das Design artspezifisch selektiver Inhibitoren mit verringerter Wirttoxizität hin. In der Zukunft sollen die 34 identifizierten Verbindungen *in vitro* auf ihre Wirksamkeit gegen den Leberegel getestet werden.

Zusammenfassend wurde in dieser Studie das Kinome des Leberegels mithilfe von *in silico* Analysen identifiziert. Das Potential von Proteinkinasen als Wirkstoffziel wurde exemplarisch gezeigt und wirksame Inhibitoren identifiziert. Außerdem wurde die erfolgreiche Umwindung von zugelassen PK-Inhibitoren gezeigt, was eine alternative Interventionsstrategie gegen den Leberegel darstellen könnte. Zusätzlich weißt die Entdeckung von FhPIM-Inhibitoren aus der MCCC-Sammlung einen deutlichen Weg für die Weiterentwicklung einer Wirkstoffziel-fokussierten Bekämpfungsstrategie. Insgesamt schafft diese Arbeit eine solide Grundlage für die Erforschung zukünftiger Interventionen gegen parasitäre Würmer auf der Basis von PK-Inhibitoren und ebenso für die Grundlagenforschung in Bezug auf die Rolle von PKs in der Zellbiologie des Leberegels.

# 6. Supplementary/Appendix

## 6.1 Supplementary figures

This section contains the supplementary figures used in this work, which provide information to support the assertions made in the introduction, result or discussion sections.

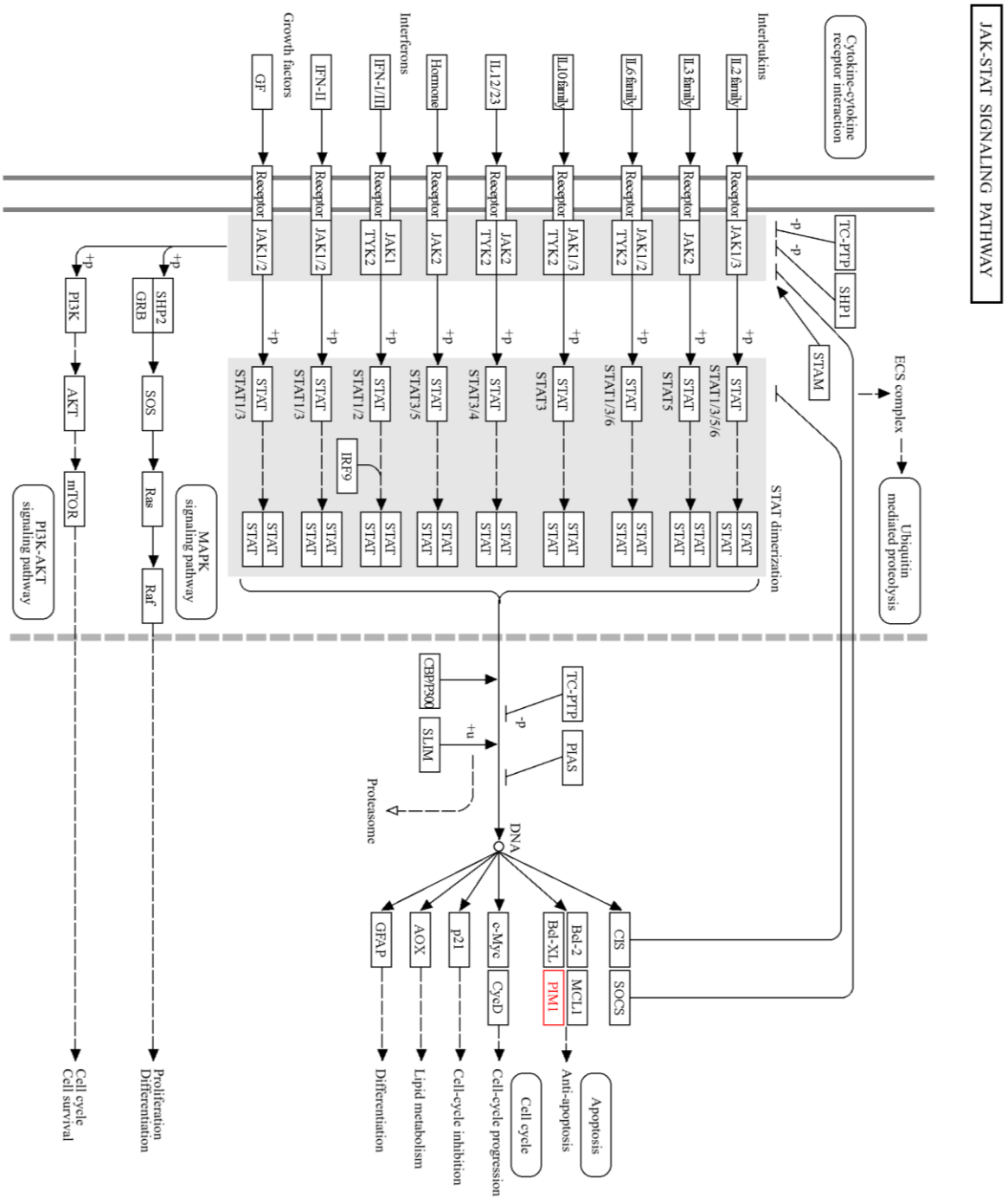


**Supplementary figure 6.1: Illustration of the role of PIM kinase in the JNK-STAT signalling pathway** obtained from KEGG metabolic pathways (191,192,381,382). PIM kinase is labelled in red box.

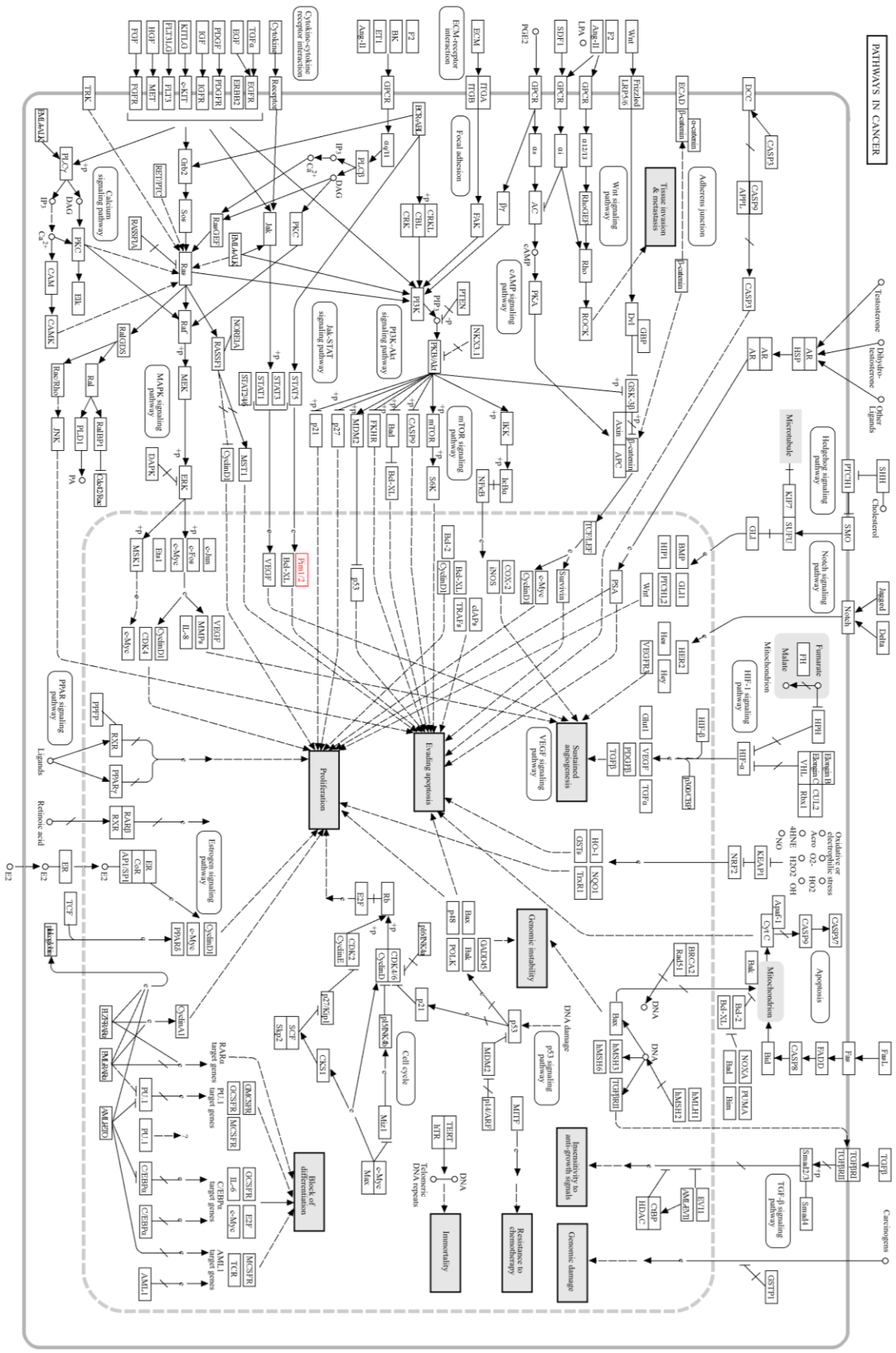


**Supplementary figure 6.2: Illustration of the role of PIM kinase in the pathways in cancer** obtained from KEGG metabolic pathways (191,192,381,382). PIM kinase is labelled in red box.

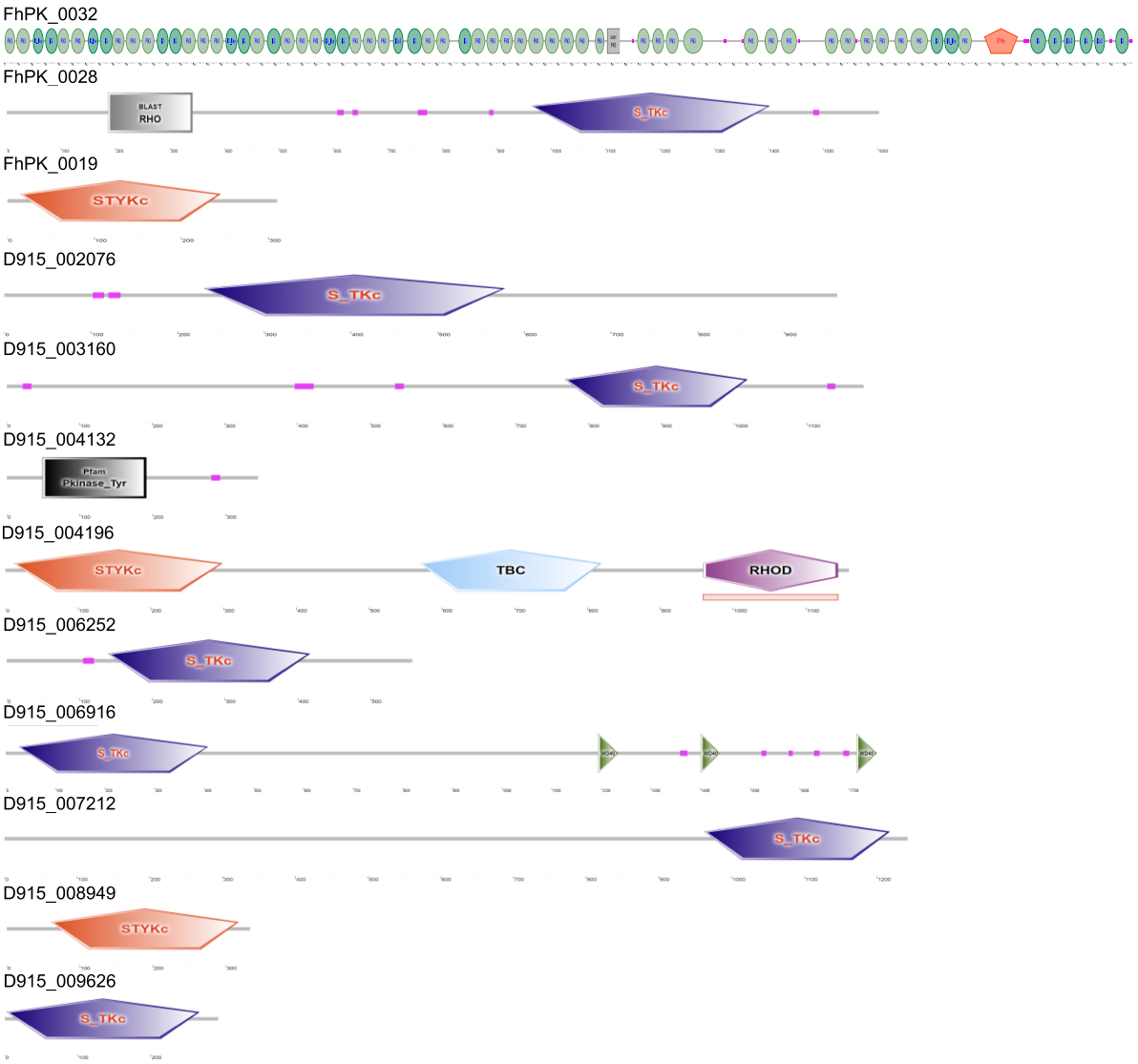


**Supplementary figure 6.3: The twelve unclassified PKs annotated from Kinnanote in the kinome of *F. hepatica***. The domain analysis of these unclassified PKs was performed in the SMART webserver (235) and complied in Inkscape (25).

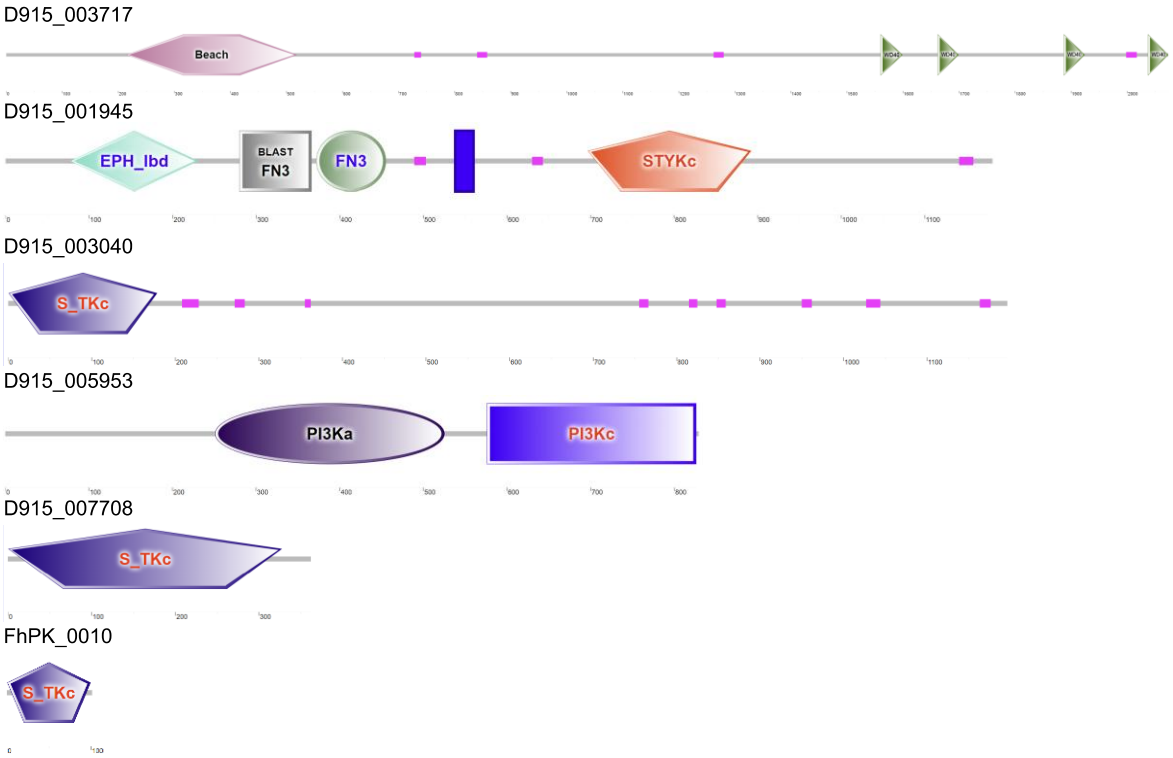


**Supplementary figure 6.4: The six twilight hits annotated from Kinnanote in the kinome of *F. hepatica***. The domain analysis of these twilights was performed in the SMART webserver (235) and complied in Inkscape (25).

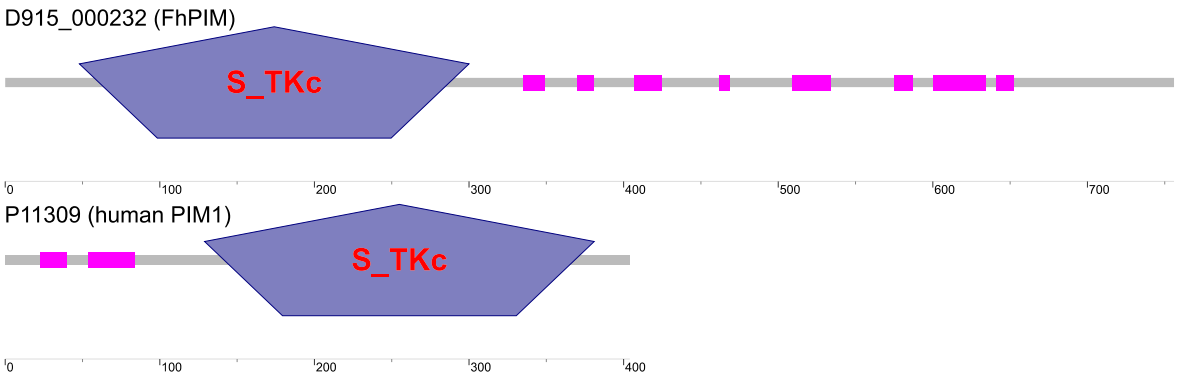


**Supplementary figure 6.5: Domain information of human PIM1 and *Fasciola* PIM kinase**. The domain analysis PKs was performed in the SMART webserver (235) and complied in Inkscape (25).

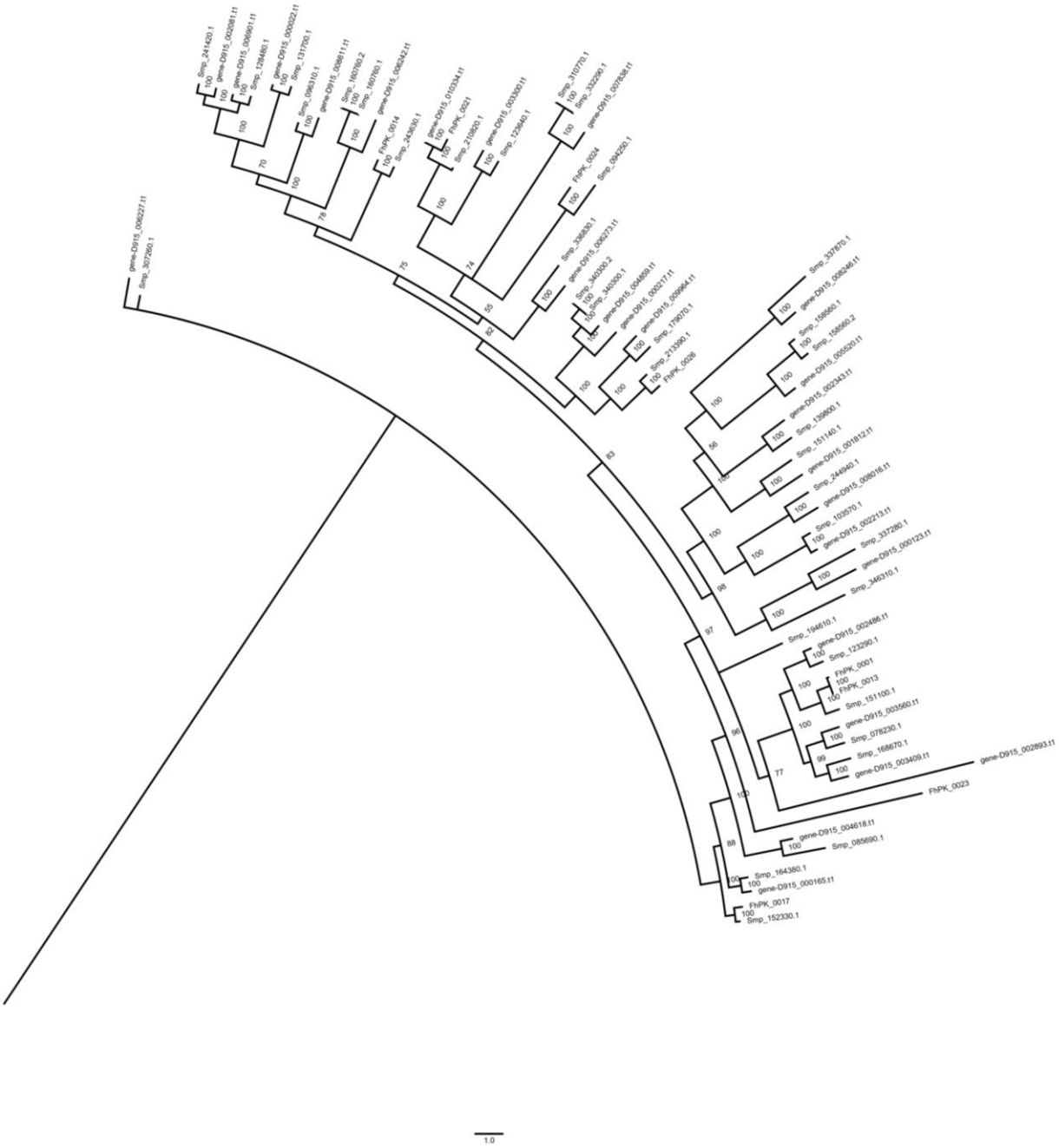


**Supplementary figure 6.6: Phylogenetic analysis of AGC PK group of *F. hepatica* and *S. mansoni*.** Subsequent to the alignment of amino acid sequences, a phylogenetic tree was constructed. The high-resolution figure of the tree displays the nodal support values (posterior probabilities generated from MrBayes v3.2.7a (221)), with sequence identifiers located at the end of each tree branch. This figure is reproduced from the supplementary data 2 of Ajmera et al., 2026 (246).

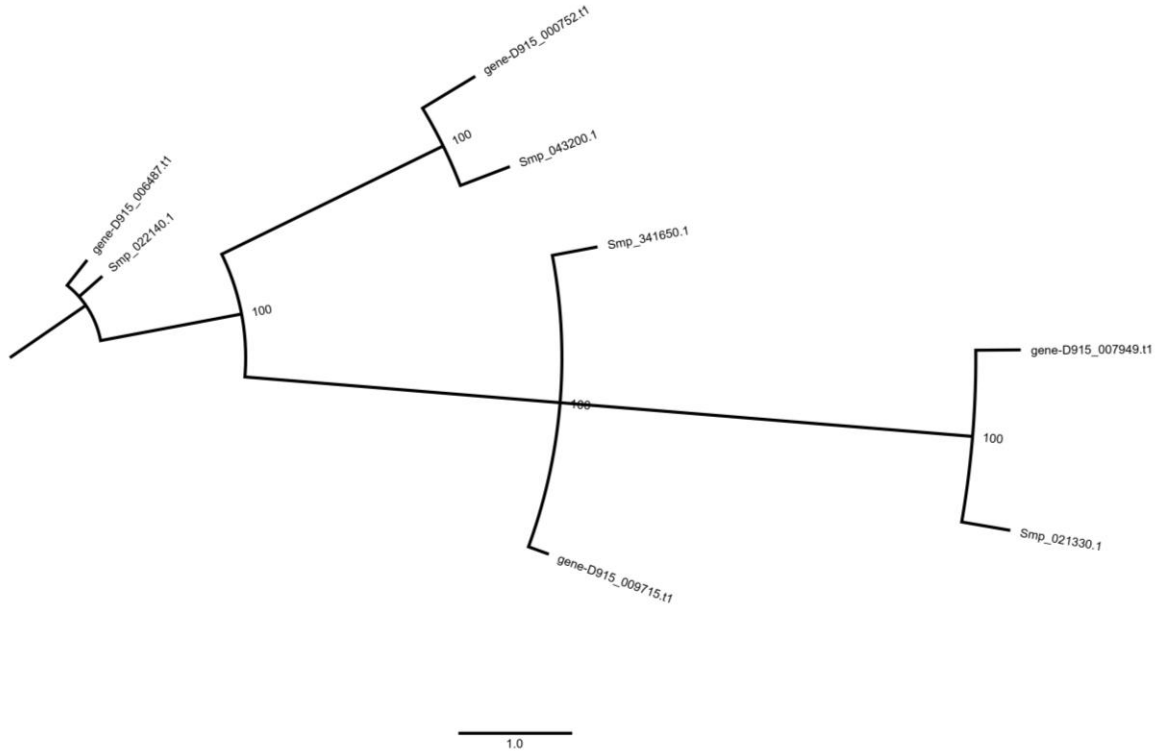


**Supplementary figure 6.7: Phylogenetic analysis of atypical PK group of *F. hepatica* and *S. mansoni***. Subsequent to the alignment of amino acid sequences, a phylogenetic tree was constructed. The high-resolution figure of the tree displays the nodal support values (posterior probabilities generated from MrBayes v3.2.7a (221)), with sequence identifiers located at the end of each tree branch. This figure is reproduced from the supplementary data 2 of Ajmera et al., 2026 (246).

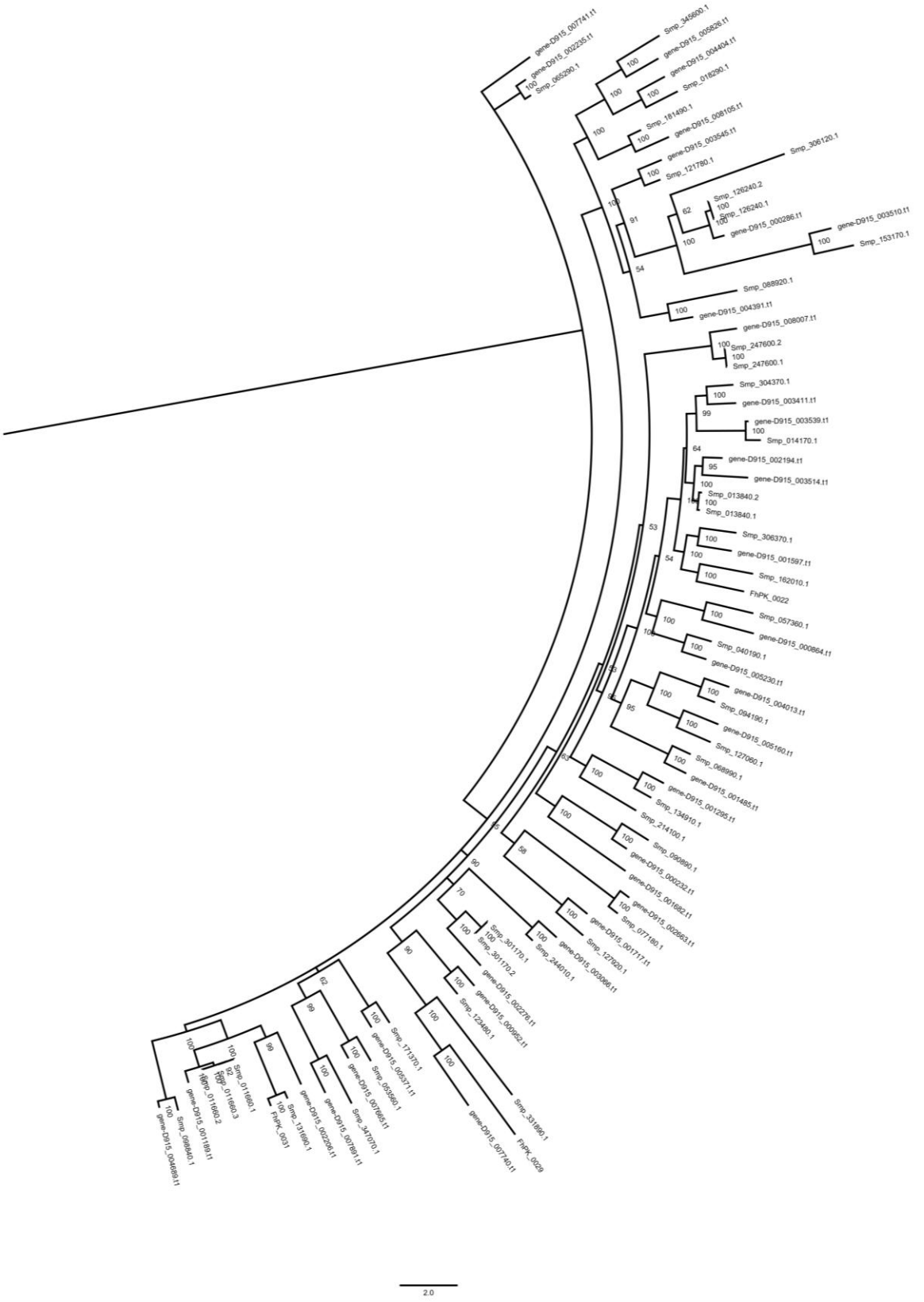


**Supplementary figure 6.8: Phylogenetic analysis of CAMK PK group of *F. hepatica* and *S. mansoni***. Subsequent to the alignment of amino acid sequences, a phylogenetic tree was constructed. The high-resolution figure of the tree displays the nodal support values (posterior probabilities generated from MrBayes v3.2.7a (221)), with sequence identifiers located at the end of each tree branch. This figure is reproduced from the supplementary data 2 of Ajmera et al., 2026 (246).

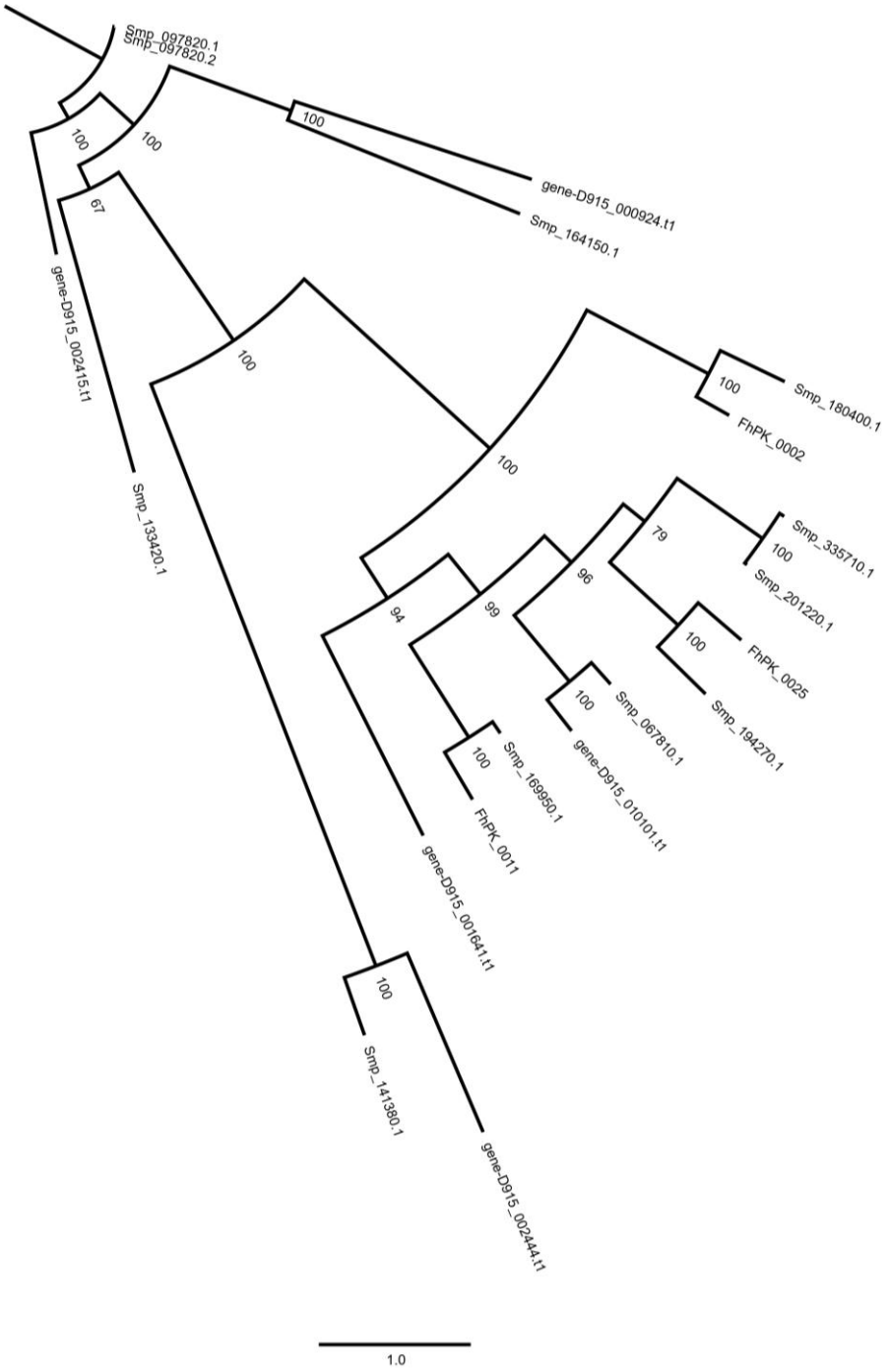


**Supplementary figure 6.9: Phylogenetic analysis of CK1 PK group of *F. hepatica* and *S. mansoni*.** Subsequent to the alignment of amino acid sequences, a phylogenetic tree was constructed. The high-resolution figure of the tree displays the nodal support values (posterior probabilities generated from MrBayes v3.2.7a (221)), with sequence identifiers located at the end of each tree branch. This figure is reproduced from the supplementary data 2 of Ajmera et al., 2026 (246).

**Supplementary figure 6.10: Phylogenetic analysis of CMGC PK group of *F. hepatica* and *S. mansoni***. Subsequent to the alignment of amino acid sequences, a phylogenetic tree was constructed. The high-resolution figure of the tree displays the nodal support values (posterior probabilities generated from MrBayes v3.2.7a (221)), with sequence identifiers located at the end of each tree branch. This figure is reproduced from the supplementary data 2 of Ajmera et al., 2026 (246).

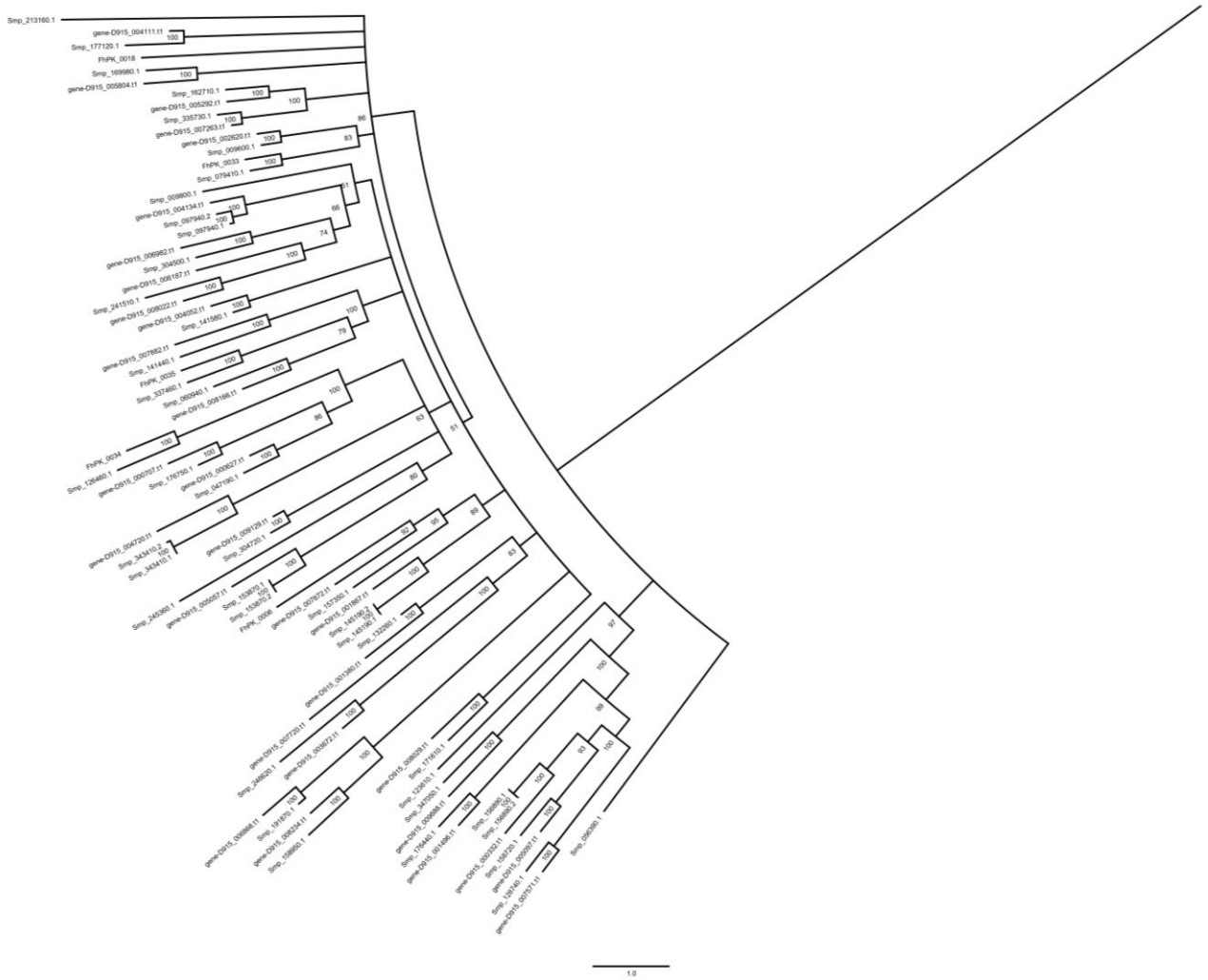

**Supplementary figure 6.11: Phylogenetic analysis of Other PK group of *F. hepatica* and *S. mansoni***. Subsequent to the alignment of amino acid sequences, a phylogenetic tree was constructed. The high-resolution figure of the tree displays the nodal support values (posterior probabilities generated from MrBayes v3.2.7a (221)), with sequence identifiers located at the end of each tree branch. This figure is reproduced from the supplementary data 2 of Ajmera et al., 2026 (246).

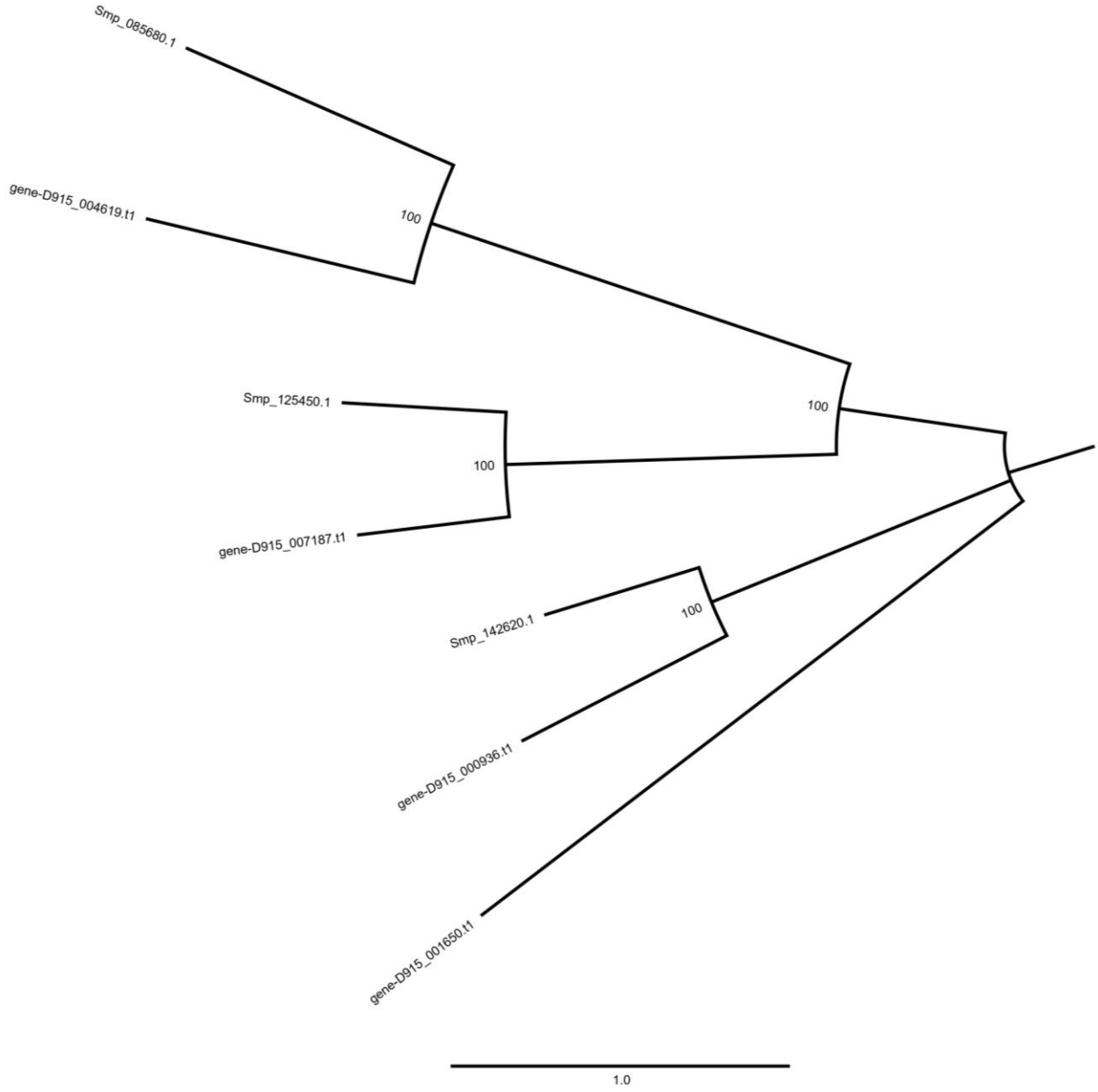


**Supplementary figure 6.12: Phylogenetic analysis of RGC PK group of *F. hepatica* and *S. mansoni***. Subsequent to the alignment of amino acid sequences, a phylogenetic tree was constructed. The high-resolution figure of the tree displays the nodal support values (posterior probabilities generated from MrBayes v3.2.7a (221)), with sequence identifiers located at the end of each tree branch. This figure is reproduced from the supplementary data 2 of Ajmera et al., 2026 (246).

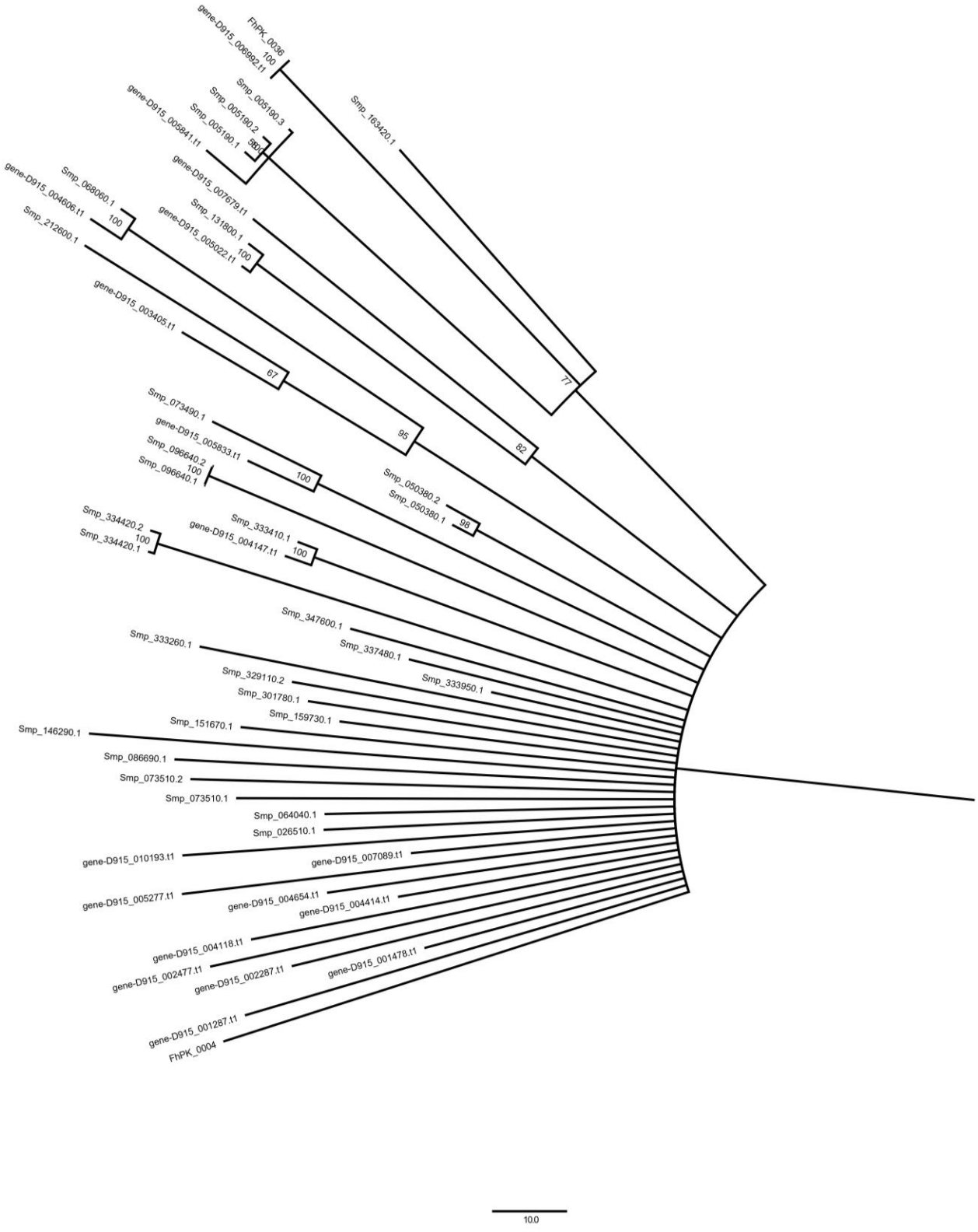


**Supplementary figure 6.13: Phylogenetic analysis of STE PK group of *F. hepatica* and *S. mansoni***. Subsequent to the alignment of amino acid sequences, a phylogenetic tree was constructed. The high-resolution figure of the tree displays the nodal support values (posterior probabilities generated from MrBayes v3.2.7a (221)), with sequence identifiers located at the end of each tree branch. This figure is reproduced from the supplementary data 2 of Ajmera et al., 2026 (246).


**Supplementary figure 6.14: Phylogenetic analysis of TK PK group of *F. hepatica* and *S. mansoni*.** Subsequent to the alignment of amino acid sequences, a phylogenetic tree was constructed. The high-resolution figure of the tree displays the nodal support values (posterior probabilities generated from MrBayes v3.2.7a (221)), with sequence identifiers located at the end of each tree branch. This figure is reproduced from the supplementary data 2 of Ajmera et al., 2026 (246).

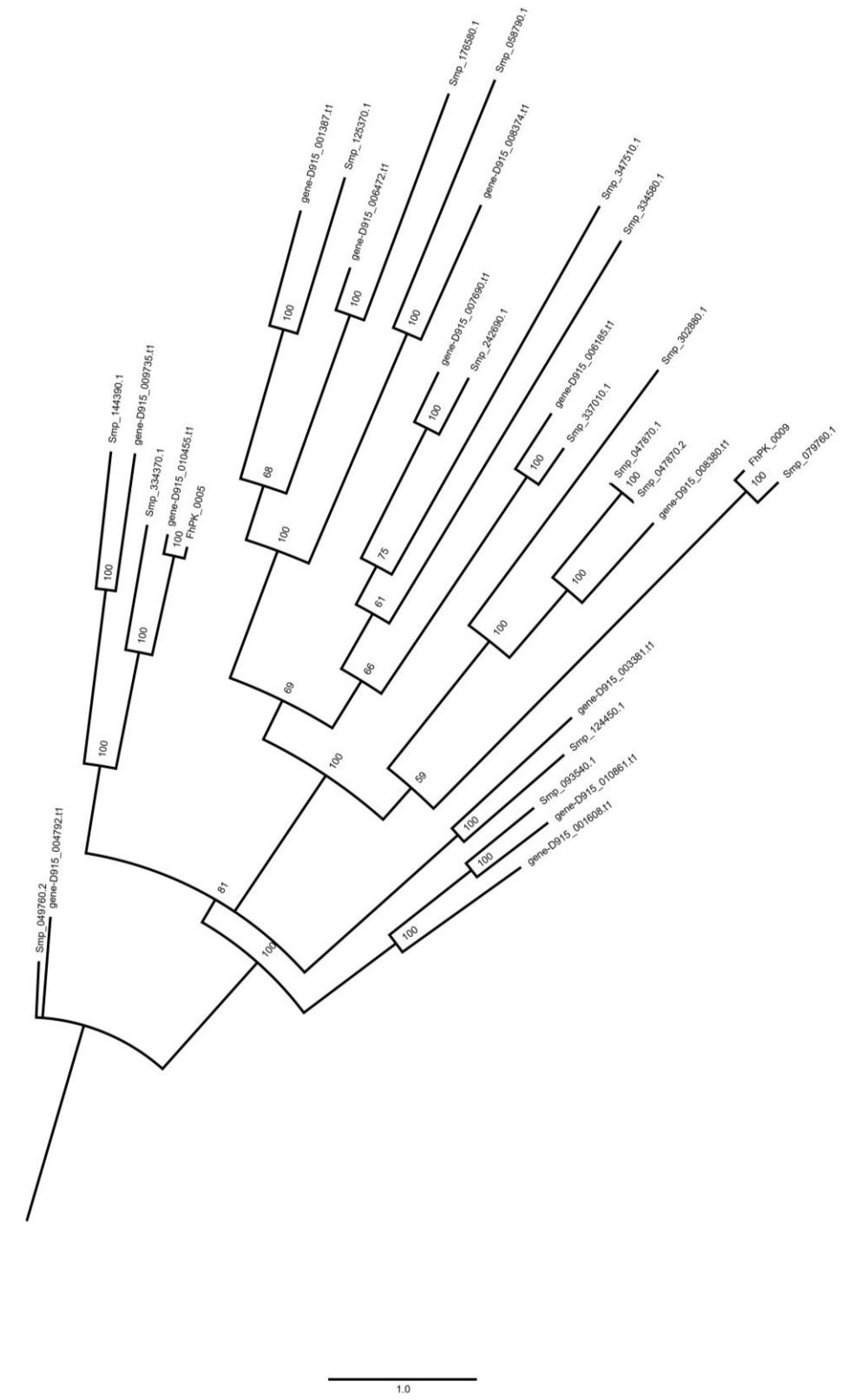


**Supplementary figure 6.15: Phylogenetic analysis of TKL PK group of *F. hepatica* and *S. mansoni***. Subsequent to the alignment of amino acid sequences, a phylogenetic tree was constructed. The high-resolution figure of the tree displays the nodal support values (posterior probabilities generated from MrBayes v3.2.7a (221)), with sequence identifiers located at the end of each tree branch. This figure is reproduced from the supplementary data 2 of Ajmera et al., 2026 (246).

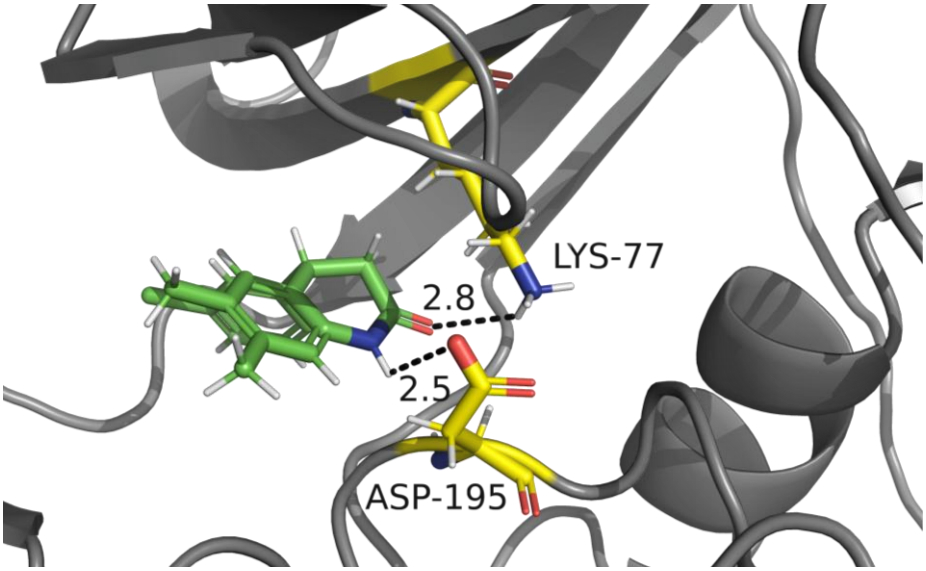


**Supplementary figure 6.16: Polar interactions of NCC-00008538** in the binding pocket of FhPIM kinase. NCC-00008538 (ligand) is displayed as sticks with green-coloured carbon atoms. The structure of FhPIM is illustrated as a cartoon in grey colour. The polar interactions are depicted as black dashed lines and their distances in angstroms (Å). Residues depicted in yellow colour are the polar interacting residues (Lys77 and Asp195) in the binding pocket of FhPIM kinase. All nitrogen, oxygen, and chlorine atoms are in blue, red, and green colours, respectively.

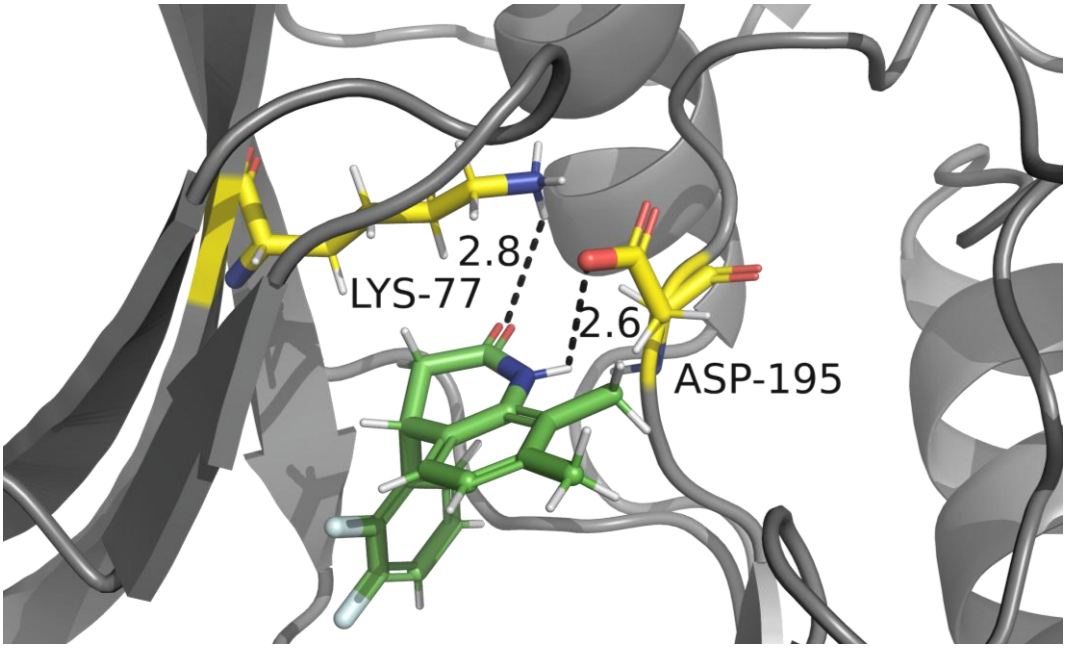


**Supplementary figure 6.17: Polar interactions of NCC-00077290** in the binding pocket of FhPIM kinase. NCC-00077290 (ligand) is displayed as sticks with green-coloured carbon atoms. The structure of FhPIM is illustrated as a cartoon in grey colour. The polar interactions are depicted as black dashed lines and their distances in angstroms (Å). Residues depicted in yellow colour are the polar interacting residues (Lys77 and Asp195) in the binding pocket of FhPIM kinase. All nitrogen, oxygen, and fluorine atoms are in blue, red, and palecyan colours, respectively.

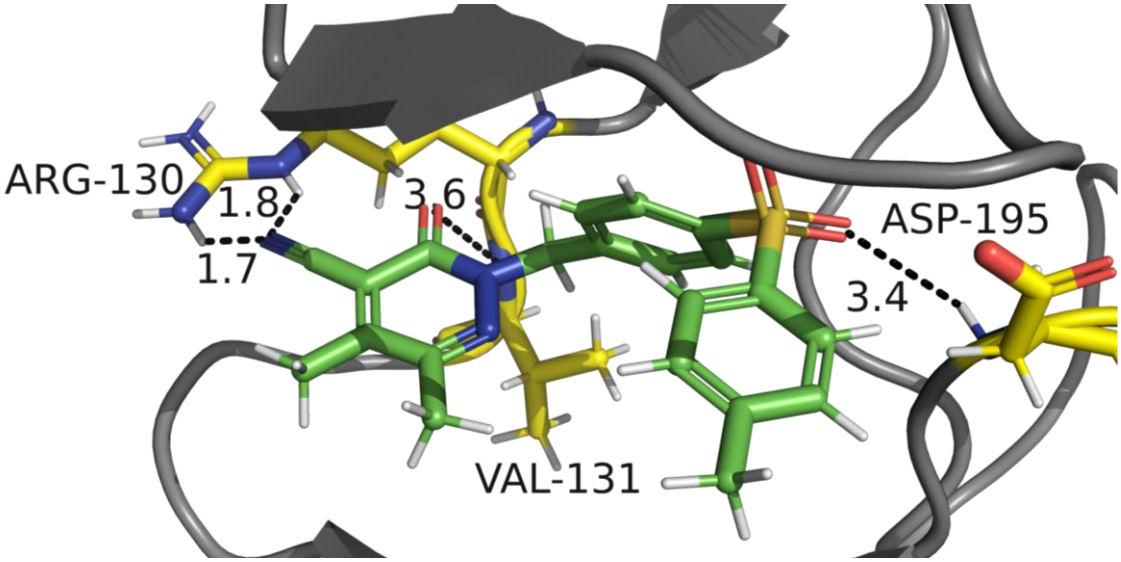


**Supplementary figure 6.18: Polar interactions of NCC-00032341** in the binding pocket of FhPIM kinase. NCC-00032341 (ligand) is displayed as sticks with green-coloured carbon atoms. The structure of FhPIM is illustrated as a cartoon in grey colour. The polar interactions are depicted as black dashed lines and their distances in angstroms (Å). Residues depicted in yellow colour are the polar interacting residues (Arg130, Val131, and Asp195) in the binding pocket of FhPIM kinase. All nitrogen, oxygen, fluorine, and sulphur atoms are in blue, red, palecyan, and yelloworange colours, respectively.

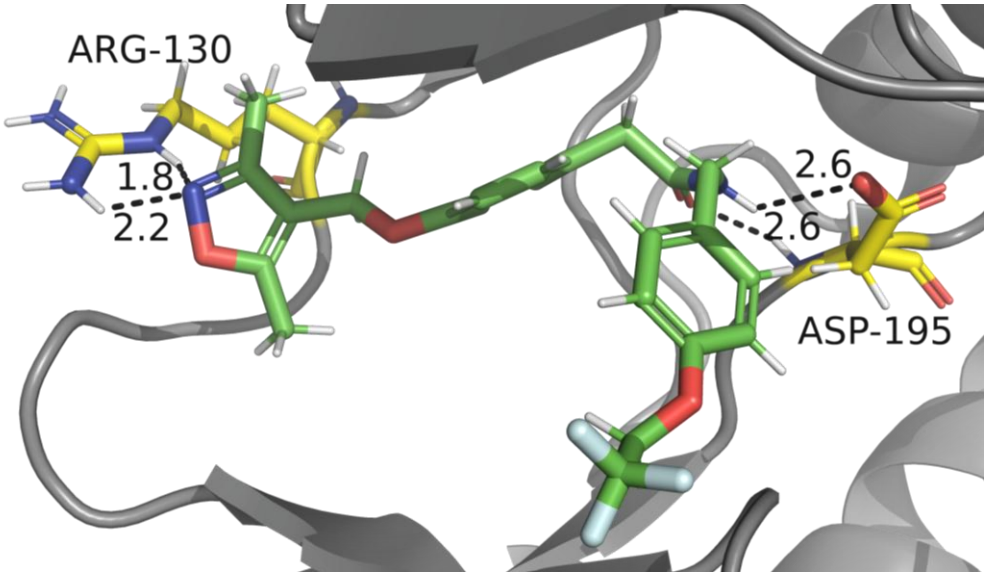


**Supplementary figure 6.19: Polar interactions of NCC-00044825** in the binding pocket of FhPIM kinase. NCC-00044825 (ligand) is displayed as sticks with green-coloured carbon atoms. The structure of FhPIM is illustrated as a cartoon in grey colour. The polar interactions are depicted as black dashed lines and their distances in angstroms (Å). Residues depicted in yellow colour are the polar interacting residues (Arg130 and Asp195) in the binding pocket of FhPIM kinase. All nitrogen, oxygen, and fluorine atoms are in blue, red, and palecyan colours, respectively.

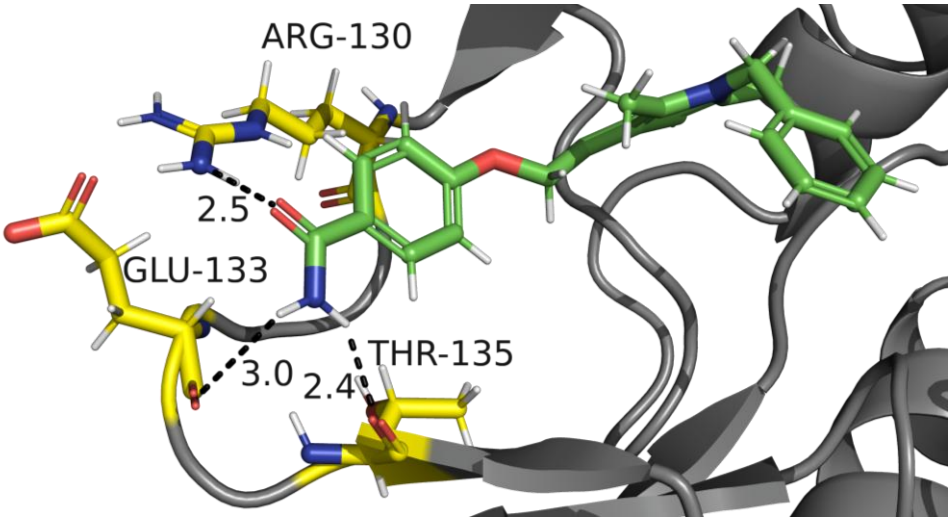


**Supplementary figure 6.20: Polar interactions of NCC-00074481** in the binding pocket of FhPIM kinase. NCC-00074481 (ligand) is displayed as sticks with green-coloured carbon atoms. The structure of FhPIM is illustrated as a cartoon in grey colour. The polar interactions are depicted as black dashed lines and their distances in angstroms (Å). Residues depicted in yellow colour are the polar interacting residues (Arg130, Glu133 and Thr135) in the binding pocket of FhPIM kinase. All nitrogen and oxygen atoms are in blue and red colours, respectively.

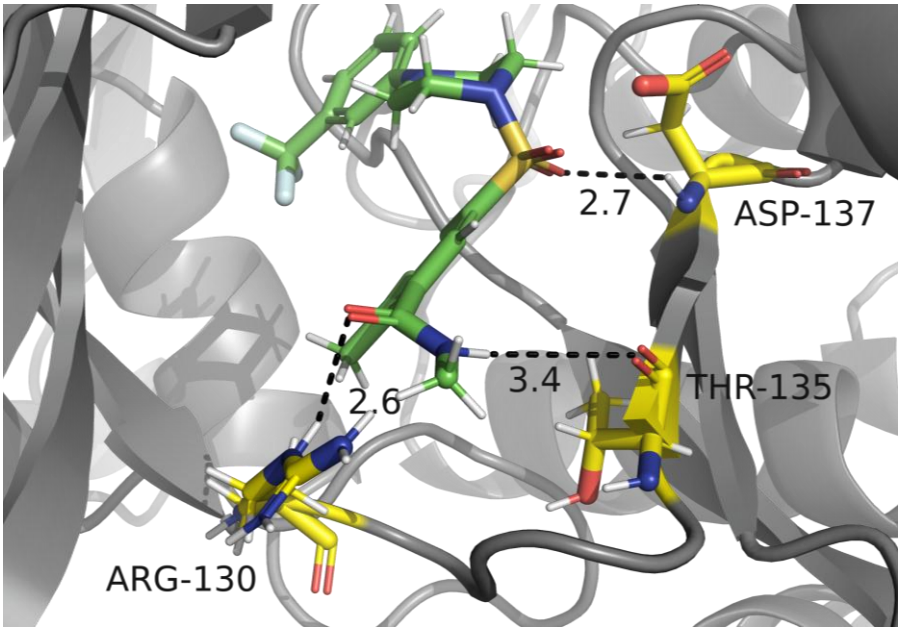


**Supplementary figure 6.21: Polar interactions of NCC-00009414** in the binding pocket of FhPIM kinase. NCC-00009414 (ligand) is displayed as sticks with green-coloured carbon atoms. The structure of FhPIM is illustrated as a cartoon in grey colour. The polar interactions are depicted as black dashed lines and their distances in angstroms (Å). Residues depicted in yellow colour are the polar interacting residues (Arg130, Thr135, and Asp137) in the binding pocket of FhPIM kinase. All nitrogen, oxygen, fluorine and sulphur atoms are in blue, red, palecyan, and yelloworange colours, respectively.

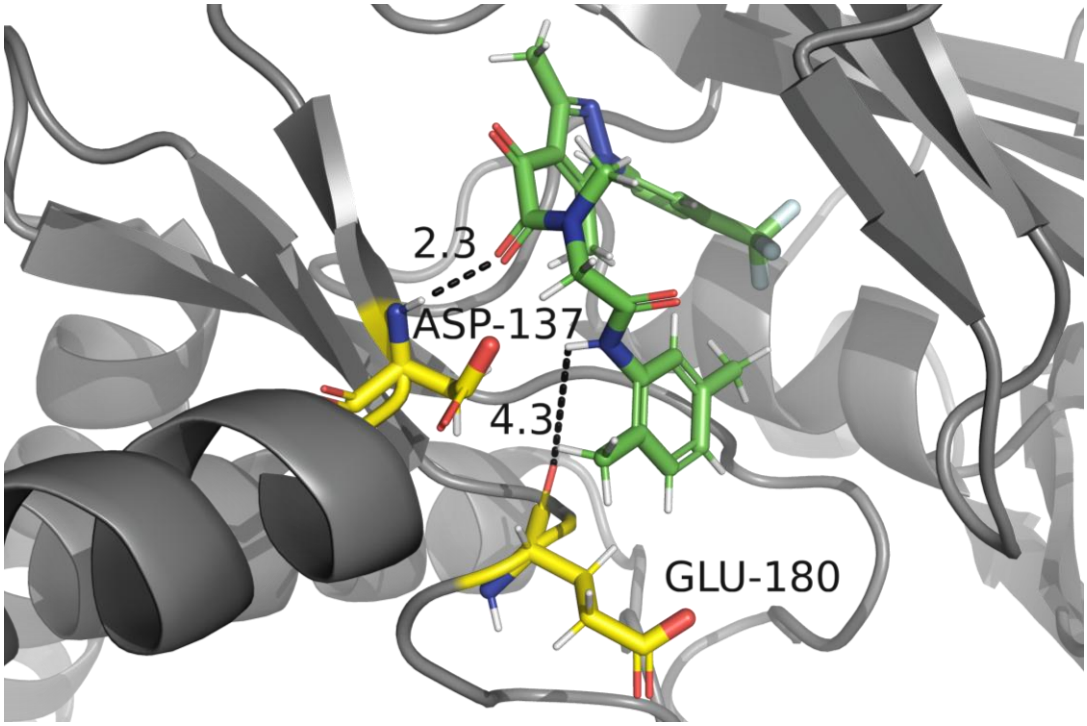


**Supplementary figure 6.22: Polar interactions of NCC-00044623** in the binding pocket of FhPIM kinase. NCC-00044623 (ligand) is displayed as sticks with green-coloured carbon atoms. The structure of FhPIM is illustrated as a cartoon in grey colour. The polar interactions are depicted as black dashed lines and their distances in angstroms (Å). Residues depicted in yellow colour are the polar interacting residues (Asp137 and Glu180) in the binding pocket of FhPIM kinase. All nitrogen, oxygen, and fluorine atoms are in blue, red, and palecyan colours, respectively.

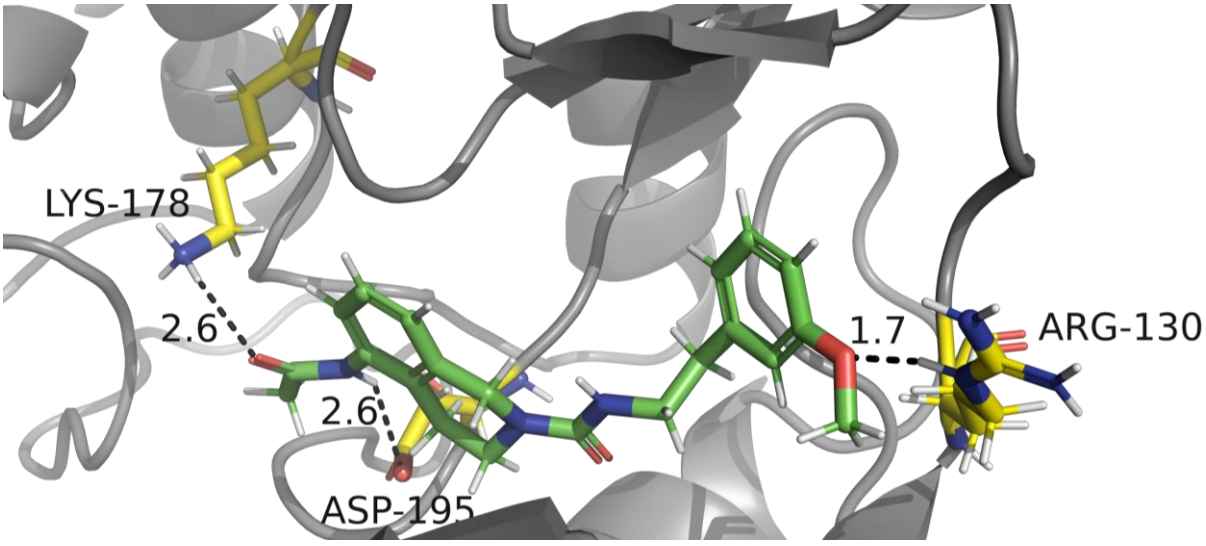


**Supplementary figure 6.23: Polar interactions of NCC-00057583** in the binding pocket of FhPIM kinase. NCC-00057583 (ligand) is displayed as sticks with green-coloured carbon atoms. The structure of FhPIM is illustrated as a cartoon in grey colour. The polar interactions are depicted as black dashed lines and their distances in angstroms (Å). Residues depicted in yellow colour are the polar interacting residues (Arg130, Lys178, and Asp195) in the binding pocket of FhPIM kinase. All nitrogen and oxygen atoms are in blue and red colours, respectively.

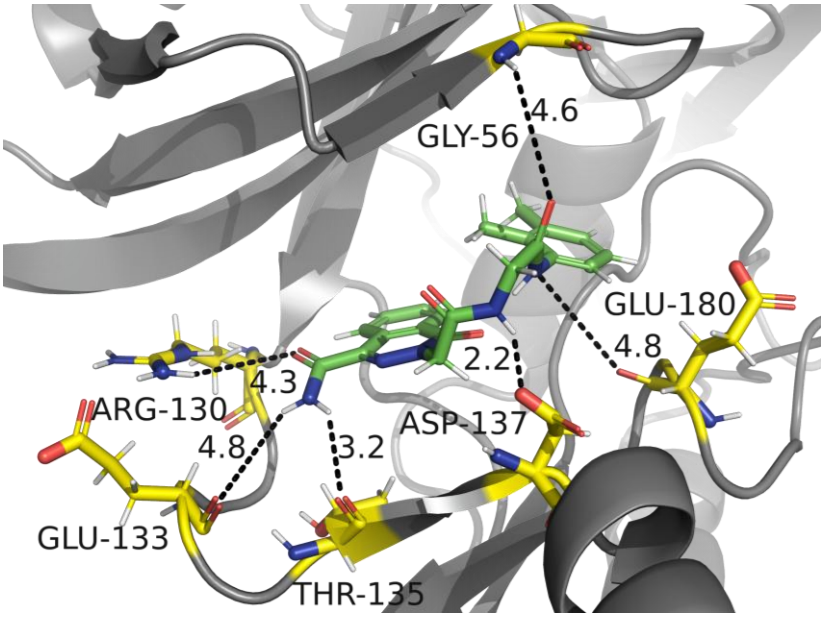


**Supplementary figure 6.24: Polar interactions of NCC-00015704** in the binding pocket of FhPIM kinase. NCC-00015704 (ligand) is displayed as sticks with green-coloured carbon atoms. The structure of FhPIM is illustrated as a cartoon in grey colour. The polar interactions are depicted as black dashed lines and their distances in angstroms (Å). Residues depicted in yellow colour are the polar interacting residues (Gly56, Arg130, Glu133, Thr135, Asp137, and Glu180) in the binding pocket of FhPIM kinase. All nitrogen and oxygen atoms are in blue and red colours, respectively.

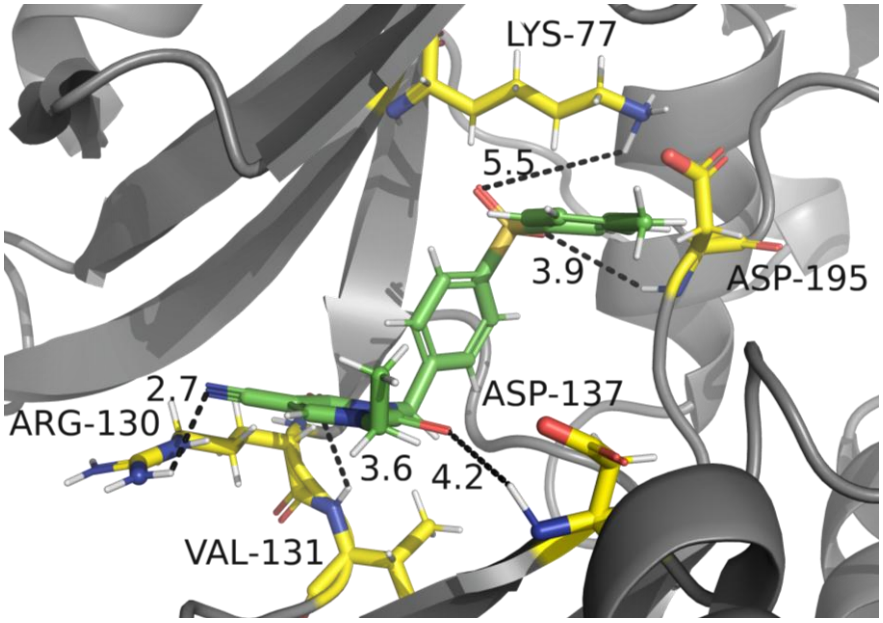


**Supplementary figure 6.25: Polar interactions of NCC-00058509** in the binding pocket of FhPIM kinase. NCC-00058509 (ligand) is displayed as sticks with green-coloured carbon atoms. The structure of FhPIM is illustrated as a cartoon in grey colour. The polar interactions are depicted as black dashed lines and their distances in angstroms (Å). Residues depicted in yellow colour are the polar interacting residues (Lys77, Arg130, Val131, Asp137, and Asp195) in the binding pocket of FhPIM kinase. All nitrogen, oxygen, and sulphur atoms are in blue, red, and yelloworange colours, respectively.

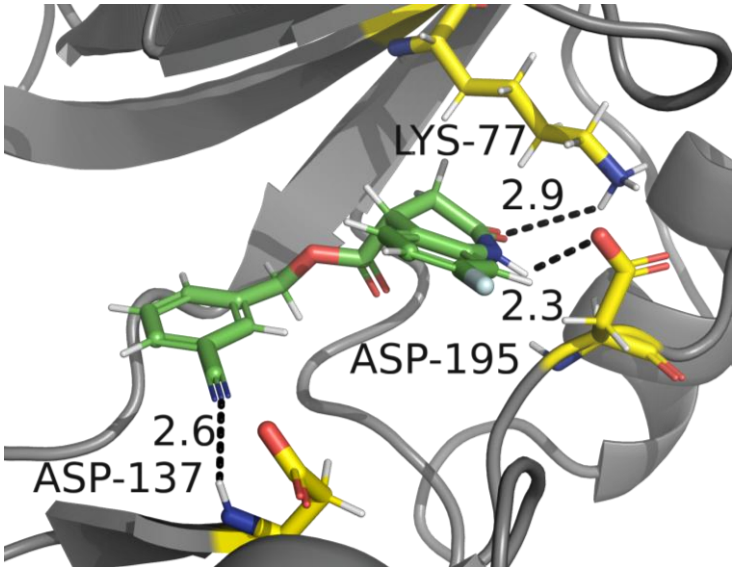


**Supplementary figure 6.26: Polar interactions of NCC-00032487** in the binding pocket of FhPIM kinase. NCC-00032487 (ligand) is displayed as sticks with green-coloured carbon atoms. The structure of FhPIM is illustrated as a cartoon in grey colour. The polar interactions are depicted as black dashed lines and their distances in angstroms (Å). Residues depicted in yellow colour are the polar interacting residues (Lys77, Asp137, and Asp195) in the binding pocket of FhPIM kinase. All nitrogen, oxygen, and fluorine atoms are in blue, red, and palecyan colours, respectively.

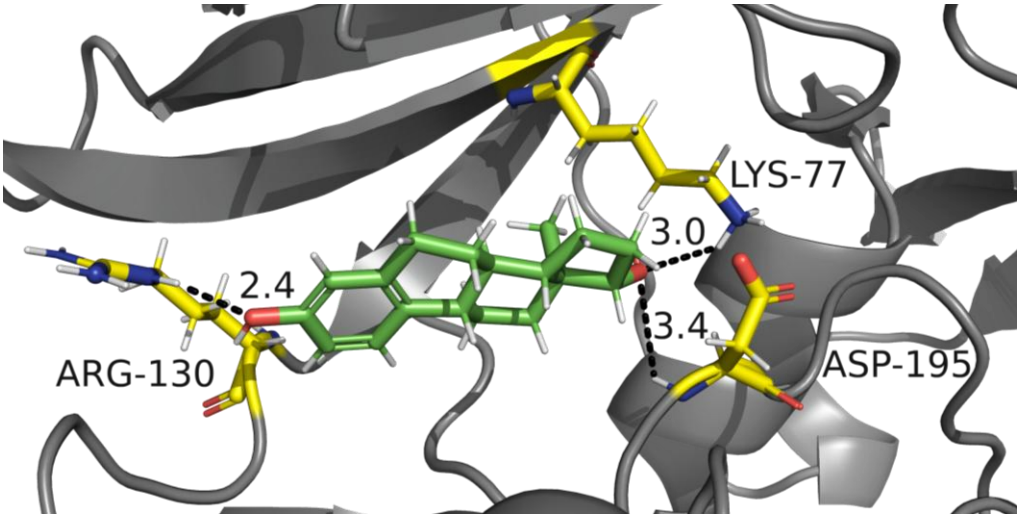


**Supplementary figure 6.27: Polar interactions of NCC-00089972** in the binding pocket of FhPIM kinase. NCC-00089972 (ligand) is displayed as sticks with green-coloured carbon atoms. The structure of FhPIM is illustrated as a cartoon in grey colour. The polar interactions are depicted as black dashed lines and their distances in angstroms (Å). Residues depicted in yellow colour are the polar interacting residues (Lys77, Arg130, and Asp195) in the binding pocket of FhPIM kinase. All nitrogen and oxygen atoms are in blue and red colours, respectively.

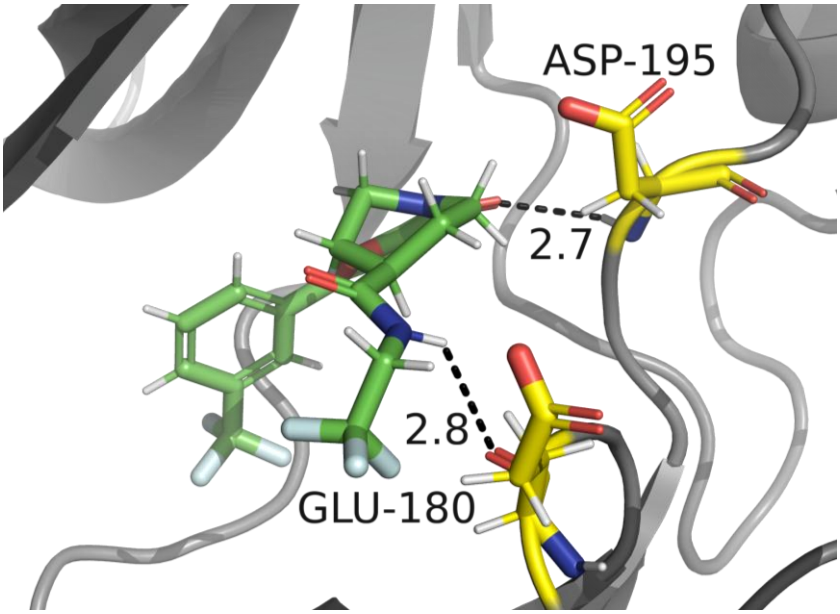


**Supplementary figure 6.28: Polar interactions of NCC-00069794** in the binding pocket of FhPIM kinase. NCC-00069794 (ligand) is displayed as sticks with green-coloured carbon atoms. The structure of FhPIM is illustrated as a cartoon in grey colour. The polar interactions are depicted as black dashed lines and their distances in angstroms (Å). Residues depicted in yellow colour are the polar interacting residues (Glu180 and Asp195) in the binding pocket of FhPIM kinase. All nitrogen, oxygen, and fluorine atoms are in blue, red, and palecyan colours, respectively.

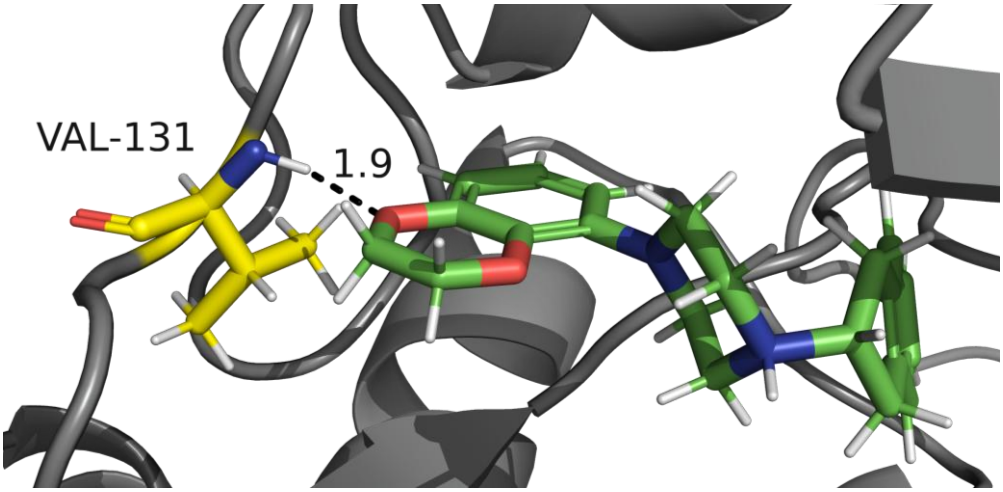


**Supplementary figure 6.29: Polar interactions of NCC-00090340** in the binding pocket of FhPIM kinase. NCC-00090340 (ligand) is displayed as sticks with green-coloured carbon atoms. The structure of FhPIM is illustrated as a cartoon in grey colour. The polar interactions are depicted as black dashed lines and their distances in angstroms (Å). Residues depicted in yellow colour are the polar interacting residues (Val131) in the binding pocket of FhPIM kinase. All nitrogen and oxygen atoms are in blue and red colours, respectively.

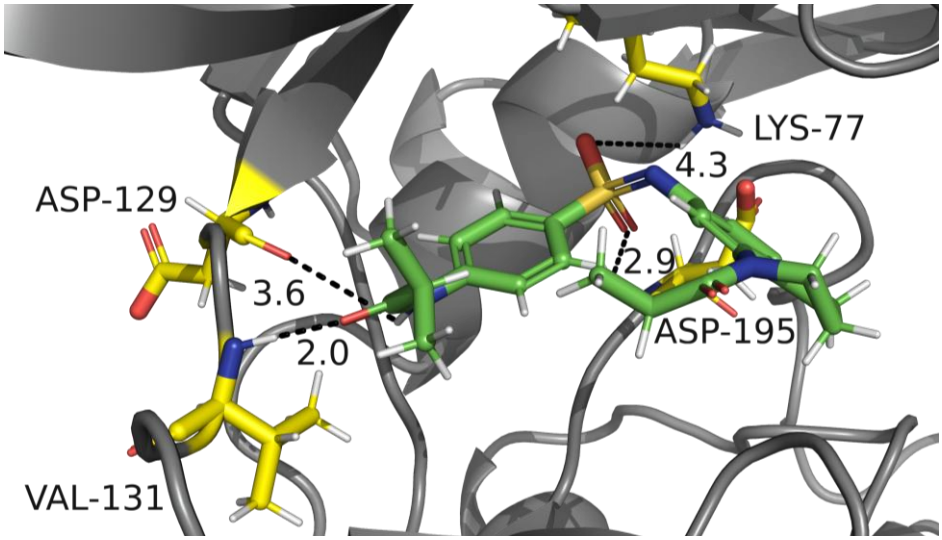


**Supplementary figure 6.30: Polar interactions of NCC-00007132** in the binding pocket of FhPIM kinase. NCC-00007132 (ligand) is displayed as sticks with green-coloured carbon atoms. The structure of FhPIM is illustrated as a cartoon in grey colour. The polar interactions are depicted as black dashed lines and their distances in angstroms (Å). Residues depicted in yellow colour are the polar interacting residues (Lys77, Asp129, Val131, and Asp195) in the binding pocket of FhPIM kinase. All nitrogen, oxygen, and sulphur atoms are in blue, red, and yelloworange colours, respectively.

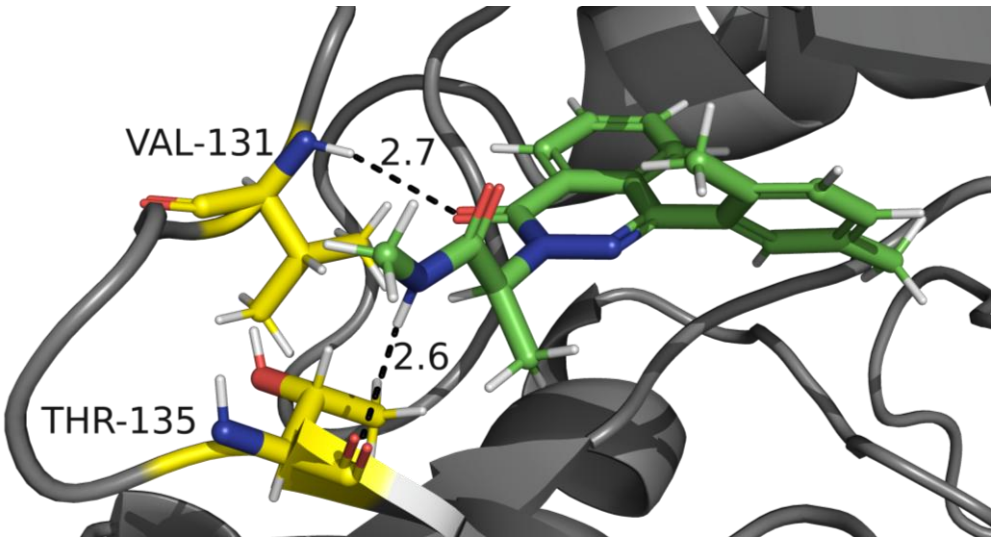


**Supplementary figure 6.31: Polar interactions of NCC-00059610** in the binding pocket of FhPIM kinase. NCC-00059610 (ligand) is displayed as sticks with green-coloured carbon atoms. The structure of FhPIM is illustrated as a cartoon in grey colour. The polar interactions are depicted as black dashed lines and their distances in angstroms (Å). Residues depicted in yellow colour are the polar interacting residues (Val131 and Thr135) in the binding pocket of FhPIM kinase. All nitrogen and oxygen atoms are in blue and red colours, respectively.

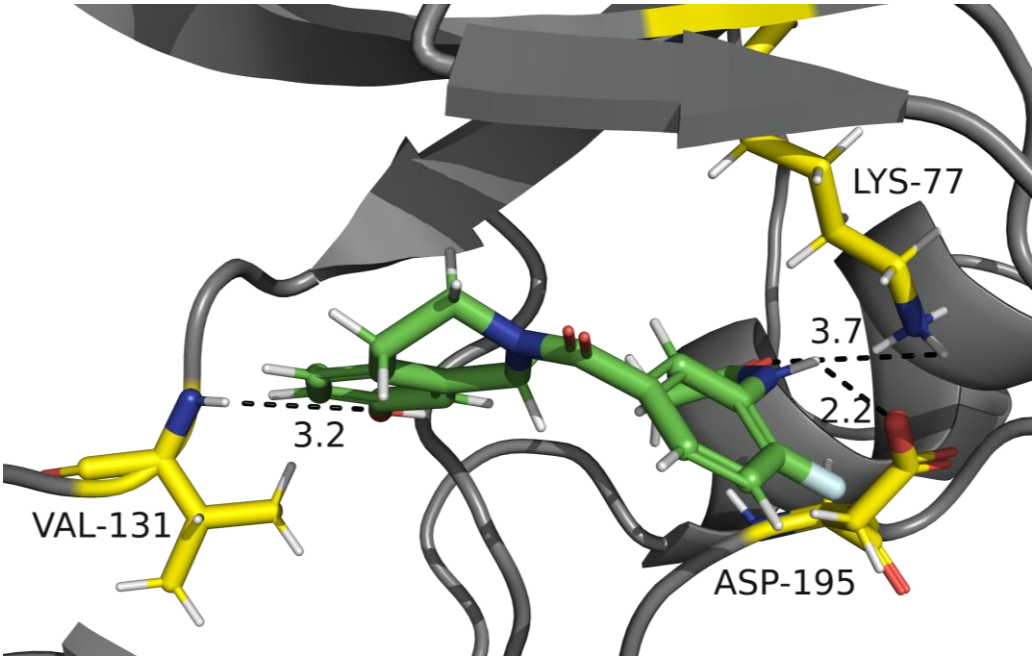


**Supplementary figure 6.32: Polar interactions of NCC-00064956** in the binding pocket of FhPIM kinase. NCC-00064956 (ligand) is displayed as sticks with green-coloured carbon atoms. The structure of FhPIM is illustrated as a cartoon in grey colour. The polar interactions are depicted as black dashed lines and their distances in angstroms (Å). Residues depicted in yellow colour are the polar interacting residues (Lys77, Val131, and Asp195) in the binding pocket of FhPIM kinase. All nitrogen, oxygen, and fluorine atoms are in blue, red, and palecyan colours, respectively.

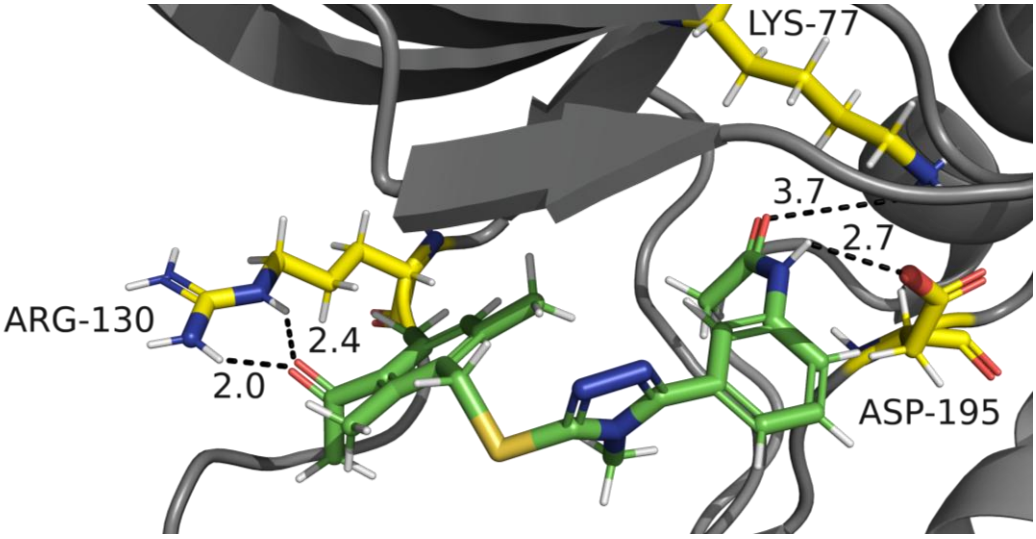


**Supplementary figure 6.33: Polar interactions of NCC-00081502** in the binding pocket of FhPIM kinase. NCC-00081502 (ligand) is displayed as sticks with green-coloured carbon atoms. The structure of FhPIM is illustrated as a cartoon in grey colour. The polar interactions are depicted as black dashed lines and their distances in angstroms (Å). Residues depicted in yellow colour are the polar interacting residues (Lys77, Arg130, and Asp195) in the binding pocket of FhPIM kinase. All nitrogen, oxygen, and sulphur atoms are in blue, red, and yelloworange colours, respectively.

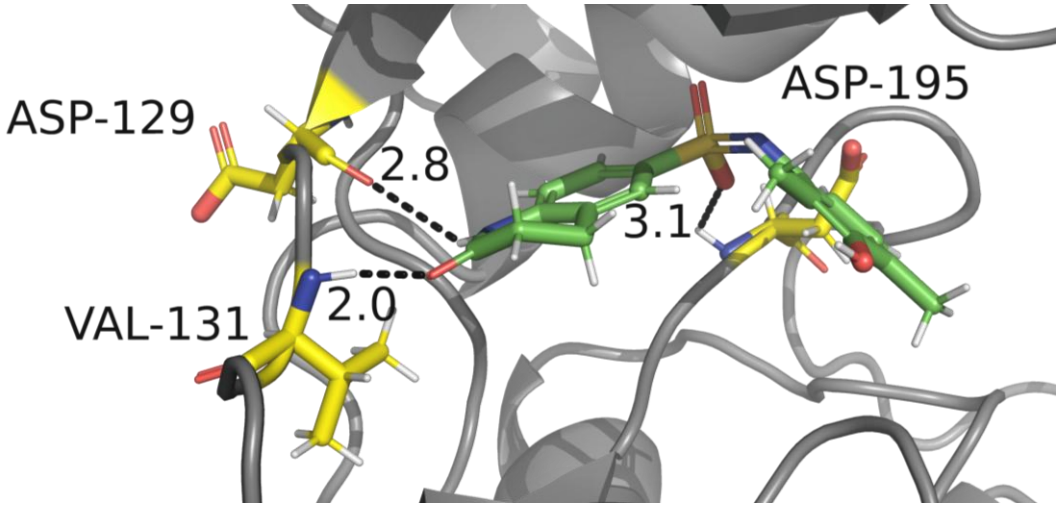


**Supplementary figure 6.34: Polar interactions of NCC-00059926** in the binding pocket of FhPIM kinase. NCC-00059926 (ligand) is displayed as sticks with green-coloured carbon atoms. The structure of FhPIM is illustrated as a cartoon in grey colour. The polar interactions are depicted as black dashed lines and their distances in angstroms (Å). Residues depicted in yellow colour are the polar interacting residues (Asp129, Val131, and Asp195) in the binding pocket of FhPIM kinase. All nitrogen, oxygen, and sulphur atoms are in blue, red, and yelloworange colours, respectively.

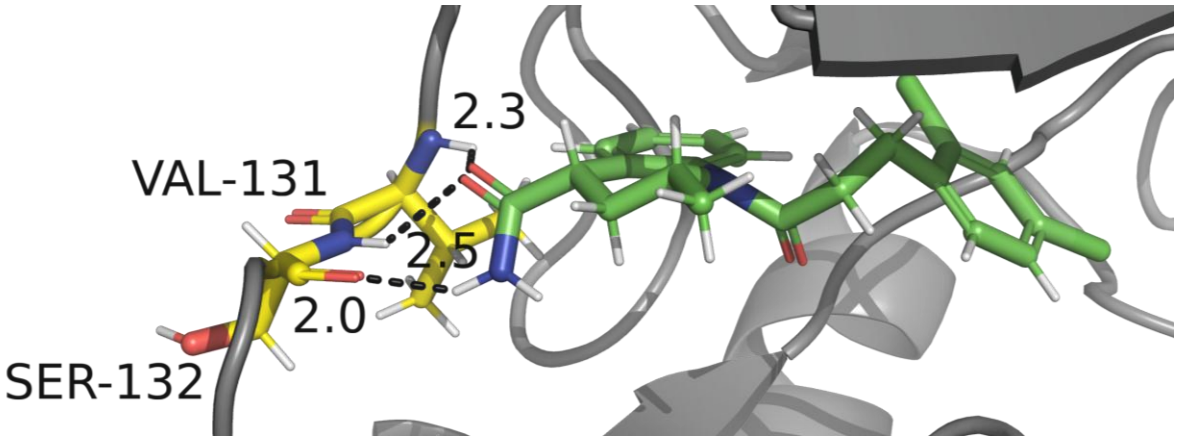


**Supplementary figure 6.35: Polar interactions of NCC-00046881** in the binding pocket of FhPIM kinase. NCC-00046881 (ligand) is displayed as sticks with green-coloured carbon atoms. The structure of FhPIM is illustrated as a cartoon in grey colour. The polar interactions are depicted as black dashed lines and their distances in angstroms (Å). Residues depicted in yellow colour are the polar interacting residues (Val131 and Ser132) in the binding pocket of FhPIM kinase. All nitrogen, oxygen, and chlorine atoms are in blue, red, and green colours, respectively.

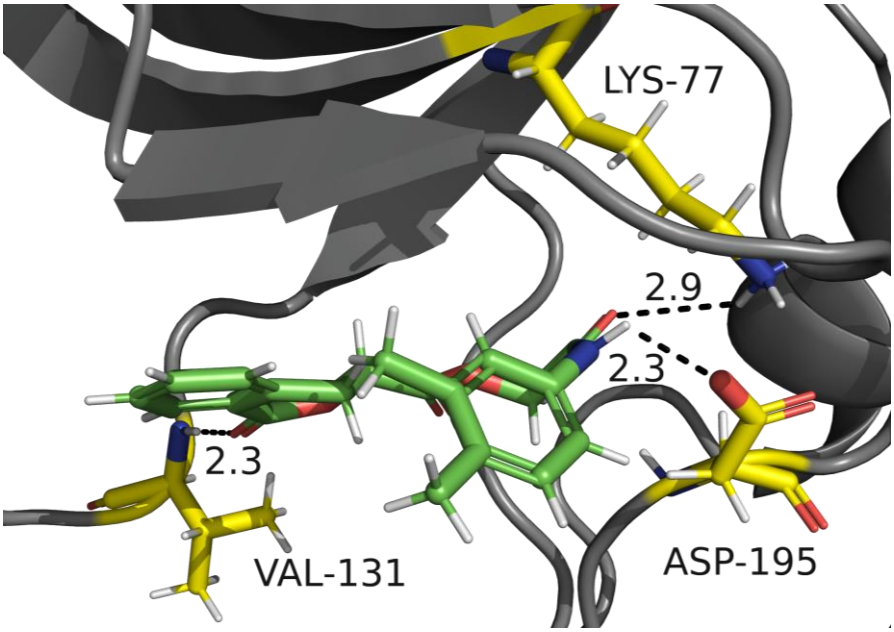


**Supplementary figure 6.36: Polar interactions of NCC-00030002** in the binding pocket of FhPIM kinase. NCC-00030002 (ligand) is displayed as sticks with green-coloured carbon atoms. The structure of FhPIM is illustrated as a cartoon in grey colour. The polar interactions are depicted as black dashed lines and their distances in angstroms (Å). Residues depicted in yellow colour are the polar interacting residues (Lys77, Val131, and Asp195) in the binding pocket of FhPIM kinase. All nitrogen, oxygen, and chlorine atoms are in blue, red, and green colours, respectively.

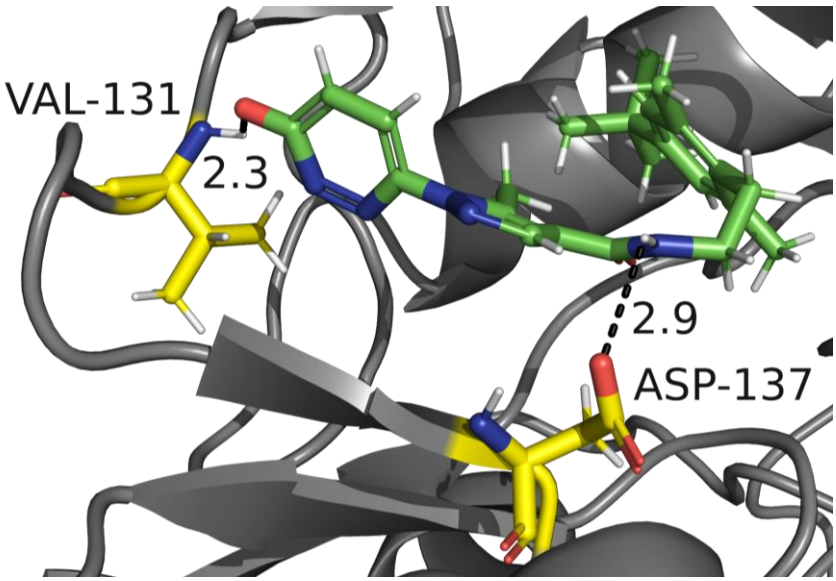


**Supplementary figure 6.37: Polar interactions of NCC-00019088** in the binding pocket of FhPIM kinase. NCC-00019088 (ligand) is displayed as sticks with green-coloured carbon atoms. The structure of FhPIM is illustrated as a cartoon in grey colour. The polar interactions are depicted as black dashed lines and their distances in angstroms (Å). Residues depicted in yellow colour are the polar interacting residues (Val131 and Asp137) in the binding pocket of FhPIM kinase. All nitrogen, oxygen, and chlorine atoms are in blue, red, and green colours, respectively.

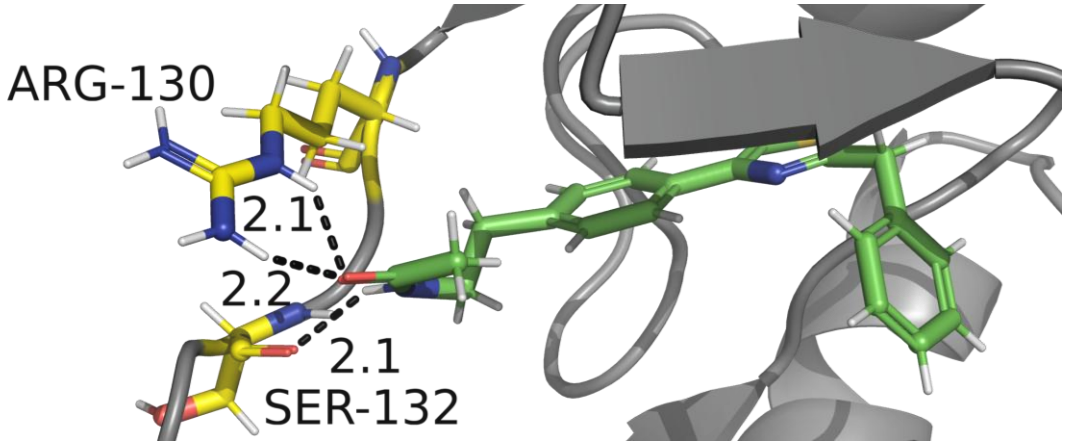


**Supplementary figure 6.38: Polar interactions of NCC-00082340** in the binding pocket of FhPIM kinase. NCC-00082340 (ligand) is displayed as sticks with green-coloured carbon atoms. The structure of FhPIM is illustrated as a cartoon in grey colour. The polar interactions are depicted as black dashed lines and their distances in angstroms (Å). Residues depicted in yellow colour are the polar interacting residues (Arg130 and Ser132) in the binding pocket of FhPIM kinase. All nitrogen, oxygen, and sulphur atoms are in blue, red, and yelloworange colours, respectively.

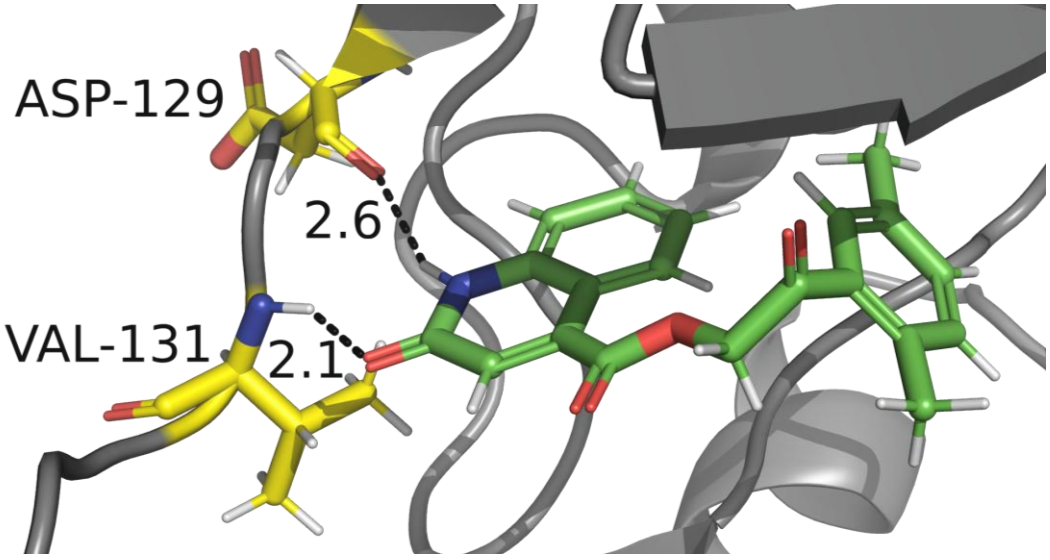


**Supplementary figure 6.39: Polar interactions of NCC-00016401** in the binding pocket of FhPIM kinase. NCC-00016401 (ligand) is displayed as sticks with green-coloured carbon atoms. The structure of FhPIM is illustrated as a cartoon in grey colour. The polar interactions are depicted as black dashed lines and their distances in angstroms (Å). Residues depicted in yellow colour are the polar interacting residues (Asp129 and Val131) in the binding pocket of FhPIM kinase. All nitrogen and oxygen atoms are in blue and red colours, respectively.

## 6.2 Supplementary tables

This section contains the supplementary tables used in this work, which provide information to support the assertions made in the result or discussion sections.

**Supplementary table 6.1: The statistical values for control vs CX-6258** treated adult and immature flukes. The mean motility score of flukes (n = 4) after 24, 48 and 72 h treatment for three independent experiments is stated below (score 0 = dead, 1 = heavily reduced, 2 = moderately reduced, 3 = normal movement). Wilcoxon rank sum test was performed to obtain the p value for each concentration vs control at different time points. The significance was assessed against control adult and immature flukes (n = 4), which exhibited the motility score of 3. NaN = Not a Number, ns = not significant (p value ≥ 0.05), * = p value < 0.05.

| Time [h] | Stage | Concentration [µM] | Mean | SEM | p value | Statistical significance |
|---|---|---|---|---|---|---|
| 24 | Adult | 25 | 3.00 | 0 | NaN | NaN |
| 24 | Adult | 50 | 2.75 | 0.25 | 0.453 | ns |
| 24 | Adult | 100 | 1.75 | 0.62 | 0.066 | ns |
| 24 | Immature | 25 | 2.75 | 0.25 | 0.453 | ns |
| 24 | Immature | 50 | 2.00 | 0 | 0.013 | * |
| 24 | Immature | 100 | 0 | 0 | 0.013 | * |
| 48 | Adult | 25 | 3.00 | 0 | NaN | NaN |
| 48 | Adult | 50 | 2.75 | 0.25 | 0.453 | ns |
| 48 | Adult | 100 | 1.00 | 0.40 | 0.020 | * |
| 48 | Immature | 25 | 2.00 | 0 | 0.013 | * |
| 48 | Immature | 50 | 0.50 | 0.28 | 0.019 | * |
| 48 | Immature | 100 | 0 | 0 | 0.013 | * |
| 72 | Adult | 25 | 3.00 | 0 | NaN | NaN |
| 72 | Adult | 50 | 2.25 | 0.47 | 0.185 | ns |
| 72 | Adult | 100 | 0.75 | 0.47 | 0.020 | * |
| 72 | Immature | 25 | 1.75 | 0.47 | 0.066 | ns |
| 72 | Immature | 50 | 0 | 0 | 0.013 | * |
| 72 | Immature | 100 | 0 | 0 | 0.013 | * |

**Supplementary table 6.2: The statistical values for control vs SGI-1776** treated adult and immature flukes. The mean motility score of flukes (n = 4) after 24, 48 and 72 h treatment for three independent experiments is stated below (score 0 = dead, 1 = heavily reduced, 2 = moderately reduced, 3 = normal movement). Wilcoxon rank sum test was performed to obtain the p value for each concentration vs control at different time points. The significance was assessed against control adult and immature flukes (n = 4), which exhibited the motility score of 3. NaN = Not a Number, ns = not significant (p value ≥ 0.05), * = p value < 0.05.

| Time [h] | Stage | Concentration [µM] | Mean | SEM | p value | Statistical significance |
|---|---|---|---|---|---|---|
| 24 | Adult | 25 | 3.00 | 0 | NaN | NaN |
| 24 | Adult | 50 | 2.50 | 0.28 | 0.181 | ns |
| 24 | Adult | 100 | 1.50 | 0.28 | 0.019 | * |
| 24 | Immature | 25 | 2.50 | 0.28 | 0.181 | ns |
| 24 | Immature | 50 | 1.50 | 0.28 | 0.019 | * |
| 24 | Immature | 100 | 0 | 0 | 0.013 | * |
| 48 | Adult | 25 | 2.75 | 0.25 | 0.453 | ns |
| 48 | Adult | 50 | 1.50 | 0.28 | 0.019 | * |
| 48 | Adult | 100 | 0 | 0 | 0.013 | * |
| 48 | Immature | 25 | 1.50 | 0.28 | 0.019 | * |
| 48 | Immature | 50 | 0.50 | 0.28 | 0.019 | * |
| 48 | Immature | 100 | 0 | 0 | 0.013 | * |
| 72 | Adult | 25 | 2.00 | 0 | 0.013 | * |
| 72 | Adult | 50 | 0.50 | 0.28 | 0.019 | * |
| 72 | Adult | 100 | 0 | 0 | 0.013 | * |
| 72 | Immature | 25 | 0.75 | 0.25 | 0.017 | * |
| 72 | Immature | 50 | 0 | 0 | 0.013 | * |
| 72 | Immature | 100 | 0 | 0 | 0.013 | * |

**Supplementary table 6.3: The statistical values for control vs vandetanib** treated adult and immature flukes. The mean motility score of flukes (n = 4) after 24, 48 and 72 h treatment for three independent experiments is stated below (score 0 = dead, 1 = heavily reduced, 2 = moderately reduced, 3 = normal movement). Wilcoxon rank sum test was performed to obtain the p value for each concentration vs control at different time points. The significance was assessed against control adult and immature flukes (n = 4), which exhibited the motility score of 3. NaN = Not a Number, ns = not significant (p value ≥ 0.05), * = p value < 0.05.

| Time [h] | Stage | Concentration [µM] | Mean | SEM | p value | Statistical significance |
|---|---|---|---|---|---|---|
| 24 | Adult | 25 | 3.00 | 0 | NaN | NaN |
| 24 | Adult | 50 | 2.25 | 0.25 | 0.060 | Ns |
| 24 | Adult | 100 | 1.00 | 0 | 0.013 | * |
| 24 | Immature | 25 | 1.50 | 0.28 | 0.019 | * |
| 24 | Immature | 50 | 0.50 | 0.28 | 0.019 | * |
| 24 | Immature | 100 | 0 | 0 | 0.013 | * |
| 48 | Adult | 25 | 2.75 | 0.25 | 0.453 | ns |
| 48 | Adult | 50 | 1.75 | 0.47 | 0.066 | ns |
| 48 | Adult | 100 | 0 | 0 | 0.013 | * |
| 48 | Immature | 25 | 0.50 | 0.28 | 0.019 | * |
| 48 | Immature | 50 | 0 | 0 | 0.013 | * |
| 48 | Immature | 100 | 0 | 0 | 0.013 | * |
| 72 | Adult | 25 | 2.50 | 0.28 | 0.181 | ns |
| 72 | Adult | 50 | 1.50 | 0.64 | 0.068 | ns |
| 72 | Adult | 100 | 0 | 0 | 0.013 | * |
| 72 | Immature | 25 | 0.50 | 0.28 | 0.019 | * |
| 72 | Immature | 50 | 0 | 0 | 0.013 | * |
| 72 | Immature | 100 | 0 | 0 | 0.013 | * |

**Supplementary table 6.4: The statistical values for control vs foretinib** treated adult and immature flukes. The mean motility score of flukes (n = 4) after 24, 48 and 72 h treatment for three independent experiments is stated below (score 0 = dead, 1 = heavily reduced, 2 = moderately reduced, 3 = normal movement). Wilcoxon rank sum test was performed to obtain the p value for each concentration vs control at different time points. The significance was assessed against control adult and immature flukes (n = 4), which exhibited the motility score of 3. NaN = Not a Number, ns = not significant (p value ≥ 0.05), * = p value < 0.05.

| Time [h] | Stage | Concentration [µM] | Mean | SEM | p value | Statistical significance |
|---|---|---|---|---|---|---|
| 24 | Adult | 25 | 3.00 | 0 | NaN | NaN |
| 24 | Adult | 50 | 3.00 | 0 | NaN | NaN |
| 24 | Adult | 100 | 2.00 | 0 | 0.013 | * |
| 24 | Immature | 25 | 2.50 | 0.28 | 0.181 | ns |
| 24 | Immature | 50 | 1.50 | 0.28 | 0.019 | * |
| 24 | Immature | 100 | 0.50 | 0.28 | 0.019 | * |
| 48 | Adult | 25 | 2.75 | 0.25 | 0.453 | ns |
| 48 | Adult | 50 | 2.50 | 0.28 | 0.181 | ns |
| 48 | Adult | 100 | 1.00 | 0.40 | 0.02 | * |
| 48 | Immature | 25 | 1.00 | 0.57 | 0.019 | * |
| 48 | Immature | 50 | 0.25 | 0.25 | 0.017 | * |
| 48 | Immature | 100 | 0.25 | 0.25 | 0.017 | * |
| 72 | Adult | 25 | 2.75 | 0.25 | 0.453 | ns |
| 72 | Adult | 50 | 1.50 | 0.28 | 0.019 | * |
| 72 | Adult | 100 | 0.50 | 0.28 | 0.019 | * |
| 72 | Immature | 25 | 0.50 | 0.28 | 0.019 | * |
| 72 | Immature | 50 | 0 | 0 | 0.013 | * |
| 72 | Immature | 100 | 0 | 0 | 0.013 | * |

**Supplementary table 6.5: The statistical values for control vs tyrosine kinase-IN-1** treated adult and immature flukes. The mean motility score of flukes (n = 4) after 24, 48 and 72 h treatment for three independent experiments is stated below (score 0 = dead, 1 = heavily reduced, 2 = moderately reduced, 3 = normal movement). Wilcoxon rank sum test was performed to obtain the p value for each concentration vs control at different time points. The significance was assessed against control adult and immature flukes (n = 4), which exhibited the motility score of 3. NaN = Not a Number, ns = not significant (p value ≥ 0.05), * = p value < 0.05.

| Time [h] | Stage | Concentration [µM] | Mean | SEM | p value | Statistical significance |
|---|---|---|---|---|---|---|
| 24 | Adult | 25 | 3.00 | 0 | NaN | NaN |
| 24 | Adult | 50 | 3.00 | 0 | NaN | NaN |
| 24 | Adult | 100 | 0.50 | 0.28 | 0.019 | * |
| 24 | Immature | 25 | 2.00 | 0 | 0.013 | * |
| 24 | Immature | 50 | 0.50 | 0.28 | 0.019 | * |
| 24 | Immature | 100 | 0.25 | 0.25 | 0.017 | * |
| 48 | Adult | 25 | 3.00 | 0 | NaN | NaN |
| 48 | Adult | 50 | 2.50 | 0.28 | 0.181 | ns |
| 48 | Adult | 100 | 0 | 0 | 0.013 | * |
| 48 | Immature | 25 | 1.00 | 0 | 0.013 | * |
| 48 | Immature | 50 | 0 | 0 | 0.013 | * |
| 48 | Immature | 100 | 0.25 | 0.25 | 0.017 | * |
| 72 | Adult | 25 | 2.75 | 0.25 | 0.453 | ns |
| 72 | Adult | 50 | 2.00 | 0.40 | 0.066 | ns |
| 72 | Adult | 100 | 0 | 0 | 0.013 | * |
| 72 | Immature | 25 | 0.75 | 0.25 | 0.017 | * |
| 72 | Immature | 50 | 0 | 0 | 0.013 | * |
| 72 | Immature | 100 | 0 | 0 | 0.013 | * |

**Supplementary table 6.6: The statistical values for control vs ruboxistaurin** treated adult and immature flukes. The mean motility score of flukes (n = 4) after 24, 48 and 72 h treatment for three independent experiments is stated below (score 0 = dead, 1 = heavily reduced, 2 = moderately reduced, 3 = normal movement). Wilcoxon rank sum test was performed to obtain the p value for each concentration vs control at different time points. The significance was assessed against control adult and immature flukes (n = 4), which exhibited the motility score of 3. NaN = Not a Number, ns = not significant (p value ≥ 0.05), * = p value < 0.05.

| Time [h] | Stage | Concentration [µM] | Mean | SEM | p value | Statistical significance |
|---|---|---|---|---|---|---|
| 24 | Adult | 25 | 2.75 | 0.25 | 0.453 | ns |
| 24 | Adult | 50 | 1.00 | 0 | 0.013 | * |
| 24 | Adult | 100 | 0 | 0 | 0.013 | * |
| 24 | Immature | 25 | 1.50 | 0.28 | 0.019 | * |
| 24 | Immature | 50 | 0 | 0 | 0.013 | * |
| 24 | Immature | 100 | 0 | 0 | 0.013 | * |
| 48 | Adult | 25 | 2.50 | 0.28 | 0.181 | ns |
| 48 | Adult | 50 | 0.50 | 0.28 | 0.019 | * |
| 48 | Adult | 100 | 0 | 0 | 0.013 | * |
| 48 | Immature | 25 | 1.00 | 0.57 | 0.019 | * |
| 48 | Immature | 50 | 0 | 0 | 0.013 | * |
| 48 | Immature | 100 | 0 | 0 | 0.013 | * |
| 72 | Adult | 25 | 2.00 | 0 | 0.013 | * |
| 72 | Adult | 50 | 0 | 0 | 0.013 | * |
| 72 | Adult | 100 | 0 | 0 | 0.013 | * |
| 72 | Immature | 25 | 0.50 | 0.28 | 0.019 | * |
| 72 | Immature | 50 | 0 | 0 | 0.013 | * |
| 72 | Immature | 100 | 0 | 0 | 0.013 | * |

**Supplementary table 6.7: The statistical values for control vs TCBZ** treated adult and immature flukes. The mean motility score of flukes (n = 4) after 24, 48 and 72 h treatment for three independent experiments is stated below (score 0 = dead, 1 = heavily reduced, 2 = moderately reduced, 3 = normal movement). Wilcoxon rank sum test was performed to obtain the p value for each concentration vs control at different time points. The significance was assessed against control adult and immature flukes (n = 4), which exhibited the motility score of 3. NaN = Not a Number, ns = not significant (p value ≥ 0.05), * = p value < 0.05.

| Time [h] | Stage | Concentration [µM] | Mean | SEM | p value | Statistical significance |
|---|---|---|---|---|---|---|
| 24 | Adult | 25 | 2.50 | 0.28 | 0.181 | ns |
| 24 | Adult | 50 | 2.00 | 0.40 | 0.066 | ns |
| 24 | Adult | 100 | 0.50 | 0.28 | 0.019 | * |
| 24 | Immature | 25 | 2.00 | 0 | 0.013 | * |
| 24 | Immature | 50 | 1.00 | 0 | 0.013 | * |
| 24 | Immature | 100 | 0 | 0 | 0.013 | * |
| 48 | Adult | 25 | 2.00 | 0.40 | 0.066 | ns |
| 48 | Adult | 50 | 1.50 | 0.28 | 0.019 | * |
| 48 | Adult | 100 | 0 | 0 | 0.013 | * |
| 48 | Immature | 25 | 2.00 | 0 | 0.013 | * |
| 48 | Immature | 50 | 1.00 | 0 | 0.013 | * |
| 48 | Immature | 100 | 0 | 0 | 0.013 | * |
| 72 | Adult | 25 | 1.50 | 0.28 | 0.019 | * |
| 72 | Adult | 50 | 1.00 | 0 | 0.013 | * |
| 72 | Adult | 100 | 0 | 0 | 0.013 | * |
| 72 | Immature | 25 | 1.00 | 0 | 0.013 | * |
| 72 | Immature | 50 | 0 | 0 | 0.013 | * |
| 72 | Immature | 100 | 0 | 0 | 0.013 | * |

**Supplementary table 6.8: 2D structures of the small-molecule PK inhibitors used in this thesis**.

| 2D structures of the small-molecule PK inhibitor used in this thesis | Name of the compound | SMILES | Molecular formula | Molecular weight (Da) |
|---|---|---|---|---|
| 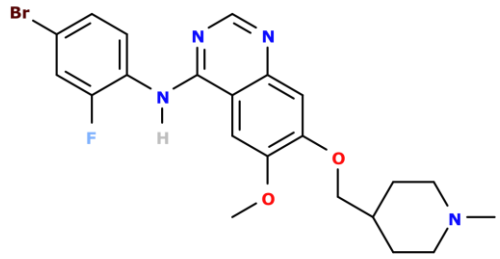 | vandetanib (ZD6474) | CN1CCC(CC1)COC2=C(C=C3C(=C2)N=CN=C3NC4=C(C=C(C=C4)Br)F)OC | C22H24BrFN4O2 | 475.35 |
| 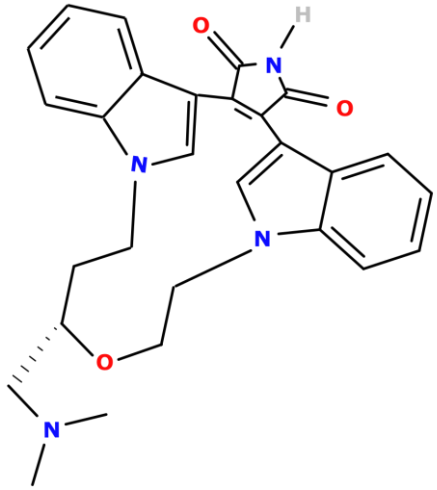 | ruboxistaurin (LY333531) HCl | CN(C)CC1CCN2C=C(C3=CC=CC=C32)C4=C(C5=CN(CCO1)C6=CC=CC=C65)C(=O)NC4=O.Cl | C28H28N4O3.HCl | 505.01 |
| 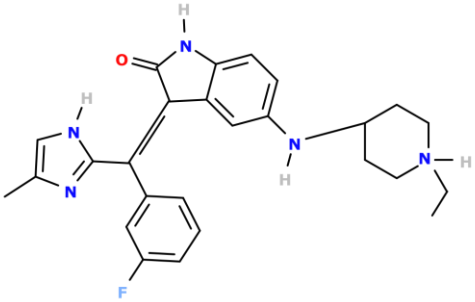 | tyrosine kinase-IN-1 (XL999) | O=C1NC2=C(C=C(NC3CCN(CC)CC3)C=C2)/C1=C(C4=CC=CC(F)=C4)/C5=NC=C(C)N5 | | 445.53 |

| | | | | |
|---|---|---|---|---|
| 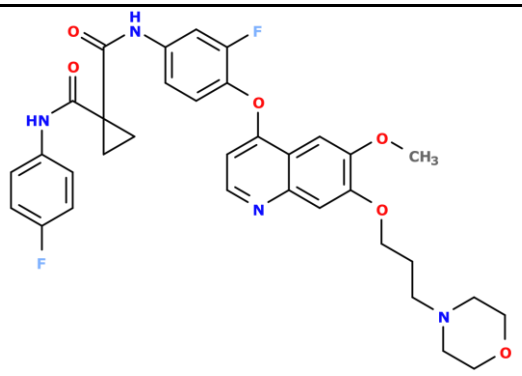 | foretinib (XL880) | COC1=CC2=C(C=CN=C2C=C1OCCCN3CCOCC3)OC4=C(C=C(C=C4)NC(=O)C5(CC5)C(=O)NC6=CC=C(C=C6)F)F | C34H34F2N4O6 | 632.65 |
| 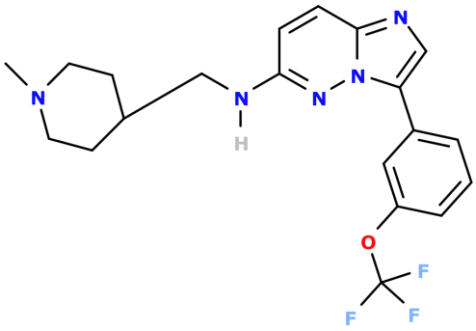 | SGI-1776 | CN1CCC(CNC(C=C2)=NN3C2=NC=C3C4=CC=CC(OC(F)(F)F)=C4)CC1 | C20H22F3N5O | 405.42 |
| 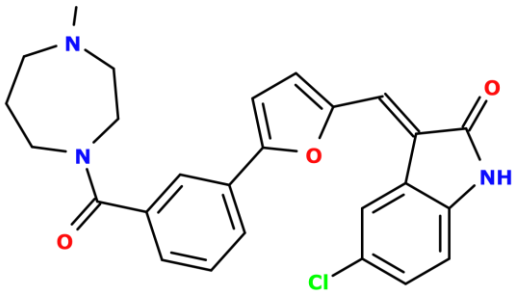 | CX-6258 HCl | CN1CCCN(CC1)C(=O)C2=CC=CC(=C2)C3=CC=C(O3)C=C4C5=C(C=CC(=C5)Cl)NC4=O.Cl | C26H24ClN3O3.HCl | 498.40 |

| | | | | |
|---|---|---|---|---|
| 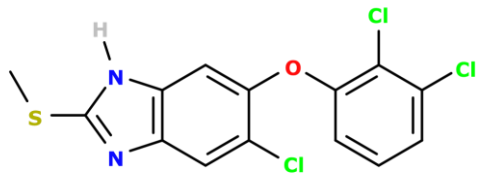 | triclabendazole | CSc1nc2cc(Cl)c(Oc3cccc(Cl)c3Cl)cc2[nH]1 | C14H9Cl3N2OS | 359.66 |

**Supplementary table 6.9: 2D structures of the ligands identified from the first round of virtual screening** of the docked ligands from the MCCC library in the binding pocket of FhPIM.

| 2D structures of the docked ligand from MCCC library in FhPIM kinase | Name of the MCCC compound | Supplier compound ID | SMILES | Molecular formula | Molecular weight (Da) |
|---|---|---|---|---|---|
| 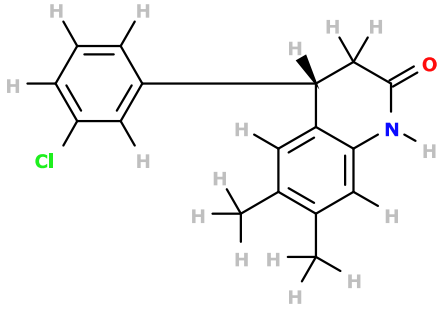 | NCC-00008538_9 | SAM003508754 | Cc1cc2NC(=O)C[C@H](c2cc1C)c1cccc(Cl)c1 | C17H16ClNO | 285.768 |
| 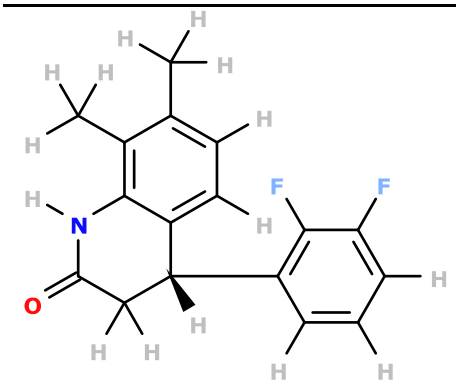 | NCC-00077290_10 | SAM003508800 | Cc1ccc2[C@@H](CC(=O)Nc2c1C)c1cccc(F)c1F | C17H15F2NO | 287.3039 |
| 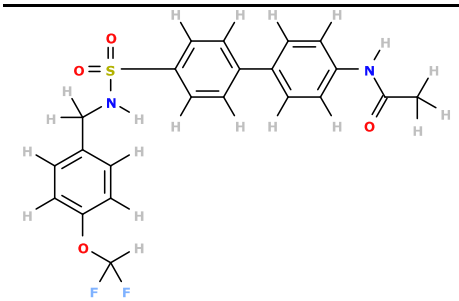 | NCC-00072436_15 | SAM003598879 | c1(ccc(cc1)S(=O)(=O)NCc1ccc(cc1)OC(F)F)c1ccc(cc1)NC(=O)C | C22H20F2N2O4S | 446.467 |

| | | | | | |
|---|---|---|---|---|---|
| 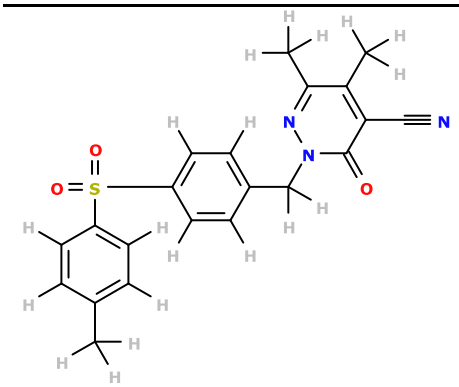 | NCC-00032341_30 | SAM003629930 | Cc1nn(c(=O)c(c1C)C#N)Cc1ccc(cc1)S(=O)(=O)c1ccc(C)cc1 | C21H19N3O3S | 393.459 |
| 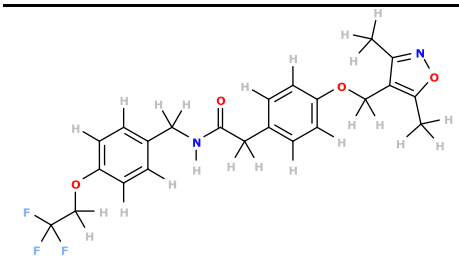 | NCC-00044825_71 | SAM003626646 | C(=O)(NCc1ccc(cc1)OCC(F)(F)F)Cc1ccc(cc1)OCc1c(noc1C)C | 448.4349 | 448.4349 |
| 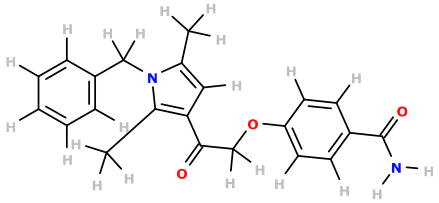 | NCC-00074481_94 | SAM003546595 | C(=O)(c1cc(C)n(c1C)Cc1ccccc1)COc1ccc(cc1)C(=O)N | C22H22N2O3 | 362.4217 |
| 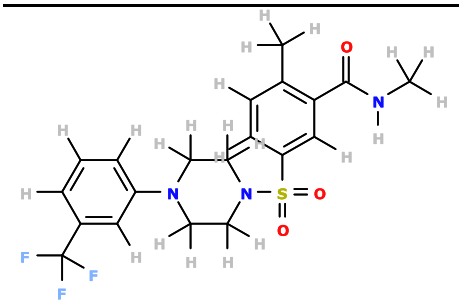 | NCC-00009414_98 | SAM003508527 | N1(CCN(CC1)c1ccc(c1)C(F)(F)F)S(=O)(=O)c1cc(c(cc1)C)C(=O)NC | C20H22F3N3O3S | 441.467 |
| 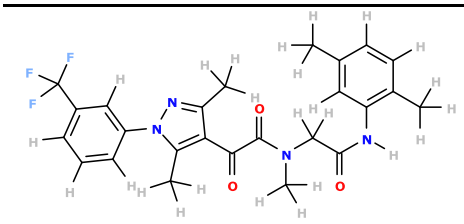 | NCC-00044623_100 | SAM003673984 | C(=O)(C(=O)N(C)CC(=O)Nc1cc(C)ccc1C)c1 | C25H25F3N4O3 | 486.4862 |

| | | | | | |
|---|---|---|---|---|---|
| | | | c(C)nn(c1C)c1cccc(c1)C(F)(F)F | | |
| 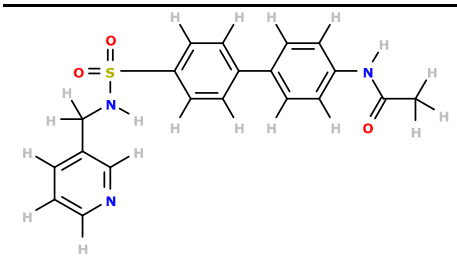 | NCC-00061091_171 | C20H19N3O3S | c1(ccc(cc1)S(=O)(=O)NCc1cccnc1)c1ccc(cc1)NC(=O)C | C20H19N3O3S | 381.448 |
| 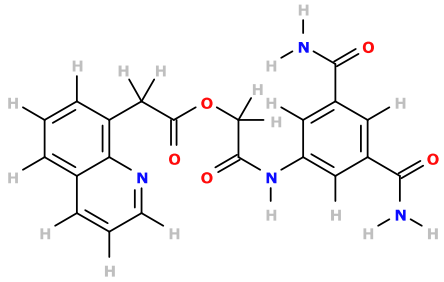 | NCC-00032141_188 | SAM003627212 | N(C(=O)COC(=O)Cc1ccccc2cccnc12)c1cc(cc(c1)C(=O)N)C(=O)N | C21H18N4O5 | 406.3914 |
| 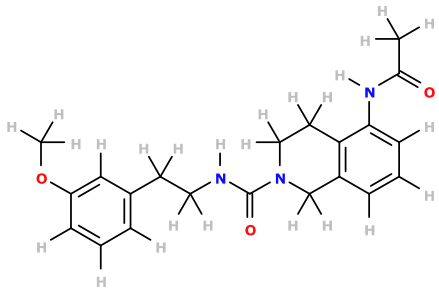 | NCC-00057583_195 | SAM003639002 | N(C(=O)N1CCc2c(C1)cccc2NC(=O)C)CCc1cccc(c1)OC | C21H25N3O3 | 367.4415 |
| 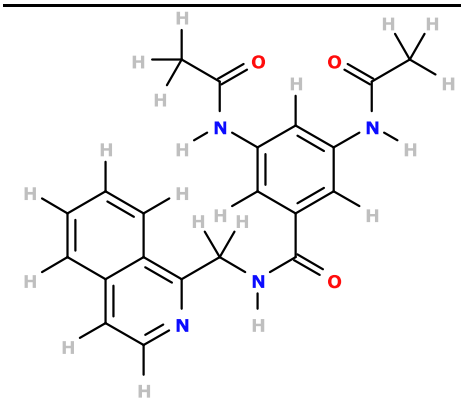 | NCC-00032797_245 | SAM003626303 | c1(cc(cc(c1)C(=O)NCc1nccc2ccccc12)NC(=O)C)NC(=O)C | C21H20N4O3 | 376.4085 |

| | | | | | |
|---|---|---|---|---|---|
| 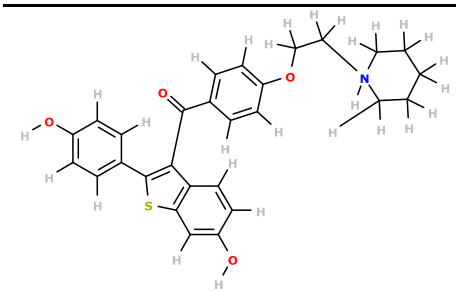 | NCC-00090515_288 | R 1402 | c1(c(sc2c1ccc(c2)O)c1ccc(cc1)O)C(=O)c1ccc(cc1)OCC[NH]1CCCCC1 | C28H27NO4S | 473.583 |
| 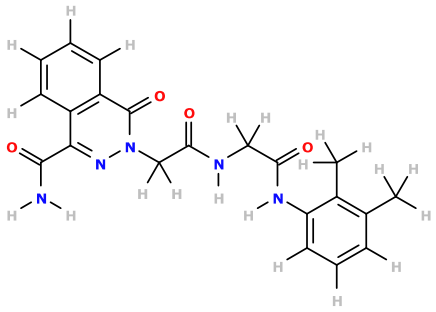 | NCC-00015704_299 | SAM003544913 | N(C(=O)Cn1nc(c2ccccc2c1=O)C(=O)N)CC(=O)Nc1cccc(C)c1C | C21H21N5O4 | 407.4225 |
| 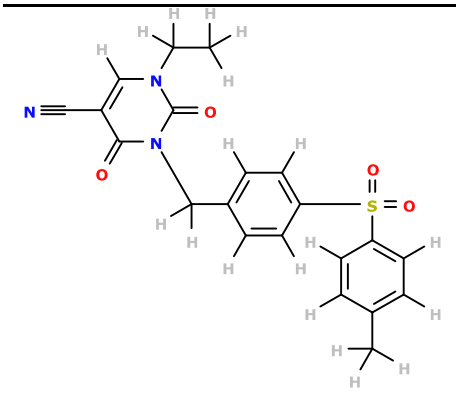 | NCC-00058509_420 | SAM003636048 | n1(cc(C#N)c(=O)n(c1=O)Cc1ccc(cc1)S(=O)(=O)c1ccc(C)cc1)CC | C21H19N3O4S | 409.458 |
| 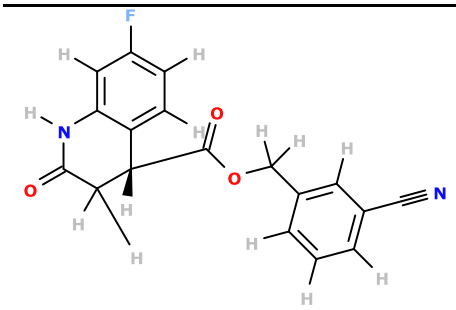 | NCC-00032487_497 | SAM003630539 | c1(cccc(c1)C#N)COC(=O)[C@H]1c2ccc(F)cc2NC(=O)C1 | C18H13FN2O3 | 324.3058 |

**Supplementary table 6.10: 2D structures of the ligands identified from the second round of virtual screening** of the docked ligands from the MCCC library in the binding pocket of FhPIM.

| 2D structures of the docked ligand from MCCC library in FhPIM kinase | Name of the MCCC compound | Supplier compound ID | SMILES | Molecular formula | Molecular weight (Da) |
|---|---|---|---|---|---|
| 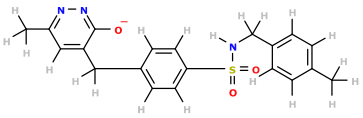 | NCC-00011396_52 | SAM003652748 | c1(ccc(cc1)Cc1cc(C)nnc1[O-])S(=O)(=O)NCc1ccc(C)cc1 | C20H21N3O3S | 383.464 |
| 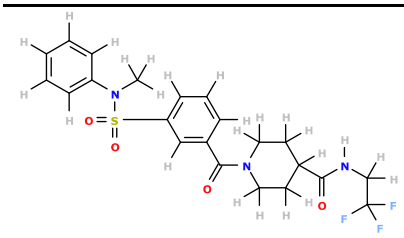 | NCC-00082673_86 | SAM003631222 | c1(cccc(c1)C(=O)N1CCC(CC1)C(=O)NCC(F)(F)F)S(=O)(=O)N(C)c1ccccc1 | C22H24F3N3O4S | 483.504 |
| 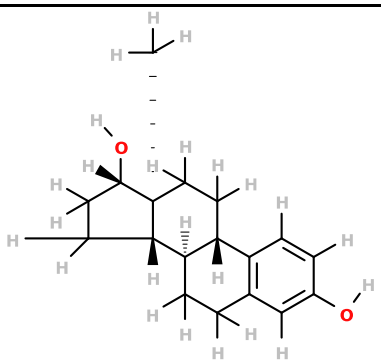 | NCC-00089972_111 | E 8875 | [C@]12([C@H]([C@H]3[C@@H](c4c(CC3)cc(cc4)O)CC1)CC[C@@H]2O)C | C18H24O2 | 272.382 |

| | | | | | |
|---|---|---|---|---|---|
| 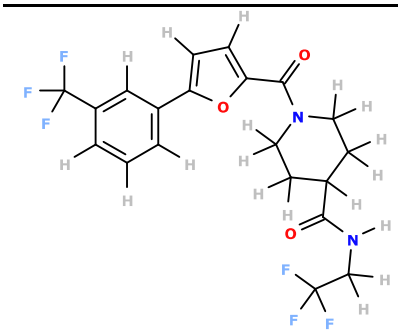 | NCC-00069794_115 | SAM003640720 | C1(CCN(CC1)C(=O)c1oc(cc1)c1cccc(c1)C(F)(F)F)C(=O)NCC(F)(F)F | C20H18F6N2O3 | 448.3589 |
| 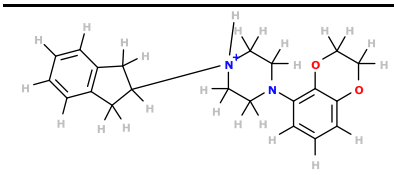 | NCC-00090340_134 | S 5321 | N1(CC[NH+](CC1)C1Cc2c(C1)cccc2)c1c2c(OCCO2)ccc1 | C21H24N2O2 | 336.4275 |
| 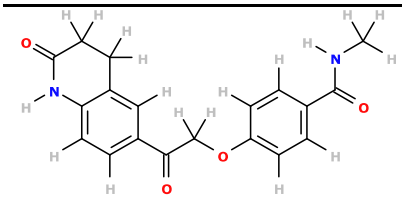 | NCC-00071469_188 | SAM003534921 | C(=O)(COc1ccc(cc1)C(=O)NC)c1ccc2NC(=O)CCc2c1 | C19H18N2O4 | 338.3572 |
| 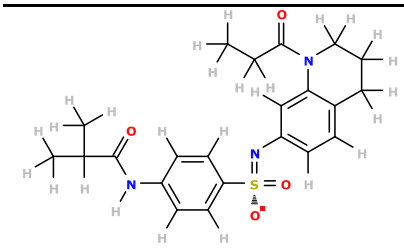 | NCC-00007132_214 | SAM003655019 | [S@@](=O)(=Nc1ccc2CCCN(c2c1)C(=O)CC)([O])c1ccc(cc1)NC(=O)C(C)C | C22H27N3O4S | 429.532 |

| | | | | | |
|---|---|---|---|---|---|
| 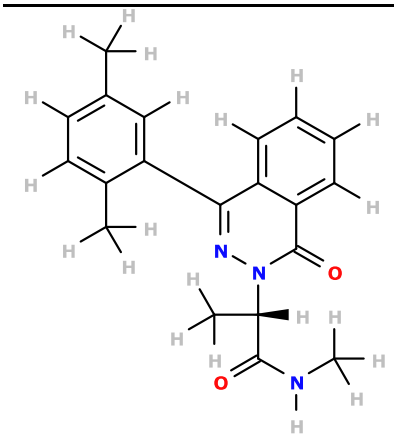 | NCC-00059610_220 | SAM003542333 | n1(nc(c2ccccc2c1=O)c1cc(C)ccc1C)[C@@H](C)C(=O)NC | C20H21N3O2 | 335.3996 |
| 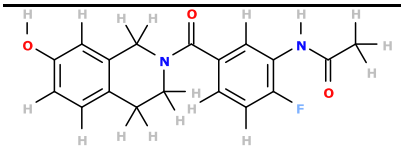 | NCC-00064956_221 | SAM003612884 | C(=O)(N1CCc2ccc(cc2C1)O)c1cc(c(cc1)F)NC(=O)C | C18H17FN2O3 | 328.3376 |
| 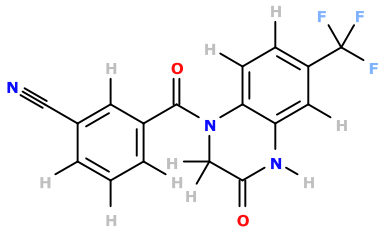 | NCC-00087073_240 | SAM003599817 | c1(cccc(c1)C#N)C(=O)N1c2ccc(cc2NC(=O)C1)C(F)(F)F | C17H10F3N3O2 | 345.2754 |
| 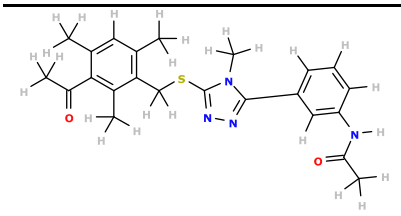 | NCC-00081502_250 | SAM003580409 | c1(nnc(n1C)SCc1c(C)cc(C)c(c1C)C(=O)C)c1cccc(c1)NC(=O)C | C23H26N4O2S | 422.543 |

| | | | | | |
|---|---|---|---|---|---|
| 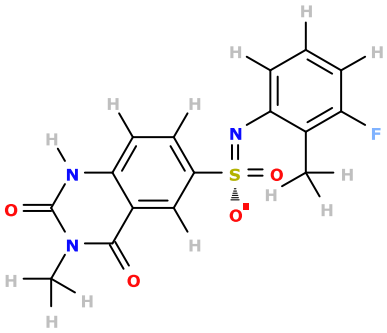 | NCC-00009498_281 | SAM003507838 | Cn1c(=O)[nH]c2ccc(cc2c1=O)[S@](=O)(=Nc1cccc(F)c1C)[O] | C16H14FN3O4S | 363.363 |
| 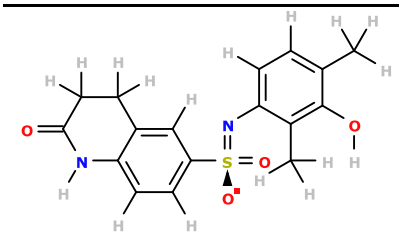 | NCC-00059926_308 | SAM003615663 | [S@](=O)(=Nc1ccc(C)c(c1C)O)([O])c1ccc2NC(=O)CCc2c1 | C17H18N2O4S | 346.401 |
| 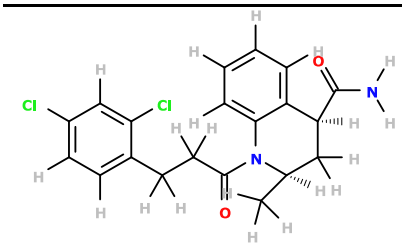 | NCC-00046881_318 | SAM003533853 | C[C@@H]1C[C@@H](c2ccccc2N1C(=O)CCc1ccc(Cl)cc1Cl)C(=O)N | C20H20Cl2N2O2 | 391.291 |
| 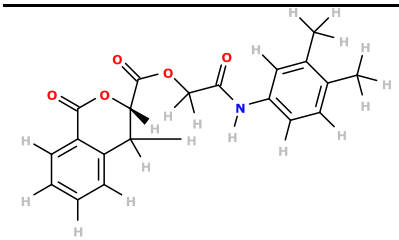 | NCC-00030002_340 | SAM003607116 | O(CC(=O)Nc1ccc(C)c(c1)C)C(=O)[C@@H]1Cc2ccccc2C(=O)O1 | C20H19NO5 | 353.3686 |
| 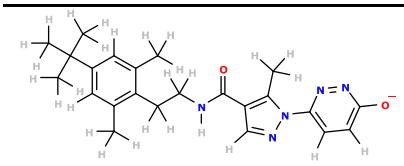 | NCC-00019088_394 | SAM003530891 | N(C(=O)c1cnn(c1C)c1ccc([O-])nn1)CC | C23H29N5O2 | 407.5087 |

| | | | | | |
|---|---|---|---|---|---|
| | | | c1c(C)cc(cc1C)C(C)(C)C | | |
| 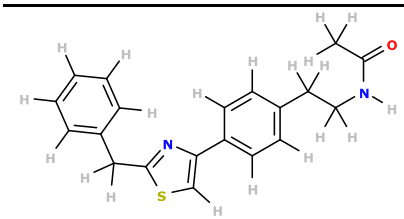 | NCC-00082340_472 | SAM003637871 | c1(ccc(cc1)c1csc(n1)Cc1ccccc1)CCNC(=O)C | C20H20N2OS | 336.451 |
| 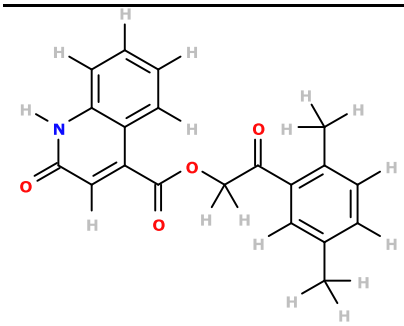 | NCC-00016401_485 | SAM003538854 | C(=O)(OCC(=O)c1c(ccc(C)c1)C)c1cc(=O)[nH]c2ccccc12 | C20H17NO4 | 335.3533 |

**Supplementary table 6.11: Clinical trials status of small-molecule PK inhibitors** (CX-6258, SGI-1776, vandetanib, foretinib, tyrosine kinase-IN-1, and ruboxistaurin) used *in vitro* against immature and adult liver flukes in this thesis.

| PK inhibitor | Clinical trial status | Pharmacological target | Known adverse effects | Administration Scheme (dosage) | References |
|---|---|---|---|---|---|
| CX-6258 | Preclinical development phase | PIM1 | Preclinical compound | Preclinical compound | (196,198,383,384) |
| SGI-176 | Terminated after phase I and then withdrawn | PIM1 | Dose limiting toxicity of cardiac QTc prolongation | 100 mg (oral) as 50 mg every 12 hours for 14 days period of a 21-day cycle | (385–387) |
| vandetanib (ZD6474) | FDA approved (medullary thyroid cancer) | Multi-receptor tyrosine kinase | Hypertension, QTc interval prolongation and increased AST and ALT levels | ≤ 300 mg/day for 56 days | (266–269,345,350) |
| foretinib (XL 880) | Investigational phase I/II but discontinued/withdrawn | Multi-receptor tyrosine kinase | Hypertension and proteinuria | 80 mg/day for 28 days | (270,271) |
| tyrosine kinase-IN-1 (XL999) | Terminated after phase II | Multi-receptor tyrosine kinase | Cardiac toxicities | 2.4 mg/kg intravenous as a four-hour infusion weekly for 8 weeks | (388,389) |
| ruboxistaurin | Investigational phase II/III | PKCβ | Nasopharyngitis | 32 mg/day for two years | (338,343,344) |

| | | | | |
|---|---|---|---|---|
| (LY33353 1) | (diabetic retinopath y) | | | |

**Supplementary table 6.12: Predicted PKs derived from the refined bioinformatic pipeline** within the kinome of the common liver fluke. The PKs that Kinannote could not classify into their family and/or sub-families were designated as NA (not applicable). The STK (unclassifiable) and twilight PKs were retained as a part of the final kinome, while the subthreshold PKs were excluded and not considered in the final kinome. (ePK = eukaryotic protein kinase)

| Predicted PK identifiers | Type of hit | Group | Family | Sub-family |
|---|---|---|---|---|
| FhPK_0001 | ePK | AGC | PKG | NA |
| FhPK_0002 | ePK | CK1 | CK1 | CK1-G |
| FhPK_0003 | not ePK | subthreshold | NA | NA |
| FhPK_0004 | ePK | STE | STE20 | MSN |
| FhPK_0005 | ePK | TKL | STKR | STKR2 |
| FhPK_0006 | ePK | Other | ULK | ULK |
| FhPK_0007 | not ePK | subthreshold | NA | NA |
| FhPK_0008 | ePK | TK | VKR | NA |
| FhPK_0009 | ePK | TKL | MLK | ILK |
| FhPK_0010 | twilight | unclassified | NA | NA |
| FhPK_0011 | ePK | CK1 | CK1 | CK1-D |
| FhPK_0012 | not ePK | subthreshold | NA | NA |
| FhPK_0013 | ePK | AGC | PKG | NA |
| FhPK_0014 | ePK | AGC | AKT | NA |
| FhPK_0015 | ePK | CMGC | MAPK | ERK7 |
| FhPK_0016 | ePK | TK | CSK | NA |
| FhPK_0017 | ePK | AGC | PKA | NA |
| FhPK_0018 | ePK | Other | CAMKK | NA |
| FhPK_0019 | ePK | STK (unclassifiable) | NA | NA |
| FhPK_0020 | ePK | TK | SEV | NA |
| FhPK_0021 | ePK | AGC | GRK | BARK |
| FhPK_0022 | ePK | CAMK | CAMKL | MARK |
| FhPK_0023 | ePK | AGC | PKA | NA |
| FhPK_0024 | ePK | AGC | PDK1 | NA |
| FhPK_0025 | ePK | CK1 | CK1 | CK1-A |

| | | | | |
|---|---|---|---|---|
| FhPK_0026 | ePK | AGC | RSK | RSKP70 |
| FhPK_0027 | ePK | CMGC | CDK | CDC2 |
| FhPK_0028 | ePK | STK (unclassifiable) | NA | NA |
| FhPK_0029 | ePK | CAMK | CAMK1 | NA |
| FhPK_0030 | ePK | TK | EGFR | NA |
| FhPK_0031 | ePK | CAMK | CASK | NA |
| FhPK_0032 | ePK | STK (unclassifiable) | NA | NA |
| FhPK_0033 | ePK | Other | PLK | SAK |
| FhPK_0034 | ePK | Other | NAK | MPSK |
| FhPK_0035 | ePK | Other | PEK | GCN2 |
| FhPK_0036 | ePK | STE | STE20 | PAKA |

**Supplementary table 6.13: Ligands evaluated in the first round of molecular docking**. A total of 484 compounds are listed in this table, which were rejected following manual visualisation and evaluation during the first round of molecular docking of the FhPIM kinase.

| Ligand name | AutoDock Vina generated energy (kcal/mol) | Ranking according to the script | Grade according to the evaluation criteria |
|---|---|---|---|
| NCC-00089825 | -11.6 | 1 | X |
| NCC-00089136 | -11.4 | 2 | C |
| NCC-00089743 | -11.3 | 3 | C |
| NCC-00089978 | -11.3 | 4 | X |
| NCC-00090330 | -11.2 | 5 | X |
| NCC-00090518 | -11.1 | 6 | X |
| NCC-00090530 | -11.1 | 7 | C |
| NCC-00089639 | -11 | 8 | X |
| NCC-00089566 | -10.8 | 11 | X |
| NCC-00090547 | -10.8 | 12 | C |
| NCC-00004318 | -10.8 | 13 | X |
| NCC-00002800 | -10.7 | 14 | C |
| NCC-00089952 | -10.7 | 16 | X |
| NCC-00090326 | -10.7 | 17 | X |
| NCC-00002821 | -10.6 | 18 | C |
| NCC-00000102 | -10.6 | 19 | X |
| NCC-00049546 | -10.6 | 20 | C |
| NCC-00000183 | -10.6 | 21 | C |
| NCC-00089740 | -10.6 | 22 | X |
| NCC-00010513 | -10.5 | 23 | C |
| NCC-00030893 | -10.5 | 24 | C |
| NCC-00090102 | -10.5 | 25 | X |
| NCC-00044374 | -10.5 | 26 | X |
| NCC-00066871 | -10.5 | 27 | X |

| | | | |
|---|---|---|---|
| NCC-00031228 | -10.5 | 28 | X |
| NCC-00018018 | -10.5 | 29 | X |
| NCC-00043155 | -10.5 | 31 | C |
| NCC-00052807 | -10.5 | 32 | C |
| NCC-00017088 | -10.5 | 33 | C |
| NCC-00038868 | -10.5 | 34 | X |
| NCC-00058085 | -10.5 | 35 | C |
| NCC-00034676 | -10.5 | 36 | C |
| NCC-00068655 | -10.5 | 37 | X |
| NCC-00029519 | -10.5 | 38 | X |
| NCC-00090670 | -10.5 | 39 | X |
| NCC-00016947 | -10.4 | 40 | X |
| NCC-00036060 | -10.4 | 41 | X |
| NCC-00011735 | -10.4 | 42 | X |
| NCC-00008558 | -10.4 | 43 | X |
| NCC-00051158 | -10.4 | 44 | X |
| NCC-00085110 | -10.4 | 45 | C |
| NCC-00084301 | -10.4 | 46 | C |
| NCC-00007602 | -10.4 | 47 | C |
| NCC-00089541 | -10.4 | 48 | C |
| NCC-00000206 | -10.4 | 49 | X |
| NCC-00075486 | -10.4 | 50 | C |
| NCC-00027798 | -10.4 | 51 | C |
| NCC-00061584 | -10.4 | 52 | X |
| NCC-00009436 | -10.4 | 53 | X |
| NCC-00018006 | -10.4 | 54 | X |
| NCC-00077998 | -10.4 | 55 | C |
| NCC-00000267 | -10.4 | 56 | X |
| NCC-00046006 | -10.4 | 57 | C |
| NCC-00054460 | -10.4 | 58 | X |
| NCC-00011399 | -10.4 | 59 | X |
| NCC-00086667 | -10.3 | 60 | C |
| NCC-00030477 | -10.3 | 61 | C |
| NCC-00090397 | -10.3 | 62 | C |
| NCC-00053237 | -10.3 | 63 | X |
| NCC-00018101 | -10.3 | 64 | X |
| NCC-00070702 | -10.3 | 65 | X |
| NCC-00005841 | -10.3 | 66 | C |
| NCC-00090465 | -10.3 | 67 | X |
| NCC-00074214 | -10.3 | 68 | X |
| NCC-00082551 | -10.3 | 69 | X |
| NCC-00011393 | -10.3 | 70 | X |
| NCC-00043950 | -10.3 | 72 | X |
| NCC-00059110 | -10.3 | 73 | X |
| NCC-00034544 | -10.3 | 74 | X |
| NCC-00011772 | -10.3 | 75 | C |
| NCC-00009031 | -10.3 | 76 | C |

| | | | |
|---|---|---|---|
| NCC-00058089 | -10.3 | 77 | C |
| NCC-00078413 | -10.3 | 78 | C |
| NCC-00041457 | -10.3 | 79 | X |
| NCC-00018484 | -10.3 | 80 | X |
| NCC-00066529 | -10.3 | 81 | C |
| NCC-00062943 | -10.3 | 82 | X |
| NCC-00085573 | -10.3 | 83 | X |
| NCC-00012317 | -10.3 | 84 | C |
| NCC-00046183 | -10.3 | 85 | C |
| NCC-00048792 | -10.2 | 86 | C |
| NCC-00046881 | -10.2 | 87 | X |
| NCC-00073815 | -10.2 | 88 | C |
| NCC-00083446 | -10.2 | 89 | X |
| NCC-00006512 | -10.2 | 90 | C |
| NCC-00033621 | -10.2 | 91 | X |
| NCC-00089739 | -10.2 | 92 | C |
| NCC-00030586 | -10.2 | 93 | X |
| NCC-00087632 | -10.2 | 95 | X |
| NCC-00000075 | -10.2 | 96 | X |
| NCC-00036261 | -10.2 | 97 | X |
| NCC-00074518 | -10.2 | 99 | X |
| NCC-00061737 | -10.2 | 101 | X |
| NCC-00070424 | -10.2 | 102 | C |
| NCC-00064661 | -10.2 | 103 | C |
| NCC-00089677 | -10.2 | 104 | C |
| NCC-00029061 | -10.2 | 105 | X |
| NCC-00061342 | -10.2 | 106 | X |
| NCC-00090115 | -10.2 | 107 | C |
| NCC-00072348 | -10.2 | 108 | C |
| NCC-00027257 | -10.2 | 109 | X |
| NCC-00062691 | -10.2 | 110 | C |
| NCC-00005199 | -10.2 | 111 | C |
| NCC-00041142 | -10.2 | 112 | C |
| NCC-00070657 | -10.2 | 113 | X |
| NCC-00061559 | -10.2 | 114 | X |
| NCC-00077025 | -10.2 | 115 | X |
| NCC-00017214 | -10.2 | 116 | C |
| NCC-00088104 | -10.2 | 117 | C |
| NCC-00083194 | -10.2 | 118 | X |
| NCC-00061845 | -10.2 | 119 | X |
| NCC-00004688 | -10.1 | 120 | C |
| NCC-00047455 | -10.1 | 121 | C |
| NCC-00069794 | -10.1 | 122 | X |
| NCC-00090277 | -10.1 | 123 | X |
| NCC-00004577 | -10.1 | 124 | C |
| NCC-00079924 | -10.1 | 125 | C |
| NCC-00064489 | -10.1 | 126 | X |

| | | | |
|---|---|---|---|
| NCC-00063845 | -10.1 | 127 | C |
| NCC-00016802 | -10.1 | 128 | C |
| NCC-00006576 | -10.1 | 129 | X |
| NCC-00032330 | -10.1 | 130 | C |
| NCC-00000243 | -10.1 | 131 | X |
| NCC-00031067 | -10.1 | 132 | X |
| NCC-00015107 | -10.1 | 133 | C |
| NCC-00090147 | -10.1 | 134 | C |
| NCC-00003799 | -10.1 | 135 | X |
| NCC-00011430 | -10.1 | 136 | C |
| NCC-00034045 | -10.1 | 137 | C |
| NCC-00007176 | -10.1 | 138 | X |
| NCC-00039041 | -10.1 | 139 | X |
| NCC-00018899 | -10.1 | 140 | X |
| NCC-00089610 | -10.1 | 141 | C |
| NCC-00083924 | -10.1 | 142 | C |
| NCC-00035095 | -10.1 | 143 | X |
| NCC-00055004 | -10.1 | 144 | C |
| NCC-00056483 | -10.1 | 145 | C |
| NCC-00052570 | -10.1 | 146 | C |
| NCC-00040335 | -10.1 | 147 | X |
| NCC-00061575 | -10.1 | 148 | C |
| NCC-00013906 | -10.1 | 149 | X |
| NCC-00035782 | -10.1 | 150 | X |
| NCC-00077817 | -10.1 | 151 | X |
| NCC-00082044 | -10.1 | 152 | X |
| NCC-00074160 | -10.1 | 153 | C |
| NCC-00090091 | -10.1 | 154 | X |
| NCC-00008652 | -10.1 | 155 | C |
| NCC-00083274 | -10.1 | 156 | C |
| NCC-00018188 | -10.1 | 157 | X |
| NCC-00036411 | -10.1 | 158 | C |
| NCC-00043780 | -10.1 | 159 | X |
| NCC-00033015 | -10.1 | 160 | X |
| NCC-00063295 | -10.1 | 161 | C |
| NCC-00089702 | -10.1 | 162 | C |
| NCC-00011066 | -10.1 | 163 | X |
| NCC-00082486 | -10.1 | 164 | C |
| NCC-00080281 | -10.1 | 165 | X |
| NCC-00030507 | -10.1 | 166 | X |
| NCC-00080727 | -10.1 | 167 | C |
| NCC-00078496 | -10.1 | 168 | C |
| NCC-00026994 | -10.1 | 169 | C |
| NCC-00029008 | -10.1 | 170 | X |
| NCC-00073413 | -10.1 | 172 | C |
| NCC-00061658 | -10.1 | 173 | X |
| NCC-00056307 | -10.1 | 174 | C |

| | | | |
|---|---|---|---|
| NCC-00016152 | -10.1 | 175 | C |
| NCC-00015745 | -10.1 | 176 | C |
| NCC-00029476 | -10.1 | 177 | C |
| NCC-00035055 | -10.1 | 178 | X |
| NCC-00087644 | -10 | 179 | X |
| NCC-00013043 | -10 | 180 | C |
| NCC-00088552 | -10 | 181 | C |
| NCC-00030088 | -10 | 182 | X |
| NCC-00002546 | -10 | 183 | X |
| NCC-00037754 | -10 | 184 | X |
| NCC-00059776 | -10 | 185 | C |
| NCC-00032080 | -10 | 186 | C |
| NCC-00059828 | -10 | 187 | C |
| NCC-00038527 | -10 | 189 | X |
| NCC-00061626 | -10 | 190 | C |
| NCC-00087112 | -10 | 191 | X |
| NCC-00011396 | -10 | 192 | C |
| NCC-00007257 | -10 | 193 | X |
| NCC-00018454 | -10 | 194 | X |
| NCC-00078778 | -10 | 196 | C |
| NCC-00037495 | -10 | 197 | C |
| NCC-00049789 | -10 | 198 | C |
| NCC-00009548 | -10 | 199 | C |
| NCC-00032036 | -10 | 200 | X |
| NCC-00070848 | -10 | 201 | C |
| NCC-00016343 | -10 | 202 | C |
| NCC-00018392 | -10 | 203 | C |
| NCC-00080609 | -10 | 204 | X |
| NCC-00090571 | -10 | 205 | X |
| NCC-00038652 | -10 | 206 | X |
| NCC-00018137 | -10 | 207 | X |
| NCC-00086964 | -10 | 208 | X |
| NCC-00054424 | -10 | 209 | X |
| NCC-00019390 | -10 | 210 | X |
| NCC-00085067 | -10 | 211 | X |
| NCC-00074080 | -10 | 212 | X |
| NCC-00087423 | -10 | 213 | C |
| NCC-00067808 | -10 | 214 | X |
| NCC-00018399 | -10 | 215 | X |
| NCC-00019764 | -10 | 216 | C |
| NCC-00020719 | -10 | 217 | X |
| NCC-00068825 | -10 | 218 | C |
| NCC-00030265 | -10 | 219 | C |
| NCC-00040611 | -10 | 220 | X |
| NCC-00059178 | -10 | 221 | C |
| NCC-00036120 | -10 | 222 | X |
| NCC-00015996 | -10 | 223 | X |

| | | | |
|---|---|---|---|
| NCC-00076357 | -10 | 224 | X |
| NCC-00077943 | -10 | 225 | C |
| NCC-00032420 | -10 | 226 | X |
| NCC-00076253 | -10 | 227 | C |
| NCC-00050511 | -10 | 228 | X |
| NCC-00013722 | -10 | 229 | X |
| NCC-00059322 | -10 | 230 | X |
| NCC-00014151 | -10 | 231 | X |
| NCC-00028367 | -10 | 232 | X |
| NCC-00003794 | -10 | 233 | C |
| NCC-00090620 | -10 | 234 | X |
| NCC-00037852 | -10 | 235 | X |
| NCC-00015210 | -10 | 236 | X |
| NCC-00011427 | -10 | 237 | C |
| NCC-00029091 | -10 | 238 | C |
| NCC-00069890 | -10 | 239 | C |
| NCC-00057134 | -10 | 240 | C |
| NCC-00038284 | -10 | 241 | C |
| NCC-00070482 | -10 | 242 | C |
| NCC-00079665 | -10 | 243 | X |
| NCC-00071000 | -10 | 244 | X |
| NCC-00064078 | -10 | 246 | C |
| NCC-00086660 | -10 | 247 | C |
| NCC-00050061 | -10 | 248 | C |
| NCC-00045989 | -10 | 249 | X |
| NCC-00087237 | -10 | 250 | X |
| NCC-00044605 | -10 | 251 | X |
| NCC-00056970 | -10 | 252 | X |
| NCC-00033922 | -10 | 253 | C |
| NCC-00018937 | -10 | 254 | C |
| NCC-00001814 | -10 | 255 | X |
| NCC-00028312 | -10 | 256 | C |
| NCC-00061721 | -10 | 257 | C |
| NCC-00077027 | -10 | 258 | C |
| NCC-00063182 | -10 | 259 | X |
| NCC-00070779 | -10 | 260 | C |
| NCC-00062235 | -10 | 261 | C |
| NCC-00047849 | -10 | 262 | C |
| NCC-00012921 | -10 | 263 | X |
| NCC-00007565 | -10 | 264 | C |
| NCC-00055984 | -10 | 265 | X |
| NCC-00059419 | -10 | 266 | X |
| NCC-00085932 | -9.9 | 267 | C |
| NCC-00071495 | -9.9 | 268 | X |
| NCC-00070300 | -9.9 | 269 | C |
| NCC-00028272 | -9.9 | 270 | C |
| NCC-00055894 | -9.9 | 271 | X |

| | | | |
|---|---|---|---|
| NCC-00005287 | -9.9 | 272 | C |
| NCC-00090078 | -9.9 | 273 | X |
| NCC-00009410 | -9.9 | 274 | X |
| NCC-00028090 | -9.9 | 275 | X |
| NCC-00033645 | -9.9 | 276 | C |
| NCC-00082686 | -9.9 | 277 | C |
| NCC-00062159 | -9.9 | 278 | C |
| NCC-00013995 | -9.9 | 279 | C |
| NCC-00033852 | -9.9 | 280 | C |
| NCC-00032608 | -9.9 | 281 | X |
| NCC-00090638 | -9.9 | 282 | X |
| NCC-00054299 | -9.9 | 283 | X |
| NCC-00047080 | -9.9 | 284 | X |
| NCC-00037589 | -9.9 | 285 | X |
| NCC-00062294 | -9.9 | 286 | C |
| NCC-00045090 | -9.9 | 287 | C |
| NCC-00037574 | -9.9 | 289 | C |
| NCC-00046519 | -9.9 | 290 | X |
| NCC-00068660 | -9.9 | 291 | X |
| NCC-00034973 | -9.9 | 292 | X |
| NCC-00054632 | -9.9 | 293 | X |
| NCC-00027356 | -9.9 | 294 | X |
| NCC-00044804 | -9.9 | 295 | C |
| NCC-00071239 | -9.9 | 296 | X |
| NCC-00090159 | -9.9 | 297 | C |
| NCC-00087196 | -9.9 | 298 | C |
| NCC-00007605 | -9.9 | 300 | X |
| NCC-00005008 | -9.9 | 301 | C |
| NCC-00057126 | -9.9 | 302 | C |
| NCC-00073811 | -9.9 | 303 | C |
| NCC-00079242 | -9.9 | 304 | X |
| NCC-00032270 | -9.9 | 305 | X |
| NCC-00067095 | -9.9 | 306 | C |
| NCC-00062429 | -9.9 | 307 | X |
| NCC-00062844 | -9.9 | 308 | X |
| NCC-00077948 | -9.9 | 309 | C |
| NCC-00019131 | -9.9 | 310 | C |
| NCC-00078593 | -9.9 | 311 | X |
| NCC-00009430 | -9.9 | 312 | X |
| NCC-00061656 | -9.9 | 313 | X |
| NCC-00064005 | -9.9 | 314 | C |
| NCC-00088999 | -9.9 | 315 | X |
| NCC-00061696 | -9.9 | 316 | C |
| NCC-00082563 | -9.9 | 317 | C |
| NCC-00084741 | -9.9 | 318 | X |
| NCC-00071358 | -9.9 | 319 | C |
| NCC-00002262 | -9.9 | 320 | X |

| | | | |
|---|---|---|---|
| NCC-00059422 | -9.9 | 321 | C |
| NCC-00045774 | -9.9 | 322 | C |
| NCC-00083413 | -9.9 | 323 | C |
| NCC-00012411 | -9.9 | 324 | C |
| NCC-00073836 | -9.9 | 325 | C |
| NCC-00035631 | -9.9 | 326 | C |
| NCC-00057630 | -9.9 | 327 | X |
| NCC-00018712 | -9.9 | 328 | C |
| NCC-00070762 | -9.9 | 329 | X |
| NCC-00056244 | -9.9 | 330 | X |
| NCC-00063250 | -9.9 | 331 | X |
| NCC-00052827 | -9.9 | 332 | C |
| NCC-00000420 | -9.9 | 333 | X |
| NCC-00074343 | -9.9 | 334 | X |
| NCC-00035105 | -9.9 | 335 | C |
| NCC-00070722 | -9.9 | 336 | X |
| NCC-00045768 | -9.9 | 337 | C |
| NCC-00047700 | -9.9 | 338 | X |
| NCC-00009760 | -9.9 | 339 | C |
| NCC-00060974 | -9.9 | 340 | C |
| NCC-00073605 | -9.9 | 341 | C |
| NCC-00055767 | -9.9 | 342 | C |
| NCC-00014180 | -9.9 | 343 | C |
| NCC-00017078 | -9.9 | 344 | X |
| NCC-00088045 | -9.9 | 345 | X |
| NCC-00090626 | -9.9 | 346 | C |
| NCC-00052717 | -9.9 | 347 | C |
| NCC-00034432 | -9.9 | 348 | X |
| NCC-00038320 | -9.9 | 349 | C |
| NCC-00046680 | -9.9 | 350 | X |
| NCC-00005640 | -9.9 | 351 | C |
| NCC-00007159 | -9.9 | 352 | X |
| NCC-00083490 | -9.9 | 353 | X |
| NCC-00052202 | -9.9 | 354 | X |
| NCC-00018146 | -9.9 | 355 | X |
| NCC-00081746 | -9.9 | 356 | C |
| NCC-00083458 | -9.9 | 357 | X |
| NCC-00029890 | -9.9 | 358 | C |
| NCC-00028108 | -9.9 | 359 | C |
| NCC-00029260 | -9.9 | 360 | X |
| NCC-00005363 | -9.9 | 361 | X |
| NCC-00007123 | -9.9 | 362 | X |
| NCC-00030956 | -9.9 | 363 | X |
| NCC-00069907 | -9.9 | 364 | C |
| NCC-00012392 | -9.9 | 365 | C |
| NCC-00088794 | -9.9 | 366 | C |
| NCC-00082859 | -9.9 | 367 | X |

| | | | |
|---|---|---|---|
| NCC-00074610 | -9.9 | 368 | X |
| NCC-00030038 | -9.9 | 369 | C |
| NCC-00015784 | -9.9 | 370 | X |
| NCC-00087203 | -9.9 | 371 | C |
| NCC-00005996 | -9.9 | 372 | C |
| NCC-00018546 | -9.9 | 373 | X |
| NCC-00000107 | -9.9 | 374 | X |
| NCC-00061321 | -9.9 | 375 | X |
| NCC-00073987 | -9.9 | 376 | C |
| NCC-00042402 | -9.9 | 377 | X |
| NCC-00043631 | -9.9 | 378 | C |
| NCC-00075095 | -9.9 | 379 | X |
| NCC-00083915 | -9.9 | 380 | C |
| NCC-00027250 | -9.9 | 381 | X |
| NCC-00014814 | -9.9 | 382 | C |
| NCC-00030185 | -9.9 | 383 | X |
| NCC-00061692 | -9.9 | 384 | C |
| NCC-00087468 | -9.9 | 385 | X |
| NCC-00027772 | -9.9 | 386 | C |
| NCC-00006238 | -9.9 | 387 | C |
| NCC-00046009 | -9.9 | 388 | X |
| NCC-00080518 | -9.9 | 389 | C |
| NCC-00038324 | -9.9 | 390 | C |
| NCC-00018245 | -9.9 | 391 | X |
| NCC-00056931 | -9.9 | 392 | C |
| NCC-00090676 | -9.9 | 393 | X |
| NCC-00005224 | -9.9 | 394 | X |
| NCC-00070534 | -9.9 | 395 | X |
| NCC-00016359 | -9.9 | 396 | C |
| NCC-00045837 | -9.9 | 397 | C |
| NCC-00032216 | -9.9 | 398 | X |
| NCC-00047373 | -9.9 | 399 | X |
| NCC-00067969 | -9.8 | 400 | X |
| NCC-00019968 | -9.8 | 401 | C |
| NCC-00028975 | -9.8 | 402 | X |
| NCC-00073017 | -9.8 | 403 | X |
| NCC-00037666 | -9.8 | 404 | C |
| NCC-00084911 | -9.8 | 405 | C |
| NCC-00038228 | -9.8 | 406 | X |
| NCC-00045253 | -9.8 | 407 | X |
| NCC-00029877 | -9.8 | 408 | C |
| NCC-00027008 | -9.8 | 409 | C |
| NCC-00076821 | -9.8 | 410 | X |
| NCC-00050838 | -9.8 | 411 | X |
| NCC-00034233 | -9.8 | 412 | C |
| NCC-00030974 | -9.8 | 413 | C |
| NCC-00001277 | -9.8 | 414 | X |

| | | | |
|---|---|---|---|
| NCC-00028318 | -9.8 | 415 | C |
| NCC-00083683 | -9.8 | 416 | X |
| NCC-00050856 | -9.8 | 417 | C |
| NCC-00018842 | -9.8 | 418 | C |
| NCC-00018888 | -9.8 | 419 | X |
| NCC-00018574 | -9.8 | 421 | X |
| NCC-00031802 | -9.8 | 422 | C |
| NCC-00017801 | -9.8 | 423 | C |
| NCC-00067411 | -9.8 | 424 | C |
| NCC-00028598 | -9.8 | 425 | X |
| NCC-00073673 | -9.8 | 426 | X |
| NCC-00030230 | -9.8 | 427 | C |
| NCC-00047625 | -9.8 | 428 | C |
| NCC-00052702 | -9.8 | 429 | C |
| NCC-00062618 | -9.8 | 430 | X |
| NCC-00007569 | -9.8 | 431 | C |
| NCC-00029109 | -9.8 | 432 | C |
| NCC-00080682 | -9.8 | 433 | X |
| NCC-00089829 | -9.8 | 434 | C |
| NCC-00016991 | -9.8 | 435 | X |
| NCC-00085849 | -9.8 | 436 | X |
| NCC-00000776 | -9.8 | 437 | X |
| NCC-00070325 | -9.8 | 438 | X |
| NCC-00090198 | -9.8 | 439 | C |
| NCC-00044694 | -9.8 | 440 | C |
| NCC-00046409 | -9.8 | 441 | X |
| NCC-00073854 | -9.8 | 442 | X |
| NCC-00083095 | -9.8 | 443 | X |
| NCC-00012442 | -9.8 | 444 | X |
| NCC-00055848 | -9.8 | 445 | X |
| NCC-00016800 | -9.8 | 446 | X |
| NCC-00062113 | -9.8 | 447 | X |
| NCC-00043027 | -9.8 | 448 | X |
| NCC-00054765 | -9.8 | 449 | X |
| NCC-00090056 | -9.8 | 450 | X |
| NCC-00033183 | -9.8 | 451 | X |
| NCC-00013850 | -9.8 | 452 | C |
| NCC-00036690 | -9.8 | 453 | C |
| NCC-00074899 | -9.8 | 454 | X |
| NCC-00088742 | -9.8 | 455 | X |
| NCC-00049610 | -9.8 | 456 | X |
| NCC-00087108 | -9.8 | 457 | C |
| NCC-00034539 | -9.8 | 458 | C |
| NCC-00053286 | -9.8 | 459 | X |
| NCC-00057182 | -9.8 | 460 | X |
| NCC-00064426 | -9.8 | 461 | X |
| NCC-00090516 | -9.8 | 462 | C |

| | | | |
|---|---|---|---|
| NCC-00035147 | -9.8 | 463 | C |
| NCC-00059211 | -9.8 | 464 | C |
| NCC-00067975 | -9.8 | 465 | C |
| NCC-00083643 | -9.8 | 466 | X |
| NCC-00036093 | -9.8 | 467 | C |
| NCC-00038198 | -9.8 | 468 | X |
| NCC-00086171 | -9.8 | 469 | C |
| NCC-00044358 | -9.8 | 470 | X |
| NCC-00085181 | -9.8 | 471 | X |
| NCC-00017803 | -9.8 | 472 | X |
| NCC-00060804 | -9.8 | 473 | C |
| NCC-00015865 | -9.8 | 474 | X |
| NCC-00043843 | -9.8 | 475 | C |
| NCC-00050435 | -9.8 | 476 | C |
| NCC-00073454 | -9.8 | 477 | C |
| NCC-00031448 | -9.8 | 478 | X |
| NCC-00008566 | -9.8 | 479 | X |
| NCC-00064855 | -9.8 | 480 | C |
| NCC-00031457 | -9.8 | 481 | C |
| NCC-00079232 | -9.8 | 482 | C |
| NCC-00074108 | -9.8 | 483 | X |
| NCC-00017495 | -9.8 | 484 | X |
| NCC-00038935 | -9.8 | 485 | C |
| NCC-00034558 | -9.8 | 486 | C |
| NCC-00001163 | -9.8 | 487 | X |
| NCC-00082526 | -9.8 | 488 | C |
| NCC-00014822 | -9.8 | 489 | C |
| NCC-00005393 | -9.8 | 490 | X |
| NCC-00085256 | -9.8 | 491 | X |
| NCC-00045772 | -9.8 | 492 | C |
| NCC-00027809 | -9.8 | 493 | X |
| NCC-00036456 | -9.8 | 494 | X |
| NCC-00049880 | -9.8 | 495 | C |
| NCC-00037791 | -9.8 | 496 | X |
| NCC-00034709 | -9.8 | 498 | X |
| NCC-00057196 | -9.8 | 499 | C |
| NCC-00014921 | -9.8 | 500 | C |

**Supplementary table 6.14: Ligands evaluated in the second round of molecular docking**. A total of 482 compounds are listed in this table, which were rejected following manual visualisation and evaluation during the second round of molecular docking of the FhPIM kinase.

| Ligand name | AutoDock Vina generated energy (kcal/mol) | Ranking according to the script | Grade according to the evaluation criteria |
|---|---|---|---|
| NCC-00089825 | -12.6 | 1 | X |
| NCC-00090676 | -11.7 | 2 | X |
| NCC-00000912 | -11.6 | 3 | X |
| NCC-00090518 | -11.6 | 4 | X |
| NCC-00089952 | -11.5 | 5 | X |
| NCC-00089541 | -11.4 | 6 | X |
| NCC-00000267 | -11.3 | 7 | X |
| NCC-00083644 | -11.2 | 8 | X |
| NCC-00000206 | -11.2 | 9 | C |
| NCC-00089743 | -11.2 | 10 | C |
| NCC-00090330 | -11.2 | 11 | X |
| NCC-00082551 | -11 | 12 | X |
| NCC-00089639 | -11 | 13 | X |
| NCC-00029890 | -10.9 | 14 | C |
| NCC-00036945 | -10.9 | 15 | X |
| NCC-00029519 | -10.9 | 16 | X |
| NCC-00074518 | -10.8 | 17 | C |
| NCC-00090192 | -10.8 | 18 | X |
| NCC-00035867 | -10.8 | 19 | C |
| NCC-00033911 | -10.7 | 20 | X |
| NCC-00090530 | -10.7 | 21 | X |
| NCC-00031876 | -10.7 | 22 | X |
| NCC-00090554 | -10.7 | 23 | X |
| NCC-00062294 | -10.7 | 24 | C |
| NCC-00083924 | -10.7 | 25 | X |
| NCC-00077998 | -10.7 | 26 | C |
| NCC-00000243 | -10.7 | 27 | X |
| NCC-00089839 | -10.7 | 28 | X |
| NCC-00090198 | -10.7 | 29 | X |
| NCC-00029032 | -10.6 | 30 | C |
| NCC-00047849 | -10.6 | 31 | X |
| NCC-00010513 | -10.6 | 32 | C |
| NCC-00056483 | -10.6 | 33 | X |
| NCC-00089740 | -10.6 | 34 | X |
| NCC-00072436 | -10.6 | 35 | C |
| NCC-00089809 | -10.6 | 36 | X |
| NCC-00084406 | -10.6 | 37 | X |
| NCC-00058089 | -10.6 | 38 | X |
| NCC-00087489 | -10.6 | 39 | X |
| NCC-00007336 | -10.6 | 40 | C |
| NCC-00001015 | -10.6 | 41 | C |
| NCC-00089136 | -10.6 | 42 | X |
| NCC-00087221 | -10.6 | 43 | X |
| NCC-00085110 | -10.6 | 44 | C |

| | | | |
|---|---|---|---|
| NCC-00089643 | -10.6 | 45 | C |
| NCC-00044049 | -10.6 | 46 | C |
| NCC-00030812 | -10.6 | 47 | X |
| NCC-00035975 | -10.6 | 48 | C |
| NCC-00009436 | -10.6 | 49 | X |
| NCC-00068655 | -10.5 | 50 | X |
| NCC-00069701 | -10.5 | 51 | X |
| NCC-00038868 | -10.5 | 53 | C |
| NCC-00046006 | -10.5 | 54 | C |
| NCC-00031333 | -10.5 | 55 | X |
| NCC-00050712 | -10.5 | 56 | C |
| NCC-00035095 | -10.5 | 57 | X |
| NCC-00036261 | -10.5 | 58 | X |
| NCC-00084170 | -10.5 | 59 | X |
| NCC-00037781 | -10.5 | 60 | C |
| NCC-00090547 | -10.5 | 61 | C |
| NCC-00028272 | -10.5 | 62 | C |
| NCC-00073521 | -10.5 | 63 | X |
| NCC-00074206 | -10.5 | 64 | C |
| NCC-00030586 | -10.5 | 65 | C |
| NCC-00073621 | -10.5 | 66 | X |
| NCC-00054460 | -10.5 | 67 | X |
| NCC-00037495 | -10.5 | 68 | C |
| NCC-00055004 | -10.5 | 69 | C |
| NCC-00031228 | -10.5 | 70 | C |
| NCC-00019097 | -10.5 | 71 | X |
| NCC-00012317 | -10.5 | 72 | X |
| NCC-00019258 | -10.5 | 73 | C |
| NCC-00086460 | -10.5 | 74 | C |
| NCC-00008992 | -10.4 | 75 | C |
| NCC-00086964 | -10.4 | 76 | C |
| NCC-00036186 | -10.4 | 77 | X |
| NCC-00061092 | -10.4 | 78 | X |
| NCC-00068455 | -10.4 | 79 | X |
| NCC-00068039 | -10.4 | 80 | X |
| NCC-00018185 | -10.4 | 81 | X |
| NCC-00014151 | -10.4 | 82 | X |
| NCC-00062943 | -10.4 | 83 | C |
| NCC-00090277 | -10.4 | 84 | X |
| NCC-00033852 | -10.4 | 85 | C |
| NCC-00017088 | -10.4 | 87 | X |
| NCC-00090465 | -10.4 | 88 | C |
| NCC-00081614 | -10.4 | 89 | X |
| NCC-00004318 | -10.4 | 90 | X |
| NCC-00068025 | -10.4 | 91 | C |
| NCC-00083683 | -10.4 | 92 | C |
| NCC-00043155 | -10.4 | 93 | X |
| NCC-00089785 | -10.4 | 94 | C |
| NCC-00064038 | -10.4 | 95 | C |
| NCC-00004403 | -10.4 | 96 | X |

| | | | |
|---|---|---|---|
| NCC-00018444 | -10.4 | 97 | X |
| NCC-00016947 | -10.4 | 98 | C |
| NCC-00027089 | -10.4 | 99 | X |
| NCC-00071183 | -10.4 | 100 | C |
| NCC-00090670 | -10.4 | 101 | X |
| NCC-00080682 | -10.4 | 102 | C |
| NCC-00090326 | -10.4 | 103 | X |
| NCC-00090638 | -10.4 | 104 | X |
| NCC-00087960 | -10.4 | 105 | X |
| NCC-00027008 | -10.4 | 106 | X |
| NCC-00045855 | -10.3 | 107 | X |
| NCC-00068825 | -10.3 | 108 | C |
| NCC-00089702 | -10.3 | 109 | X |
| NCC-00017726 | -10.3 | 110 | C |
| NCC-00008995 | -10.3 | 112 | X |
| NCC-00052807 | -10.3 | 113 | C |
| NCC-00073903 | -10.3 | 114 | C |
| NCC-00015301 | -10.3 | 116 | X |
| NCC-00082925 | -10.3 | 117 | C |
| NCC-00007176 | -10.3 | 118 | X |
| NCC-00055767 | -10.3 | 119 | C |
| NCC-00050460 | -10.3 | 120 | C |
| NCC-00045847 | -10.3 | 121 | C |
| NCC-00083194 | -10.3 | 122 | X |
| NCC-00060604 | -10.3 | 123 | X |
| NCC-00009548 | -10.3 | 124 | C |
| NCC-00036012 | -10.3 | 125 | C |
| NCC-00036241 | -10.3 | 126 | C |
| NCC-00017922 | -10.3 | 127 | C |
| NCC-00077025 | -10.3 | 128 | X |
| NCC-00049659 | -10.3 | 129 | C |
| NCC-00038675 | -10.3 | 130 | C |
| NCC-00078099 | -10.3 | 131 | C |
| NCC-00029008 | -10.3 | 132 | X |
| NCC-00070848 | -10.3 | 133 | C |
| NCC-00049897 | -10.3 | 135 | C |
| NCC-00045980 | -10.3 | 136 | C |
| NCC-00053263 | -10.3 | 137 | X |
| NCC-00057781 | -10.3 | 138 | C |
| NCC-00014591 | -10.3 | 139 | X |
| NCC-00042402 | -10.3 | 140 | X |
| NCC-00079785 | -10.3 | 141 | X |
| NCC-00009942 | -10.3 | 142 | C |
| NCC-00056766 | -10.3 | 143 | X |
| NCC-00061952 | -10.3 | 144 | X |
| NCC-00035461 | -10.3 | 145 | C |
| NCC-00029863 | -10.3 | 146 | X |
| NCC-00049847 | -10.3 | 147 | X |
| NCC-00085853 | -10.3 | 148 | C |
| NCC-00019858 | -10.3 | 149 | C |

| | | | |
|---|---|---|---|
| NCC-00043922 | -10.3 | 150 | X |
| NCC-00016920 | -10.3 | 151 | C |
| NCC-00061089 | -10.3 | 152 | X |
| NCC-00072054 | -10.3 | 153 | C |
| NCC-00089986 | -10.3 | 154 | C |
| NCC-00044030 | -10.3 | 155 | C |
| NCC-00007644 | -10.3 | 156 | X |
| NCC-00059419 | -10.3 | 157 | C |
| NCC-00000127 | -10.3 | 158 | C |
| NCC-00052899 | -10.3 | 159 | C |
| NCC-00036495 | -10.2 | 160 | C |
| NCC-00080750 | -10.2 | 161 | X |
| NCC-00001951 | -10.2 | 162 | C |
| NCC-00013521 | -10.2 | 163 | X |
| NCC-00003916 | -10.2 | 164 | X |
| NCC-00008307 | -10.2 | 165 | X |
| NCC-00037575 | -10.2 | 166 | X |
| NCC-00069754 | -10.2 | 167 | X |
| NCC-00000164 | -10.2 | 168 | X |
| NCC-00040335 | -10.2 | 169 | C |
| NCC-00012302 | -10.2 | 170 | C |
| NCC-00005412 | -10.2 | 171 | X |
| NCC-00052202 | -10.2 | 172 | C |
| NCC-00029923 | -10.2 | 173 | C |
| NCC-00070424 | -10.2 | 174 | X |
| NCC-00061943 | -10.2 | 175 | X |
| NCC-00090571 | -10.2 | 176 | C |
| NCC-00077817 | -10.2 | 177 | X |
| NCC-00060974 | -10.2 | 178 | X |
| NCC-00045078 | -10.2 | 179 | C |
| NCC-00015704 | -10.2 | 180 | X |
| NCC-00002277 | -10.2 | 181 | X |
| NCC-00013250 | -10.2 | 182 | C |
| NCC-00055026 | -10.2 | 183 | C |
| NCC-00046076 | -10.2 | 184 | C |
| NCC-00031448 | -10.2 | 185 | X |
| NCC-00017760 | -10.2 | 186 | X |
| NCC-00015210 | -10.2 | 187 | X |
| NCC-00041142 | -10.2 | 189 | C |
| NCC-00078413 | -10.2 | 190 | C |
| NCC-00034709 | -10.2 | 191 | C |
| NCC-00003669 | -10.2 | 192 | X |
| NCC-00027307 | -10.2 | 193 | X |
| NCC-00057327 | -10.2 | 194 | X |
| NCC-00043161 | -10.2 | 195 | X |
| NCC-00090165 | -10.2 | 196 | X |
| NCC-00059322 | -10.2 | 197 | X |
| NCC-00046193 | -10.2 | 198 | X |
| NCC-00062870 | -10.2 | 199 | C |
| NCC-00070885 | -10.2 | 200 | X |

| | | | |
|---|---|---|---|
| NCC-00082965 | -10.2 | 201 | C |
| NCC-00077005 | -10.2 | 202 | X |
| NCC-00044717 | -10.2 | 203 | X |
| NCC-00037487 | -10.2 | 204 | X |
| NCC-00045768 | -10.2 | 205 | X |
| NCC-00067943 | -10.2 | 206 | X |
| NCC-00056573 | -10.2 | 207 | C |
| NCC-00000670 | -10.2 | 208 | X |
| NCC-00012191 | -10.2 | 209 | C |
| NCC-00036653 | -10.2 | 210 | C |
| NCC-00035565 | -10.2 | 211 | X |
| NCC-00044111 | -10.2 | 212 | C |
| NCC-00065681 | -10.2 | 213 | X |
| NCC-00011811 | -10.2 | 215 | X |
| NCC-00052201 | -10.2 | 216 | X |
| NCC-00032308 | -10.2 | 217 | X |
| NCC-00048380 | -10.2 | 218 | X |
| NCC-00055894 | -10.2 | 219 | X |
| NCC-00016579 | -10.2 | 222 | X |
| NCC-00089644 | -10.2 | 223 | X |
| NCC-00028975 | -10.2 | 224 | X |
| NCC-00020491 | -10.2 | 225 | X |
| NCC-00017034 | -10.2 | 226 | X |
| NCC-00012114 | -10.2 | 227 | X |
| NCC-00067155 | -10.2 | 228 | C |
| NCC-00018392 | -10.2 | 229 | C |
| NCC-00061460 | -10.2 | 230 | X |
| NCC-00038415 | -10.2 | 231 | X |
| NCC-00067338 | -10.2 | 232 | X |
| NCC-00066874 | -10.2 | 233 | X |
| NCC-00083518 | -10.2 | 234 | X |
| NCC-00064078 | -10.2 | 235 | X |
| NCC-00030893 | -10.2 | 236 | X |
| NCC-00056038 | -10.2 | 237 | C |
| NCC-00089958 | -10.2 | 238 | X |
| NCC-00041405 | -10.1 | 239 | C |
| NCC-00050951 | -10.1 | 241 | C |
| NCC-00010014 | -10.1 | 242 | C |
| NCC-00089494 | -10.1 | 243 | C |
| NCC-00030620 | -10.1 | 244 | X |
| NCC-00085812 | -10.1 | 245 | X |
| NCC-00003736 | -10.1 | 246 | X |
| NCC-00087644 | -10.1 | 247 | X |
| NCC-00033260 | -10.1 | 248 | C |
| NCC-00044944 | -10.1 | 249 | X |
| NCC-00057664 | -10.1 | 251 | C |
| NCC-00043416 | -10.1 | 252 | X |
| NCC-00001758 | -10.1 | 253 | C |
| NCC-00085315 | -10.1 | 254 | X |
| NCC-00074610 | -10.1 | 255 | X |

| | | | |
|---|---|---|---|
| NCC-00035971 | -10.1 | 256 | C |
| NCC-00084301 | -10.1 | 257 | X |
| NCC-00026758 | -10.1 | 258 | X |
| NCC-00083110 | -10.1 | 259 | C |
| NCC-00047477 | -10.1 | 260 | C |
| NCC-00007585 | -10.1 | 261 | C |
| NCC-00086630 | -10.1 | 262 | C |
| NCC-00013906 | -10.1 | 263 | X |
| NCC-00018437 | -10.1 | 264 | X |
| NCC-00002858 | -10.1 | 265 | C |
| NCC-00017457 | -10.1 | 266 | X |
| NCC-00090410 | -10.1 | 267 | X |
| NCC-00062474 | -10.1 | 268 | X |
| NCC-00087972 | -10.1 | 269 | C |
| NCC-00012398 | -10.1 | 270 | X |
| NCC-00080281 | -10.1 | 271 | X |
| NCC-00084911 | -10.1 | 272 | X |
| NCC-00090533 | -10.1 | 273 | C |
| NCC-00012421 | -10.1 | 274 | X |
| NCC-00037780 | -10.1 | 275 | X |
| NCC-00000662 | -10.1 | 276 | C |
| NCC-00085015 | -10.1 | 277 | C |
| NCC-00074998 | -10.1 | 278 | C |
| NCC-00069165 | -10.1 | 279 | C |
| NCC-00061170 | -10.1 | 280 | C |
| NCC-00036999 | -10.1 | 282 | X |
| NCC-00061584 | -10.1 | 283 | C |
| NCC-00053666 | -10.1 | 284 | X |
| NCC-00063690 | -10.1 | 285 | C |
| NCC-00038211 | -10.1 | 286 | X |
| NCC-00031357 | -10.1 | 287 | X |
| NCC-00056791 | -10.1 | 288 | X |
| NCC-00019789 | -10.1 | 289 | C |
| NCC-00078516 | -10.1 | 290 | C |
| NCC-00061365 | -10.1 | 291 | C |
| NCC-00070400 | -10.1 | 292 | X |
| NCC-00032757 | -10.1 | 293 | X |
| NCC-00090067 | -10.1 | 294 | C |
| NCC-00088794 | -10.1 | 295 | C |
| NCC-00017214 | -10.1 | 296 | C |
| NCC-00042958 | -10.1 | 297 | X |
| NCC-00052809 | -10.1 | 298 | X |
| NCC-00017495 | -10.1 | 299 | C |
| NCC-00080637 | -10.1 | 300 | X |
| NCC-00082839 | -10.1 | 301 | C |
| NCC-00033490 | -10.1 | 302 | X |
| NCC-00027455 | -10.1 | 303 | X |
| NCC-00084815 | -10.1 | 304 | X |
| NCC-00076334 | -10.1 | 305 | X |
| NCC-00081762 | -10.1 | 306 | C |

| | | | |
|---|---|---|---|
| NCC-00044623 | -10.1 | 307 | C |
| NCC-00082098 | -10.1 | 309 | C |
| NCC-00001364 | -10.1 | 310 | X |
| NCC-00073817 | -10.1 | 311 | C |
| NCC-00065133 | -10.1 | 312 | C |
| NCC-00063932 | -10.1 | 313 | X |
| NCC-00074545 | -10.1 | 314 | C |
| NCC-00043152 | -10.1 | 315 | C |
| NCC-00055789 | -10.1 | 316 | X |
| NCC-00057682 | -10.1 | 317 | C |
| NCC-00017897 | -10.1 | 319 | X |
| NCC-00082896 | -10.1 | 320 | C |
| NCC-00008632 | -10.1 | 321 | C |
| NCC-00083458 | -10.1 | 322 | X |
| NCC-00014391 | -10.1 | 323 | C |
| NCC-00050178 | -10.1 | 324 | C |
| NCC-00067137 | -10.1 | 325 | X |
| NCC-00088183 | -10.1 | 326 | X |
| NCC-00013850 | -10.1 | 327 | C |
| NCC-00040634 | -10.1 | 328 | C |
| NCC-00081318 | -10.1 | 329 | C |
| NCC-00089714 | -10.1 | 330 | X |
| NCC-00084769 | -10.1 | 331 | C |
| NCC-00033654 | -10.1 | 332 | X |
| NCC-00007257 | -10.1 | 333 | C |
| NCC-00020610 | -10.1 | 334 | C |
| NCC-00057188 | -10.1 | 335 | C |
| NCC-00044574 | -10.1 | 336 | C |
| NCC-00090288 | -10.1 | 337 | C |
| NCC-00075699 | -10.1 | 338 | C |
| NCC-00019159 | -10.1 | 339 | C |
| NCC-00090091 | -10.1 | 341 | X |
| NCC-00009414 | -10.1 | 342 | X |
| NCC-00083235 | -10.1 | 343 | X |
| NCC-00038209 | -10.1 | 344 | X |
| NCC-00017274 | -10.1 | 345 | C |
| NCC-00066871 | -10.1 | 346 | C |
| NCC-00015865 | -10.1 | 347 | X |
| NCC-00008538 | -10.1 | 348 | X |
| NCC-00030507 | -10.1 | 349 | C |
| NCC-00047862 | -10.1 | 350 | C |
| NCC-00059211 | -10.1 | 351 | C |
| NCC-00051158 | -10.1 | 352 | X |
| NCC-00034815 | -10.1 | 353 | C |
| NCC-00062232 | -10.1 | 354 | C |
| NCC-00084163 | -10.1 | 355 | C |
| NCC-00028738 | -10.1 | 356 | C |
| NCC-00033668 | -10.1 | 357 | X |
| NCC-00037317 | -10 | 358 | C |
| NCC-00086897 | -10 | 359 | X |

| | | | |
|---|---|---|---|
| NCC-00011530 | -10 | 360 | X |
| NCC-00090532 | -10 | 361 | C |
| NCC-00036192 | -10 | 362 | X |
| NCC-00062766 | -10 | 363 | X |
| NCC-00063471 | -10 | 364 | X |
| NCC-00078433 | -10 | 365 | X |
| NCC-00049042 | -10 | 366 | X |
| NCC-00055060 | -10 | 367 | X |
| NCC-00080536 | -10 | 368 | X |
| NCC-00013371 | -10 | 369 | C |
| NCC-00069234 | -10 | 370 | X |
| NCC-00003291 | -10 | 371 | C |
| NCC-00038929 | -10 | 372 | X |
| NCC-00061874 | -10 | 373 | C |
| NCC-00086675 | -10 | 374 | X |
| NCC-00089931 | -10 | 375 | X |
| NCC-00036860 | -10 | 376 | C |
| NCC-00043906 | -10 | 377 | C |
| NCC-00083214 | -10 | 378 | X |
| NCC-00055394 | -10 | 379 | C |
| NCC-00038424 | -10 | 380 | X |
| NCC-00070657 | -10 | 381 | X |
| NCC-00052186 | -10 | 382 | C |
| NCC-00028369 | -10 | 383 | X |
| NCC-00055208 | -10 | 384 | X |
| NCC-00029163 | -10 | 385 | X |
| NCC-00067097 | -10 | 386 | X |
| NCC-00064004 | -10 | 387 | X |
| NCC-00070660 | -10 | 388 | C |
| NCC-00027250 | -10 | 389 | C |
| NCC-00008088 | -10 | 390 | C |
| NCC-00018188 | -10 | 391 | X |
| NCC-00033645 | -10 | 392 | C |
| NCC-00058693 | -10 | 393 | X |
| NCC-00064489 | -10 | 395 | C |
| NCC-00011399 | -10 | 396 | C |
| NCC-00056116 | -10 | 397 | C |
| NCC-00070103 | -10 | 398 | C |
| NCC-00011735 | -10 | 399 | X |
| NCC-00040553 | -10 | 400 | X |
| NCC-00015581 | -10 | 401 | X |
| NCC-00039871 | -10 | 402 | X |
| NCC-00017403 | -10 | 403 | X |
| NCC-00046639 | -10 | 404 | C |
| NCC-00089981 | -10 | 405 | X |
| NCC-00057671 | -10 | 406 | X |
| NCC-00064946 | -10 | 407 | X |
| NCC-00036926 | -10 | 408 | X |
| NCC-00053423 | -10 | 409 | X |
| NCC-00030517 | -10 | 410 | C |

| | | | |
|---|---|---|---|
| NCC-00039930 | -10 | 411 | C |
| NCC-00016943 | -10 | 412 | X |
| NCC-00057646 | -10 | 413 | X |
| NCC-00053286 | -10 | 414 | X |
| NCC-00071495 | -10 | 415 | X |
| NCC-00070061 | -10 | 416 | X |
| NCC-00028424 | -10 | 417 | X |
| NCC-00058342 | -10 | 418 | X |
| NCC-00075285 | -10 | 419 | C |
| NCC-00062570 | -10 | 420 | X |
| NCC-00044804 | -10 | 421 | X |
| NCC-00037314 | -10 | 422 | X |
| NCC-00077723 | -10 | 423 | X |
| NCC-00074356 | -10 | 424 | C |
| NCC-00053770 | -10 | 425 | C |
| NCC-00036411 | -10 | 426 | C |
| NCC-00068545 | -10 | 427 | X |
| NCC-00068810 | -10 | 428 | C |
| NCC-00081925 | -10 | 429 | C |
| NCC-00031866 | -10 | 430 | C |
| NCC-00082910 | -10 | 431 | X |
| NCC-00007569 | -10 | 432 | X |
| NCC-00026994 | -10 | 433 | C |
| NCC-00004368 | -10 | 434 | X |
| NCC-00055008 | -10 | 435 | C |
| NCC-00018906 | -10 | 436 | X |
| NCC-00010672 | -10 | 437 | C |
| NCC-00016903 | -10 | 438 | X |
| NCC-00031301 | -10 | 439 | X |
| NCC-00052208 | -10 | 440 | C |
| NCC-00033015 | -10 | 441 | C |
| NCC-00004577 | -10 | 442 | C |
| NCC-00089566 | -10 | 443 | X |
| NCC-00030454 | -10 | 444 | X |
| NCC-00000148 | -10 | 445 | C |
| NCC-00003813 | -10 | 446 | C |
| NCC-00011094 | -10 | 447 | X |
| NCC-00044121 | -10 | 448 | C |
| NCC-00089914 | -10 | 449 | X |
| NCC-00037589 | -10 | 450 | X |
| NCC-00030833 | -10 | 451 | C |
| NCC-00069317 | -10 | 452 | X |
| NCC-00060638 | -10 | 453 | C |
| NCC-00018734 | -10 | 454 | X |
| NCC-00089829 | -10 | 455 | C |
| NCC-00036148 | -10 | 456 | X |
| NCC-00062675 | -10 | 457 | C |
| NCC-00044694 | -10 | 458 | X |
| NCC-00084785 | -10 | 459 | C |
| NCC-00046946 | -10 | 460 | C |

| | | | |
|---|---|---|---|
| NCC-00061839 | -10 | 461 | X |
| NCC-00088438 | -10 | 462 | C |
| NCC-00034192 | -10 | 463 | X |
| NCC-00047606 | -10 | 464 | C |
| NCC-00050470 | -10 | 465 | C |
| NCC-00061658 | -10 | 466 | C |
| NCC-00081933 | -10 | 467 | C |
| NCC-00080612 | -10 | 468 | C |
| NCC-00073846 | -10 | 469 | C |
| NCC-00035552 | -10 | 470 | C |
| NCC-00028598 | -10 | 471 | X |
| NCC-00042159 | -10 | 473 | C |
| NCC-00018461 | -10 | 474 | X |
| NCC-00033011 | -10 | 475 | X |
| NCC-00086883 | -10 | 476 | X |
| NCC-00030956 | -10 | 477 | C |
| NCC-00081551 | -10 | 478 | C |
| NCC-00036479 | -10 | 479 | X |
| NCC-00008558 | -10 | 480 | X |
| NCC-00019091 | -10 | 481 | X |
| NCC-00085179 | -10 | 482 | X |
| NCC-00047674 | -10 | 483 | C |
| NCC-00009351 | -10 | 484 | X |
| NCC-00038493 | -10 | 486 | X |
| NCC-00090604 | -10 | 487 | C |
| NCC-00011748 | -10 | 488 | X |
| NCC-00017026 | -10 | 489 | X |
| NCC-00012045 | -10 | 490 | X |
| NCC-00089621 | -10 | 491 | X |
| NCC-00055109 | -10 | 492 | C |
| NCC-00040621 | -10 | 493 | C |
| NCC-00050463 | -10 | 494 | X |
| NCC-00046183 | -10 | 495 | X |
| NCC-00009266 | -10 | 496 | C |
| NCC-00020096 | -10 | 497 | X |
| NCC-00050253 | -10 | 498 | C |
| NCC-00045969 | -10 | 499 | X |
| NCC-00059582 | -10 | 500 | C |

## 6.3 Supplementary codes

### 6.3.1 Code for the Iteration nested loop conditions for reducing the redundancies

Code for the iteration nested loop with IF conditions for reducing the redundancies in R v4.3.4 is stated below:

```
> # Create an empty vector to store the row indices to remove
> rows_to_remove <- c()
> # Loop through each row
> for (c in 1:nrow(dataframe)) {
+   # Get the current row values
+   curr_contig <- dataframe$Fh_scaffold[c]
+   curr_strand <- dataframe$strand[c]
+   curr_start <- dataframe$start[c]
+   curr_end <- dataframe$end[c]
+   # Loop through all other rows
+   for (r in 1:nrow(dataframe)) {
+     if (c != r) {  # Skip the current row if we are looking at the same row as what is the current row
+       # Check if conditions are met
+       if (dataframe$Fh_scaffold[r] == curr_contig && # Contig is the same as current
+           dataframe$strand[r] == curr_strand && # Strand is the same as current
+            dataframe$start[r] <= curr_start && # The start position is smaller than the current start
+           dataframe$end[r] >= curr_end) { # The end position is larger than the current end
+            rows_to_remove <- append(rows_to_remove, c)  # If all conditions above are true, current row is fully contained in another row
+         # Add current row index to rows_to_remove
```

```
+         break  # No need to check further, move to the next row
+       }
+     }
+   }
+ }
```

### 6.3.2 Code for the Iteration nested loop conditions for reducing the overlapping genes

Code for the iteration loop with IF conditions for reducing the overlapping genes in R v4.3.4 is the stated below:

```
# new loop code for overlapping filtration
> overlapping_genes <- c()
> overlap_lengths <- vector("numeric", nrow(dataframe))
> gene_lengths <- vector("numeric", nrow(dataframe))
> overlap_ratios <- vector("numeric", nrow(dataframe))
> # Loop through each row
> for (c in 1:nrow(dataframe)) {
+   # Get the current row values
+   curr_contig <- dataframe$Fh_scaffold[c]
+   curr_strand <- dataframe$strand[c]
+   curr_start <- dataframe$start[c]
+   curr_end <- dataframe$end[c]
+
+   # Loop through all other rows
+   for (r in 1:nrow(dataframe)) {
+     if (c != r) { # Skip the current row if we are looking at the same row as the current row
+       # Check if conditions are met
```

```
+       if (dataframe$Fh_scaffold[r] == curr_contig && # Contig is the same as current
+           dataframe$strand[r] == curr_strand && # Strand is the same as current
+           ((dataframe$start[r] <= curr_start && dataframe$end[r] >= curr_start) ||
+            (dataframe$start[r] <= curr_end && dataframe$end[r] >= curr_end))) {
+           overlapping_genes <- append(overlapping_genes, c) # If all conditions are met, the current row overlaps with another one
+         # Calculate the length of overlap
+         overlap_start <- max(dataframe$start[c], dataframe$start[r])
+         overlap_end <- min(dataframe$end[c], dataframe$end[r])
+         overlap_length <- overlap_end - overlap_start + 1
+
+         # Calculate the ratio of overlap to gene sequence length
+         gene_length <- dataframe$end[c] - dataframe$start[c] + 1
+         overlap_ratio <- overlap_length / gene_length
+
+         # Store the collected data in the vectors
+         overlap_lengths[c] <- overlap_length
+         gene_lengths[c] <- gene_length
+         overlap_ratios[c] <- overlap_ratio
+       }
+     }
+   }
+ }
```

## 6.4 Supplementary information

### 6.4.1 Protein sequence of FhPIM kinase (D915_000232) in a FASTA format

Protein sequence in a FASTA format of FhPIM kinase (D915_000232) which was obtained from Parasite Wormbase (245).

>gene-D915_000232.t1 peptide: gene-D915_000232.t1 pep:protein_coding
MAQITTHYSNTRTNFQLPPNGRLVRRSSEELGLQIVVHEGHAAFLQRYVLGTRFGGGGFGH
VHRARSLCDNREVVVKEIRSDKVPCWCQVDSQLMPMEVVLLTMCQGLPGVVGFLDAFNLG
QSWVIVMDRVSETTCDMFDYIGERGTLPEREAAHYFYQLAGILLACHRVGVLHRDIKDENILI
NRATNELVLIDFGSGAFLESRLYTDFDGTRVYCPPEWILNSCYHGKQAEVWSLGVLLYDML
CGDIPFVNDKGIIGGKLRYRNESLSEEARDLIRNCLSMDPEKRPTLLEILQHPWMCRYRPKR
VEGQPASMLTALLAVDEASTLSVEQKRSLADADNDNSSSPSLTHDSVTRRLLSTHGTSNLH
ASSLSSISSSPPSTCDLGFLDEEPKLACPVFNLDRDSNTKETLQTTNTTGATPHTHAQSEPV
PGVTSRPLMLSSQPVEKREQKMSTNNEVILISDSSSRSSFHNVTRSSLGSSERLEDHLCMH
GRSPVASFEPSTIPSQPRLHSNESGSSSGYYSRSESLSSNESHQLISATNAGNSATCLTSSH
AASVICVPSTVTAVTTTRPFCSSTVLTTSHSLSHPGRIAVHTHNWRSGSAGIASSASSSCGS
SSDNSSSSSSSVSSNPSFNKLNPCHVPIPPTVSSTTTLYATGLLQWPLLFSTHKSTPISTSPT
FQTTRPASVHPIVSSSVPATQSSPVAPISIRSASDQIDRLCQSLHPSSPTLAVSHPQKPTTWF
WGDGTRLDQNWRPMS

### 6.4.2 Protein sequence of HsPIM1 kinase (P11309) in a FASTA format

Protein sequence in a FASTA format of HsPIM1 kinase (P11309) which was obtained from Uniprot (241,242).

>sp|P11309|PIM1_HUMAN Serine/threonine-protein kinase pim-1 OS=Homo sapiens OX=9606 GN=PIM1 PE=1 SV=4
MLLSKINSLAHLRAAPCNDLHATKLAPGKEKEPLESQYQVGPLLGSGGFGSVYSGIRVSDNL
PVAIKHVEKDRISDWGELPNGTRVPMEVVLLKKVSSGFSGVIRLLDWFERPDSFVLILERPE
PVQDLFDFITERGALQEELARSFFWQVLEAVRHCHNCGVLHRDIKDENILIDLNRGELKLIDF
GSGALLKDTVYTDFDGTRVYSPPEWIRYHRYHGRSAAVWSLGILLYDMVCGDIPFEHDEEII
RGQVFFRQRVSSECQHLIRWCLALRPSDRPTFEEIQNHPWMQDVLLPQETAEIHLHSLSPG
PSK

# 7. References


1. Mehmood K, Zhang H, Sabir AJ, Abbas RZ, Ijaz M, Durrani AZ, et al. A review on epidemiology, global prevalence and economical losses of fasciolosis in ruminants. Microb Pathog. 2017 Aug 1;109:253–62. doi:10.1016/j.micpath.2017.06.006 PubMed PMID: 28602837.

2. World Health Organisation. Global report on neglected tropical diseases 2025 [Internet]. [cited 2025 Nov 1]. Available from: https://www.who.int/teams/control-of-neglected-tropical-diseases/global-report-on-neglected-tropical-diseases-2025

3. WHO team: Control of Neglected tropical disease (NTD). Soil-transmitted helminthiases: estimates of the number of children needing preventive chemotherapy and number treated, 2009 [Internet]. Geneva; 2011 [cited 2025 Oct 12]. Available from: https://www.who.int/publications/i/item/who-wer8625-257-267

4. Littewood DT, Rohde K, Bray RA, Herniou EA. Phylogeny of the platyhelminthes and the evolution of parasitism. Biological Journal of the Linnean Society. 1999 Sep 1;68(1–2):257–87. doi:https://doi.org/10.1111/j.1095-8312.1999.tb01169.x

5. Cwiklinski K, Dalton JP, Dufresne PJ, La Course J, Williams DJL, Hodgkinson J, et al. The *Fasciola hepatica* genome: Gene duplication and polymorphism reveals adaptation to the host environment and the capacity for rapid evolution. Genome Biol. 2015 Apr 3;16(1):71. doi:10.1186/s13059-015-0632-2 PubMed PMID: 25887684.

6. Cwiklinski K, O'Neill SM, Donnelly S, Dalton JP. A prospective view of animal and human fasciolosis. Parasite Immunology. Blackwell Publishing Ltd; 2016. p. 558–68. doi:10.1111/pim.12343 PubMed PMID: 27314903.

7. Maule AG, Marks NJ, editors. Parasitic flatworms: Molecular biology, biochemistry, immunology and physiology. London: CABI International; 2006. 1–448 p.

8. Toledo R, Fried B, editors. Digenetic trematodes. 3rd ed. Springer Cham; 2023. 1–585 p. doi:https://doi.org/10.1007/978-3-031-60121-7

9. Schoch CL, Ciufo S, Domrachev M, Hotton CL, Kannan S, Khovanskaya R, et al. NCBI Taxonomy: A comprehensive update on curation, resources and tools. Database. 2020;2020:baaa062. doi:10.1093/database/baaa062 PubMed PMID: 32761142.

10. Robinson MW, Dalton JP. Zoonotic helminth infections with particular emphasis on fasciolosis and other trematodiases. Philosophical Transactions of the Royal Society B:

Biological Sciences. 2009 Sep 27;364(1530):2763–76. doi:10.1098/rstb.2009.0089 PubMed PMID: 19687044.

11. Torgerson P, Claxton J. Epidemiology and Control. In: Dalton J, editor. Fasciolosis. CAB international; 1999. p. 113–50.

12. Thomas AP. The Life History of the Liver-Fluke (*Fasciola hepetica*). J Cell Sci. 1883 Jan 1;2(89):99–133. doi:https://doi.org/10.1242/jcs.s2-23.89.99

13. Dalton JP, editor. Fasciolosis. 2nd ed. CABI International; 2021. 1–501 p. doi:10.1079/9781789246162.0000

14. Mas-Coma Santiago and Valero MA and BMD. Fascioliasis. In: Toledo Rafael and Fried B, editor. Digenetic Trematodes. Cham: Springer International Publishing; 2024. p. 157–201. doi:10.1007/978-3-031-60121-7_5

15. Howell AK, Williams DJL. The Epidemiology and Control of Liver Flukes in Cattle and Sheep. Veterinary Clinics of North America: Food Animal Practice. 2020 Mar 1;36(1):109–23. doi:https://doi.org/10.1016/j.cvfa.2019.12.002

16. Dixon KE. The physiology of excystment of the metacercaria of *Fasciola hepatica* L. Parasitology. 1966;56(3):431–56. doi:10.1017/S0031182000068931

17. Happich FA, Boray JC. Quantitative diagnosis of chronic fasciolosis. 2. The estimation of daily total egg production of *Fasciola hepatica* and the number of adult flukes in sheep by faecal egg counts. Australian Veterinary Journal. 1969 May 22;45(7):329–31. doi:10.1111/j.1751-0813.1969.tb05012.x

18. Happich FA, Boray JC. Quantitative diagnosis of chronic fasciolosis. 1. comparative studies on quantitative faecal examinations for chronic *Fasciola hepatica* infection in sheep. Aust Vet J. 1969;45(7):326–8.

19. Threadgold LT. *Fasciola hepatica*: Ultrastructure and histochemistry of the glycocalyx of the tegument. Exp Parasitol. 1976 Feb 1;39(1):119–34. doi:https://doi.org/10.1016/0014-4894(76)90019-9

20. Bils RF, Martin WE. Fine structure and development of the trematode integument. Trans Am Microsc Soc. 1966;85(1):78–88. doi:https://doi.org/10.2307/3224777

21. Dalton JP, Skelly P, Halton DW. Role of the tegument and gut in nutrient uptake by parasitic platyhelminths. Can J Zool. 2004;82(2):211–32. doi:10.1139/z03-213

22. Sukhdeo SC, Sukhdeo MVK, Mettrick DF. Neurocytology of the cerebral ganglion of *Fasciola hepatica* (Platyhelminthes). Journal of Comparative Neurology. 1988 Dec 15;278(3):337–43. doi:https://doi.org/10.1002/cne.902780304

23. Hanna R. *Fasciola hepatica*: Histology of the reproductive organs and differential effects of triclabendazole on drug-sensitive and drug-resistant fluke isolates and on flukes from selected field cases. Pathogens. 2015 Jun 26;4(3):431–56. doi:10.3390/pathogens4030431

24. Meepool A, Wanichanon C, Viyanant V, Sobhon P. Development and roles of vitelline cells in eggshell formation in *Fasciola gigantica*. Invertebr Reprod Dev. 2006 Jan 1;49(1–2):9–17. doi:10.1080/07924259.2006.9652189

25. Inkscape [Internet]. Inkscape Project; 2024. Available from: https://inkscape.org

26. de Waal T, Mehmood K. Trematode infection in ruminants. Front Vet Sci. 2021 Jul 14;8:719577. doi:10.3389/fvets.2021.719577

27. Tolan Jr. RW. Fascioliasis due to *Fasciola hepatica* and *Fasciola gigantica* infection: An update on this 'neglected' neglected tropical disease. Lab Med. 2011 Feb 1;42(2):107–16. doi:https://doi.org/10.1309/LMLFBB8PW4SA0YJI

28. Keiser J, Utezinger J. Emerging Foodborne Trematodiasis. Emerg Infect Dis. 2005 Oct;11(10):1507–14. doi:10.3201/eid1110.050614 PubMed PMID: 1631868.

29. PIEDRAFITA D, SPITHILL TW, SMITH RE, RAADSMA HW. Improving animal and human health through understanding liver fluke immunology. Parasite Immunol. 2010 Aug;32(8):572–81. doi:https://doi.org/10.1111/j.1365-3024.2010.01223.x

30. Mas-Coma S, Bargues MD, Valero MA. Fascioliasis and other plant-borne trematode zoonoses. Int J Parasitol. 2005 Oct 1;35(11–12):1255–78. doi:https://doi.org/10.1016/j.ijpara.2005.07.010

31. Charlier J, De Cat A, Forbes A, Vercruysse J. Measurement of antibodies to gastrointestinal nematodes and liver fluke in meat juice of beef cattle and associations with carcass parameters. Vet Parasitol. 2009 Dec 23;166(3–4):235–40. doi:https://doi.org/10.1016/j.vetpar.2009.09.040

32. Mezo M, González-Warleta M, Castro-Hermida JA, Muiño L, Ubeira FM. Association between anti-*F. hepatica* antibody levels in milk and production losses in dairy cows. Vet Parasitol. 2011 Aug 25;180(3–4):237–42. doi:https://doi.org/10.1016/j.vetpar.2011.03.009

33. Charlier J, Hostens M, Jacobs J, van Ranst B, Duchateau L, Vercruysse J. Integrating fasciolosis control in the dry cow management: The effect of closantel treatment on milk production. PLoS One. 2012 Aug 20;7(8):e43216. doi:10.1371/journal.pone.0043216 PubMed PMID: 22916226.

34. Köstenberger K, Tichy A, Bauer K, Pless P, Wittek T. Associations between fasciolosis and milk production, and the impact of anthelmintic treatment in dairy herds. Parasitol Res. 2017 Jul;116(7):1981–7. doi:10.1007/s00436-017-5481-3

35. Charlier J, Duchateau L, Claerebout E, Williams D, Vercruysse J. Associations between anti-*Fasciola hepatica* antibody levels in bulk-tank milk samples and production parameters in dairy herds. Prev Vet Med. 2007 Jan 1;78(1):57–66. doi:https://doi.org/10.1016/j.prevetmed.2006.09.010

36. May K, Bohlsen E, König S, Strube C. *Fasciola hepatica* seroprevalence in Northern German dairy herds and associations with milk production parameters and milk ketone bodies. Vet Parasitol. 2020 Jan 1;277:109016. doi:https://doi.org/10.1016/j.vetpar.2019.109016

37. López-Díaz MC, Carro MC, Cadórniga C, Díez-Baños P, Mezo M. Puberty and serum concentrations of ovarian steroids during prepuberal period in friesian heifers artificially infected with *Fasciola hepatica*. Theriogenology. 1998 Sep 1;50(4):587–93. doi:https://doi.org/10.1016/S0093-691X(98)00163-0

38. Mitchell G. Update on fasciolosis in cattle and sheep. In Pract. 2002 Jul;24(7):378–85. doi:https://doi.org/10.1136/inpract.24.7.378

39. Boray JC. Experimental fascioliasis in Australia. In: Dawes B, editor. Advances in Parasitology. Academic Press; 1969. p. 95–210. (Advances in Parasitology). doi:https://doi.org/10.1016/S0065-308X(08)60435-2

40. Beesley NJ, Caminade C, Charlier J, Flynn RJ, Hodgkinson JE, Martinez-Moreno A, et al. *Fasciola* and fasciolosis in ruminants in Europe: Identifying research needs. Transbound Emerg Dis. 2018 May;65(S1):199–216. doi:https://doi.org/10.1111/tbed.12682

41. Dixon RC, Wescott RB. A fast and accurate fecal examination technique for diagnosis of *Fasciola hepatica*. In: annual meeting of the american association of veterinary parasitologists. 1987. p. 28.

42. Cringoli G, Rinaldi L, Maurelli MP, Utzinger J. FLOTAC: New multivalent techniques for qualitative and quantitative copromicroscopic diagnosis of parasites in animals and humans. Nat Protoc. 2010 Mar;5(3):503–15. doi:10.1038/nprot.2009.235

43. Cringoli G, Maurelli MP, Levecke B, Bosco A, Vercruysse J, Utzinger J, et al. The Mini-FLOTAC technique for the diagnosis of helminth and protozoan infections in humans and animals. Nat Protoc. 2017 Sep;12(9):1723–32. doi:10.1038/nprot.2017.067

44. Rufino-Moya PJ, Zafra Leva R, Martínez-Moreno Á, Buffoni L, Valderas García E, Pérez Arévalo J, et al. Advancement in diagnosis, treatment, and vaccines against *Fasciola hepatica*: A comprehensive review. Pathogens. 2024 Aug 7;13(8):699. doi:10.3390/pathogens13080669

45. Alvarez Rojas CA, Jex AR, Gasser RB, Scheerlinck JPY. Chapter Two - Techniques for the Diagnosis of *Fasciola* Infections in Animals: Room for Improvement. In: Rollinson D, Stothard JR, editors. Advances in parasitology. Academic Press; 2014. p. 65–107. (Advances in Parasitology). doi:https://doi.org/10.1016/B978-0-12-800182-0.00002-7

46. Dalton JP, Neill SO, Stack C, Collins P, Walshe A, Sekiya M, et al. *Fasciola hepatica* cathepsin L-like proteases: Biology, function, and potential in the development of first generation liver fluke vaccines. Int J Parasitol. 2003 Sep 30;33(11):1173–81. doi:https://doi.org/10.1016/S0020-7519(03)00171-1

47. O'Neill SM, Parkinson M, Strauss W, Angles R, Dalton JP. Immunodiagnosis of *Fasciola hepatica* infection (fascioliasis) in a human population in the Bolivian Altiplano using purified cathepsin L cysteine proteinase. Am J Trop Med Hyg. 1998 Apr 1;58(4):417–23. doi:https://doi.org/10.4269/ajtmh.1998.58.417

48. Anand N, Sharma S. Approaches to design and synthesis of antiparasitic drugs. Vol. 25. Elsevier; 1997. doi:https://doi.org/10.1016/S0165-7208(97)80030-X

49. Alvarez LI, Lanusse CE, Williams DJL, Fairweather I, Hodgkinson JE. Flukicidal drugs: pharmacotherapeutics and drug resistance. In: Dalton J, editor. Fasciolosis. 2nd edition. CABI; 2021. p. 211–55. doi:10.1079/9781789246162.0007

50. Kelley JM, Elliott TP, Beddoe T, Anderson G, Skuce P, Spithill TW. Current threat of triclabendazole resistance in *Fasciola hepatica*. Trends Parasitol. 2016 Jun 1;32(6):458–69. doi:10.1016/j.pt.2016.03.002 PubMed PMID: 27049013.

51. Novartis Pharmaceuticals. www.clinicaltrials.gov [Internet]. 2022 [cited 2025 Dec 1]. Study of safety, tolerability and clinical outcomes of EGATEN (Triclabendazole) in

fascioliasis patients (6 years of age or older). Available from: https://clinicaltrials.gov/study/NCT04230148

52. Hodgkinson J, Cwiklinski K, Beesley NJ, Paterson S, Williams DJL. Identification of putative markers of triclabendazole resistance by a genome-wide analysis of genetically recombinant *Fasciola hepatica*. Parasitology. 2013/05/31. 2013 Oct;140(12):1523–33. doi:10.1017/S0031182013000528

53. van De N, Le TH, Agramunt VH, Mas-Coma S. Early postnatal and preschool-age infection by *fasciola* spp.: Report of five cases from Vietnam and worldwide review. Am J Trop Med Hyg. 2020 Jul 6;103(4):1578–89. doi:10.4269/ajtmh.20-0139 PubMed PMID: 32618259.

54. Stitt AW, Fairweather I. *Fasciola hepatica*: Tegumental surface changes in adult and juvenile flukes following treatment in vitro with the sulphoxide metabolite of triclabendazole (Fasinex). Parasitol Res. 1993 Jul;79(7):529–36. doi:https://doi.org/10.1007/BF00932235

55. Stitt AW, Fairweather I. The effect of the sulphoxide metabolite of triclabendazole ('Fasinex') on the tegument of mature and immature stages of the liver fluke, *Fasciola hepatica*. Parasitology. 1994 Jun;108(5):555–67. doi:https://doi.org/10.1017/S0031182000077428

56. Toner E, Brennan GP, Hanna REB, Edgar HW, Fairweather I. Tegumental surface changes in adult *Fasciola hepatica* in response to treatment *in vivo* with triclabendazole in the sheep host. Vet Parasitol. 2010 Sep 20;172(3–4):238–48. doi:https://doi.org/10.1016/j.vetpar.2010.05.012

57. Stitt AW, Fairweather I. *Fasciola hepatica*: Disruption of the vitelline cells *in vitro* by the sulphoxide metabolite of triclabendazole. Parasitol Res. 1996 Apr;82(4):333–9. doi:https://doi.org/10.1007/s004360050122

58. Stitt AW, Fairweather I. Spermatogenesis in *Fasciola hepatica*: An ultrastructural comparison of the effects of the anthelmintic, thiabendazole ("Fasinex") and the microtubule inhibitor, tubulozole. Invertebr Reprod Dev. 1992 Dec 1;22(1–3):139–50. doi:10.1080/07924259.1992.9672266

59. Lacey E. The role of the cytoskeletal protein, tubulin, in the mode of action and mechanism of drug resistance to benzimidazoles. Int J Parasitol. 1988 Nov 1;18(7):885–936. doi:https://doi.org/10.1016/0020-7519(88)90175-0

60. Fairweather I, Boray JC. Fasciolicides: Efficacy, actions, resistance and its management. The Veterinary Journal. 1999 Sep 1;158(2):81–112. doi:https://doi.org/10.1053/tvjl.1999.0377

61. Ryan LA, Hoey E, Trudgett A, Fairweather I, Fuchs M, Robinson MW, et al. *Fasciola hepatica* expresses multiple α- and β-tubulin isotypes. Mol Biochem Parasitol. 2008 May 1;159(1):73–8. doi:10.1016/j.molbiopara.2008.02.001 PubMed PMID: 18372053.

62. Kotze AC, Prichard RK. Chapter nine - anthelmintic resistance in *Haemonchus contortus*: History, mechanisms and diagnosis. In: Gasser RB, Samson-Himmelstjerna G Von, editors. Advances in Parasitology. Academic Press; 2016. p. 397–428. doi:https://doi.org/10.1016/bs.apar.2016.02.012

63. Fairweather I, Brennan GP, Hanna REB, Robinson MW, Skuce PJ. Drug resistance in liver flukes. Int J Parasitol Drugs Drug Resist. 2020 Apr 1;12:39–59. doi:10.1016/j.ijpddr.2019.11.003 PubMed PMID: 32179499.

64. Olivares-Ferretti P, Beltrán JF, Salazar LA, Fonseca-Salamanca F. Protein modelling and molecular docking analysis of *Fasciola hepatica* β-Tubulin's interaction sites, with triclabendazole, triclabendazole sulphoxide and triclabendazole sulphone. Acta Parasitol. 2023 Sep 1;68(3):535–47. doi:10.1007/s11686-023-00692-z PubMed PMID: 37330945.

65. Overend DJ, Bowen FL. Resistance of *Fasciola hepatica* to triclabendazole. Aust Vet J. 1995;72(7):275–6. doi:https://doi.org/10.1111/j.1751-0813.1995.tb03546.x

66. Kahl A, von Samson-Himmelstjerna G, Helm C, Hodgkinson J, Williams D, Weiher W, et al. Efficacy of flukicides against *Fasciola hepatica* and first report of triclabendazole resistance on German sheep farms. Int J Parasitol Drugs Drug Resist. 2023 Dec 1;23:94–105. doi:10.1016/j.ijpddr.2023.11.001 PubMed PMID: 38006779.

67. Sanabria R, Ceballos L, Moreno L, Romero J, Lanusse C, Alvarez L. Identification of a field isolate of *Fasciola hepatica* resistant to albendazole and susceptible to triclabendazole. Vet Parasitol. 2013 Mar 13;193(1–3):105–10. doi:https://doi.org/10.1016/j.vetpar.2012.11.033

68. Martínez-Valladares M, Cordero-Pérez C, Rojo-Vázquez FA. Efficacy of an anthelmintic combination in sheep infected with *Fasciola hepatica* resistant to albendazole and clorsulon. Exp Parasitol. 2014 Jan 1;136:59–62. doi:https://doi.org/10.1016/j.exppara.2013.10.010

69. Novobilský A, Höglund J. First report of closantel treatment failure against *Fasciola hepatica* in cattle. Int J Parasitol Drugs Drug Resist. 2015 Dec 1;5(3):172–7. doi:https://doi.org/10.1016/j.ijpddr.2015.07.003

70. Robles-Pérez D, Martínez-Pérez JM, Rojo-Vázquez FA, Martínez-Valladares M. The diagnosis of fasciolosis in feces of sheep by means of a PCR and its application in the detection of anthelmintic resistance in sheep flocks naturally infected. Vet Parasitol. 2013 Oct 18;197(1–2):277–82. doi:https://doi.org/10.1016/j.vetpar.2013.05.006

71. ROBINSON MW, TRUDGETT A, HOEY EM, FAIRWEATHER I. Triclabendazole-resistant *Fasciola hepatica*: β-tubulin and response to *in vitro* treatment with triclabendazole. Parasitology. 2002 Mar;124(3):325–38. doi:10.1017/S003118200100124X

72. Fuchs MA, Ryan LA, Chambers EL, Moore CM, Fairweather I, Trudgett A, et al. Differential expression of liver fluke β-tubulin isotypes at selected life cycle stages. Int J Parasitol. 2013 Dec 1;43(14):1133–9. doi:https://doi.org/10.1016/j.ijpara.2013.08.007

73. Robey RW, Pluchino KM, Hall MD, Fojo AT, Bates SE, Gottesman MM. Revisiting the role of ABC transporters in multidrug-resistant cancer. Nat Rev Cancer. 2018 Jul;18(7):452–64. doi:10.1038/s41568-018-0005-8

74. Kotze AC, Hunt PW, Skuce P, von Samson-Himmelstjerna G, Martin RJ, Sager H, et al. Recent advances in candidate-gene and whole-genome approaches to the discovery of anthelmintic resistance markers and the description of drug/receptor interactions. Int J Parasitol Drugs Drug Resist. 2014 Dec 1;4(3):164–84. doi:10.1016/j.ijpddr.2014.07.007

75. Wilkinson R, Law CJ, Hoey EM, Fairweather I, Brennan GP, Trudgett A. An amino acid substitution in *Fasciola hepatica* P-glycoprotein from triclabendazole-resistant and triclabendazole-susceptible populations. Mol Biochem Parasitol. 2012 Nov 1;186(1):69–72. doi:https://doi.org/10.1016/j.molbiopara.2012.08.008

76. Solana MV, Domínguez MF, Scarcella S, Radio S, Smircich P, Fernández S, et al. Different SNPs in *Fasciola hepatica* P-glycoprotein from diverse Latin American populations are not associated with Triclabendazole resistance. Mol Biochem Parasitol. 2018 Sep 1;224:57–60. doi:https://doi.org/10.1016/j.molbiopara.2018.07.005

77. Elliott TP, Spithill TW. The T687G SNP in a P-glycoprotein gene of *Fasciola hepatica* is not associated with resistance to triclabendazole in two resistant Australian populations.

Mol Biochem Parasitol. 2014 Nov 1;198(1):45–7. doi:https://doi.org/10.1016/j.molbiopara.2014.11.006

78. Robinson MW, Lawson J, Trudgett A, Hoey EM, Fairweather I. The comparative metabolism of triclabendazole sulphoxide by triclabendazole-susceptible and triclabendazole-resistant *Fasciola hepatica*. Parasitol Res. 2004 Feb;92(3):205–10. doi:10.1007/s00436-003-1003-6

79. Choi YJ, Rosa BA, Fernandez-Baca M V., Ore RA, Martin J, Ortiz P, et al. Independent origins and non-parallel selection signatures of triclabendazole resistance in *Fasciola hepatica*. Nat Commun. 2025 Mar 27;16(1):2996. doi:10.1038/s41467-025-57796-5 PubMed PMID: 40148292.

80. Zajíčková M, Nguyen LT, Skálová L, Raisová Stuchlíková L, Matoušková P. Anthelmintics in the future: Current trends in the discovery and development of new drugs against gastrointestinal nematodes. Drug Discov Today. 2020 Feb 1;25(2):430–7. doi:https://doi.org/10.1016/j.drudis.2019.12.007

81. Nixon SA, Welz C, Woods DJ, Costa-Junior L, Zamanian M, Martin RJ. Where are all the anthelmintics? Challenges and opportunities on the path to new anthelmintics. Int J Parasitol Drugs Drug Resist. 2020 Dec 1;14:8–16. doi:https://doi.org/10.1016/j.ijpddr.2020.07.001

82. O'Connor KA, Roth BL. Finding new tricks for old drugs: An efficient route for public-sector drug discovery. Nat Rev Drug Discov. 2005 Dec;4(12):1005–14. doi:10.1038/nrd1900 PubMed PMID: 16341065.

83. Panic G, Duthaler U, Speich B, Keiser J. Repurposing drugs for the treatment and control of helminth infections. Int J Parasitol Drugs Drug Resist. 2014 Dec 1;4(3):185–200. doi:https://doi.org/10.1016/j.ijpddr.2014.07.002

84. Alvarez-Mercado JM, Ibarra-Velarde F, Alonso-Díaz MÁ, Vera-Montenegro Y, Avila-Acevedo JG, García-Bores AM. *In vitro* antihelmintic effect of fifteen tropical plant extracts on excysted flukes of *Fasciola hepatica*. BMC Vet Res. 2015 Feb 27;11(1):45. doi:10.1186/s12917-015-0362-4

85. Lorsuwannarat N, Piedrafita D, Chantree P, Sansri V, Songkoomkrong S, Bantuchai S, et al. The *in vitro* anthelmintic effects of plumbagin on newly excysted and 4-weeks-old juvenile parasites of *Fasciola gigantica*. Exp Parasitol. 2014 Jan 1;136:5–13. doi:https://doi.org/10.1016/j.exppara.2013.10.004

86. Abdelaal MMO, Brennan GP, Hanna REB, Abdel-Aziz A, Fairweather I. Disruption of egg production by triclabendazole-resistant *Fasciola hepatica* following treatment with a commercial preparation of myrrh (Mirazid). Acta Parasitol. 2017 Jun 1;62(2):336–47. doi:10.1515/ap-2017-0041

87. Abdelaal MMO, Brennan GP, Abdel-Aziz A, Fairweather I. Ultrastructural changes to the tegumental system and gastrodermal cells of adult *Fasciola hepatica* following treatment *in vivo* with a commercial preparation of myrrh (Mirazid). J Helminthol. 2016/10/20. 2017 Nov;91(6):672–85. doi:DOI: 10.1017/S0022149X16000705

88. Brown D. Unfinished business: Target-based drug discovery. Drug Discov Today. 2007 Dec 1;12(23–24):1007–12. doi:https://doi.org/10.1016/j.drudis.2007.10.017

89. Wolf C, Gunkel N. Target identification and validation in antiparasitic drug discovery. In: Selzer PM, editor. Antiparasitic and Antibacterial Drug Discovery. 2009. p. 59–73. doi:https://doi.org/10.1002/9783527626816.ch5

90. Sharma KR, Colvis CM, Rodgers GP, Sheeley DM. Illuminating the druggable genome: Pathways to progress. Drug Discov Today. 2024 Mar;29(3):103805. doi:https://doi.org/10.1016/j.drudis.2023.103805

91. Park SK, Friedrich L, Yahya NA, Rohr CM, Chulkov EG, Maillard D, et al. Mechanism of praziquantel action at a parasitic flatworm ion channel. Sci Transl Med. 2021 Dec 22;13(625):eabj5832. doi:10.1126/scitranslmed.abj5832 PubMed PMID: 34936384.

92. Rohr CM, Sprague DJ, Park SK, Malcolm NJ, Marchant JS. Natural variation in the binding pocket of a parasitic flatworm TRPM channel resolves the basis for praziquantel sensitivity. Proc Natl Acad Sci U S A. 2023 Jan 3;120(1). doi:10.1073/pnas.2217732120 PubMed PMID: 36574686.

93. Sprague DJ, Park SK, Gramberg S, Bauer L, Rohr CM, Chulkov EG, et al. Target-based discovery of a broad-spectrum flukicide. Nat Struct Mol Biol. 2024 Sep;31(9):1386–93. doi:10.1038/s41594-024-01298-3

94. Spithill TW, Toet H, Rathinasamy V, Zerna G, Swan J, Cameron T, et al. Vaccines for *Fasciola*: New thinking for an old problem. In: Dalton JP, editor. CABI. 2nd ed. CABI; 2021. p. 379–422. doi:10.1079/9781789246162.0012

95. Toet H, Piedrafita DM, Spithill TW. Liver fluke vaccines in ruminants: Strategies, progress and future opportunities. Int J Parasitol. 2014 Oct 15;44(12):915–27. doi:https://doi.org/10.1016/j.ijpara.2014.07.011

96. Luci´ L, Piacenza L, Acosta D, Basmadjian I, Dalton JP, Carmona C. Vaccination with cathepsin L proteinases and with leucine aminopeptidase induces high levels of protection against fascioliasis in sheep. Infect Immun. 1999 Apr 1;67(4):1954–61. doi:https://doi.org/10.1128/iai.67.4.1954-1961.1999

97. Dalton JP, Mcgonigle S, Rolph TP, And †, Andrews SJ. Induction of protective immunity in cattle against infection with *Fasciola hepatica* by vaccination with cathepsin L proteinases and with hemoglobin. Infect Immun. 1996 Dec;64(12):5066–74. doi:https://doi.org/10.1128/iai.64.12.5066-5074.1996

98. Ravidà A, Cwiklinski K, Aldridge AM, Clarke P, Thompson R, Gerlach JQ, et al. *Fasciola hepatica* surface tegument: Glycoproteins at the interface of parasite and host. Molecular & Cellular Proteomics. 2016 Oct 1;15(10):3139–53. doi:https://doi.org/10.1074/mcp.M116.059774

99. Meevissen MHJ, Yazdanbakhsh M, Hokke CH. *Schistosoma mansoni* egg glycoproteins and C-type lectins of host immune cells: Molecular partners that shape immune responses. Exp Parasitol. 2012 Sep 1;132(1):14–21. doi:https://doi.org/10.1016/j.exppara.2011.05.005

100. McManus DP. Recent progress in the development of liver fluke and blood fluke vaccines. Vaccines (Basel). 2020 Sep 22;8(3):553. doi:10.3390/vaccines8030553

101. Villa-Mancera A, Reynoso-Palomar A, Utrera-Quintana F, Carreón-Luna L. Cathepsin L1 mimotopes with adjuvant Quil A induces a Th1/Th2 immune response and confers significant protection against *Fasciola hepatica* infection in goats. Parasitol Res. 2014 Jan;113(1):243–50. doi:10.1007/s00436-013-3650-6

102. Villa-Mancera A, Alcalá-Canto Y, Reynoso-Palomar A, Olmedo-Juárez A, Olivares-Pérez J. Vaccination with cathepsin L phage-exposed mimotopes, single or in combination, reduce size, fluke burden, egg production and viability in sheep experimentally infected with *Fasciola hepatica*. Parasitol Int. 2021 Aug 1;83:102355. doi:https://doi.org/10.1016/j.parint.2021.102355

103. Villa-Mancera A, Alcalá-Canto Y, Olivares-Pérez J, Molina-Mendoza P, Hernández-Guzmán K, Utrera-Quintana F, et al. Vaccination with cathepsin L mimotopes of *Fasciola hepatica* in goats reduces worm burden, morphometric measurements, and reproductive structures. Microb Pathog. 2021 Jun 1;155:104859. doi:https://doi.org/10.1016/j.micpath.2021.104859

104. Chen Q, Chen B, Zhang C. Intelligent Strategies for Pathway Mining. Springer International Publishing; 2014. doi:https://doi.org/10.1007/978-3-319-04172-8

105. Cohen P. Protein kinases—the major drug targets of the twenty-first century? Nat Rev Drug Discov. 2002 Apr 1;1(4):309–15. doi:https://doi.org/10.1038/nrd773

106. Roskoski R. A historical overview of protein kinases and their targeted small molecule inhibitors. Pharmacol Res. 2015 Oct 1;100:1–23. doi:10.1016/j.phrs.2015.07.010 PubMed PMID: 26207888.

107. Hunter T. Signaling—2000 and beyond. Cell. 2000;100(1):113–27. doi:https://doi.org/10.1016/S0092-8674(00)81688-8

108. Cohen P. The regulation of protein function by multisite phosphorylation – a 25 year update. Trends Biochem Sci. 2000 Dec 1;25(12):596–601. doi:https://doi.org/10.1016/S0968-0004(00)01712-6

109. Manning G, Whyte D, Martinez R, Hunter T, Sudarsanam S. The protein kinase complement of the human genome. Science (1979). 2002 Dec 6;298(5600):1992–1934. doi:10.1126/science.1075762

110. Hanks SK. Genomic analysis of the eukaryotic protein kinase superfamily: A perspective. Genome Biol. 2003 Apr;4(5):111. doi:10.1186/gb-2003-4-5-111

111. Röhm S, Krämer A, Knapp S. Function, structure and topology of protein kinases. In: Laufer S, editor. Proteinkinase Inhibitors. Cham: Springer International Publishing; 2021. p. 1–24. doi:10.1007/7355_2020_97

112. Ten Eyck LF, Taylor SS, Kornev AP. Conserved spatial patterns across the protein kinase family. Biochimica et Biophysica Acta (BBA) - Proteins and Proteomics. 2008 Jan 1;1784(1):238–43. doi:https://doi.org/10.1016/j.bbapap.2007.11.002

113. Taylor SS, Kornev AP. Protein kinases: Evolution of dynamic regulatory proteins. Trends Biochem Sci. 2011 Feb 1;36(2):65–77. doi:https://doi.org/10.1016/j.tibs.2010.09.006

114. Modi V, Dunbrack RL. A Structurally-Validated Multiple Sequence Alignment of 497 Human Protein Kinase Domains. Sci Rep. 2019;9(1):19790. doi:10.1038/s41598-019-56499-4

115. Xie Y, Li H, Luo X, Li H, Gao Q, Zhang L, et al. IBS 2.0: An upgraded illustrator for the visualization of biological sequences. Nucleic Acids Res. 2022 Jul 5;50(W1):W420–6. doi:10.1093/nar/gkac373 PubMed PMID: 35580044.

116. Laufer S, editor. Proteinkinase Inhibitors. Springer; 2021. 1–256 p. doi:https://doi.org/10.1007/978-3-030-68180-7

117. Hunter T, Lindberg RA, Middlemas DS, Tracy S, Van Der Geer P. Receptor protein tyrosine kinases and phosphatases. Cold Spring Harb Symp Quant Biol. 1992 Jan 1;57:25–41. doi:10.1101/sqb.1992.057.01.005

118. Hanks SK, Hunter T. Protein kinases 6. The eukaryotic protein kinase superfamily: kinase (catalytic) domain structure and classification. FASEB journal. 1995 May;9(8):576–96. doi:10.1096/fasebj.9.8.7768349

119. Hanks SK, Quinn AM, Hunter T. The protein kinase family: Conserved features and deduced phylogeny of the catalytic domains. Science (1979). 1988 Jul 1;241(4861):42–52. doi:10.1126/science.3291115

120. Manning G, Plowman GD, Hunter T, Sudarsanam S. Evolution of protein kinase signaling from yeast to man. Trends Biochem Sci. 2002 Oct 1;27(10):514–20. doi:https://doi.org/10.1016/S0968-0004(02)02179-5

121. KinBase - the kinase database [Internet]. [cited 2024 Mar 10]. Available from: http://kinase.com/web/current/kinbase/

122. Hunter T. [1] Protein kinase classification. In: Hunter T, Sefton BM, editors. Methods in Enzymology. Academic Press; 1991. p. 3–37. doi:https://doi.org/10.1016/0076-6879(91)00125-G

123. Kanev GK, de Graaf C, de Esch IJP, Leurs R, Würdinger T, Westerman BA, et al. The landscape of atypical and eukaryotic protein kinases. Trends Pharmacol Sci. 2019 Nov 1;40(11):818–32. doi:10.1016/j.tips.2019.09.002 PubMed PMID: 31677919.

124. Lundquist PK, Davis JI, van Wijk KJ. ABC1K atypical kinases in plants: Filling the organellar kinase void. Trends in Plant Science. 2012. p. 546–55. doi:10.1016/j.tplants.2012.05.010 PubMed PMID: 22694836.

125. Roskoski R. Properties of FDA-approved small molecule protein kinase inhibitors: A 2022 update. Pharmacological Research. Academic Press; 2022. doi:10.1016/j.phrs.2021.106037 PubMed PMID: 34921994.

126. Bournez C, Carles F, Peyrat G, Aci-Sèche S, Bourg S, Meyer C, et al. Comparative assessment of protein kinase inhibitors in public databases and in PKIDB. Molecules. 2020 Jul 15;25(14):3226. doi:10.3390/molecules25143226 PubMed PMID: 32679723.

127. Carles F, Bourg S, Meyer C, Bonnet P. PKIDB: A curated, annotated and updated database of protein kinase inhibitors in clinical trials. Molecules. 2018 Apr 15;23(4):908. doi:10.3390/molecules23040908 PubMed PMID: 29662024.

128. Doerig C, Grevelding CG. Targeting kinases in Plasmodium and Schistosoma: Same goals, different challenges. Biochimica et Biophysica Acta (BBA) - Proteins and Proteomics. 2015 Oct 1;1854(10):1637–43. doi:https://doi.org/10.1016/j.bbapap.2015.03.002

129. Stroehlein AJ, Young ND, Gasser RB. Advances in kinome research of parasitic worms - implications for fundamental research and applied biotechnological outcomes. Biotechnol Adv. 2018 Jul 1;36(4):915–34. doi:10.1016/j.biotechadv.2018.02.013 PubMed PMID: 29477756.

130. Arora N, Raj A, Anjum F, Kaur R, Rawat SS, Kumar R, et al. Unveiling *Taenia solium* kinome profile and its potential for new therapeutic targets. Expert Rev Proteomics. 2020 Jan 2;17(1):85–94. doi:10.1080/14789450.2020.1719835 PubMed PMID: 31968176.

131. Liu GH, Korhonen PK, Young ND, Lu J, Wang T, Fu YT, et al. *Dipylidium caninum* draft genome - a new resource for comparative genomic and genetic explorations of flatworms. Genomics. 2021 May 1;113(3):1272–80. doi:https://doi.org/10.1016/j.ygeno.2021.02.019

132. Stroehlein AJ, Young ND, Korhonen PK, Jabbar A, Hofmann A, Sternberg PW, et al. The *Haemonchus contortus* kinome - A resource for fundamental molecular investigations and drug discovery. Parasit Vectors. 2015 Dec 8;8(1):623. doi:10.1186/s13071-015-1231-5 PubMed PMID: 26644012.

133. Stroehlein AJ, Young ND, Korhonen PK, Chang BCH, Nejsum P, Pozio E, et al. Whipworm kinomes reflect a unique biology and adaptation to the host animal. Int J Parasitol. 2017 Nov 1;47(13):857–66. doi:10.1016/j.ijpara.2017.04.005 PubMed PMID: 28606697.

134. Giuliani S, Silva AC, Borba JVVB, Ramos PIP, Paveley RA, Muratov EN, et al. Computationally-guided drug repurposing enables the discovery of kinase targets and inhibitors as new schistosomicidal agents. PLoS Comput Biol. 2018 Oct 22;14(10):e1006515. doi:10.1371/journal.pcbi.1006515 PubMed PMID: 30346968.

135. Stroehlein AJ, Young ND, Jex AR, Sternberg PW, Tan P, Boag PR, et al. Defining the *Schistosoma haematobium* kinome enables the prediction of essential kinases as anti-

schistosome drug targets. Sci Rep. 2015 Dec 4;5(1):17759. doi:10.1038/srep17759 PubMed PMID: 26635209.

136. Andrade LF, Nahum LA, Avelar LGA, Silva LL, Zerlotini A, Ruiz JC, et al. Eukaryotic protein kinases (ePKs) of the helminth parasite *Schistosoma mansoni*. BMC Genomics. 2011 Dec;12:1–9. doi:10.1186/1471-2164-12-215 PubMed PMID: 21548963.

137. Grevelding CG, Langner S, Dissous C. Kinases: Molecular stage directors for schistosome development and differentiation. Trends Parasitol. 2018 Mar 1;34(3):246–60. doi:10.1016/j.pt.2017.12.001 PubMed PMID: 29276074.

138. Das KC, Kalita P, Tripathi T. Genome-wide identification and characterization of eukaryotic protein kinases. Frontiers in Biosciences. 2020 Jun 1;25(9):1787–827. doi:https://doi.org/10.2741/4878

139. Adderley J, Doerig C. Comparative analysis of the kinomes of *Plasmodium falciparum*, *Plasmodium vivax* and their host *Homo sapiens*. BMC Genomics. 2022 Mar 26;23(1):237. doi:10.1186/s12864-022-08457-0 PubMed PMID: 35346035.

140. Ward P, Equinet L, Packer J, Doerig C. Protein kinases of the human malaria parasite *Plasmodium falciparum*: The kinome of a divergent eukaryote. BMC Genomics. 2004 Oct 12;5(1):79. doi:10.1186/1471-2164-5-79

141. Kar PP, Araveti PB, Srivastava A. Deciphering the kinome of *Theileria annulata* for identification of drug targets and anti-theilerial drug. Ticks Tick Borne Dis. 2022 Nov 1;13(6). doi:10.1016/j.ttbdis.2022.102049

142. Borba JVB, Silva AC, Ramos PIP, Grazzia N, Miguel DC, Muratov EN, et al. Unveiling the kinomes of *Leishmania infantum* and *L. braziliensis* empowers the discovery of new kinase targets and antileishmanial compounds. Comput Struct Biotechnol J. 2019 Jan 1;17:352–61. doi:10.1016/j.csbj.2019.02.005

143. Parsons M, Worthey EA, Ward PN, Mottram JC. Comparative analysis of the kinomes of three pathogenic trypanosomatids: *Leishmania major*, *Trypanosoma brucei* and *Trypanosoma cruzi*. BMC Genomics. 2005 Sep 15;6(1):127. doi:10.1186/1471-2164-6-127 PubMed PMID: 16164760.

144. Dissous C, Grevelding CG. Piggy-backing the concept of cancer drugs for schistosomiasis treatment: A tangible perspective? Trends Parasitol. 2011 Feb 1;27(2):59–66. doi:10.1016/j.pt.2010.09.001 PubMed PMID: 20920890.

145. Moreira BP, Weber MHW, Haeberlein S, Mokosch AS, Spengler B, Grevelding CG, et al. Drug repurposing and *De novo* drug discovery of protein kinase inhibitors as new drugs against schistosomiasis. Molecules. 2022 Feb 19;27(4):1414. doi:10.3390/molecules27041414 PubMed PMID: 35209202.

146. Moreira BP, Gava SG, Haeberlein S, Gueye S, Santos ESS, Weber MHW, et al. Identification of potent schistosomicidal compounds predicted as type II-kinase inhibitors against *Schistosoma mansoni* c-Jun N-terminal kinase SMJNK. Frontiers in Parasitology. 2024 Apr 26;3:1494407. doi:10.3389/fpara.2024.1394407

147. Moreira BP, Batista ICA, Tavares NC, Armstrong T, Gava SG, Torres GP, et al. Docking-based virtual screening enables prioritizing protein kinase inhibitors with *in vitro* phenotypic activity against *Schistosoma mansoni*. Front Cell Infect Microbiol. 2022 Jul 5;12:913301. doi:10.3389/fcimb.2022.913301 PubMed PMID: 35865824.

148. Lucet IS, Tobin A, Drewry D, Wilks AF, Doerig C. *Plasmodium* kinases as targets for new-generation antimalarials. Future Med Chem. 2012 Dec 1;4(18):2295–310. doi:10.4155/fmc.12.183

149. Borba JVVB, Silva AC, Lima MNN, Mendonca SS, Furnham N, Costa FTM, et al. Chemogenomics and bioinformatics approaches for prioritizing kinases as drug targets for neglected tropical diseases. In: Advances in Protein Chemistry and Structural Biology. Academic Press Inc.; 2021. p. 187–223. doi:10.1016/bs.apcsb.2020.10.006 PubMed PMID: 33632465.

150. Despommier DD. *Trichinella spiralis* and the concept of niche. J Parasitol. 1993 Aug 1;79(4):472–82. doi:10.2307/3283370

151. Garnick E. Niche breadth in parasites: An evolutionarily stable strategy model, with special reference to the protozoan parasite *Leishmania*. Theor Popul Biol. 1992 Aug 1;42(1):62–103. doi:https://doi.org/10.1016/0040-5809(92)90005-E

152. Maizels RM, Pearce EJ, Artis D, Yazdanbakhsh M, Wynn TA. Regulation of pathogenesis and immunity in helminth infections. Journal of Experimental Medicine. 2009 Sep 28;206(10):2059–66. doi:10.1084/jem.20091903

153. Maizels RM, McSorley HJ. Regulation of the host immune system by helminth parasites. Journal of Allergy and Clinical Immunology. 2016 Sep 1;138(3):666–75. doi:https://doi.org/10.1016/j.jaci.2016.07.007

154. McSorley HJ, Hewitson JP, Maizels RM. Immunomodulation by helminth parasites: Defining mechanisms and mediators. Int J Parasitol. 2013 Mar 1;43(3–4):301–10. doi:https://doi.org/10.1016/j.ijpara.2012.11.011

155. Taylor CM, Wang Q, Rosa BA, Huang SCC, Powell K, Schedl T, et al. Discovery of anthelmintic drug targets and drugs using chokepoints in nematode metabolic pathways. PLoS Pathog. 2013 Aug 1;9(8):e1003505. doi:https://doi.org/10.1371/journal.ppat.1003505

156. Swierczewski BE, Davies SJ. A *schistosome* cAMP-Dependent protein kinase catalytic subunit is essential for parasite viability. PLoS Negl Trop Dis. 2009 Aug 25;3(8):e505. doi:https://doi.org/10.1371/journal.pntd.0000505

157. Vicogne J, Cailliau K, Tulasne D, Browaeys E, Yan YT, Fafeur V, et al. Conservation of epidermal growth factor receptor function in the human parasitic helminth *Schistosoma mansoni*. Journal of Biological Chemistry. 2004 Sep 3;279(36):37407–14. doi:https://doi.org/10.1074/jbc.M313738200

158. Gava SG, Tavares NC, Falcone FH, Oliveira G, Mourão MM. Profiling transcriptional regulation and functional roles of *Schistosoma mansoni* c-Jun N-terminal kinase. Front Genet. 2019 Oct 18;10:1036. doi:https://doi.org/10.3389/fgene.2019.01036

159. Andrade LF de, Mourao M de M, Geraldo JA, Coelho FS, Silva LL, Neves RH, et al. Regulation of *Schistosoma mansoni* development and reproduction by the mitogen-activated protein kinase signaling pathway. PLoS Negl Trop Dis. 2014 Jun 19;8(6):e2949.

160. Avelar L das GA, Gava SG, Neves RH, Silva MCS, Araújo N, Tavares NC, et al. Smp38 MAP kinase regulation in *Schistosoma mansoni*: Roles in survival, oviposition, and protection against oxidative stress. Front Immunol. 2019 Jan 24;10:21. doi:https://doi.org/10.3389/fimmu.2019.00021

161. Chauhan A, Sun Y, Pani B, Quenumzangbe F, Sharma J, Singh BB, et al. Helminth induced suppression of macrophage activation is correlated with inhibition of calcium channel activity. PLoS One. 2014 Jul 11;9(7):e101023. doi:https://doi.org/10.1371/journal.pone.0101023

162. Brehm K, Koziol U. Chapter four - *Echinococcus*–Host interactions at cellular and molecular levels. In: Thompson RCA, Deplazes P, Lymbery AJ, editors. Advances in Parasitology. Academic Press; 2017. p. 147–212. doi:https://doi.org/10.1016/bs.apar.2016.09.001

163. Gao HJ, Sun XD, Luo YP, Pang HS, Ma XM, Zhang T, et al. Anti-echinococcal effect of verapamil involving the regulation of the calcium/calmodulin-dependent protein kinase II response in vitro and in a murine infection model. Parasit Vectors. 2021;14(1):108. doi:10.1186/s13071-021-04618-4

164. Vicogne J, Pin JP, Lardans V, Capron M, Noël C, Dissous C. An unusual receptor tyrosine kinase of *Schistosoma mansoni* contains a venus flytrap module. Mol Biochem Parasitol. 2003 Jan 1;126(1):51–62. doi:https://doi.org/10.1016/S0166-6851(02)00249-9

165. Ahier A, Rondard P, Gouignard N, Khayath N, Huang S, Trolet J, et al. A new family of receptor tyrosine kinases with a venus flytrap binding domain in insects and other invertebrates activated by aminoacids. PLoS One. 2009 May 21;4(5):e5651. doi:https://doi.org/10.1371/journal.pone.0005651

166. Dissous C, Morel M, Vanderstraete M. Venus kinase receptors: Prospects in signaling and biological functions of these invertebrate kinases. Front Endocrinol (Lausanne). 2014 May 13;5:72. doi:10.3389/fendo.2014.00072

167. Vanderstraete M, Gouignard N, Cailliau K, Morel M, Lancelot J, Bodart JF, et al. Dual targeting of insulin and venus kinase receptors of *Schistosoma mansoni* for novel anti-schistosome Therapy. PLoS Negl Trop Dis. 2013 May 16;7(5):e2226. doi:10.1371/journal.pntd.0002226

168. Dissous C. Venus kinase receptors at the crossroads of insulin signaling: Their role in reproduction for helminths and insects. Front Endocrinol (Lausanne). 2015 Aug 3;6:118. doi:10.3389/fendo.2015.00118

169. Morawietz CM, Houhou H, Puckelwaldt O, Hehr L, Dreisbach D, Mokosch A, et al. Targeting kinases in *Fasciola hepatica*: Anthelminthic effects and tissue distribution of selected kinase inhibitors. Front Vet Sci. 2020 Dec 21;7:611270. doi:10.3389/fvets.2020.611270

170. McCusker P, Clarke NG, Armstrong R, Wells D, Robb E, McVeigh P, et al. Polo-like kinase 1 regulates growth in juvenile *Fasciola hepatica*. PLoS Pathog. 2025 Dec 2;21(12):e1013406. doi:https://doi.org/10.1371/journal.ppat.1013406

171. Gramberg S, Puckelwaldt O, Schmitt T, Lu Z, Haeberlein S. Spatial transcriptomics of a parasitic flatworm provides a molecular map of drug targets and drug resistance genes. Nat Commun. 2024 Oct 16;15(1):8918. doi:10.1038/s41467-024-53215-3

172. Robertson SA, Renslo AR. Drug discovery for neglected tropical diseases at the sandler center. Future Med Chem. 2011 Aug 1;3(10):1279–88. doi:10.4155/fmc.11.85

173. Hoover D, Friedmann M, Reeves R, Magnuson NS. Recombinant human pim-1 protein exhibits serine/threonine kinase activity. Journal of Biological Chemistry. 1991 Jul 25;266(21):14018–23. doi:https://doi.org/10.1016/S0021-9258(18)92804-8

174. Allen JD, Verhoeven E, Domen J, van der Valk M, Berns A. PIM-2 transgene induces lymphoid tumors, exhibiting potent synergy with c-myc. Oncogene. 1997 Sep;15(10):1133–41. doi:https://doi.org/10.1038/sj.onc.1201288

175. Nawijn MC, Alendar A, Berns A. For better or for worse: The role of Pim oncogenes in tumorigenesis. Nat Rev Cancer. 2011 Jan;11(1):23–34. doi:10.1038/nrc2986

176. Wu J, Chu E, Kang Y. PIM Kinases in Multiple Myeloma. Cancers (Basel). 2021 Aug 26;13(17):4304. doi:10.3390/cancers13174304

177. Liu Z, Han M, Ding K, Fu R. The role of Pim kinase in immunomodulation. Am J Cancer Res. 2020 Dec 1;10(12):4085–97.

178. Nock S, Karim E, Unsworth AJ. Pim kinases: Important regulators of cardiovascular disease. Int J Mol Sci. 2023 Jul 18;24(14):11582. doi:10.3390/ijms241411582

179. Qian KC, Wang L, Hickey ER, Studts J, Barringer K, Peng C, et al. Structural basis of constitutive activity and a unique nucleotide binding mode of human Pim-1 kinase. Journal of Biological Chemistry. 2005 Feb 18;280(7):6130–7. doi:https://doi.org/10.1074/jbc.M409123200

180. Johnson LN, Noble MEM, Owen DJ. Active and inactive protein kinases: Structural basis for regulation. Cell. 1996 Apr 19;85(2):149–58. doi:10.1016/S0092-8674(00)81092-2

181. Amaravadi R, Thompson CB. The survival kinases Akt and Pim as potential pharmacological targets. J Clin Invest. 2005 Oct 3;115(10):2618–24. doi:10.1172/JCI26273

182. Kunder R, Velyunskiy M, Dunne SF, Cho BK, Kanojia D, Begg L, et al. Synergistic PIM kinase and proteasome inhibition as a therapeutic strategy for MYC-overexpressing triple-negative breast cancer. Cell Chem Biol. 2022 Mar 17;29(3):358–72. doi:https://doi.org/10.1016/j.chembiol.2021.08.011

183. Jackson LJ, Pheneger JA, Pheneger TJ, Davis G, Wright AD, Robinson JE, et al. The role of PIM kinases in human and mouse CD4+ T cell activation and inflammatory bowel

disease. Cell Immunol. 2012 Jan 1;272(2):200–13. doi:https://doi.org/10.1016/j.cellimm.2011.10.011

184. Losman J, Chen XP, Jiang H, PAN PY, Kashiwada M, Giallourakis C, et al. IL-4 signaling is regulated through the recruitment of phosphatases, kinases, and SOCS proteins to the receptor complex. In: Cold Spring Harbor symposia on quantitative biology. Cold Spring Harbor Laboratory Press; 1999. p. 405–16. doi:doi:10.1101/sqb.1999.64.405

185. Wang Z, Bhattacharya N, Mixter PF, Wei W, Sedivy J, Magnuson NS. Phosphorylation of the cell cycle inhibitor p21Cip1/WAF1 by Pim-1 kinase. Biochimica et Biophysica Acta (BBA) - Molecular Cell Research. 2002 Dec 16;1593(1):45–55. doi:https://doi.org/10.1016/S0167-4889(02)00347-6

186. Bhattacharya N, Wang Z, Davitt C, McKenzie IF, Xing P xiang, Magnuson NS. Pim-1 associates with protein complexes necessary for mitosis. Chromosoma. 2002 Jul;111(2):80–95. doi:10.1007/s00412-002-0192-6

187. Bachmann M, Kosan C, Xing PX, Montenarh M, Hoffmann I, Möröy T. The oncogenic serine/threonine kinase Pim-1 directly phosphorylates and activates the G2/M specific phosphatase Cdc25C. Int J Biochem Cell Biol. 2006 Mar 1;38(3):430–43. doi:https://doi.org/10.1016/j.biocel.2005.10.010

188. Aho TLT, Sandholm J, Peltola KJ, Mankonen HP, Lilly M, Koskinen PJ. Pim-1 kinase promotes inactivation of the pro-apoptotic Bad protein by phosphorylating it on the Ser112 gatekeeper site. FEBS Lett. 2004 Jul 30;571(1–3):43–9. doi:https://doi.org/10.1016/j.febslet.2004.06.050

189. Peltola KJ, Paukku K, Aho TLT, Ruuska M, Silvennoinen O, Koskinen PJ. Pim-1 kinase inhibits STAT5-dependent transcription via its interactions with SOCS1 and SOCS3. Blood. 2004 May 15;103(10):3744–50. doi:https://doi.org/10.1182/blood-2003-09-3126

190. Chen XP, Losman JA, Cowan S, Donahue E, Fay S, Vuong BQ, et al. Pim serine/threonine kinases regulate the stability of Socs-1 protein. Proceedings of the National Academy of Sciences. 2002 Feb 19;99(4):2175–80. doi:10.1073/pnas.042035699

191. Ogata H, Goto S, Sato K, Fujibuchi W, Bono H, Kanehisa M. KEGG: Kyoto encyclopedia of genes and genomes. Nucleic Acids Res. 1999 Jan 1;27(1):29–34. doi:10.1093/nar/27.1.29

192. Kanehisa M, Furumichi M, Tanabe M, Sato Y, Morishima K. KEGG: new perspectives on genomes, pathways, diseases and drugs. Nucleic Acids Res. 2017 Jan 4;45(D1):D353–61. doi:10.1093/nar/gkw1092

193. Chen LS, Redkar S, Taverna P, Cortes JE, Gandhi V. Mechanisms of cytotoxicity to Pim kinase inhibitor, SGI-1776, in acute myeloid leukemia. Blood, The Journal of the American Society of Hematology. 2011 Jul 21;118(3):693–702. doi:10.1182/blood-2010-12-323022

194. Kelly KR, Oberheu K, Medina E, Espitia CM, Mahalingam D, Taverna P, et al. Targeting PIM kinase activity with the novel small molecule inhibitor SGI-1776 significantly augments the efficacy of cytarabine in models of acute myeloid leukemia. Blood. 2010 Nov 19;116(21):3253. doi:10.1182/blood.V116.21.3253.3253

195. Chen LS, Redkar S, Bearss D, Wierda WG, Gandhi V. Pim kinase inhibitor, SGI-1776, induces apoptosis in chronic lymphocytic leukemia cells. Blood. 2009 Nov 5;114(19):4150–7. doi:10.1182/blood-2009-03-212852

196. Haddach M, Michaux J, Schwaebe MK, Pierre F, O'Brien SE, Borsan C, et al. Discovery of CX-6258. A potent, selective, and orally efficacious pan-PIM kinases inhibitor. ACS Med Chem Lett. 2012 Feb 9;3(2):135–9. doi:10.1021/ml200259q

197. Bogusz J, Zrubek K, Rembacz KP, Grudnik P, Golik P, Romanowska M, et al. Structural analysis of PIM1 kinase complexes with ATP-competitive inhibitors. Sci Rep. 2017 Oct 17;7(1):13399. doi:10.1038/s41598-017-13557-z PubMed PMID: 29042609.

198. Melms JC, Vallabhaneni S, Mills CE, Yapp C, Chen JY, Morelli E, et al. Inhibition of haspin kinase promotes cell-intrinsic and extrinsic antitumor activity. Cancer Res. 2020 Feb 15;80(4):798–810. doi:10.1158/0008-5472.CAN-19-2330

199. Jumper J, Evans R, Pritzel A, Green T, Figurnov M, Ronneberger O, et al. Highly accurate protein structure prediction with AlphaFold. Nature. 2021 Aug;596(7873):583–9. doi:10.1038/s41586-021-03819-2 PubMed PMID: 34265844.

200. Varadi M, Bertoni D, Magana P, Paramval U, Pidruchna I, Radhakrishnan M, et al. AlphaFold protein structure database in 2024: Providing structure coverage for over 214 million protein sequences. Nucleic Acids Res. 2024 Jan 5;52(D1):D368–75. doi:10.1093/nar/gkad1011 PubMed PMID: 37933859.

201. Varadi M, Anyango S, Deshpande M, Nair S, Natassia C, Yordanova G, et al. AlphaFold protein structure database: Massively expanding the structural coverage of protein-

sequence space with high-accuracy models. Nucleic Acids Res. 2022 Jan 7;50(D1):D439–44. doi:10.1093/nar/gkab1061 PubMed PMID: 34791371.

202. Anaconda Software Distribution. Anaconda Documentation [Internet]. Anaconda Inc.; 2020. Available from: https://anaconda.com/

203. Eberhardt J, Santos-Martins D, Tillack AF, Forli S. AutoDock Vina 1.2.0: New docking methods, expanded force field, and python bindings. J Chem Inf Model. 2021 Jul 19;61(8):3891–8. doi:10.1021/acs.jcim.1c00203 PubMed PMID: 34278794.

204. Trott O, Olson AJ. AutoDock Vina: Improving the speed and accuracy of docking with a new scoring function, efficient optimization, and multithreading. J Comput Chem. 2010 Jan 30;31(2):455–61. doi:10.1002/jcc.21334 PubMed PMID: 19499576.

205. Quinlan AR, Hall IM. BEDTools: A flexible suite of utilities for comparing genomic features. Bioinformatics. 2010 Mar 15;26(6):841–2. doi:10.1093/bioinformatics/btq033 PubMed PMID: 20110278.

206. Altschul SF, Gish W, Miller W, Myers EW, Lipman DJ. Basic Local Alignment Search Tool. J Mol Biol. 1990 Oct 5;215(3):403–10. doi:https://doi.org/10.1016/S0022-2836(05)80360-2

207. Camacho C, Coulouris G, Avagyan V, Ma N, Papadopoulos J, Bealer K, et al. BLAST+: Architecture and applications. BMC Bioinformatics. 2009 Dec 15;10(1):421. doi:10.1186/1471-2105-10-421 PubMed PMID: 20003500.

208. Kanehisa M, Sato Y, Morishima K. BlastKOALA and GhostKOALA: KEGG tools for functional characterization of genome and metagenome sequences. J Mol Biol. 2016 Feb 22;428(4):726–31. doi:10.1016/j.jmb.2015.11.006 PubMed PMID: 26585406.

209. Mirdita M, Schütze K, Moriwaki Y, Heo L, Ovchinnikov S, Steinegger M. ColabFold: Making protein folding accessible to all. Nat Methods. 2022 Jun 1;19(6):679–82. doi:10.1038/s41592-022-01488-1 PubMed PMID: 35637307.

210. Madeira F, Madhusoodanan N, Lee J, Eusebi A, Niewielska A, Tivey ARN, et al. The EMBL-EBI job dispatcher sequence analysis tools framework in 2024. Nucleic Acids Res. 2024 Jul 5;52(W1):W521–5. doi:10.1093/nar/gkae241 PubMed PMID: 38597606.

211. Rice P, Longden I, Bleasby A. EMBOSS: The European molecular biology open software suite. Trends in genetics. 2000 Jun 1;16(6):276–7.

212. Slater GSC, Birney E. Automated generation of heuristics for biological sequence comparison. BMC Bioinformatics. 2005 Dec;6:1–11. doi:10.1186/1471-2105-6-31 PubMed PMID: 15713233.

213. Rambaut A. FigTree v1.4.4 [Internet]. [cited 2024 Jun 12]. Available from: https://github.com/rambaut/figtree/releases

214. Pertea G, Pertea M. GFF utilities: GffRead and GffCompare. F1000Res. 2020 Apr 28;9:ISCB Comm J-304. doi:10.12688/f1000research.23297.1 PubMed PMID: 32489650.

215. Eddy SR. Profile hidden Markov models. Bioinformatics. 1998;14(9):755–63. doi:10.1093/bioinformatics/14.9.755

216. Finn RD, Clements J, Eddy SR. HMMER web server: Interactive sequence similarity searching. Nucleic Acids Res. 2011 May 18;39(SUPPL. 2):W29-37. doi:10.1093/nar/gkr367 PubMed PMID: 21593126.

217. Jones P, Binns D, Chang HY, Fraser M, Li W, McAnulla C, et al. InterProScan 5: Genome-scale protein function classification. Bioinformatics. 2014 May 1;30(9):1236–40. doi:10.1093/bioinformatics/btu031 PubMed PMID: 24451626.

218. Goldberg JM, Griggs AD, Smith JL, Haas BJ, Wortman JR, Zeng Q. Kinannote, a computer program to identify and classify members of the eukaryotic protein kinase superfamily. Bioinformatics. 2013 Oct 1;29(19):2387–94. doi:10.1093/bioinformatics/btt419 PubMed PMID: 23904509.

219. Katoh K, Standley DM. MAFFT multiple sequence alignment software version 7: Improvements in performance and usability. Mol Biol Evol. 2013 Jan 16;30(4):772–80. doi:10.1093/molbev/mst010 PubMed PMID: 23329690.

220. Tamura K, Stecher G, Kumar S. MEGA11: Molecular Evolutionary Genetics Analysis Version 11. Mol Biol Evol. 2021 Jul 1;38(7):3022–7. doi:10.1093/molbev/msab120 PubMed PMID: 33892491.

221. Ronquist F, Teslenko M, Van Der Mark P, Ayres DL, Darling A, Höhna S, et al. Mrbayes 3.2: Efficient bayesian phylogenetic inference and model choice across a large model space. Syst Biol. 2012 May 1;61(3):539–42. doi:10.1093/sysbio/sys029 PubMed PMID: 22357727.

222. Edgar RC. MUSCLE: Multiple sequence alignment with high accuracy and high throughput. Nucleic Acids Res. 2004;32(5):1792–7. doi:10.1093/nar/gkh340 PubMed PMID: 15034147.

223. Edgar RC. Muscle5: High-accuracy alignment ensembles enable unbiased assessments of sequence homology and phylogeny. Nat Commun. 2022 Nov 15;13(1):6968. doi:10.1038/s41467-022-34630-w PubMed PMID: 36379955.

224. O'Boyle NM, Banck M, James CA, Morley C, Vandermeersch T, Hutchison GR. Open Babel: An open chemical toolbox. J Cheminform. 2011 Dec;3(10):1–4. doi:10.1186/1758-2946-3-33 PubMed PMID: 21982300.

225. Emms DM, Kelly S. OrthoFinder: Phylogenetic orthology inference for comparative genomics. Genome Biol. 2019 Dec;20(1):1–14. doi:10.1186/s13059-019-1832-y PubMed PMID: 31727128.

226. Li L, Stoeckert CJ, Roos DS. OrthoMCL: Identification of ortholog groups for eukaryotic genomes. Genome Res. 2003 Sep 1;13(9):2178–89. doi:10.1101/gr.1224503 PubMed PMID: 12952885.

227. Fischer S, Brunk BP, Chen F, Gao X, Harb OS, Iodice JB, et al. Using OrthoMCL to assign proteins to OrthoMCL-DB groups or to cluster proteomes into new ortholog groups. Curr Protoc Bioinformatics. 2011 Sep;35(1):6–12. doi:10.1002/0471250953.bi0612s35 PubMed PMID: 21901743.

228. Mi H, Ebert D, Muruganujan A, Mills C, Albou LP, Mushayamaha T, et al. PANTHER version 16: A revised family classification, tree-based classification tool, enhancer regions and extensive API. Nucleic Acids Res. 2021 Jan 8;49(D1):D394–403. doi:10.1093/nar/gkaa1106 PubMed PMID: 33290554.

229. Wang M, Kong L. pblat: A multithread blat algorithm speeding up aligning sequences to genomes. BMC Bioinformatics. 2019 Dec;20:1–4. doi:10.1186/s12859-019-2597-8 PubMed PMID: 30646844.

230. Mistry J, Chuguransky S, Williams L, Qureshi M, Salazar GA, Sonnhammer ELL, et al. Pfam: The protein families database in 2021. Nucleic Acids Res. 2021 Jan 8;49(D1):D412–9. doi:10.1093/nar/gkaa913 PubMed PMID: 33125078.

231. Schrödinger LLC. The PyMOL Molecular Graphics System, Version~3.0. 2015.

232. Python Language Reference. Python Documentation [Internet]. Python Software Foundation; 2001. Available from: https://python.org/

233. R Core Team. R: A language and environment for statistical computing [Internet]. Vienna, Austria: R Foundation for Statistical Computing; 2023 [cited 2024 Jul 24]. Available from: https://www.R-project.org/ doi:doi.org/10.59350/t79xt-tf203

234. Burley SK, Bhatt R, Bhikadiya C, Bi C, Biester A, Biswas P, et al. Updated resources for exploring experimentally-determined PDB structures and Computed Structure Models at the RCSB Protein Data Bank. Nucleic Acids Res. 2025 Jan 6;53(D1):D564–74. doi:10.1093/nar/gkae1091 PubMed PMID: 39607707.

235. Letunic I, Khedkar S, Bork P. SMART: Recent updates, new developments and status in 2020. Nucleic Acids Res. 2021 Jan 8;49(D1):D458–60. doi:10.1093/nar/gkaa937 PubMed PMID: 33104802.

236. Gutermuth T, Penner P, Sieg J, Dolfus U, Rarey M. SmartChemist─Simplifying communication about organic chemical structures. J Chem Inf Model. 2025 Jun 9;65(17):9075–81. doi:10.1021/acs.jcim.5c00599

237. Pandurangan AP, Stahlhacke J, Oates ME, Smithers B, Gough J. The SUPERFAMILY 2.0 database: A significant proteome update and a new webserver. Nucleic Acids Res. 2019 Jan 8;47(D1):D490–4. doi:10.1093/nar/gky1130 PubMed PMID: 30445555.

238. Waterhouse A, Bertoni M, Bienert S, Studer G, Tauriello G, Gumienny R, et al. SWISS-MODEL: Homology modelling of protein structures and complexes. Nucleic Acids Res. 2018 Jul 2;46(W1):W296–303. doi:10.1093/nar/gky427 PubMed PMID: 29788355.

239. Wickham H, Averick M, Bryan J, Chang W, McGowan L, François R, et al. Welcome to the Tidyverse. J Open Source Softw. 2019 Nov 21;4(43):1686. doi:10.21105/joss.01686

240. Irwin JJ, Shoichet BK, Mysinger MM, Huang N, Colizzi F, Wassam P, et al. Automated docking screens: A feasibility study. J Med Chem. 2009 Sep 24;52(18):5712–20. doi:10.1021/jm9006966 PubMed PMID: 19719084.

241. Apweiler R, Bairoch A, Wu CH, Baker WC, Boeckmann B, Ferro S, et al. UniProt: the Universal Protein knowledgebase. Nucleic Acids Res. 2004 Jan 1;32(90001):115D – 119. doi:10.1093/nar/gkh131

242. Bateman A, Martin MJ, Orchard S, Magrane M, Adesina A, Ahmad S, et al. UniProt: The universal protein knowledgebase in 2025. Nucleic Acids Res. 2025 Jan 6;53(D1):D609–17. doi:10.1093/nar/gkae1010 PubMed PMID: 39552041.

243. Pettersen EF, Goddard TD, Huang CC, Couch GS, Greenblatt DM, Meng EC, et al. UCSF Chimera - A visualization system for exploratory research and analysis. J Comput Chem. 2004 Oct;25(13):1605–12. doi:10.1002/jcc.20084 PubMed PMID: 15264254.

244. Pettersen EF, Goddard TD, Huang CC, Meng EC, Couch GS, Croll TI, et al. UCSF ChimeraX: Structure visualization for researchers, educators, and developers. Protein Science. 2021 Jan 1;30(1):70–82. doi:10.1002/pro.3943 PubMed PMID: 32881101.

245. Howe KL, Bolt BJ, Shafie M, Kersey P, Berriman M. WormBase ParaSite − a comprehensive resource for helminth genomics. Mol Biochem Parasitol. 2017 Jul 1;215:2–10. doi:10.1016/j.molbiopara.2016.11.005 PubMed PMID: 27899279.

246. Ajmera S, Puckelwaldt O, Stroehlein AJ, Haeberlein S. Curation of the *Fasciola hepatica* kinome as a resource for drug target discovery. BMC Genomics. 2026 Jan 16;27:98. doi:10.1186/s12864-025-12513-w

247. Van Dongen SM. Graph clustering by flow simulation. [Utrecht]: University of Utrecht; 2000.

248. Weiner SJ, Kollman PA, Case DA, Singh UC, Ghio C, Alagona G, et al. A new force field for molecular mechanical simulation of nucleic acids and proteins. J Am Chem Soc. 1984 Feb;106(3):765–84.

249. Jacobs MD, Black J, Futer O, Swenson L, Hare B, Fleming M, et al. Pim-1 ligand-bound structures reveal the mechanism of serine/threonine kinase inhibition by LY294002. Journal of Biological Chemistry. 2005 Apr 8;280(14):13728–34. doi:https://doi.org/10.1074/jbc.M413155200

250. Heyder L, Hochban PMM, Taylor C, Chevillard F, Siefker C, Iking C, et al. Pose, duplicate, then elaborate: Steps towards increased affinity for inhibitors targeting the specificity surface of the PIM-1 kinase. Eur J Med Chem. 2023 Jan 5;245:114914. doi:10.1016/j.ejmech.2022.114914 PubMed PMID: 36410167.

251. Karaman MW, Herrgard S, Treiber DK, Gallant P, Atteridge CE, Campbell BT, et al. A quantitative analysis of kinase inhibitor selectivity. Nat Biotechnol. 2008 Jan;26(1):127–32. doi:10.1038/nbt1358

252. Lipinski CA. Lead- and drug-like compounds: The rule-of-five revolution. Drug Discov Today Technol. 2004 Dec 1;1(4):337–41. doi:10.1016/j.ddtec.2004.11.007 PubMed PMID: 24981612.

253. Lipinski CA, Lombardo F, Dominy BW, Feeney PJ. Experimental and computational approaches to estimate solubility and permeability in drug discovery and development settings. Adv Drug Deliv Rev. 1997 Jan 15;23(1):3–25. doi:https://doi.org/10.1016/S0169-409X(96)00423-1

254. Halgren TA. Merck molecular force field. I. Basis, form, scope, parameterization, and performance of MMFF94. J Comput Chem. 1996 Apr;17(5–6):490–519. doi:10.1002/(SICI)1096-987X(199604)17:5/6<490::AID-JCC1>3.0.CO;2-P

255. Molecular Operating Environment (MOE) [Internet]. Montreal: Chemical Computing Group ULC; 2022. Available from: https://www.chemcomp.com/

256. Bissantz C, Kuhn B, Stahl M. A medicinal chemist's guide to molecular interactions. J Med Chem. 2010 Jul 22;53(14):5061–84. doi:10.1021/jm100112j PubMed PMID: 20345171.

257. Bender BJ, Gahbauer S, Luttens A, Lyu J, Webb CM, Stein RM, et al. A practical guide to large-scale docking. Nat Protoc. 2021 Oct 1;16(10):4799–832. doi:10.1038/s41596-021-00597-z PubMed PMID: 34561691.

258. Chowdhury I, Dashi G, Keskitalo S. CMGC kinases in health and cancer. Cancers (Basel). 2023 Jul 28;15(15):3838. doi:10.3390/cancers15153838

259. Nawaratna SSK, You H, Jones MK, McManus DP, Gobert GN. Calcium and Ca 2+ /Calmodulin-dependent kinase II as targets for helminth parasite control. Biochem Soc Trans. 2018 Dec 17;46(6):1743–51. doi:10.1042/BST20180480 PubMed PMID: 30420417.

260. Pearce LR, Komander D, Alessi DR. The nuts and bolts of AGC protein kinases. Nat Rev Mol Cell Biol. 2010 Jan;11(1):9–22. doi:10.1038/nrm2822 PubMed PMID: 20027184.

261. Wedge SR, Ogilvie DJ, Dukes M, Kendrew J, Chester R, Jackson JA, et al. ZD6474 inhibits vascular endothelial growth factor signaling, angiogenesis, and tumor growth following oral administration. Cancer Res. 2002 Aug 15;62(16):4645–55.

262. Jirousek MR, Gillig JR, Gonzalez CM, Heath WF, Mcdonald Iii JH, Neel DA, et al. ,13H-dibenzo[e,k]pyrrolo[3,4-h][1,4,13]oxadiazacyclohexadecene-1,3(2H)-dione (LY333531) and related analogues: Isozyme selective inhibitors of protein kinase C. J Med Chem. 1996 Jul 5;39(14):2664–71. doi:https://doi.org/10.1021/jm950588y

263. Qian F, Engst S, Yamaguchi K, Peiwen Y, Won KA, Mock L, et al. Inhibition of tumor cell growth, invasion, and metastasis by EXEL-2880 (XL880, GSK1363089), a novel inhibitor of HGF and VEGF receptor tyrosine kinases. Cancer Res. 2009 Oct 15;69(20):8009–16. doi:10.1158/0008-5472.CAN-08-4889 PubMed PMID: 19808973.

264. You WK, Sennino B, Williamson CW, Falcón B, Hashizume H, Yao LC, et al. VEGF and c-Met blockade amplify angiogenesis inhibition in Pancreatic Islet Cancer. Cancer Res. 2011 Jul 15;71(14):4758–68. doi:10.1158/0008-5472.CAN-10-2527 PubMed PMID: 21613405.

265. Morabito A, Piccirillo MC, Falasconi F, De Feo G, Del Giudice A, Bryce J, et al. Vandetanib (ZD6474), a dual inhibitor of vascular endothelial growth factor receptor (VEGFR) and epidermal growth factor receptor (EGFR) tyrosine kinases: Current status and future directions. Oncologist. 2009 Apr 1;14(4):378–90. doi:10.1634/theoncologist.2008-0261 PubMed PMID: 19349511.

266. Herbst RS, Heymach J V., O'Reilly MS, Onn A, Ryan AJ. Vandetanib (ZD6474): An orally available receptor tyrosine kinase inhibitor that selectively targets pathways critical for tumor growth and angiogenesis. Expert Opin Investig Drugs. 2007 Feb;16(2):239–49. doi:10.1517/13543784.16.2.239 PubMed PMID: 17243944.

267. FDA. FDA [Internet]. 2011 [cited 2025 Oct 30]. FDA approves new treatment for rare form of thyroid cancer. Available from: https://web.archive.org/web/20120302105514/http://www.fda.gov/NewsEvents/Newsroom/PressAnnouncements/2011/ucm250168.htm

268. Deshpande H, Roman S, Thumar J, Sosa JA. Vandetanib (ZD6474) in the treatment of medullary thyroid cancer. Clin Med Insights Oncol. 2011 Jan;5(CMO-S6197):213–21. doi:10.4137/CMO.S6197

269. Lee SH, Lee JK, Ahn MJ, Kim DW, Sun JM, Keam B, et al. Vandetanib in pretreated patients with advanced non-small cell lung cancer-harboring RET rearrangement: A phase II clinical trial. Annals of Oncology. 2017 Feb 1;28(2):292–7. doi:10.1093/annonc/mdw559 PubMed PMID: 27803005.

270. GlaxoSmithKline. www.clinicaltrials.gov [Internet]. 2016 [cited 2025 Oct 30]. A phase II study to evaluate Foretinib in genomic subpopulations of subjects with non-small-cell lung cancer (NSCLC). Available from: https://clinicaltrials.gov/study/NCT02034097

271. Shapiro GI, McCallum S, Adams LM, Sherman L, Weller S, Swann S, et al. A Phase 1 dose-escalation study of the safety and pharmacokinetics of once-daily oral foretinib, a

multi-kinase inhibitor, in patients with solid tumors. Invest New Drugs. 2013 Jun;31(3):742–50. doi:10.1007/s10637-012-9881-z PubMed PMID: 23054208.

272. Koike A, Becker F, Sennhenn P, Kim J, Zhang J, Hannus S, et al. Targeting *Echinococcus multilocularis* PIM kinase for improving anti-parasitic chemotherapy. PLoS Negl Trop Dis. 2022 Oct 3;16(10):e0010483. doi:10.1371/journal.pntd.0010483 PubMed PMID: 36190997.

273. McNulty SN, Tort JF, Rinaldi G, Fischer K, Rosa BA, Smircich P, et al. Genomes of *Fasciola hepatica* from the Americas reveal colonization with *Neorickettsia* endobacteria related to the agents of potomac horse and human sennetsu fevers. PLoS Genet. 2017 Jan 1;13(1). doi:10.1371/journal.pgen.1006537 PubMed PMID: 28060841.

274. Puckelwaldt O. Uncovering the cellular diversity of *Fasciola hepatica* utilizing single-cell transcriptomics. Institute of Parasitology, JLU Giessen; 2024. doi:https://doi.org/10.22029/jlupub-19504

275. van Linden OPJ, Kooistra AJ, Leurs R, de Esch IJP, de Graaf C. KLIFS: A knowledge-based structural database to navigate kinase–ligand interaction space. J Med Chem. 2014 Jan 23;57(2):249–77. doi:10.1021/jm400378w

276. Qian KC, Wang L, Hickey ER, Studts J, Barringer K, Peng C, et al. Structural basis of constitutive activity and a unique nucleotide binding mode of human PIM-1 kinase. Journal of Biological Chemistry. 2005 Feb 18;280(7):6130–7. doi:10.1074/jbc.M409123200 PubMed PMID: 15525646.

277. Lee SJ, Han BG, Cho JW, Choi JS, Lee J, Song HJ, et al. Crystal structure of Pim1 kinase in complex with a pyrido[4,3-D]pyrimidine derivative suggests a unique binding mode. PLoS One. 2013 Jul 31;8(7):e70358. doi:https://doi.org/10.1371/journal.pone.0070358

278. Laurent Brault, Christelle Gasser, Franz Bracher, Kilian Huber, Stefan Knapp, Jürg Schwaller. PIM serine/threonine kinases in the pathogenesis and therapy of hematologic malignancies and solid cancers. Haematologica. 2010 Feb 9;95(6):1004–15. doi:10.3324/haematol.2009.017079

279. Robert X, Gouet P. Deciphering key features in protein structures with the new ENDscript server. Nucleic Acids Res. 2014 Jul 1;42(W1):W320–4. doi:10.1093/nar/gku316

280. Torres PHM, Sodero ACR, Jofily P, Silva-Jr FP. Key topics in molecular docking for drug design. Int J Mol Sci. 2019 Sep 15;20(18):4574. doi:10.3390/ijms20184574

281. Meng XY, Zhang HX, Mezei M, Cui M. Molecular docking: A powerful approach for structure-based drug discovery. Curr Comput Aided Drug Des. 2011 Jun 1;7(2):146–57. doi:10.2174/157340911795677602

282. Ishchenko A, Zhang L, Le Brazidec JY, Fan J, Chong JH, Hingway A, et al. Structure-based design of low-nanomolar PIM kinase inhibitors. Bioorg Med Chem Lett. 2015 Feb 1;25(3):474–80. doi:10.1016/j.bmcl.2014.12.041 PubMed PMID: 25575657.

283. Burger MT, Han W, Lan J, Nishiguchi G, Bellamacina C, Lindval M, et al. Structure guided optimization, *in vitro* activity, and *in vivo* activity of pan-PIM kinase inhibitors. ACS Med Chem Lett. 2013 Dec 12;4(12):1193–7. doi:10.1021/ml400307j

284. Burger MT, Nishiguchi G, Han W, Lan J, Simmons R, Atallah G, et al. Identification of N-(4-((1R,3S,5S)-3-amino-5-methylcyclohexyl)pyridin-3-yl)-6-(2,6-difluorophenyl)-5-fluoropicolinamide (PIM447), a potent and selective proviral insertion site of moloney murine leukemia (PIM) 1, 2, and 3 kinase inhibitor in clinical trials for hematological malignancies. J Med Chem. 2015 Nov 12;58(21):8373–86. doi:10.1021/acs.jmedchem.5b01275 PubMed PMID: 26505898.

285. Keiser J, Utzinger J. Chapter 8 - The drugs we have and the drugs we need against major helminth infections. In: Zhou XN, Bergquist R, Olveda R, Utzinger J, editors. Advances in Parasitology. Academic Press; 2010. p. 197–230. doi:https://doi.org/10.1016/S0065-308X(10)73008-6

286. Prichard RK, Basáñez MG, Boatin BA, McCarthy JS, García HH, Yang GJ, et al. A research agenda for helminth diseases of humans: Intervention for control and elimination. PLoS Negl Trop Dis. 2012 Apr 24;6(4):e1549. doi:https://doi.org/10.1371/journal.pntd.0001549

287. Caffrey CR. *Schistosomiasis* and its treatment. Future Med Chem. 2015 Apr 1;7(6):675–6. doi:10.4155/fmc.15.27

288. Caffrey CR, Utzinger J, Keiser J. Drug discovery for trematodiases: Challenges and progress. In: Selzer PM, Caffrey CR, editors. Parasitic Helminths. 2012. p. 323–39. doi:https://doi.org/10.1002/9783527652969.ch20

289. Mahurkar ND, Gawhale ND, Lokhande MN, Uke SJ, Kodape MM. Benzimidazole: A versatile scaffold for drug discovery and beyond - A comprehensive review of synthetic

approaches and recent advancements in medicinal chemistry. Results Chem. 2023 Dec 1;6:101139. doi:https://doi.org/10.1016/j.rechem.2023.101139

290. Robinson MW, McFerran N, Trudgett A, Hoey L, Fairweather I. A possible model of benzimidazole binding to β-tubulin disclosed by invoking an inter-domain movement. J Mol Graph Model. 2004 Dec;23(3):275–84. doi:https://doi.org/10.1016/j.jmgm.2004.08.001

291. Gelmedin V, Dissous C, Grevelding CG. Re-positioning protein-kinase inhibitors against schistosomiasis. Future Med Chem. 2015 Apr 1;7(6):737–52. doi:10.4155/fmc.15.31 PubMed PMID: 25996067.

292. Varjosalo M, Keskitalo S, Van Drogen A, Nurkkala H, Vichalkovski A, Aebersold R, et al. The protein interaction landscape of the human CMGC kinase group. Cell Rep. 2013 Apr 25;3(4):1306–20. doi:https://doi.org/10.1016/j.celrep.2013.03.027

293. Krishna M, Narang H. The complexity of mitogen-activated protein kinases (MAPKs) made simple. Cellular and Molecular Life Sciences. 2008 Nov;65(22):3525–44. doi:10.1007/s00018-008-8170-7

294. Yue J, López JM. Understanding MAPK signaling pathways in apoptosis. Int J Mol Sci. 2020 Mar 28;21(7):2346. doi:10.3390/ijms21072346 PubMed PMID: 32231094.

295. Skelding KA, Rostas JAP. The role of molecular regulation and targeting in regulating calcium/calmodulin stimulated protein kinases. In: Islam MdS, editor. Calcium Signaling. 1st ed. Dordrecht: Springer Netherlands; 2012. p. 703–30. doi:10.1007/978-94-007-2888-2_31

296. You H, McManus DP, Hu W, Smout MJ, Brindley PJ, Gobert GN. Transcriptional responses of *in vivo* praziquantel exposure in *schistosomes* identifies a functional role for calcium signalling pathway member CamKII. PLoS Pathog. 2013 Mar 28;9(3):e1003254. doi:https://doi.org/10.1371/journal.ppat.1003254

297. Hirst NL, Lawton SP, Walker AJ. CaMKII regulates neuromuscular activity and survival of the human blood fluke *Schistosoma mansoni*. Sci Rep. 2022 Nov 18;12(1):19831. doi:10.1038/s41598-022-23962-8

298. Deehan MR, Harnett W, Harnett MM. A filarial nematode-secreted phosphorylcholine-containing glycoprotein uncouples the B cell antigen receptor from extracellular signal-regulated kinase-mitogen-activated protein kinase by promoting the surface Ig-mediated recruitment of Src homology 2 domain-containing tyrosine phosphatase-1

and Pac-1 mitogen-activated kinase-phosphatase 1. The Journal of Immunology. 2001 Jun 15;166(12):7462–8. doi:https://doi.org/10.4049/jimmunol.166.12.7462

299. Harnett MM, Deehan MR, Williams DM, Harnett W. Induction of signalling anergy via the T-cell receptor in cultured Jurkat T cells by pre-exposure to a filarial nematode secreted product. Parasite Immunol. 1998 Nov;20(11):551–63. doi:10.1046/j.1365-3024.1998.00181.x PubMed PMID: 9988312.

300. Steinhart R, Kazimirsky G, Okhrimenko H, Ben-Hur T, Brodie C. PKCε induces astrocytic differentiation of multipotential neural precursor cells. Glia. 2007 Jan 15;55(2):224–32. doi:https://doi.org/10.1002/glia.20454

301. Gallicano GI, Yousef MC, Capco DG. PKC - A pivotal regulator of early development. BioEssays. 1997 Jan 1;19(1):29–36. doi:https://doi.org/10.1002/bies.950190107

302. Eckert JJ, McCallum A, Mears A, Rumsby MG, Cameron IT, Fleming TP. Specific PKC isoforms regulate blastocoel formation during mouse preimplantation development. Dev Biol. 2004 Oct 15;274(2):384–401. doi:https://doi.org/10.1016/j.ydbio.2004.07.027

303. Ludtmann MHR, Rollinson D, Emery AM, Walker AJ. Protein kinase C signalling during miracidium to mother sporocyst development in the helminth parasite, *Schistosoma mansoni*. Int J Parasitol. 2009 Sep 1;39(11):1223–33. doi:https://doi.org/10.1016/j.ijpara.2009.04.002

304. Bahia D, Avelar L, Mortara RA, Khayath N, Yan Y, Noël C, et al. SmPKC1, a new protein kinase C identified in the platyhelminth parasite *Schistosoma mansoni*. Biochem Biophys Res Commun. 2006 Jul 7;345(3):1138–48. doi:https://doi.org/10.1016/j.bbrc.2006.05.025

305. Bahia D, Avelar LGA, Vigorosi F, Cioli D, Oliveira GC, Mortara RA. The distribution of motor proteins in the muscles and flame cells of the *Schistosoma mansoni* miracidium and primary sporocyst. Parasitology. 2006/06/02. 2006 Sep;133(3):321–9. doi:DOI: 10.1017/S0031182006000400

306. Ressurreição M, Kirk RS, Rollinson D, Emery AM, Page NM, Walker AJ. Sensory protein kinase signaling in *Schistosoma mansoni* cercariae: Host location and invasion. Journal of Infectious Diseases. 2015;212(10):1787–97. doi:10.1093/infdis/jiv464 PubMed PMID: 26401028.

307. Ressurreição M, De Saram P, Kirk RS, Rollinson D, Emery AM, Page NM, et al. Protein kinase C and extracellular signal-regulated kinase regulate movement, attachment,

pairing and egg release in *Schistosoma mansoni*. PLoS Negl Trop Dis. 2014 Jun 12;8(6):e2924. doi:https://doi.org/10.1371/journal.pntd.0002924

308. Graham MK, Fairweather I, McGeown JG. Second messengers mediating mechanical responses to the FaRP GYIRFamide in the fluke *Fasciola hepatica*. American Journal of Physiology-Regulatory, Integrative and Comparative Physiology. 2000 Dec 1;279(6):R2089–94. doi:10.1152/ajpregu.2000.279.6.R2089

309. Puckelwaldt O, Gramberg S, Ajmera S, Koepke J, Samakovlis C, Haeberlein S. Single-cell transcriptomics identifies a p21-activated kinase important for survival of the zoonotic parasite *Fasciola hepatica*. bioRxiv. 2024 Mar 27;2024.03.26.586785. doi:10.1101/2024.03.26.586785

310. Hubbard SR, Till JH. Protein tyrosine kinase structure and function. Annu Rev Biochem. 2000 Jul;69(1):373–98. doi:https://doi.org/10.1146/annurev.biochem.69.1.373

311. Robinson DR, Wu YM, Lin SF. The protein tyrosine kinase family of the human genome. Oncogene. 2000 Nov;19(49):5548–57. doi:https://doi.org/10.1038/sj.onc.1203957

312. Hubbard SR, Miller WT. Receptor tyrosine kinases: mechanisms of activation and signaling. Curr Opin Cell Biol. 2007 Apr 1;19(2):117–23. doi:10.1016/j.ceb.2007.02.010 PubMed PMID: 17306972.

313. Katz M, Amit I, Yarden Y. Regulation of MAPKs by growth factors and receptor tyrosine kinases. Biochim Biophys Acta Mol Cell Res. 2007 Aug 1;1773(8):1161–76. doi:10.1016/j.bbamcr.2007.01.002 PubMed PMID: 17306385.

314. Sudhesh Dev S, Zainal Abidin SA, Farghadani R, Othman I, Naidu R. Receptor tyrosine kinases and their signaling pathways as therapeutic targets of curcumin in cancer. Front Pharmacol. 2021 Nov 15;12:772510. doi:10.3389/fphar.2021.772510

315. Beckmann S, Hahnel S, Cailliau K, Vanderstraete M, Browaeys E, Dissous C, et al. Characterization of the Src/Abl hybrid kinase SmTK6 of *Schistosoma mansoni*. Journal of Biological Chemistry. 2011 Dec 9;286(49):42325–36. doi:10.1074/jbc.M110.210336 PubMed PMID: 22013071.

316. Sundaram M V. RTK/ras/MAPK signaling. WormBook. 2006 Feb 11;1–19. doi:10.1895/wormbook.1.80.1

317. Simão FA, Waterhouse RM, Ioannidis P, Kriventseva E V., Zdobnov EM. BUSCO: Assessing genome assembly and annotation completeness with single-copy orthologs.

Bioinformatics. 2015 Oct 1;31(19):3210–2. doi:10.1093/bioinformatics/btv351 PubMed PMID: 26059717.

318. Yang Z, Rannala B. Molecular phylogenetics: Principles and Practice. Nature Reviews Genetics. 2012. p. 303–14. doi:10.1038/nrg3186 PubMed PMID: 22456349.

319. Stroehlein AJ, Young ND, Gasser RB. Improved strategy for the curation and classification of kinases, with broad applicability to other eukaryotic protein groups. Sci Rep. 2018 Dec 1;8(1). doi:10.1038/s41598-018-25020-8 PubMed PMID: 29717207.

320. Martin DMA, Miranda-Saavedra D, Barton GJ. Kinomer v. 1.0: a database of systematically classified eukaryotic protein kinases. Nucleic Acids Res. 2009 Jan 1;37(suppl_1):D244–50. doi:10.1093/nar/gkn834

321. Klug DM, Gelb MH, Pollastri MP. Repurposing strategies for tropical disease drug discovery. Bioorg Med Chem Lett. 2016 Jun 1;26(11):2569–76. doi:https://doi.org/10.1016/j.bmcl.2016.03.103

322. Cowan N, Keiser J. Repurposing of anticancer drugs: *in vitro* and *in vivo* activities against *Schistosoma mansoni*. Parasit Vectors. 2015 Aug 13;8(1):1–9. doi:10.1186/s13071-015-1023-y PubMed PMID: 26265386.

323. Chu CN, Lee TKW. Targeting protein kinases in cancer stem cells. Essays Biochem. 2022 Sep 16;66(4):399–412. doi:10.1042/EBC20220002 PubMed PMID: 35607921.

324. Wendt GR, Collins JJ. Schistosomiasis as a disease of stem cells. Curr Opin Genet Dev. 2016 Oct 1;40:95–102. doi:10.1016/j.gde.2016.06.010 PubMed PMID: 27392295.

325. Wang B, Lee J, Li P, Saberi A, Yang H, Liu C, et al. Stem cell heterogeneity drives the parasitic life cycle of <i>Schistosoma mansoni<i>. Sánchez Alvarado A, editor. Elife. 2018 Jul 10;7:e35449. doi:10.7554/eLife.35449

326. Collins III JJ, Wang B, Lambrus BG, Tharp ME, Iyer H, Newmark PA. Adult somatic stem cells in the human parasite *Schistosoma mansoni*. Nature. 2013 Feb 28;494(7438):476–9. doi:10.1038/nature11924

327. Doerig C. Protein kinases as targets for anti-parasitic chemotherapy. Biochimica et Biophysica Acta (BBA) - Proteins and Proteomics. 2004 Mar 11;1697(1–2):155–68. doi:https://doi.org/10.1016/j.bbapap.2003.11.021

328. Kaufmann S. Paul Ehrlich: Founder of chemotherapy. Nat Rev Drug Discov. 2008 May 7;7(5):373. doi:10.1038/nrd2582

329. Klaeger S, Heinzlmeir S, Wilhelm M, Polzer H, Vick B, Koenig PA, et al. The target landscape of clinical kinase drugs. Science (1979). 2017 Dec 1;358(6367):eaan4368. doi:10.1126/science.aan4368 PubMed PMID: 29191878.

330. Garuti L, Roberti M, Bottegoni G. Multi-kinase inhibitors. Curr Med Chem. 2015 Feb 1;22(6):695–712. doi:https://doi.org/10.2174/0929867321666141216125528

331. Ashburn TT, Thor KB. Drug repositioning: Identifying and developing new uses for existing drugs. Nat Rev Drug Discov. 2004 Aug 1;3(8):673–83. doi:10.1038/nrd1468

332. Vieth M, Sutherland JJ, Robertson DH, Campbell RM. Kinomics: Characterizing the therapeutically validated kinase space. Drug Discov Today. 2005 Jun 15;10(12):839–46. doi:10.1016/S1359-6446(05)03477-X PubMed PMID: 15970266.

333. Cohen MH, Johnson JR, Justice R, Pazdur R. Approval summary: Imatinib mesylate for one or three years in the adjuvant treatment of gastrointestinal stromal tumors. Oncologist. 2012 Jul 1;17(7):992–7. doi:10.1634/theoncologist.2012-0109

334. Houhou H, Puckelwaldt O, Strube C, Haeberlein S. Reference gene analysis and its use for kinase expression profiling in *Fasciola hepatica*. Sci Rep. 2019 Nov 1;9(1):15867.

335. Wang JYJ. Cell responses to DNA damage. In: Boffetta P, Hainaut P, editors. Encyclopedia of Cancer. 3rd ed. Oxford: Academic Press; 2019. p. 315–25. doi:https://doi.org/10.1016/B978-0-12-801238-3.98754-3

336. Komander D, Kular GS, Schüttelkopf AW, Deak M, Prakash KRC, Bain J, et al. Interactions of LY333531 and other bisindolyl maleimide inhibitors with PDK1. Structure. 2004 Feb 1;12(2):215–26. doi:10.1016/j.str.2004.01.005 PubMed PMID: 14962382.

337. Tang S, Xiao V, Wei L, Whiteside CI, Kotra LP. Protein kinase C isozymes and their selectivity towards ruboxistaurin. Proteins: Structure, Function and Genetics. 2008 Jul;72(1):447–60. doi:10.1002/prot.21942 PubMed PMID: 18214957.

338. Javey G, Schwartz SG, Flynn HW, Aiello LP, Sheetz MJ. Ruboxistaurin: Review of safety and efficacy in the treatment of diabetic retinopathy. Clin Med Insights Ther. 2010 Jan;2:CMS5046. doi:https://doi.org/10.4137/CMT.S5046

339. Burkey JL, Campanale KM, Barbuch R, O'Bannon D, Rash J, Benson C, et al. Disposition of [14C] ruboxistaurin in humans. Drug Metabolism and Disposition. 2006 Nov 1;34(11):1909–17. doi:https://doi.org/10.1124/dmd.106.009894

340. Hennessy DR, Lacey E, Steel JW, Prichad RK. The kinetics of triclabendazole disposition in sheep. J Vet Pharmacol Ther. 1987 Mar 1;10(1):64–72. doi:https://doi.org/10.1111/j.1365-2885.1987.tb00078.x

341. Gramberg SF. Transcriptome analyses across tissues in the liver fluke *Fasciola hepatica* - from gene expression to drug target characterization. Institute of Parasitology, JLU Giessen; 2025. doi:https://doi.org/10.22029/jlupub-20244

342. EMEA. Withdrawal assessment report for Arxxant-Ruboxistaurin (as mesilate monohydrate) [Internet]. London; 2007 May. Available from: http://www.emea.europa.eu doi:https://www.ema.europa.eu/documents/withdrawal-report/withdrawal-assessment-report-arxxant_en.pdf

343. Sheetz MJ, Aiello LP, Davis MD, Danis R, Bek T, Cunha-Vaz J, et al. The effect of the oral PKCβ inhibitor ruboxistaurin on vision loss in two phase 3 studies. Invest Ophthalmol Vis Sci. 2013 Mar 1;54(3):1750–7. doi:10.1167/iovs.12-11055 PubMed PMID: 23404115.

344. McGill JB, King GL, Berg PH, Price KL, Kles KA, Bastyr EJ, et al. Clinical safety of the selective PKC-β inhibitor, ruboxistaurin. Expert Opin Drug Saf. 2006 Nov 1;5(6):835–45. doi:10.1517/14740338.5.6.835 PubMed PMID: 17044810.

345. Inoue K, Torimura T, Nakamura T, Iwamoto H, Masuda H, Abe M, et al. Vandetanib, an inhibitor of VEGF receptor-2 and EGF receptor, suppresses tumor development and improves prognosis of liver cancer in mice. Clinical Cancer Research. 2012 Jul 15;18(14):3924–33. doi:10.1158/1078-0432.CCR-11-2041 PubMed PMID: 22611027.

346. Kipryushina YO, Yakovlev K V., Odintsova NA. Vascular endothelial growth factors: A comparison between invertebrates and vertebrates. Cytokine Growth Factor Rev. 2015 Dec 1;26(6):687–95. doi:10.1016/j.cytogfr.2015.04.001 PubMed PMID: 26066416.

347. D'Aniello S, Irimia M, Maeso I, Pascual-Anaya J, Jiménez-Delgado S, Bertrand S, et al. Gene expansion and retention leads to a diverse tyrosine kinase superfamily in amphioxus. Mol Biol Evol. 2008 Sep 1;25(9):1841–54. doi:10.1093/molbev/msn132 PubMed PMID: 18550616.

348. Horiike A, Yoh K, Seto T, Satouchi M, Nishio M, Yamamoto N, et al. NSCLC, metastatic 1203PD LURET study: Phase 2 study of vandetanib in patients with advanced RET-rearranged non-small cell lung cancer (NSCLC). Annals of Oncology. 2016 Oct 1;27:vi416–54. doi:10.1093/annonc/mdw383.4

349. Gustafson DL, Bradshaw-Pierce EL, Merz AL, Zirrolli JA. Tissue distribution and metabolism of the tyrosine kinase inhibitor ZD6474 (Zactima) in tumor-bearing nude mice following oral dosing. Journal of Pharmacology and Experimental Therapeutics. 2006 Aug 1;318(2):872–80. doi:10.1124/jpet.106.102376 PubMed PMID: 16644900.

350. Michael Vozniak J, Jacobs JM. Vandetanib. J Adv Pract Oncol. 2012 Mar 1;3(2):112–6. PubMed PMID: 25031937.

351. Weil A, Martin P, Smith R, Oliver S, Langmuir P, Read J, et al. Pharmacokinetics of vandetanib in subjects with renal or hepatic impairment. Clin Pharmacokinet. 2010 Sep;49(9):607–18. doi:10.2165/11534330-000000000-00000

352. Banas V, Elfawal MA, Rosa BA, Mahoney M, Kauffman J, Goetz E, et al. Discovery of human PIM kinase inhibitors as a class of anthelmintic drugs to treat intestinal nematode infections. ACS Infect Dis. 2025 Jan 20;11(2):506–17. doi:10.1021/acsinfecdis.4c00864

353. McCusker P, McVeigh P, Rathinasamy V, Toet H, McCammick E, O'Connor A, et al. Stimulating neoblast-like cell proliferation in juvenile *Fasciola hepatica* supports growth and progression towards the adult phenotype *in vitro*. PLoS Negl Trop Dis. 2016 Sep 13;10(9):e0004994. doi:https://doi.org/10.1371/journal.pntd.0004994

354. Cohen MS, Zhang C, Shokat KM, Taunton J. Structural bioinformatics-based design of selective, irreversible kinase inhibitors. Science (1979). 2005 May 27;308(5726):1318–21. doi:10.1126/science1108367

355. Zhou Y, Xiang S, Yang F, Lu X. Targeting gatekeeper mutations for kinase drug discovery. J Med Chem. 2022 Nov 17;65(23):15540–58. doi:10.1021/acs.jmedchem.2c01361

356. Aledo JC. Methionine in proteins: The Cinderella of the proteinogenic amino acids. Protein Science. 2019 Oct 1;28(10):1785–96. doi:https://doi.org/10.1002/pro.3698

357. Tong M, Seeliger MA. Targeting conformational plasticity of protein kinases. ACS Chem Biol. 2015 Jan 16;10(1):190–200. doi:10.1021/cb500870a

358. Huse M, Kuriyan J. The conformational plasticity of protein kinases. Cell. 2002 May 3;109(3):275–82. doi:https://doi.org/10.1016/S0092-8674(02)00741-9

359. Yumura S, Kitagawa D, Moritsugu K, Nakayama A, Shinada T, Sawa M, et al. Conserved gatekeeper methionine regulates the binding and access of kinase inhibitors

to ATP sites of MAP2K1, 4, and 7: Clues for developing selective inhibitors. Bioorg Med Chem Lett. 2024 Nov 1;112:129914. doi:https://doi.org/10.1016/j.bmcl.2024.129914

360. The managed chemical compound collection library, University of Nottingham [Internet]. [cited 2026 May 11]. Available from: https://uat-mccc-frontend.azurewebsites.net/

361. Rost B. Twilight zone of protein sequence alignments. Protein Eng. 1999 Feb 1;12(2):85–94. doi:10.1093/protein/12.2.85

362. Baker D, Sali A. Protein structure prediction and structural genomics. Science (1979). 2001 Oct 5;294(5540):93–6. doi:10.1126/science.1065659

363. Sánchez R, Sali A. Large-scale protein structure modeling of the *Saccharomyces cerevisiae* genome. Proceedings of the National Academy of Sciences. 1998 Nov 10;95(23):13597–602. doi:10.1073/pnas.95.23.13597

364. Bordoli L, Kiefer F, Arnold K, Benkert P, Battey J, Schwede T. Protein structure homology modeling using SWISS-MODEL workspace. Nat Protoc. 2009 Jan;4(1):1–13. doi:10.1038/nprot.2008.197

365. Haddad Y, Adam V, Heger Z. Ten quick tips for homology modeling of high-resolution protein 3D structures. PLoS Comput Biol. 2020 Apr 2;16(4):e1007449. doi:10.1371/journal.pcbi.1007449

366. Krieger E, Nabuurs SB, Vriend G. Homology modeling. In: Bourne PE, Weissig H, editors. Structural Bioinformatics. 2003. p. 509–23. (Methods of Biochemical Analysis). doi:10.1002/0471721204.ch25

367. Winiewska-Szajewska M, Paprocki D, Marzec E, Poznański J. Effect of histidine protonation state on ligand binding at the ATP-binding site of human protein kinase CK2. Sci Rep. 2024 Jan 17;14(1):1463. doi:10.1038/s41598-024-51905-y

368. Reynolds WF, Peat IR, Freedman MH, Lyerla JR. Determination of the tautomeric form of the imidazole ring of L-histidine in basic solution by carbon-13 magnetic resonance spectroscopy. J Am Chem Soc. 1973 Jan 1;95(2):328–31. doi:10.1021/ja00783a006

369. Zoë Fisher S, Raum HN, Weininger U. Proton occupancies in histidine side chains of carbonic anhydrase II by neutron crystallography and NMR – differences, similarities and opportunities. ChemBioChem. 2025 Mar 3;26(5):e202400930. doi:https://doi.org/10.1002/cbic.202400930

370. Kim MO, Nichols SE, Wang Y, McCammon JA. Effects of histidine protonation and rotameric states on virtual screening of *M. tuberculosis* RmlC. J Comput Aided Mol Des. 2013 Apr 12;27(3):235–46. doi:10.1007/s10822-013-9643-9

371. Scapin G, Patel SB, Lisnock J, Becker JW, LoGrasso P V. The structure of JNK3 in complex with small molecule inhibitors: Structural basis for potency and selectivity. Chem Biol. 2003 Aug 1;10(8):705–12. doi:https://doi.org/10.1016/S1074-5521(03)00159-5

372. Carrera AC, Alexandrov K, Roberts TM. The conserved lysine of the catalytic domain of protein kinases is actively involved in the phosphotransfer reaction and not required for anchoring ATP. Proceedings of the National Academy of Sciences. 1993 Jan 15;90(2):442–6. doi:10.1073/pnas.90.2.442

373. Siefker C. Characterisation and differentiation of kinase binding pockets in PKA and Pim1 by small molecule fragments using protein crystallography. Institute for Pharmaceutical Chemistry, Philipps University Marburg; 2018. doi:https://doi.org/10.17192/z2018.0229

374. Taylor C. Discovery and development of novel inhibitors for the kinase Pim-1 and G-protein coupled receptor smoothened. Institute for Pharmaceutical Chemistry, Philipps University Marburg; 2021. doi:https://doi.org/10.17192/z2019.0241

375. Jacobs MD, Black J, Futer O, Swenson L, Hare B, Fleming M, et al. PIM-1 ligand-bound structures reveal the mechanism of serine/threonine kinase inhibition by LY294002. Journal of Biological Chemistry. 2005 Apr 8;280(14):13728–34. doi:10.1074/jbc.M413155200 PubMed PMID: 15657054.

376. Wang X, Blackaby W, Allen V, Chan GKY, Chang JH, Chiang PC, et al. Optimization of pan-Pim kinase activity and oral bioavailability leading to diaminopyrazole (GDC-0339) for the treatment of multiple myeloma. J Med Chem. 2019 Feb 4;62(4):2140–53. doi:10.1021/acs.jmedchem.8b01857

377. Fabbro D, Cowan-Jacob SW, Moebitz H. Ten things you should know about protein kinases: IUPHAR Review 14. Br J Pharmacol. 2015 Jun 1;172(11):2675–700. doi:https://doi.org/10.1111/bph.13096

378. Nagar B, Bornmann WG, Pellicena P, Schindler T, Veach DR, Miller WT, et al. Crystal structures of the kinase domain of c-Abl in complex with the small molecule inhibitors PD173955 and imatinib (STI-571). Cancer Res. 2002 Aug 1;62(15):4236–43. PubMed PMID: 12154025.

379. Nolen B, Taylor S, Ghosh G. Regulation of protein kinases: Controlling activity through activation segment conformation. Mol Cell. 2004 Sep 10;15(5):661–75. doi:10.1016/j.molcel.2004.08.024

380. Adams JA. Kinetic and catalytic mechanisms of protein kinases. Chem Rev. 2001 Aug 1;101(8):2271–90. doi:10.1021/cr000230w

381. Kanehisa M, Goto S, Furumichi M, Tanabe M, Hirakawa M. KEGG for representation and analysis of molecular networks involving diseases and drugs. Nucleic Acids Res. 2010 Jan 1;38(suppl_1):D355–60. doi:10.1093/nar/gkp896

382. Kanehisa M, Goto S. KEGG: Kyoto encyclopedia of genes and genomes. Nucleic Acids Res. 2000 Jan 1;28(1):27–30. doi:10.1093/nar/28.1.27

383. Rebello RJ, Kusnadi E, Cameron DP, Pearson HB, Lesmana A, Devlin JR, et al. The dual inhibition of RNA Pol I transcription and PIM kinase as a new therapeutic approach to treat advanced prostate cancer. Clinical Cancer Research. 2016 Nov 15;22(22):5539–52. doi:10.1158/1078-0432.CCR-16-0124

384. Sun Z, Zeng L, Zhang M, Zhang Y, Yang N. PIM1 inhibitor synergizes the anti-tumor effect of osimertinib via STAT3 dephosphorylation in EGFR-mutant non-small cell lung cancer. Ann Transl Med. 2020 Mar;8(6):366. doi:10.21037/atm.2020.02.43

385. Astex Pharmaceuticals Inc. www.clinicaltrials.gov [Internet]. 2010 [cited 2026 Feb 10]. Safety of SGI-1776, a PIM kinase inhibitor in refractory prostate cancer and relapsed/ refractory non Hodgkin's lymphoma (NCT00848601). Available from: https://clinicaltrials.gov/study/NCT00848601?intr=SGI-1776&viewType=Card&rank=2&tab=study

386. Astex Pharmaceuticals Inc. www.clinicaltrials.gov [Internet]. 2012 [cited 2026 Feb 10]. Study of SGI-1776, a PIM kinase inhibitor, in subjects with relapsed/refractory leukemias (NCT01239108). Available from: https://clinicaltrials.gov/study/NCT01239108?intr=SGI-1776&viewType=Card&rank=1

387. Batra V, Maris JM, Kang MH, Reynolds CP, Houghton PJ, Alexander D, et al. Initial testing (stage 1) of SGI-1776, a PIM1 kinase inhibitor, by the pediatric preclinical testing program. Pediatr Blood Cancer. 2012 Oct 1;59(4):749–52. doi:https://doi.org/10.1002/pbc.23364

388. Symphony Evolution Inc. www.clinicaltrials.gov [Internet]. 2007 [cited 2025 Oct 30]. A phase 2 study of XL999 administered intravenously to subjects with metastatic colorectal cancer. Available from: https://clinicaltrials.gov/study/NCT00277303

389. Symphony Evolution Inc. www.clinicaltrials.gov [Internet]. 2008 [cited 2025 Oct 30]. A phase 2 study of XL999 administered intravenously to subjects with non-small-cell lung cancer. Available from: https://clinicaltrials.gov/study/NCT00277329

# 8. Contributions

## 8.1 Publications

**Please note:**

Previously published content (text passages, illustrations) has been appropriately referenced throughout this document, citing the below-mentioned publications. Text passages are referenced paragraph-by-paragraph, illustrations in the respective figure legends. Co-author contributions are consistent with the information provided in the publication and are indicated again in relevant sections. Lack of specific mark or a reference to a trademark or a patent does not imply that this work or part of it can be used or copied without the copyright permission.

**Part of this thesis have been published in or is in the process of being published in:**

**Ajmera, S.**, Puckelwaldt, O., Stroehlein, A., Haeberlein, S. (2026). Curation of the *Fasciola hepatica* kinome as a resource for drug target discovery. **BMC Genomics**; 27(1): 98. https://doi.org/10.1186/s12864-025-12513-w.

**Ajmera, S.**, Puckelwaldt, O., Martinez, J., Shamsara, J., Moreira, B., Falcone, F., Kolb, P., Haeberlein, S. (2026). Leveraging PIM kinase in *Fasciola hepatica* to identify novel fasciolicidal compounds from the MCCC compound library. **(In preparation, submission envisaged at International Journal of Parasitology: Drug and Drug resistance)**

**Further publications:**

Puckelwaldt, O., Gramberg, S., **Ajmera, S.**, Koepke, J., Shamsara, J., Samakovlis, C., Kolb, P., Haeberlein, S. (2026). Single-cell transcriptomics identifies a p21-activated kinase important for survival of the zoonotic parasite *Fasciola hepatica*. **iScience**. **(accepted)**

Welsch, S., Puckelwaldt, O., **Ajmera, S.**, Magari, F., Haeberlein, S., Grünweller, A., Grevelding, C. (2026). The DEAD-box RNA helicase eIF4A is a crucial factor for stem-cell activity and reproduction of the parasite *Schistosoma mansoni*. **Frontiers in Cellular and Infection Microbiology**; 15:1731808. https://doi.org/10.3389/fcimb.2025.1731808.

Sanna, A., Stettler, F., Boloukulu, E., Miller-Büchner, P., Koepke, J., **Ajmera, S.**, Teppe, L., Lafee, M., Hamarsheh, D., Roderfeld, M., Bartkuhn, M., Haeberlein, S. (2026). *Fasciola hepatica* bypass host glucose dependency. **(In preparation, envisaged to be published in Current Research in Parasitology & Vector-Borne Diseases)**

## 8.2 Conferences

**This work has been presented at the following conferences:**

2025 - Tagung der DVG-Fachgruppe Parasitologie und parasitäre Krankheiten - Giessen, Germany

Talk: *Fasciola hepatica* kinome: A roadmap to anthelmintic compounds.

2025 - Joint Parasitology Spring Meeting - Wuerzburg, Germany.

Poster: *Fasciola hepatica* kinome: A roadmap towards anthelmintic compounds.

2024 - 7th DRUID retreat - Marburg, Germany.

Talk: *Fasciola hepatica* kinome: A roadmap towards anthelmintic compounds.

Poster: Navigating the kinase landscape of *Fasciola hepatica*: A roadmap for drug target discovery.

2024 - Anti-helmintics VI - Toronto, Canada.

Poster: *Fasciola hepatica* kinome: A roadmap to anthelmintic compounds.

2024 - 17th GGL Annual Conference - Giessen, Germany.

Poster: Traversing the *Fasciola hepatica* kinome: Paving the way for new therapeutic breakthroughs.

2024 - International conference of the LOEWE center DRUID - Seeon-Seebruck, Germany.

Poster: Navigating the kinase landscape of *Fasciola hepatica*: A roadmap for drug target discovery.

2023 - 6th DRUID retreat - Marburg, Germany.

Poster: Exploring the *Fasciola hepatica* kinome for discovery of novel drug target and candidates.

2023 - 16th GGL Annual Conference - Giessen, Germany.

Poster: DISCOVERING THE *Fasciola hepatica* KINOME FOR THE DETECTION OF NOVEL DRUG TARGETS AND DRUG CANDIDATES.

2023 - 30th Annual meeting of the German Society for Parasitology - Giessen, Germany.

Poster: EXPLORING THE *FASCIOLA HEPATICA* KINOME FOR THE DISCOVERY OF NOVEL DRUG TARGETS AND DRUG CANDIDATES.

2023 - 6th Spring symposium DRUID - Marburg, Germany.

Poster: Exploring the *Fasciola hepatica* kinome for discovery of novel drug target and candidates.